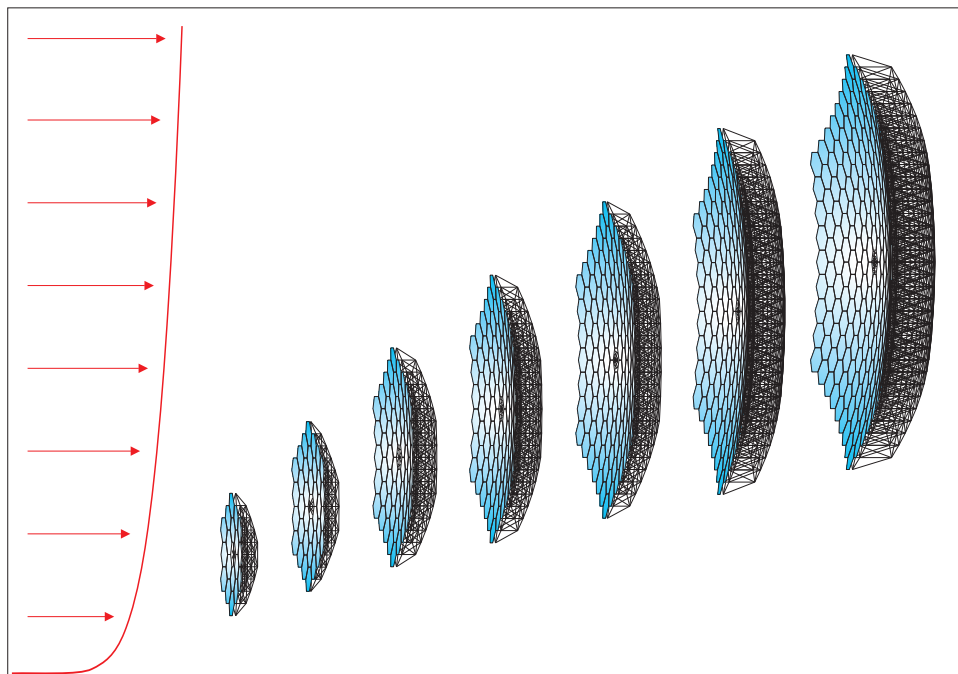


# Twelve Lectures on Structural Dynamics

André PREUMONT



2013

---

Active Structures Laboratory  
Department of Mechanical Engineering and Robotics

---



*Il n'y a que la vérité qui persuade,  
même sans avoir besoin de paraître avec toutes les preuves.  
Elle entre si naturellement dans l'esprit,  
que quand on l'apprend pour la première fois,  
il semble qu'on ne fasse que s'en souvenir.*

Fontenelle,  
*Entretiens sur la pluralité des mondes*, 1686



## Preface

---

Nowadays, with the amazing computing capability of computers and the availability of sophisticated, user-friendly computer-aided analysis software, the main difficulty for the analyst is to interpret the results and to make sure that the analysis includes all the relevant physical phenomena. The majority of structural failures occur because physical phenomena are overlooked, or greatly underestimated, rather than as a result of computational errors (e.g. the flutter of the Takoma suspension bridge, or the recent Fukushima tsunami disaster). To build confidence in the design, the analyst first develops a crude model, a model of minimum complexity which still reflects the main physical phenomena. What minimum complexity means depends on the problem; for example, a point mass with two degrees of freedom is sufficient to explain the stable operation of a rotor at supercritical velocities, but it is impossible to account for the dependency of the natural frequencies on the rotor speed without including the gyroscopic effects; the effect of prestresses on the natural frequencies cannot be accounted for without the inclusion of nonlinear strains (Green strain tensor). Similarly, analytical results may appear unnecessary at a time where extensive parametric studies may be performed numerically very quickly, but knowledge of the parametric dependence of critical properties such as natural frequency on design parameters (dimensions, material properties,...) is invaluable in design, especially when scale effects are involved.

This book is based on the vibration course that I teach in the joint masters program ULB/VUB at the university of Brussels, and the random vibration course that I taught for a decade at the university of Liege. It has also been strongly influenced by my research work in the active control of structures, where we usually work with models of moderate size, but

## VIII

which accounts for all the relevant features of the system dynamics. The book is focused on modeling, with very little, if any, attention paid to the numerical methods that I consider as mature and well-established, and which are well covered in the excellent books written by those more qualified than me (e.g. Geradin & Rixen).

I would like to pay a tribute to my own teachers at the university of Liege where I was initiated into structural analysis. Some forty years later, I still have vivid memories of the sparkling lectures of Prof. Ch. Massonnet on the strength of materials and of Prof. B. Fraeijis de Veubeke on vibrations (all without notes); and later Michel Geradin advised me during my doctorate. Reading the wonderful books from S.H. Crandall; Y.C. Fung; Y.K. Lin; and L. Meirovitch, and a few others also made a lasting impression on me. Finally, I wish to thank my coworkers at ULB for their enthusiasm and raising many questions that I have attempted to answer in this book. A special thanks goes to Renaud Bastaits who helped me to produce these notes, and did artfully most of the figures.

André Preumont  
Bruxelles, December 2012.

# Contents

<b>1 Single degree-of-freedom linear oscillator</b>	<b>1</b>
1.1 Free response . . . . .	1
1.2 Impulse response . . . . .	3
1.3 Convolution integral . . . . .	4
1.4 Harmonic response . . . . .	5
1.4.1 Undamped oscillator . . . . .	5
1.4.2 Damped oscillator . . . . .	7
1.5 Frequency Response Function . . . . .	8
1.6 Beat phenomenon . . . . .	10
1.7 State space form . . . . .	11
1.8 Problems . . . . .	13
<b>2 Multiple degree-of-freedom systems</b>	<b>17</b>
2.1 Governing equations . . . . .	17
2.2 Free response of the undamped system . . . . .	20
2.2.1 Eigenvalue problem . . . . .	20
2.2.2 Orthogonality relationships . . . . .	22
2.2.3 Multiple natural frequencies . . . . .	23
2.2.4 Rigid body modes . . . . .	23
2.2.5 Free response from initial conditions . . . . .	24
2.3 Modal decomposition . . . . .	25
2.3.1 Modal truncation . . . . .	26
2.4 Damping . . . . .	26
2.5 Dynamic flexibility matrix . . . . .	27
2.5.1 Structure with rigid body modes* . . . . .	30
2.5.2 Example* . . . . .	32
2.6 Anti-resonances . . . . .	34
2.6.1 Anti-resonances and constrained system . . . . .	37
2.7 Natural frequencies of a $n$ -storey building* . . . . .	39
2.8 Problems . . . . .	41

X CONTENTS

<b>3 Lagrangian dynamics</b>	<b>45</b>
3.1 Introduction . . . . .	45
3.2 Generalized coordinates, kinematic constraints . . . . .	46
3.2.1 Virtual displacements . . . . .	48
3.3 Principle of virtual work . . . . .	49
3.4 D'Alembert's principle . . . . .	51
3.5 Hamilton's principle . . . . .	52
3.6 Lagrange's equations . . . . .	55
3.6.1 Vibration of a linear non-gyroscopic discrete system	58
3.6.2 Dissipation function . . . . .	58
3.6.3 Example 1: Pendulum with a sliding mass . . . . .	59
3.6.4 Example 2: Rotating pendulum . . . . .	60
3.6.5 Example 3: Rotating spring mass system . . . . .	62
3.6.6 Example 4: Gyroscopic effects . . . . .	63
3.7 Lagrange's equations with constraints . . . . .	66
3.8 Conservation laws . . . . .	67
3.8.1 Jacobi integral . . . . .	67
3.8.2 Ignorable coordinate . . . . .	69
3.8.3 Example: The spherical pendulum . . . . .	71
3.9 Prestresses, geometric strain energy . . . . .	71
3.9.1 Green strain tensor . . . . .	72
3.9.2 Geometric strain energy due to prestress . . . . .	74
3.9.3 Buckling . . . . .	76
3.10 Negative stiffness . . . . .	76
3.11 Problems . . . . .	77
<b>4 Continuous systems</b>	<b>81</b>
4.1 Planar vibration of a beam (Euler-Bernoulli) . . . . .	81
4.1.1 Hamilton's principle . . . . .	83
4.2 Beam with axial prestress . . . . .	85
4.3 Free vibration of a beam . . . . .	87
4.3.1 Decoupling the boundary conditions . . . . .	88
4.3.2 Simply supported beam . . . . .	89
4.3.3 Free-free beam . . . . .	91
4.4 Orthogonality relationships . . . . .	93
4.5 Modal decomposition . . . . .	95
4.6 Vibration of a string . . . . .	96
4.7 Axial vibration of a bar . . . . .	98
4.7.1 Free vibration . . . . .	99
4.8 Static buckling of a beam* . . . . .	100

4.8.1	Simply supported beam . . . . .	101
4.8.2	Clamped-free beam . . . . .	102
4.9	Bending vibration of thin plates* . . . . .	103
4.9.1	Kirchhoff plate . . . . .	103
4.9.2	Free vibration of a simply supported rectangular plate	106
4.9.3	Free vibration of a clamped circular plate . . . . .	107
4.9.4	Rotating modes . . . . .	111
4.10	Response of a disk to a rotating point force* . . . . .	112
4.10.1	Constant rotating point force . . . . .	112
4.10.2	Harmonic rotating point force . . . . .	114
4.11	Problems . . . . .	115
<b>5</b>	<b>Rayleigh-Ritz method</b>	<b>117</b>
5.1	introduction . . . . .	117
5.2	Shape functions . . . . .	118
5.3	Axial vibration of a bar . . . . .	120
5.4	Planar vibration of a beam . . . . .	122
5.4.1	Damping . . . . .	125
5.4.2	Beam with axial load . . . . .	125
5.4.3	Simply supported beam with uniform axial load .	126
5.5	Rayleigh quotient . . . . .	127
5.5.1	Continuous beam . . . . .	127
5.5.2	Discrete system . . . . .	128
5.5.3	Principle of stationarity . . . . .	129
5.5.4	Recursive search of eigenvectors . . . . .	131
5.6	Building with gravity loads . . . . .	132
5.6.1	Single storey building . . . . .	132
5.6.2	Building with $n$ -identical floors . . . . .	134
5.7	Problems . . . . .	134
<b>6</b>	<b>Finite elements</b>	<b>139</b>
6.1	Introduction . . . . .	139
6.2	Formulation for a plane truss . . . . .	140
6.2.1	Bar element . . . . .	140
6.2.2	Truss structure . . . . .	143
6.3	Planar structure made of beams . . . . .	144
6.3.1	Beam element . . . . .	145
6.3.2	Beam structure . . . . .	147
6.3.3	Boundary conditions . . . . .	148
6.3.4	Convergence . . . . .	149

## XII CONTENTS

6.3.5	Geometric stiffness of a planar beam element . . . . .	151
6.4	Guyan reduction . . . . .	152
6.4.1	Examples . . . . .	154
6.5	Craig-Bampton reduction . . . . .	158
6.6	Problems . . . . .	159
<b>7</b>	<b>Seismic excitation</b>	<b>161</b>
7.1	Introduction . . . . .	161
7.2	Equation of motion for a single axis excitation . . . . .	161
7.2.1	Modal coordinates . . . . .	164
7.2.2	Support reaction, dynamic mass . . . . .	165
7.3	Example: $n$ -storey building . . . . .	166
7.4	Multi-axis excitation*	168
7.4.1	Modal coordinates . . . . .	169
7.4.2	Support reactions . . . . .	171
7.5	Cascade analysis . . . . .	172
7.6	Problems . . . . .	174
<b>8</b>	<b>Random vibration</b>	<b>175</b>
8.1	Introduction . . . . .	175
8.2	Stationary random process . . . . .	175
8.3	Correlation function and power spectral density . . . . .	176
8.3.1	PSD estimation from time histories . . . . .	178
8.3.2	Cumulative mean square response . . . . .	179
8.3.3	Gaussian process . . . . .	180
8.3.4	White noise . . . . .	180
8.4	Stationary response of a SISO linear system . . . . .	181
8.4.1	Random response of a linear oscillator . . . . .	182
8.4.2	White noise approximation . . . . .	184
8.4.3	Band limited white noise excitation . . . . .	184
8.4.4	Kanai-Tajimi spectrum . . . . .	185
8.5	Spectral moments, Rice formulae, central frequency . . . . .	186
8.6	Envelope of a narrow band process . . . . .	187
8.7	FRF estimation and coherence function . . . . .	189
8.8	Random response of MIMO systems . . . . .	191
8.8.1	Response in modal coordinates . . . . .	192
8.8.2	Correlation and PSD matrices . . . . .	193
8.8.3	Boundary layer noise . . . . .	195
8.8.4	Wind response of a tall building . . . . .	196
8.8.5	Vehicle moving on a rough road . . . . .	198

8.9	Mean square response . . . . .	199
8.9.1	Role of the cross-correlations . . . . .	200
8.10	Example: The seismic response of a n-storey building . .	202
8.11	Problems . . . . .	205
<b>9</b>	<b>Peak factor &amp; random fatigue</b>	<b>207</b>
9.1	Introduction . . . . .	207
9.1.1	Threshold crossings . . . . .	207
9.1.2	Fatigue . . . . .	208
9.2	Peak factor . . . . .	208
9.2.1	Maxima . . . . .	208
9.2.2	First-crossing problem . . . . .	209
9.2.3	Peak factor . . . . .	212
9.3	Response spectrum . . . . .	213
9.3.1	Maximum structural response . . . . .	215
9.3.2	Relation between $S_v(\omega, \xi)$ and $\Phi_0(\omega)$ . . . . .	216
9.4	Random fatigue . . . . .	217
9.4.1	S-N curve . . . . .	217
9.4.2	Linear damage theory . . . . .	218
9.4.3	Uniaxial loading . . . . .	218
9.4.4	Biaxial loading . . . . .	220
9.4.5	Finite element formulation . . . . .	221
9.5	Problems . . . . .	221
<b>10</b>	<b>Rotor dynamics</b>	<b>223</b>
10.1	Introduction . . . . .	223
10.2	Jeffcott rotor . . . . .	224
10.2.1	Unbalance response . . . . .	225
10.2.2	Complex coordinates . . . . .	226
10.2.3	Free whirl . . . . .	227
10.2.4	Jeffcott rotor with viscous damping . . . . .	227
10.2.5	Stability in presence of damping . . . . .	230
10.3	Gyroscopic effects . . . . .	230
10.3.1	Kinetic energy of a rigid disk . . . . .	232
10.3.2	Dynamics including gyroscopic effects . . . . .	235
10.3.3	Free whirl, Campbell diagram . . . . .	235
10.3.4	Unbalance response . . . . .	238
10.3.5	Response to an asynchronous force . . . . .	238
10.4	Rigid rotor on elastic supports . . . . .	240
10.5	Anisotropy of the shaft and the supports . . . . .	243

XIV CONTENTS

10.5.1 Anisotropic supports . . . . .	243
10.5.2 Anisotropic shaft . . . . .	246
10.5.3 Unbalance response of an anisotropic shaft . . . . .	248
10.5.4 Stability of an anisotropic shaft . . . . .	249
10.6 Vibrating angular rate sensor . . . . .	250
10.7 Problems . . . . .	252
<b>11 Vibration alleviation</b>	<b>255</b>
11.1 Introduction . . . . .	255
11.2 Dynamic vibration absorber . . . . .	256
11.3 Narrow band disturbance . . . . .	257
11.4 Wide band disturbance . . . . .	258
11.4.1 Equal peak design . . . . .	260
11.5 Multiple d.o.f. systems . . . . .	263
11.6 Example: n-storey building . . . . .	264
11.6.1 Model construction . . . . .	265
11.6.2 Design of the DVA . . . . .	266
11.6.3 Random response of the structure with DVA . . . . .	267
11.7 Vibration isolation . . . . .	269
11.8 Linear isolator . . . . .	270
11.9 Relaxation isolator . . . . .	272
11.10 Six-axis isolator . . . . .	275
11.11 Isolation by kinematic coupling . . . . .	278
11.12 Centrifugal Pendulum Vibration Absorber . . . . .	280
11.13 Model of a car suspension . . . . .	281
11.14 Problems . . . . .	283
<b>12 Introduction to active vibration control</b>	<b>287</b>
12.1 The virtue of collocated control . . . . .	287
12.1.1 Collocated control . . . . .	290
12.1.2 Non-collocated control . . . . .	291
12.2 Active suspension: the “sky-hook” damper . . . . .	292
12.3 Active mass damper . . . . .	295
12.3.1 System modeling . . . . .	297
12.3.2 System response . . . . .	298
12.4 Active truss . . . . .	301
12.4.1 Open-loop transfer function . . . . .	302
12.4.2 Active damping by integral force feedback . . . . .	304
12.4.3 Beta controller . . . . .	307
12.5 Problems . . . . .	308

CONTENTS XV

**Bibliography 311**

**Index 315**



# 1

---

## Single degree-of-freedom linear oscillator

*La vraie science est une ignorance  
qui se sait.*

Montaigne, *Essais*, 1572-1588

### 1.1 Free response

Consider the linear, single degree-of-freedom (d.o.f.) oscillator of Fig.1.1.a; it consists of a mass  $m$  attached to the ground by a linear spring of stiffness  $k$  and a linear viscous damper of constant  $c$ ;  $f$  is the external force applied to the system, taken positive in the direction of the motion  $x$ . The free body diagram of the mass  $m$  is shown in Fig.1.1.b; the spring force  $kx$  and the damping force  $c\dot{x}$  are opposing the motion. From Newton's law, the equation of the motion is

$$\begin{aligned} m\ddot{x} &= f - c\dot{x} - kx \\ m\ddot{x} + c\dot{x} + kx &= f \end{aligned} \quad (1.1)$$

In all the following discussion, it is assumed that the damping is moderate, so that the free response is oscillatory; it is governed by the homogeneous equation

$$m\ddot{x} + c\dot{x} + kx = 0 \quad (1.2)$$

A non trivial ( $\neq 0$ ) solution  $x = Ae^{st}$  exists if and only if

$$ms^2 + cs + k = 0 \quad (1.3)$$

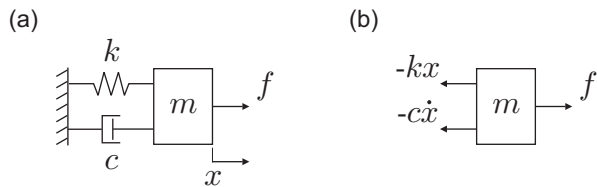


**Fig. 1.1.** (a) Single degree-of-freedom linear oscillator. (b) Free body diagram.

This is the *characteristic equation*, the solution of which are the *eigenvalues* of the system:

$$s = -\frac{c}{2m} \pm j\sqrt{\frac{k}{m} - \frac{c^2}{4m^2}} \quad (1.4)$$

and, upon defining the (undamped) *natural frequency*  $\omega_n$  and the *fraction of critical damping*, or in short *damping ratio*  $\xi$  according to:

$$\omega_n^2 = \frac{k}{m} \quad \text{and} \quad \xi\omega_n = \frac{c}{2m} \quad (1.5)$$

$$s = -\xi\omega_n \pm j\omega_n\sqrt{1 - \xi^2} \quad (1.6)$$

where it has been assumed that  $\xi < 1$ , which is the condition for the response to be oscillatory. In most practical problems in structural dynamics,  $\xi \ll 1$ . The solutions of the characteristic equation are called the *poles* of the system in linear system theory. They are located as shown in Fig. 1.2 where the relationship between  $\omega_n$ ,  $\xi$  and the position of the poles in the complex plane is highlighted. The imaginary part of the eigenvalue,  $\omega_d = \omega_n\sqrt{1 - \xi^2}$ , is often called the *damped natural frequency*. For most practical applications,  $\omega_d \simeq \omega_n$ . The most general solution of Equ.(1.3) is

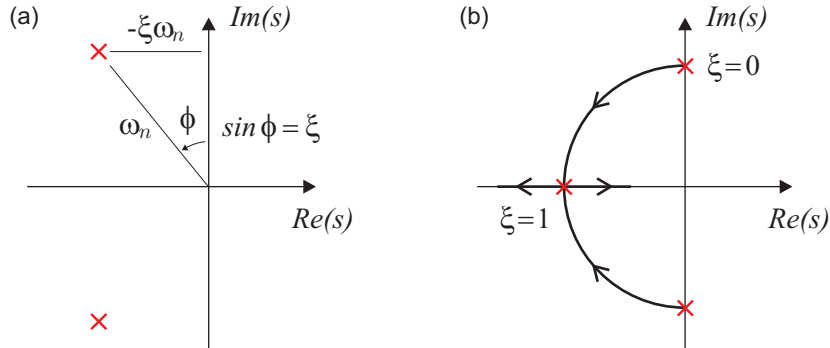


**Fig. 1.2.** (a) Position of the poles of the linear oscillator in the complex plane and their relation to  $\omega_n$  and  $\xi$ . (b) Evolution of the poles with the damping ratio  $\xi$ . For  $\xi = 1$ , the two poles coincide on the real axis at  $s = -\omega_n$  and the free response is no longer oscillatory.

$$x = e^{-\xi\omega_n t}(Ae^{j\omega_d t} + Be^{-j\omega_d t}) = e^{-\xi\omega_n t}(A_1 \cos \omega_d t + B_1 \sin \omega_d t) \quad (1.7)$$

where  $A, B, A_1, B_1$  are constants depending on the initial conditions (two initial conditions are necessary since the motion is governed by a second order differential equation).

## 1.2 Impulse response

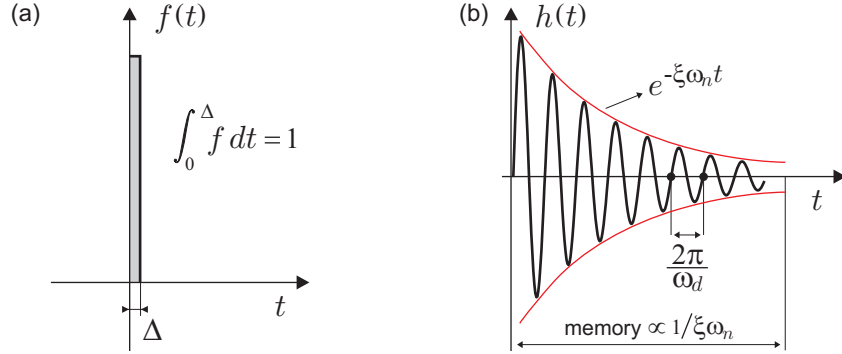


**Fig. 1.3.** (a) Unit impulse force. (b) Impulse response of the linear oscillator.

A unit impulse force (Fig.1.3.a) is a very large force applied during a very short time  $\Delta$  and such that

$$\int_0^\Delta f dt = 1 \quad (1.8)$$

The limit as  $\Delta \rightarrow 0$  is a Dirac impulse  $\delta(t)$ . The response of the linear oscillator initially at rest [ $x(0) = 0, \dot{x}(0) = 0$ ] to a unit impulse is called the *impulse response* and it is denoted  $h(t)$ ; it can be evaluated by integrating Equ.(1.1) over the short period  $\Delta$  to evaluate the state of the system after the impulse.

$$\int_0^\Delta m\ddot{x} dt = \int_0^\Delta f dt - \int_0^\Delta c\dot{x} dt - \int_0^\Delta kx dt$$

Taking into account that the spring force  $kx$  and the damping force  $c\dot{x}$  have always finite amplitudes, the last two integrals vanish when taking the limit for  $\Delta \rightarrow 0$ ; this leads to

$$\lim_{\Delta \rightarrow 0} m\dot{x}(\Delta) = m\dot{x}(0^+) = 1 \quad (1.9)$$

This means that the net effect of the impulse load is to change the initial velocity to  $\dot{x}(0^+) = 1/m$  while keeping  $x(0) = 0$ . Note that this is independent of the detailed shape of the impulse load provided it satisfies Equ.(1.8). Returning to Equ.(1.7), the constants can now be determined:

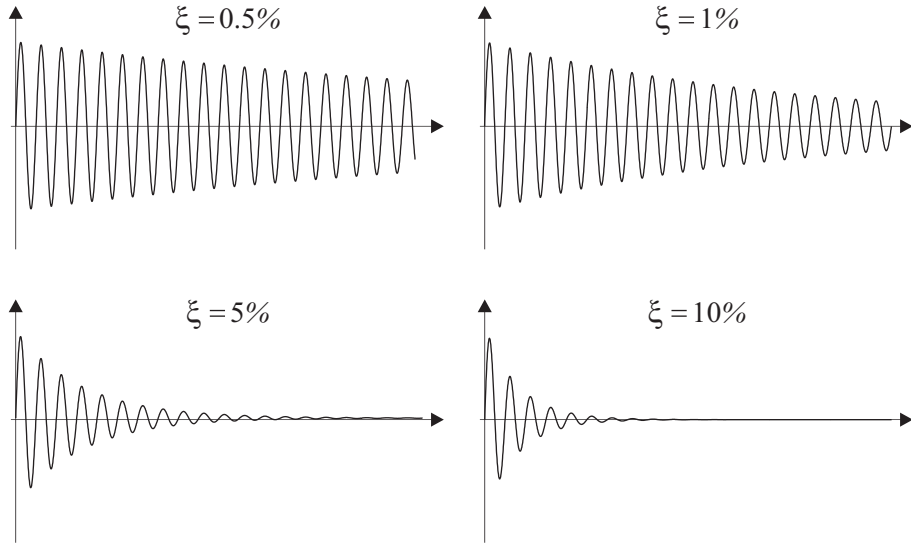


**Fig. 1.4.** Impulse response of the linear oscillator for various values of the damping ratio.

From  $x(0) = 0$ ,  $A_1 = 0$ , and from  $\dot{x}(0) = 1/m$ ,  $B_1 = 1/m\omega_d$ . Thus, the impulse response reads

$$h(t) = \frac{1}{m\omega_d} e^{-\xi\omega_n t} \sin \omega_d t \quad (1.10)$$

It is represented in Fig.1.3.b; it is a damped sine function; the duration with significant values of  $h(t)$  can be looked at as the *memory* of the system; after that time, the system has forgotten the disturbance and returns to its rest equilibrium position. The attenuation rate of the impulse response is controlled by the damping ratio  $\xi$ ; the larger the damping, the shorter the memory of the system. Figure 1.4 shows typical impulse responses for various values of  $\xi$  of practical interest; for  $\xi = 0.1$ , the response is reduced by about half after only one cycle; for  $\xi = 0.05$ , halving the response takes about two cycles; for  $\xi = 0.01$ , it takes about 10 cycles, etc... (these numbers are always good to know).

### 1.3 Convolution integral

Consider a *linear* system of impulse response  $h(t)$  initially at rest, and excited by the forcing function  $f(t)$  [ $f(t) = 0$  for  $t < 0$ ]. The response of the system can be evaluated by first slicing the forcing function into small

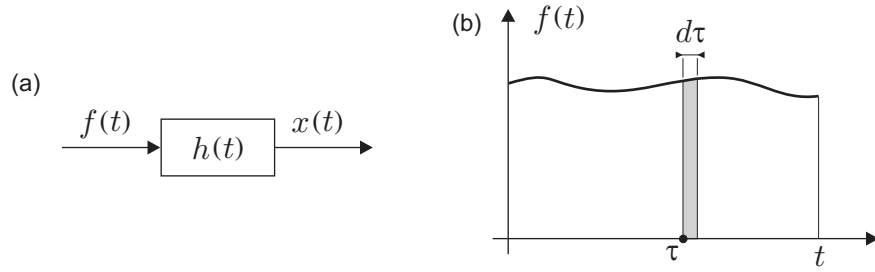


**Fig. 1.5.** (a) Input-output relationship of a linear system. (b) Decomposition of the forcing function into a train of impulse loads.

intervals  $d\tau$  (shaded area in Fig 1.5.b) and replacing these by impulse loads with the same impulse,  $f(\tau)d\tau$ . The response at  $t$  to a single impulse  $f(\tau)d\tau$  is, by definition

$$x(t) = \int_0^t h(t-\tau)f(\tau)d\tau \quad (1.11)$$

A *causal* system is such that the response cannot anticipate the excitation; this means that  $h(t) = 0$  for  $t < 0$ . For such a system, the upper limit may be changed to  $\infty$ . If the forcing function is applied also for negative times, the lower limit must be extended to  $-\infty$ , leading to<sup>1</sup>

$$x(t) = \int_{-\infty}^{\infty} h(t-\tau)f(\tau)d\tau = \int_{-\infty}^{\infty} h(u)f(t-u)du = h(t) \star f(t) \quad (1.12)$$

This is the *convolution integral*, denoted by  $\star$ . Note that the critical point in our discussion is the use of the principle of superposition, which requires that the system be linear. The above equation is not restricted to a linear oscillator; it applies to any linear system of impulse response  $h(t)$ .

## 1.4 Harmonic response

### 1.4.1 Undamped oscillator

Consider an undamped oscillator excited with an harmonic force  $f = Fe^{j\omega t}$  supposed applied from  $t = -\infty$ , so that any transient response has disappeared and only the forced response remains:

$$m\ddot{x} + kx = Fe^{j\omega t} \quad (1.13)$$

---

<sup>1</sup> The second integral is readily obtained by the change of variables  $u = t - \tau$ .

The use of the complex exponential function  $e^{j\omega t}$  is not strictly necessary in the undamped case because the response can only be in phase or in *antiphase* with the excitation, that is with a phase difference of  $180^0$ . However, the use of complex exponentials instead of sine and cosine functions will simplify considerably the discussion when the damping is introduced. Equ.(1.13) should be understood as follows: the real part of  $x$  (projection on the real axis) gives the response to  $f = F \cos \omega t$  and the imaginary part is the response to  $f = F \sin \omega t$ .

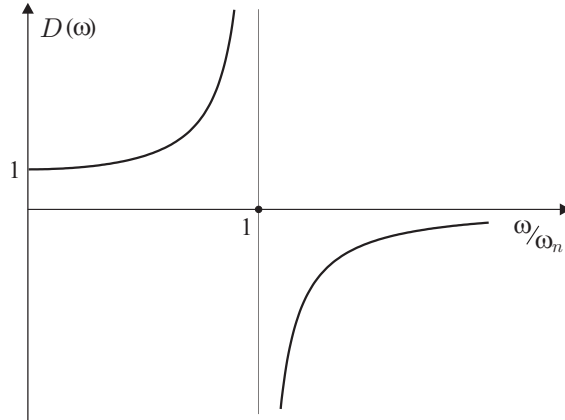


**Fig. 1.6.** Dynamic amplification of the undamped linear oscillator.

The solution of Equ.(1.13) has the form  $x = X e^{j\omega t}$ . Upon substituting, one gets

$$(-m\omega^2 + k)X = F$$

or, using  $\omega_n^2 = k/m$ ,

$$X = \left\{ \frac{F}{k} \right\} \left\{ \frac{1}{1 - (\omega/\omega_n)^2} \right\} = \left\{ \frac{F}{k} \right\} D(\omega) \quad (1.14)$$

where  $F/k$  is the static response and  $D(\omega) = [1 - (\omega/\omega_n)^2]^{-1}$  is the *dynamic amplification* of the system (Fig.1.6). When the frequency of the excitation is lower than the resonance frequency,  $\omega < \omega_n$ , the dynamic amplification is positive, which means that the response is in phase with the excitation; when  $\omega > \omega_n$ , the dynamic amplification is negative, meaning that the response is in antiphase with the excitation.

### 1.4.2 Damped oscillator

For a damped oscillator, the governing equation becomes

$$m\ddot{x} + c\dot{x} + kx = Fe^{j\omega t}$$

or

$$\ddot{x} + 2\xi\omega_n\dot{x} + \omega_n^2x = \frac{F}{m}e^{j\omega t} \quad (1.15)$$

The solution has, once again, the form  $x = Xe^{j\omega t}$ , with  $X$  being a complex quantity. Substituting into the equation, one finds

$$X = \left\{ \frac{F}{k} \right\} \left\{ \frac{1}{1 - (\omega/\omega_n)^2 + 2j\xi\omega/\omega_n} \right\} = \left\{ \frac{F}{k} \right\} \cdot D(\omega) \quad (1.16)$$

where the dynamic amplification  $D(\omega)$  is a complex valued function:

$$D(\omega) = \frac{1}{1 - (\omega/\omega_n)^2 + 2j\xi\omega/\omega_n} \quad (1.17)$$

The amplitude and phase diagrams, also called *Bode plots*, of the dynamic amplification,  $D(\omega) = |D(\omega)|e^{j\phi(\omega)}$ , is shown in Fig. 1.7.

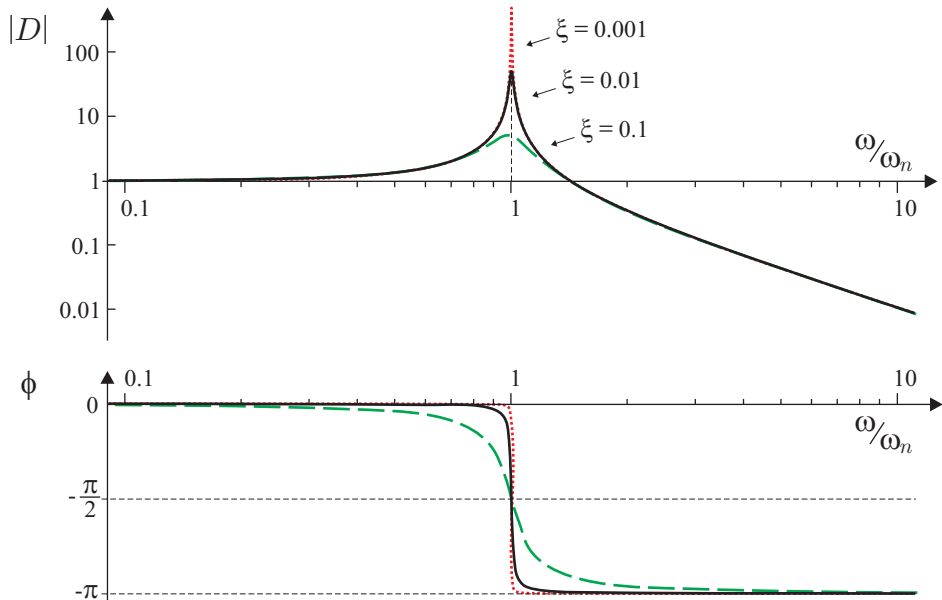


**Fig. 1.7.** Dynamic amplification of the damped linear oscillator  $D(\omega) = |D(\omega)|e^{j\phi(\omega)}$ . Amplitude  $|D|$  and phase  $\phi$  diagrams (Bode plots).

The damping strongly affects the dynamic amplification in the vicinity of the resonance  $\omega_n$ ; for low damping, very large dynamic amplifications occur. The maximum does not occur strictly at  $\omega = \omega_n$  but, for small  $\xi$ ,  $|D|_{\max} \simeq |D(\omega_n)| = 1/2\xi$  is a sufficient approximation.  $Q = 1/2\xi$  is called the *quality factor* of the oscillator. While in the undamped case, the phase shift is either  $0^\circ$  or  $180^\circ$ , the phase shift evolves gradually from  $0^\circ$  to  $180^\circ$  and most of the shift occurs in the vicinity of  $\omega_n$ , within a frequency band  $2\xi\omega_n$  called the *bandwidth* of the oscillator. The phase shift is exactly  $90^\circ$  at  $\omega = \omega_n$  (*phase resonance*). The amplitude of the Bode plot is often graduated in decibels (dB), defined as  $20 \log A$  (thus,  $A = 1$  is 0 dB,  $A = 10$  is 20 dB,  $A = 100$  is 40 dB, etc...)

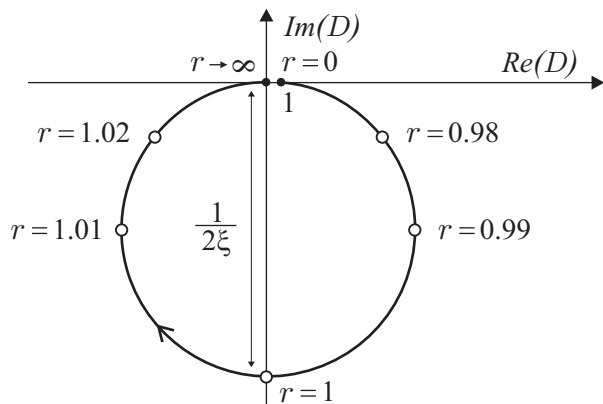


**Fig. 1.8.** Nyquist plot of Dynamic amplification of the linear oscillator  $D(\omega) = |D(\omega)|e^{j\phi(\omega)}$ . [ $r = \omega/\omega_n$ ].

An alternative representation called *Nyquist* plot is shown in Fig.1.8. The diagram consists of a direct representation of the complex value of  $D(\omega)$ . The curve is close to a circle of diameter  $1/2\xi$ ; it is graduated in  $r = \omega/\omega_n$ , with a strong magnification of the frequency band close to  $r = 1$  where the large amplitudes and most of the phase shift occur.

## 1.5 Frequency Response Function

Consider an arbitrary linear system of impulse response  $h(t)$ , excited by an harmonic input  $f = F e^{j\omega t}$ . The response of the system can be evaluated from Equ.(1.12)

$$x(t) = \int_{-\infty}^{\infty} h(\tau) f(t - \tau) d\tau$$

Substituting  $f = Fe^{j\omega t}$ ,

$$x(t) = \int_{-\infty}^{\infty} h(\tau) F e^{j\omega(t-\tau)} d\tau = F e^{j\omega t} \int_{-\infty}^{\infty} h(\tau) e^{-j\omega\tau} d\tau$$

This equation says that the response  $x(t)$  is also harmonic,  $x(t) = X(\omega)e^{j\omega t}$ . The ratio between the complex amplitude of the output and that of the input,

$$H(\omega) = \frac{X(\omega)}{F(\omega)} \quad (1.18)$$

is called the *Frequency Response Function* (FRF) of the system. From the previous equation, one sees that  $H(\omega)$  is the Fourier transform of the impulse response  $h(t)$ :

$$H(\omega) = \int_{-\infty}^{\infty} h(\tau) e^{-j\omega\tau} d\tau \quad (1.19)$$

The convolution theorem of the Fourier transform allows a more powerful statement: If  $F(\omega)$  is the Fourier transform of the input to the linear system of impulse response  $h(t)$ , then the Fourier transform of the output,  $X(\omega)$ , is given by the product of  $F(\omega)$  and  $H(\omega)$  (Fig.1.9)

$$x(t) = h(t) * f(t) \iff X(\omega) = H(\omega)F(\omega) \quad (1.20)$$

(the double arrow is used to represent Fourier transform pairs).<sup>2</sup> This fundamental result of linear system theory tells us that if the input of the system does not have any component in some frequency band, there will not be any component in the output in that frequency band.

The frequency distribution of the energy in a signal is governed by Parseval's theorem:

$$\int_{-\infty}^{\infty} f^2(t) dt = \frac{1}{2\pi} \int_{-\infty}^{\infty} |F(\omega)|^2 d\omega \quad (1.21)$$

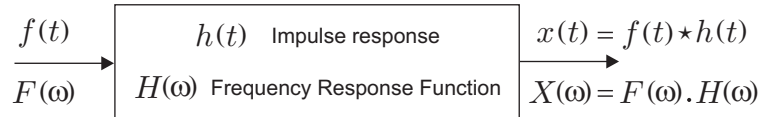


**Fig. 1.9.** Input-output relationship of a linear system in the time domain and in the frequency domain.  $[h(t) \iff H(\omega)]$  constitute a Fourier transform pair.

<sup>2</sup> The Fourier transform is one of the magic tools of mathematics which is used in almost all fields of physics; see (Papoulis, 1962) for a clear exposition, although the book was written before the Fast Fourier Transform.

$|F(\omega)|^2/2\pi$  is called the *energy spectrum* of  $f(t)$ . Using the previous equation, one observes that the energy spectrum of the output is related to that of the input through the square of the FRF amplitude,  $|H(\omega)|^2$ .

## 1.6 Beat phenomenon

The beat is associated with the transient response of a lightly damped system to an harmonic excitation at a frequency close to one of its resonance frequencies. To analyze it, consider the response of an undamped oscillator to an harmonic force  $f = F \cos \omega t$  starting from rest at  $t = 0$ .

$$m\ddot{x} + kx = F \cos \omega t \quad t > 0 \quad (1.22)$$

The impulse response of an undamped linear oscillator is  $h(t) = \frac{1}{m\omega_n} \sin \omega_n t$ . From the convolution theorem, the response may be written

$$x(t) = \int_0^t F \cos \omega \tau \cdot h(t - \tau) d\tau$$

and, upon solving the integral,

$$x(t) = \frac{F}{m} \frac{\cos \omega t - \cos \omega_n t}{\omega_n^2 - \omega^2} \quad (1.23)$$

The beat occurs when  $\omega$  is close to  $\omega_n$ ; with the notations  $\omega + \omega_n = 2\omega_0 \simeq 2\omega_n$  and  $\omega - \omega_n = 2\Delta$ ,

$$x(t) = \frac{F}{m} \frac{\sin \omega_0 t \sin \Delta t}{2\omega_0 \Delta} = \frac{F}{m} \frac{\sin \omega_0 t}{2\omega_0} \frac{\sin \Delta t}{\Delta} \quad (1.24)$$

Thus, the response consists of an harmonic component at the frequency equal to the half sum,  $\omega_0 = (\omega + \omega_n)/2 \simeq \omega_n$ , modulated by another harmonic function at the frequency equal to the half difference,  $\Delta = (\omega - \omega_n)/2$ , Fig.1.10. For  $\Delta \rightarrow 0$ ,  $\frac{\sin \Delta t}{\Delta} \rightarrow t$  and the amplitude increases linearly with  $t$ :

$$x(t) = \frac{F}{m} \frac{\sin \omega_n t}{2\omega_n} t \quad (1.25)$$

The response is  $\pi/2$  out of phase with the excitation.

The beat is a transient phenomenon; it always disappears after some time, even with a small damping (Problem 1.1). For a perfect tuning ( $\omega = \omega_n$ ), the response still increases linearly at the beginning, but saturates at a maximum value fixed by the dynamic amplification at resonance,  $1/2\xi$ . For an imperfect tuning ( $\omega \neq \omega_n$ ), the response still oscillates

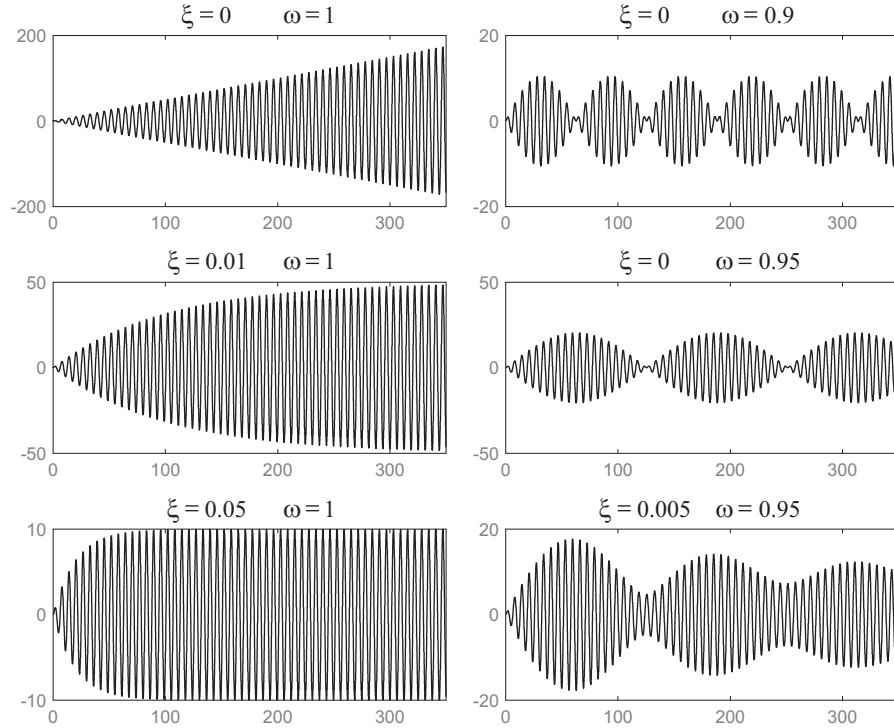


**Fig. 1.10.** Transient response of the linear oscillator  $\ddot{x} + 2\xi\dot{x} + x = \cos \omega t$  ( $t > 0$ ) for various values of the excitation frequency  $\omega$  and the damping ratio  $\xi$ .

at the beginning, but the beat disappears after a few cycles of the modulating function; the transient period before achieving the steady state is controlled by the “memory” of the system,  $\propto (\xi\omega_n)^{-1}$ . Various situations are illustrated in Fig. 1.10.

## 1.7 State space form

For numerical analysis, e.g. with *MATLAB*, it is often convenient to write second order differential equations as a set of first order equations; this is known as the state space form:

$$\dot{\mathbf{x}} = A\mathbf{x} + B\mathbf{u} \quad (1.26)$$

$A$  is the system matrix,  $B$  is the input matrix,  $\mathbf{u}$  is the input vector and  $\mathbf{x}$  is the state vector containing the state variables. This system equation is supplemented by the output equation

$$\mathbf{y} = C\mathbf{x} + D\mathbf{u} \quad (1.27)$$

where  $\mathbf{y}$  is the output vector,  $C$  is the output matrix, and  $D$  is the feedthrough matrix.

For the linear oscillator

$$\ddot{x} + 2\xi\omega_n\dot{x} + \omega_n^2x = \frac{f}{m} \quad (1.28)$$

the state variables can be selected as

$$x_1 = x, \quad x_2 = \dot{x} \quad (1.29)$$

With this choice, Equ.(1.28) can be rewritten as a set of two first order equations

$$\begin{aligned} \dot{x}_1 &= x_2 \\ \dot{x}_2 &= -2\xi\omega_nx_2 - \omega_n^2x_1 + f/m \end{aligned} \quad (1.30)$$

or

$$\begin{Bmatrix} \dot{x}_1 \\ \dot{x}_2 \end{Bmatrix} = \begin{bmatrix} 0 & 1 \\ -\omega_n^2 & -2\xi\omega_n \end{bmatrix} \begin{Bmatrix} x_1 \\ x_2 \end{Bmatrix} + \begin{Bmatrix} 0 \\ \frac{1}{m} \end{Bmatrix} f \quad (1.31)$$

This equation explicitly shows the system and input matrices  $A$  and  $B$ . If one measures the displacement,  $y = x_1$ , the output matrix is  $C = (1 \ 0)$  while if one uses a velocity sensor,  $y = x_2$  and  $C = (0 \ 1)$ ;  $D = 0$  in these cases. An accelerometer can only be accounted for by using a feedthrough matrix  $D$  in addition to  $C$ . In fact, from Equ.(1.30), one gets

$$y = \ddot{x} = \dot{x}_2 = (-\omega_n^2 - 2\xi\omega_n) \begin{Bmatrix} x_1 \\ x_2 \end{Bmatrix} + \frac{1}{m}f \quad (1.32)$$

The output and feedthrough matrices are respectively  $C = (-\omega_n^2 \ -2\xi\omega_n)$  and  $D = 1/m$ .

The choice (1.29) for the state variables is not unique and it may be convenient to make another choice :

$$x_1 = \omega_n x, \quad x_2 = \dot{x} \quad (1.33)$$

The advantage of this representation is that both state variables express a velocity, and that the free response trajectories in the phase plane  $(x_1, x_2)$  are slowly decaying spirals (Problem 1.2). With this choice, Equ.(1.28) can be rewritten

$$\begin{Bmatrix} \dot{x}_1 \\ \dot{x}_2 \end{Bmatrix} = \begin{bmatrix} 0 & \omega_n \\ -\omega_n & -2\xi\omega_n \end{bmatrix} \begin{Bmatrix} x_1 \\ x_2 \end{Bmatrix} + \begin{Bmatrix} 0 \\ \frac{1}{m} \end{Bmatrix} f \quad (1.34)$$

This form is sometimes preferred to (1.31) because the system matrix is dimensionally homogeneous (all the state variables have the dimension of a velocity).

## 1.8 Problems

**P.1.1** Analyze numerically the beat phenomenon for the oscillator

$$\ddot{x} + 2\xi\dot{x} + x = \cos\omega t \quad (t > 0)$$

for various values of  $\omega$  and  $\xi$ , and reconstruct Fig.1.10. Show that for imperfect tuning ( $\omega \neq 1$ ) the process is stabilized by the damping after a few cycles of the modulating function, and that, for perfect tuning ( $\omega = 1$ ), the steady state amplitude is  $1/2\xi$ .

**P.1.2** Consider the single d.o.f. oscillator described by Equ.(1.34). For non-zero initial conditions, sketch the free response in the phase plane ( $x_1, x_2$ ). Show that the image point rotates clockwise along a spiral trajectory. Relate the decay rate of the spiral to the damping ratio.

**P.1.3** A single storey building is often modelled as a rigid slab  $m$  supported by massless columns clamped at both ends (Fig.1.11.a). Based on this assumption, estimate the natural frequency of this single d.o.f. oscillator. [Hint: The tip displacement and tip rotation of a clamped free beam loaded respectively by a point force and a moment acting at the

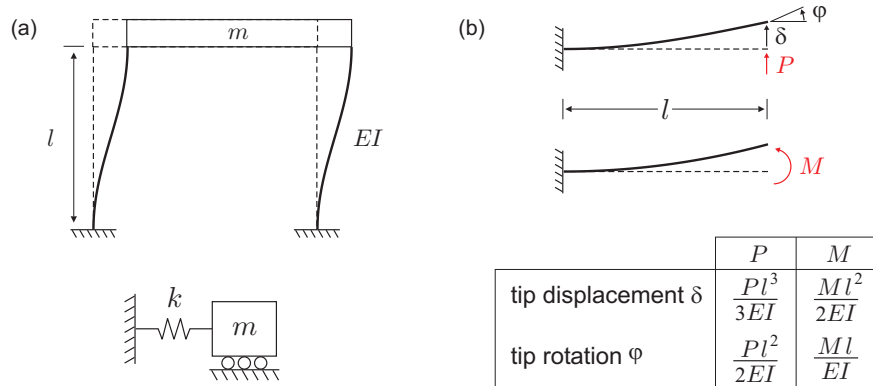


**Fig. 1.11.** (a) Model of a single story building. (b) Clamped-free beam loaded at the free end.

free end are given in Fig.1.11.b. Based on this, show that the equivalent stiffness of the storey is  $k = 2 \times (12EI/l^3)$ .]

**P.1.4** Reconsider the previous problem with the assumption that the massless columns are clamped at the base and hinged at the slab.

**P.1.5** Consider a rigid bar of mass  $m$  and length  $l$  and articulated at  $O$ , Fig.1.12. It is supported by a spring  $k$  and a damper  $c$  at a distance  $b$  from  $O$ , and it is excited by the input displacement  $z$  acting on a spring  $k_1$  attached to the bar at a distance  $a$  from  $O$ . Write the equation of motion of the equivalent single d.o.f. oscillator. [Hint: Write the rotation equilibrium about the articulation  $O$ .]

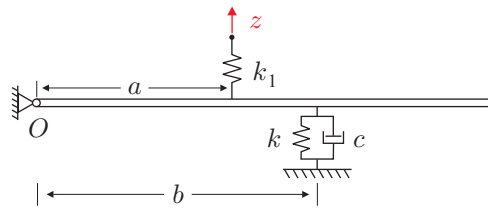


**Fig. 1.12.** Single d.o.f. model of a rigid bar of mass  $m$  and length  $L$ , articulated at  $O$ .

**P.1.6** Write the equation governing the torsional vibration of a disk of mass moment of inertia  $J$  attached to a circular shaft of torsional stiffness  $K_\theta$  [ $K_\theta = GI_p/l$  where  $l$  is the length of the shaft,  $I_p$  is the polar moment of inertia of the cross section and  $G$  is the shear modulus of the material].

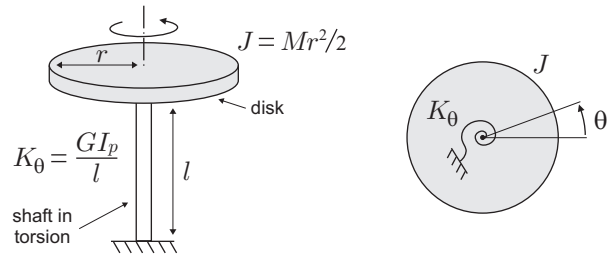


**Fig. 1.13.** Torsional vibration of a disk.

**P.1.7** Write the equation governing the vibration of the system of Fig.1.14, formed of point mass attached to the tip of massless clamped beam (of length  $l$  and bending stiffness  $EI$ ) and a spring [Hint: use the results of Fig.1.11].

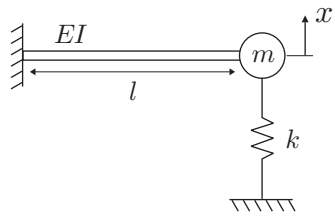


Fig. 1.14.

**P.1.8** Consider the state space equations of a linear oscillator. Write the output equation (the matrices  $C$  and  $D$ ) for an accelerometer measuring  $\ddot{x}$  if the state variables (1.33) are used.



---

## Multiple degree-of-freedom systems

*je sais bien ce que je fuis, et non  
pas ce que je cherche.*

Montaigne, *Essais*, 1572-1588

### 2.1 Governing equations

Consider the lumped mass system with two d.o.f. of Fig.2.1; the free body diagrams of the two masses are also represented. From Newton's law, the equations governing the motion of the two masses are

$$m_1 \ddot{x}_1 = f_1 + c(\dot{x}_2 - \dot{x}_1) + k(x_2 - x_1) - kx_1 - c\dot{x}_1$$

$$m_2 \ddot{x}_2 = f_2 + c(\dot{x}_1 - \dot{x}_2) + k(x_1 - x_2) - kx_2 - c\dot{x}_2$$

or, in matrix form

$$\begin{bmatrix} m_1 & 0 \\ 0 & m_2 \end{bmatrix} \begin{Bmatrix} \ddot{x}_1 \\ \ddot{x}_2 \end{Bmatrix} + \begin{bmatrix} 2c & -c \\ -c & 2c \end{bmatrix} \begin{Bmatrix} \dot{x}_1 \\ \dot{x}_2 \end{Bmatrix} + \begin{bmatrix} 2k & -k \\ -k & 2k \end{bmatrix} \begin{Bmatrix} x_1 \\ x_2 \end{Bmatrix} = \begin{Bmatrix} f_1 \\ f_2 \end{Bmatrix}$$

This equation has the general form

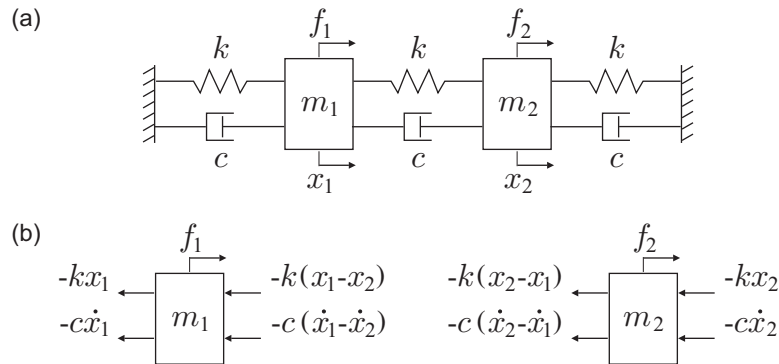


**Fig. 2.1.** (a) Two degree-of-freedom lumped mass system. (b) Free body diagrams.

$$M\ddot{\mathbf{x}} + C\dot{\mathbf{x}} + K\mathbf{x} = \mathbf{f} \quad (2.1)$$

where  $\mathbf{x} = (x_1, x_2)^T$  is the vector containing the d.o.f. of the system,

$$M = \begin{bmatrix} m_1 & 0 \\ 0 & m_2 \end{bmatrix}$$

is the mass matrix; it is diagonal in this case, because this example considers a *lumped mass* system;

$$K = \begin{bmatrix} 2k & -k \\ -k & 2k \end{bmatrix}$$

is the stiffness matrix and

$$C = \begin{bmatrix} 2c & -c \\ -c & 2c \end{bmatrix}$$

is the viscous damping matrix. Equation (2.2) is the general form governing the dynamics of a non-gyroscopic linear multi d.o.f. system. The components of the vector  $\mathbf{x}$  are the degrees of freedom of the model; they may be displacements, rotations, or generalized coordinates, depending on the way the model has been built. The size of the matrices  $M, C, K$  is equal to the number of degrees of freedom and they are *symmetric* and *semi-positive definite*:

$$K = K^T$$

$$\mathbf{x}^T K \mathbf{x} \geq 0, \quad \text{for all } \mathbf{x}$$

and similarly for  $M$  and  $C$ . In fact, it is easy to check that the kinetic energy of the system (of the two point masses) and the strain energy stored in the 3 springs, respectively

$$T = \frac{1}{2}m_1\dot{x}_1^2 + \frac{1}{2}m_2\dot{x}_2^2$$

$$V = \frac{1}{2}kx_1^2 + \frac{1}{2}k(x_2 - x_1)^2 + \frac{1}{2}kx_2^2$$

may be written as

$$T = \frac{1}{2}\dot{\mathbf{x}}^T M \dot{\mathbf{x}}, \quad V = \frac{1}{2}\mathbf{x}^T K \mathbf{x} \quad (2.2)$$

The strain energy in the system is strictly positive if the displacement field  $\mathbf{x}$  involves elastic deformations in the structure; it is equal to 0 if

$\mathbf{x}$  consists of rigid body displacements. Similarly, the kinetic energy is strictly positive, except if some d.o.f. have no inertia associated to them.

As a second example leading to Equ.(2.1), consider the building of Fig.2.2.a; it consists of 5 identical floors of mass  $m$ , connected by massless columns of height  $l$  and bending stiffness  $EI$ , clamped at both ends. Using the result of problem 1.3, the system may be modeled by 5 identical point masses  $m$  connected by springs of elastic constant  $k = 24EI/l^3$  representing the lateral stiffness of one floor. The system has 5 d.o.f. because its kinematics is fully described by the 5 coordinates  $\mathbf{x} = (x_1, \dots, x_5)^T$  of the point masses.

The dynamic equilibrium of mass  $i$  reads (Fig.2.2.c)

$$m\ddot{x}_i = k(x_{i+1} - x_i) - k(x_i - x_{i-1}) + f_i \quad (i = 2, 3, 4)$$

where  $f_i$  is the external force directly applied to mass  $i$ . The equations governing the d.o.f. 1 and 5 are slightly different:

$$m\ddot{x}_1 = k(x_2 - x_1) - kx_1 + f_1$$

$$m\ddot{x}_5 = -k(x_5 - x_4) + f_5$$

This system of 5 second order differential equations may be written in the matrix form (2.1) with the diagonal mass matrix  $M = mI_5$  and the stiffness matrix

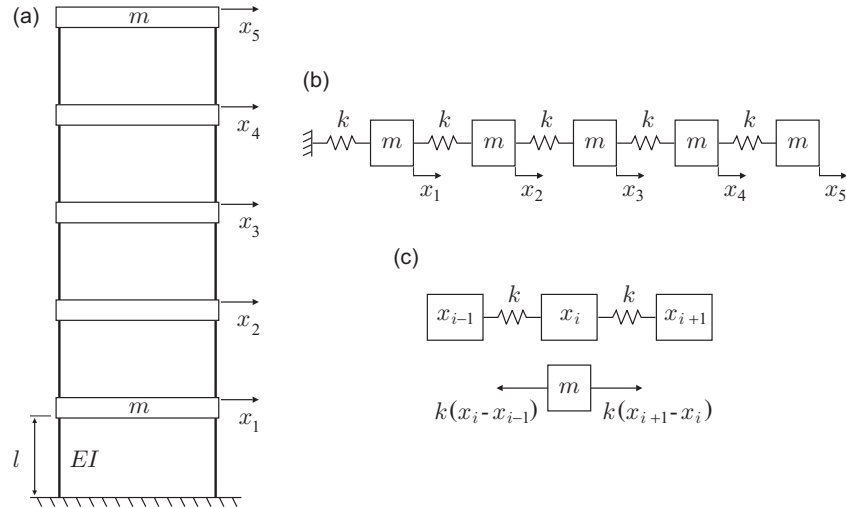


**Fig. 2.2.** (a) Model of a building with 5 identical rigid floors connected with massless columns of height  $l$  and bending stiffness  $EI$ . (b) Equivalent spring-mass system, with  $k = 24EI/l^3$ . (c) Free body diagram of mass  $i$ .

$$K = \begin{bmatrix} 2k & -k & 0 & 0 & 0 \\ -k & 2k & -k & 0 & 0 \\ 0 & -k & 2k & -k & 0 \\ 0 & 0 & -k & 2k & -k \\ 0 & 0 & 0 & -k & k \end{bmatrix}$$

Once again, it is easy to check that the total kinetic energy

$$T = \sum_{i=1}^5 \frac{1}{2} m \dot{x}_i^2$$

and the strain energy stored in the column, of the building

$$V = \sum_{i=1}^5 \frac{1}{2} k (x_i - x_{i-1})^2$$

may be written according to Equ.(2.2).

## 2.2 Free response of the undamped system

### 2.2.1 Eigenvalue problem

Consider the free response ( $\mathbf{f} = 0$ ) of the undamped (conservative) system ( $C = 0$ )

$$M\ddot{\mathbf{x}} + K\mathbf{x} = 0 \quad (2.3)$$

Proceeding as for the single d.o.f. oscillator, a non trivial solution  $\mathbf{x} = \phi e^{st}$  exists if  $s$  and  $\phi$  satisfy

$$(K + s^2 M)\phi = 0 \quad (2.4)$$

It is an eigenvalue problem; the eigenvalues  $s$  (the poles of the system) are solutions of the characteristic equation

$$\det(K + s^2 M) = 0 \quad (2.5)$$

They are purely imaginary,  $s = \pm j\omega_i$ , because  $K$  and  $M$  are symmetric semi-positive definite ( $\omega_i$  are called the *natural* frequencies, or the *resonance* frequencies); the number of natural frequencies is equal to the number of d.o.f.; they are usually ordered by increasing frequencies ( $\omega_1 \leq \omega_2 \leq \dots \leq \omega_n$ ). To every natural frequency  $\omega_i$  corresponds a *mode shape*  $\phi_i$ , solution of

$$(K - \omega_i^2 M) \phi_i = 0 \quad (2.6)$$

The properties of  $K$  and  $M$  guarantee that the mode shapes  $\phi_i$  are real. Note that Equ.(2.6) defines only the shape, but not the amplitude of the mode which can be scaled arbitrarily. The mode shapes are not just mathematical quantities: they can be observed even on lightly damped structures by exciting them at a natural frequency.

As an example, consider the two mass system of the previous section in the particular case where  $m_1 = m_2 = m$ . The eigenvalue problem (2.6) reads

$$\begin{bmatrix} 2k - \omega^2 m & -k \\ -k & 2k - \omega^2 m \end{bmatrix} \begin{Bmatrix} x_1 \\ x_2 \end{Bmatrix} = 0 \quad (2.7)$$

The solutions of

$$\det \begin{bmatrix} 2k - \omega^2 m & -k \\ -k & 2k - \omega^2 m \end{bmatrix} = 0$$

are

$$\omega_1^2 = \frac{k}{m} \quad \text{and} \quad \omega_2^2 = \frac{3k}{m}$$

The corresponding mode shapes may be determined by substituting these values into (2.7). Since the determinant vanishes, the solution may be determined by considering a single line of this system of equation. Considering the first line, one finds:

$$\omega_1^2 = \frac{k}{m} \Rightarrow (2k - k)x_1 - kx_2 = 0 \Rightarrow x_1 = x_2 \Rightarrow \phi_1 = \begin{Bmatrix} x_1 \\ x_1 \end{Bmatrix}$$

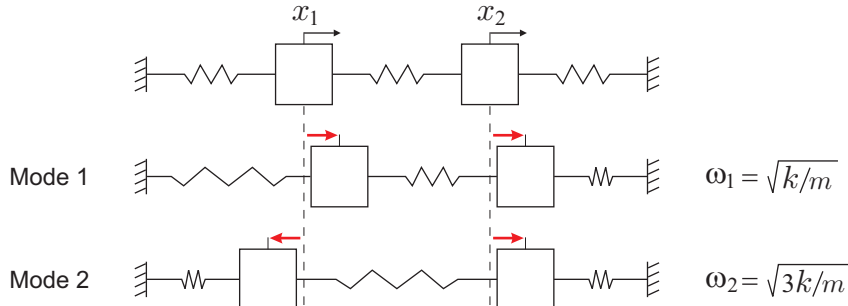


**Fig. 2.3.** Mode shapes of the two degree-of-freedom lumped mass system.

$$\omega_2^2 = \frac{3k}{m} \Rightarrow (2k-3k)x_1 - kx_2 = 0 \Rightarrow x_1 = -x_2 \Rightarrow \phi_2 = \begin{Bmatrix} x_1 \\ -x_1 \end{Bmatrix}$$

They are represented in Fig.2.3. For the first mode, the motion of the two masses is equal and in the same direction; for the second mode, the two masses move in opposite directions.

### 2.2.2 Orthogonality relationships

Left multiplying Equ.(2.6) by  $\phi_j^T$ , one gets the scalar equation

$$\phi_j^T K \phi_i = \omega_i^2 \phi_j^T M \phi_i$$

and, upon permuting  $i$  and  $j$ , one gets similarly,

$$\phi_i^T K \phi_j = \omega_j^2 \phi_i^T M \phi_j$$

Subtracting these equations, taking into account that a scalar is equal to its transpose, and that  $K$  and  $M$  are symmetric, one gets

$$0 = (\omega_i^2 - \omega_j^2) \phi_j^T M \phi_i$$

which shows that the mode shapes corresponding to distinct natural frequencies are orthogonal with respect to the mass matrix.

$$\phi_j^T M \phi_i = 0 \quad (\omega_i \neq \omega_j)$$

It follows from the foregoing equations that the mode shapes are also orthogonal with respect to the stiffness matrix. The orthogonality conditions are often written as

$$\phi_i^T M \phi_j = \mu_i \delta_{ij} \quad (2.8)$$

$$\phi_i^T K \phi_j = \mu_i \omega_i^2 \delta_{ij} \quad (2.9)$$

where  $\delta_{ij}$  is the Kronecker delta ( $\delta_{ij} = 1$  if  $i = j$ ,  $\delta_{ij} = 0$  if  $i \neq j$ ),  $\mu_i$  is the *modal mass* (also called generalized mass) of mode  $i$ . From the foregoing equations,

$$\omega_i^2 = \frac{\phi_i^T K \phi_i}{\phi_i^T M \phi_i} \quad (2.10)$$

We will come back to this important result when we study the *Rayleigh quotient*.

Since the mode shapes can be scaled arbitrarily, it is a common practice to normalize them in such a way that  $\mu_i = 1$ . If one defines the matrix

of the mode shapes  $\Phi = (\phi_1, \phi_2, \dots, \phi_n)$ , the orthogonality relationships read

$$\Phi^T M \Phi = \text{diag}(\mu_i) \quad (2.11)$$

$$\Phi^T K \Phi = \text{diag}(\mu_i \omega_i^2) \quad (2.12)$$

Because of these orthogonality conditions, the mode shapes are often called the *normal modes*.

### 2.2.3 Multiple natural frequencies

To demonstrate the orthogonality conditions, we have used the fact that the natural frequencies were distinct. If several modes have the same natural frequency (as often occurs in practice because of symmetry), they form a subspace of dimension equal to the multiplicity of the eigenvalue. Any vector in this subspace is a solution of the eigenvalue problem (Problem 2.5), and it is always possible to find a set of vectors such that the orthogonality conditions are satisfied.

### 2.2.4 Rigid body modes

A rigid body mode  $\mathbf{u}_i$  is such that there is no strain energy associated with it:  $\mathbf{u}_i^T K \mathbf{u}_i = 0$ . It is also solution of

$$K \mathbf{u}_i = 0 \quad (2.13)$$

This can be demonstrated by showing that if it were  $\neq 0$ , say  $K \mathbf{u}_i = \mathbf{a}$ , this would violate the condition that  $K$  is semi-positive definite. Indeed, the vector  $\mathbf{a} + \lambda \mathbf{u}_i$ , where  $\lambda$  is an arbitrary scalar parameter, satisfies

$$(\mathbf{a} + \lambda \mathbf{u}_i)^T K (\mathbf{a} + \lambda \mathbf{u}_i) \geq 0 \quad \text{for all } \lambda$$

or equivalently

$$\mathbf{a}^T K \mathbf{a} + 2\lambda \mathbf{a}^T K \mathbf{u}_i + \lambda^2 \mathbf{u}_i^T K \mathbf{u}_i \geq 0 \quad \text{for all } \lambda$$

Since  $\mathbf{u}_i^T K \mathbf{u}_i = 0$  and  $K \mathbf{u}_i = \mathbf{a}$ ,

$$\mathbf{a}^T K \mathbf{a} + 2\lambda \mathbf{a}^T \mathbf{a} \geq 0 \quad \text{for all } \lambda$$

Both  $\mathbf{a}^T K \mathbf{a}$  and  $\mathbf{a}^T \mathbf{a}$  are  $\geq 0$ . If  $\mathbf{a} \neq 0$ , the free parameter  $\lambda$  can always be chosen negative enough, in such a way that this inequality is violated. Thus  $\mathbf{a}$  must be 0 and Equ.(2.13) is demonstrated. It simply states that

the rigid body modes can be regarded as solutions of the eigenvalue problem (2.6) with  $\omega_i = 0$ .

In summary, any linear structure with  $n$  d.o.f. has  $n$  normal modes satisfying the orthogonal relationships (2.8) and (2.9), even in presence of multiple natural frequencies; the rigid body modes correspond to a natural frequency equal to zero.

### 2.2.5 Free response from initial conditions

The general solution of Equ(2.3) from non-zero initial conditions is

$$\mathbf{x} = \sum_{i=1}^n (A_i \cos \omega_i t + B_i \sin \omega_i t) \boldsymbol{\phi}_i \quad (2.14)$$

where the  $2n$  constants  $A_i$  and  $B_i$  can be determined from the initial conditions  $\mathbf{x}(0), \dot{\mathbf{x}}(0)$ . The orthogonality conditions (2.8) allow to determine these constants independently for each mode: left multiplying the foregoing equation and its time derivative by  $\boldsymbol{\phi}_k^T M$ , one gets:

$$\begin{aligned} \boldsymbol{\phi}_k^T M \mathbf{x} &= \mu_k (A_k \cos \omega_k t + B_k \sin \omega_k t) \\ \boldsymbol{\phi}_k^T M \dot{\mathbf{x}} &= \mu_k (-\omega_k A_k \sin \omega_k t + \omega_k B_k \cos \omega_k t) \end{aligned}$$

and, at  $t = 0$ ,

$$A_k = \frac{\boldsymbol{\phi}_k^T M \mathbf{x}(0)}{\mu_k} \quad B_k = \frac{\boldsymbol{\phi}_k^T M \dot{\mathbf{x}}(0)}{\mu_k \omega_k}$$

Finally,

$$\mathbf{x} = \sum_{i=1}^n \left[ \frac{\boldsymbol{\phi}_i^T M \mathbf{x}(0)}{\mu_i} \cos \omega_i t + \frac{\boldsymbol{\phi}_i^T M \dot{\mathbf{x}}(0)}{\mu_i \omega_i} \sin \omega_i t \right] \boldsymbol{\phi}_i \quad (2.15)$$

Note that, since  $\omega_i$  appears at the denominator, this result is not valid if there are rigid body modes. However, if one takes the limit for  $\omega_i \rightarrow 0$ , taking into account that  $\sin \omega_i t / \omega_i \rightarrow t$  and  $\cos \omega_i t \rightarrow 1$ , Equ.(2.14) becomes

$$\mathbf{x} = \sum_{i=1}^r (A_i + B_i t) \mathbf{u}_i + \sum_{i=r+1}^n (A_i \cos \omega_i t + B_i \sin \omega_i t) \boldsymbol{\phi}_i \quad (2.16)$$

where  $r$  is the number of rigid body modes. The constants  $A_i$  and  $B_i$  can be determined in the same way as before.

### 2.3 Modal decomposition

We now return to the general equation assuming a lightly damped system<sup>1</sup> and use the normal modes of the undamped system as new set of coordinates.

$$M\ddot{\mathbf{x}} + C\dot{\mathbf{x}} + K\mathbf{x} = \mathbf{f} \quad (2.17)$$

Let us perform a change of variables from physical coordinates  $\mathbf{x}$  to modal coordinates according to

$$\mathbf{x} = \Phi\mathbf{z} \quad (2.18)$$

where  $\mathbf{z}$  is the vector of modal amplitudes. Substituting into Equ.(2.17),

$$M\Phi\ddot{\mathbf{z}} + C\Phi\dot{\mathbf{z}} + K\Phi\mathbf{z} = \mathbf{f}$$

Left multiplying by  $\Phi^T$  and using the orthogonality relationships (2.8) and (2.9), one gets

$$\text{diag}(\mu_i)\ddot{\mathbf{z}} + \Phi^T C \Phi \dot{\mathbf{z}} + \text{diag}(\mu_i \omega_i^2) \mathbf{z} = \Phi^T \mathbf{f} \quad (2.19)$$

If the matrix  $\Phi^T C \Phi$  is diagonal, the damping is said *classical* or *normal*. In this case, the modal fraction of critical damping  $\xi_i$  (in short *modal damping*) is defined by

$$\Phi^T C \Phi = \text{diag}(2\xi_i \mu_i \omega_i) \quad (2.20)$$

Under this condition, the modal equations are decoupled and Equ.(2.19) can be rewritten

$$\ddot{\mathbf{z}} + 2\xi \Omega \dot{\mathbf{z}} + \Omega^2 \mathbf{z} = \mu^{-1} \Phi^T \mathbf{f} \quad (2.21)$$

with the notations

$$\begin{aligned} \xi &= \text{diag}(\xi_i) \\ \Omega &= \text{diag}(\omega_i) \\ \mu &= \text{diag}(\mu_i) \end{aligned} \quad (2.22)$$

This is a set of decoupled equations governing the response of the normal modes. Mode  $i$  follows

$$\ddot{z}_i + 2\xi_i \omega_i \dot{z}_i + \omega_i^2 z_i = \frac{1}{\mu_i} \phi_i^T \mathbf{f} \quad (2.23)$$

which is the equation of a single d.o.f. oscillator of mass  $\mu_i$ , frequency  $\omega_i$  and damping ratio  $\xi_i$ ; the generalized force  $\phi_i^T \mathbf{f}$  is the work of the external force  $\mathbf{f}$  on mode  $\phi_i$ .

---

<sup>1</sup> This assumption means that the poles of the system are complex conjugate pairs localized close to the imaginary axis.

### 2.3.1 Modal truncation

If one accepts the assumption of classical damping, the only difference between Equ.(2.17) and (2.21) lies in the change of coordinates (2.18). However, in physical coordinates, the number of degrees of freedom of a discretized model such as (2.17) is usually large, especially if the geometry is complicated, because of the difficulty of accurately representing the stiffness of the structure. The number of modes is equal to the number of d.o.f.; however, among them, only the low frequency modes have a physical meaning; the high frequency ones depend on the model (which does not mean that their global contribution to the response is not important). This number of degrees of freedom is unnecessarily large to represent the structural response in a limited bandwidth ( $\omega \leq \omega_b$ ). If a structure is excited by a band-limited excitation, its response is dominated by the modes whose natural frequencies belong to the bandwidth of the excitation, and the integration of Equ.(2.21) can often be restricted to these modes. The number of degrees of freedom contributing effectively to the response is therefore reduced drastically in modal coordinates. Overall, the structural response may be split into the modes responding *dynamically* ( $i < m$ , with  $\omega_m > \omega_b$ ) and those responding in a *quasi-static* manner ( $i > m$ ), for which all the contributions involving time derivatives may be neglected:

$$\begin{aligned}\ddot{z}_i + 2\xi_i\omega_i\dot{z}_i + \omega_i^2 z_i &= \phi_i^T \mathbf{f} / \mu_i & (i < m) \\ \omega_i^2 z_i &= \phi_i^T \mathbf{f} / \mu_i & (i > m)\end{aligned}\quad (2.24)$$

## 2.4 Damping

The damping matrix  $C$  represents the various dissipation mechanisms in the structure, which are usually poorly known. To compensate for this lack of knowledge, it is customary to make assumptions on its form. One of the most popular hypotheses is the *Rayleigh damping*:

$$C = \alpha M + \beta K \quad (2.25)$$

The coefficients  $\alpha$  and  $\beta$  are selected to fit the structure under consideration. One can readily check that the Rayleigh damping complies with condition (2.20) and that the corresponding modal damping ratios are

$$\xi_i = \frac{1}{2} \left( \frac{\alpha}{\omega_i} + \beta \omega_i \right) \quad (2.26)$$

The two free parameters  $\alpha$  and  $\beta$  can be selected in order to match the modal damping of two modes. The Rayleigh damping tends to overestimate the damping of the high frequency modes (Problem 2.7).

It turns out that the assumption of modal damping, Equ.(2.20) is in very good agreement with experiments when the damping is small, and that the modal damping ratios  $\xi_i$  are much easier to determine from experiments than the full damping matrix  $C$ . The following values of the modal damping ratio can be regarded as typical: satellites and space structures are generally very lightly damped ( $\xi \simeq 0.001 - 0.005$ ), because of the extensive use of fiber reinforced composites, the absence of aerodynamic damping, and the low strain level. Mechanical engineering applications (steel structures, piping,...) are in the range of  $\xi \simeq 0.01 - 0.02$ ; most dissipation takes place in the joints, and the damping increases with the strain level. For civil engineering applications,  $\xi \simeq 0.05$  is typical and, when radiation damping through the ground is involved, it may reach  $\xi \simeq 0.20$ , depending on the local soil conditions. The assumption of modal damping is questionable when the damping is large, as in problems involving soil-structure interaction. Lightly damped structures are usually easier to model, but the detrimental effect of resonances is more pronounced. Refer to Fig.1.2 and 1.7 to visualize the effect of  $\xi$ , respectively on the location of the poles in the complex plane and on the dynamic amplification.

## 2.5 Dynamic flexibility matrix

Consider the steady state harmonic response of Equ.(2.17) to a vector excitation  $\mathbf{f} = \mathbf{F}e^{j\omega t}$ . The response is also harmonic with the same frequency,  $\mathbf{x} = \mathbf{X}e^{j\omega t}$ , and the amplitudes of  $\mathbf{F}$  and  $\mathbf{X}$  are related by

$$\mathbf{X} = [-\omega^2 M + j\omega C + K]^{-1} \mathbf{F} = G(\omega) \mathbf{F} \quad (2.27)$$

The matrix  $G(\omega)$  is called the *dynamic flexibility matrix*; it is a dynamic generalization of the static flexibility matrix,  $G(0) = K^{-1}$ . The modal expansion of  $G(\omega)$  can be obtained by transforming into modal coordinates  $\mathbf{x} = \Phi \mathbf{z}$  as we did earlier. The modal response is also harmonic,  $\mathbf{z} = \mathbf{Z}e^{j\omega t}$  and one finds easily that

$$\mathbf{Z} = \text{diag}\left\{\frac{1}{\mu_i(\omega_i^2 + 2j\xi_i\omega_i\omega - \omega^2)}\right\} \Phi^T \mathbf{F}$$

leading to

$$\mathbf{X} = \Phi \mathbf{Z} = \Phi \operatorname{diag}\left\{\frac{1}{\mu_i(\omega_i^2 + 2j\xi_i\omega_i\omega - \omega^2)}\right\} \Phi^T \mathbf{F}$$

Comparing with (2.27), one finds the modal expansion of the dynamic flexibility matrix:

$$G(\omega) = [-\omega^2 M + j\omega C + K]^{-1} = \sum_{i=1}^n \frac{\phi_i \phi_i^T}{\mu_i(\omega_i^2 + 2j\xi_i\omega_i\omega - \omega^2)} \quad (2.28)$$

where the sum extends to all the modes.  $G_{lk}(\omega)$  expresses the complex amplitude of the structural response of d.o.f.  $l$  when a unit harmonic force  $e^{j\omega t}$  is applied at d.o.f.  $k$ .  $G(\omega)$  can be rewritten

$$G(\omega) = \sum_{i=1}^n \frac{\phi_i \phi_i^T}{\mu_i \omega_i^2} D_i(\omega) \quad (2.29)$$

where

$$D_i(\omega) = \frac{1}{1 - \omega^2/\omega_i^2 + 2j\xi_i\omega/\omega_i} \quad (2.30)$$

is the *dynamic amplification factor* of mode  $i$ .  $D_i(\omega)$  is equal to 1 at  $\omega = 0$ , it exhibits large values in the vicinity of  $\omega_i$ ,  $|D_i(\omega_i)| = (2\xi_i)^{-1}$ , and then decreases beyond  $\omega_i$  (Fig.2.4).<sup>2</sup>

According to the definition of  $G(\omega)$  the Fourier transform of the response  $\mathbf{X}(\omega)$  is related to the Fourier transform  $\mathbf{F}(\omega)$  of an arbitrary transient excitation by

$$\mathbf{X}(\omega) = G(\omega) \mathbf{F}(\omega)$$

This equation is the vector generalization of Equ.(1.20); it means that all the frequency components work independently, and if the excitation has no energy at one frequency, there is no energy in the response at that frequency.

From Fig.2.4, one sees that when the excitation has a limited bandwidth,  $\omega < \omega_b$ , the contribution of all the high frequency modes (i.e. such that  $\omega_k \gg \omega_b$ ) to  $G(\omega)$  can be evaluated by assuming  $D_k(\omega) \simeq 1$ . As a result, if  $m$  is selected in such a way that  $\omega_m$  is slightly larger than  $\omega_b$ , the modal expansion may be split according to

$$G(\omega) \simeq \sum_{i=1}^m \frac{\phi_i \phi_i^T}{\mu_i \omega_i^2} D_i(\omega) + \sum_{i=m+1}^n \frac{\phi_i \phi_i^T}{\mu_i \omega_i^2} \quad (2.31)$$

---

<sup>2</sup>  $Q_i = 1/2\xi_i$  is often called the *quality factor* of mode  $i$ .

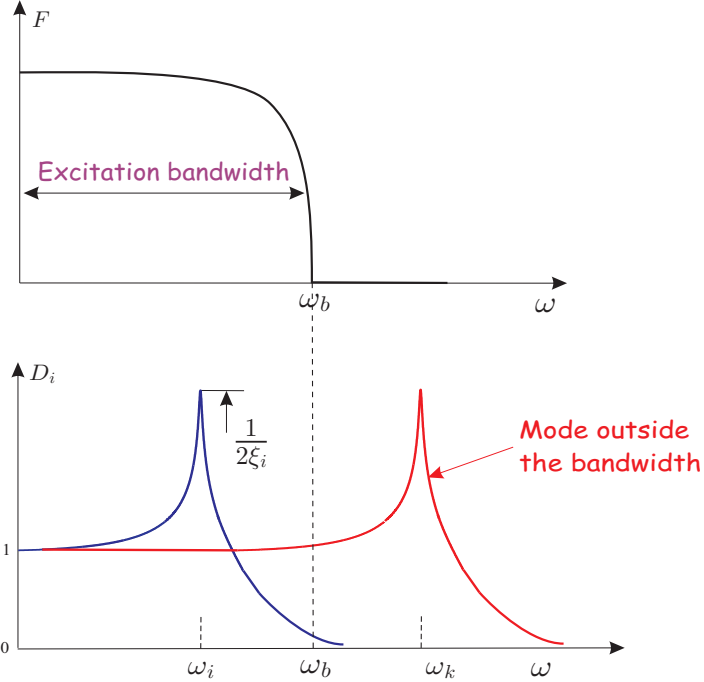


**Fig. 2.4.** Fourier spectrum of the excitation  $F$  with a limited frequency content  $\omega < \omega_b$  and dynamic amplification  $D_i$  of mode  $i$  such that  $\omega_i < \omega_b$  and  $\omega_k \gg \omega_b$ .

This approximation is valid for  $\omega < \omega_m$ . The first term in the right hand side is the contribution of all the modes which respond dynamically and the second term is a quasi-static correction for the high frequency modes. Taking into account the modal expansion of the static flexibility matrix,

$$G(0) = K^{-1} = \sum_{i=1}^n \frac{\phi_i \phi_i^T}{\mu_i \omega_i^2} \quad (2.32)$$

$G(\omega)$  can be rewritten in terms of the low frequency modes only:

$$G(\omega) \simeq \sum_{i=1}^m \frac{\phi_i \phi_i^T}{\mu_i \omega_i^2} D_i(\omega) + K^{-1} - \sum_{i=1}^m \frac{\phi_i \phi_i^T}{\mu_i \omega_i^2} \quad (2.33)$$

The quasi-static correction of the high frequency modes is often called the *residual mode*, denoted by  $R$ . Unlike all the terms involving  $D_i(\omega)$  which reduce to 0 as  $\omega \rightarrow \infty$ ,  $R$  is independent of the frequency and introduces a *feedthrough* (constant) component in the dynamic flexibility matrix.

### 2.5.1 Structure with rigid body modes\*

The approximation (2.33) applies only at low frequency,  $\omega < \omega_m$ . If the structure has  $r$  rigid body modes, the first sum can be split into rigid and flexible modes; however, the residual mode cannot be used any more, because  $K^{-1}$  no longer exists. This problem can be solved in the following way. The displacements are partitioned into their rigid and flexible contributions according to

$$\mathbf{x} = \mathbf{x}_r + \mathbf{x}_e = \Phi_r \mathbf{z}_r + \Phi_e \mathbf{z}_e \quad (2.34)$$

where  $\Phi_r$  and  $\Phi_e$  are the matrices whose columns are the rigid body modes and the flexible modes, respectively. Assuming no damping, to make things formally simpler, and taking into account that the rigid body modes satisfy  $K\Phi_r = 0$ , we obtain the equation of motion

$$M\Phi_r \ddot{\mathbf{z}}_r + M\Phi_e \ddot{\mathbf{z}}_e + K\Phi_e \mathbf{z}_e = \mathbf{f} \quad (2.35)$$

Left multiplying by  $\Phi_r^T$  and using the orthogonality relations (2.8) and (2.9), we see that the rigid body modes are governed by

$$\Phi_r^T M \Phi_r \ddot{\mathbf{z}}_r = \Phi_r^T \mathbf{f}$$

or

$$\ddot{\mathbf{z}}_r = \mu_r^{-1} \Phi_r^T \mathbf{f} \quad (2.36)$$

Substituting this result into Equ.(2.35), we get

$$\begin{aligned} M\Phi_e \ddot{\mathbf{z}}_e + K\Phi_e \mathbf{z}_e &= \mathbf{f} - M\Phi_r \ddot{\mathbf{z}}_r \\ &= \mathbf{f} - M\Phi_r \mu_r^{-1} \Phi_r^T \mathbf{f} = (I - M\Phi_r \mu_r^{-1} \Phi_r^T) \mathbf{f} \end{aligned}$$

or

$$M\Phi_e \ddot{\mathbf{z}}_e + K\Phi_e \mathbf{z}_e = P^T \mathbf{f} \quad (2.37)$$

where we have defined the projection matrix

$$P = I - \Phi_r \mu_r^{-1} \Phi_r^T M \quad (2.38)$$

such that  $P^T \mathbf{f}$  is orthogonal to the rigid body modes. In fact, we can easily check that

$$P\Phi_r = 0 \quad (2.39)$$

$$P\Phi_e = \Phi_e \quad (2.40)$$

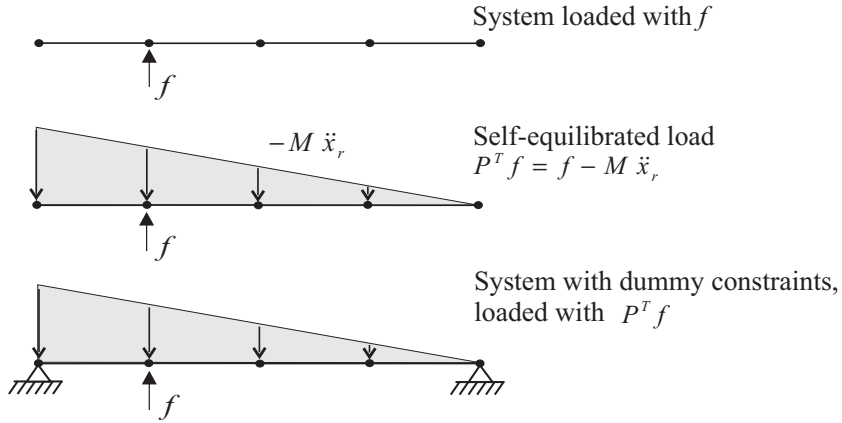


**Fig. 2.5.** Structure with rigid body modes.

$P$  can therefore be regarded as a filter which leaves unchanged the flexible modes and eliminates the rigid body modes.

If we follow the same procedure as in the foregoing section, we need to evaluate the elastic contribution of the static deflection, which is the solution of

$$K\mathbf{x}_e = P^T \mathbf{f} \quad (2.41)$$

Since  $K\Phi_r = 0$ , the solution may contain an arbitrary contribution from the rigid body modes. On the other hand,  $P^T \mathbf{f} = \mathbf{f} - M\dot{\mathbf{x}}_r$  is the superposition of the external forces and the inertia forces associated with the motion as a rigid body; it is self-equilibrated, because it is orthogonal to the rigid body modes. Since the system is in equilibrium as a rigid body, a particular solution of Equ.(2.41) can be obtained by adding *dummy constraints* to remove the rigid body modes (Fig.2.5). The modified system is statically determinate and its stiffness matrix can be inverted. If we denote by  $G_{iso}$  the flexibility matrix of the modified system, the general solution of (2.41) is

$$\mathbf{x}_e = G_{iso}P^T \mathbf{f} + \Phi_r \mathbf{c}$$

where  $\mathbf{c}$  is a vector of arbitrary constants. The contribution of the rigid body modes can be eliminated with the projection matrix  $P$ , leading to

$$\mathbf{x}_e = PG_{iso}P^T \mathbf{f} \quad (2.42)$$

$PG_{iso}P^T$  is the pseudo-static flexibility matrix of the flexible modes. On the other hand, left multiplying Equ.(2.35) by  $\Phi_e^T$ , we get

$$\Phi_e^T M \Phi_e \ddot{\mathbf{z}}_e + \Phi_e^T K \Phi_e \mathbf{z}_e = \Phi_e^T \mathbf{f}$$

where the diagonal matrix  $\Phi_e^T K \Phi_e$  is regular. It follows that the pseudo-static deflection can be written alternatively

$$\mathbf{x}_e = \Phi_e \mathbf{z}_e = \Phi_e (\Phi_e^T K \Phi_e)^{-1} \Phi_e^T \mathbf{f} \quad (2.43)$$

Comparing with Equ.(2.42), we get

$$PG_{iso}P^T = \Phi_e (\Phi_e^T K \Phi_e)^{-1} \Phi_e^T = \sum_{r+1}^n \frac{\phi_i \phi_i^T}{\mu_i \omega_i^2} \quad (2.44)$$

This equation is identical to Equ.(2.32) when there are no rigid body modes. From this result, we can extend Equ.(2.33) to systems with rigid body modes:

$$G(\omega) \simeq \sum_{i=1}^r \frac{\phi_i \phi_i^T}{-\mu_i \omega_i^2} + \sum_{i=r+1}^m \frac{\phi_i \phi_i^T}{\mu_i \omega_i^2} D_i(\omega) + R \quad (2.45)$$

where the contribution from the residual mode is

$$R = \sum_{m+1}^n \frac{\phi_i \phi_i^T}{\mu_i \omega_i^2} = PG_{iso}P^T - \sum_{r+1}^m \frac{\phi_i \phi_i^T}{\mu_i \omega_i^2} \quad (2.46)$$

Note that  $G_{iso}$  is the flexibility matrix of the system obtained by adding dummy constraints to remove the rigid body modes. Obviously, this can be achieved in many different ways and it may look surprising that they all lead to the same result (2.46). In fact, different boundary conditions lead to different displacements under the self-equilibrated load  $P^T f$ , but they differ only by a contribution of the rigid body modes, which is destroyed by the projection matrix  $P$ , leading to the same  $PG_{iso}P^T$ . Let us illustrate the procedure with an example.

### 2.5.2 Example\*

Consider the system of three identical masses of Fig.2.6. There is one rigid body mode and two flexible ones:

$$\Phi = (\Phi_r, \Phi_e) = \begin{bmatrix} 1 & 1 & 1 \\ 1 & 0 & -2 \\ 1 & -1 & 1 \end{bmatrix}$$

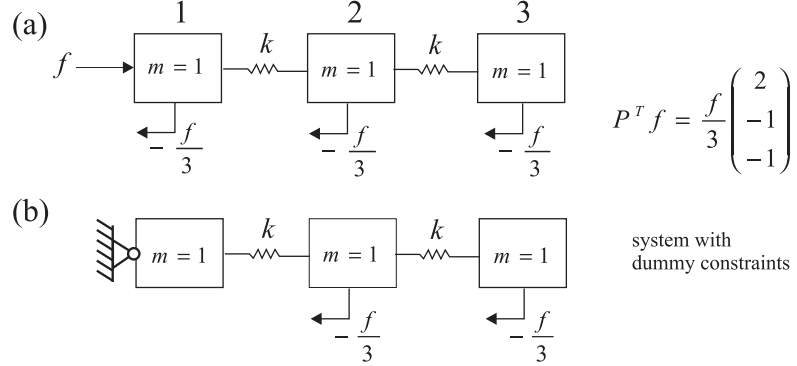


**Fig. 2.6.** Three mass system: (a) self-equilibrated forces associated with a force  $f$  applied to mass 1; (b) dummy constraints.

and

$$\Phi^T M \Phi = \text{diag}(3, 2, 6) \quad \Phi^T K \Phi = k \cdot \text{diag}(0, 2, 18)$$

From Equ.(2.38), the projection matrix is

$$P = \begin{bmatrix} 1 & 0 & 0 \\ 0 & 1 & 0 \\ 0 & 0 & 1 \end{bmatrix} - \left\{ \begin{bmatrix} 1 \\ 1 \\ 1 \end{bmatrix} \right\} \cdot \frac{1}{3} \cdot (1, 1, 1) = \begin{bmatrix} 1 & 0 & 0 \\ 0 & 1 & 0 \\ 0 & 0 & 1 \end{bmatrix} - \frac{1}{3} \begin{bmatrix} 1 & 1 & 1 \\ 1 & 1 & 1 \\ 1 & 1 & 1 \end{bmatrix}$$

or

$$P = \frac{1}{3} \begin{bmatrix} 2 & -1 & -1 \\ -1 & 2 & -1 \\ -1 & -1 & 2 \end{bmatrix}$$

We can readily check that

$$P\Phi = P(\Phi_r, \Phi_e) = (0, \Phi_e)$$

and the self-equilibrated loads associated with a force  $f$  applied to mass 1 is, Fig.2.6.a

$$P^T \mathbf{f} = \frac{1}{3} \begin{bmatrix} 2 & -1 & -1 \\ -1 & 2 & -1 \\ -1 & -1 & 2 \end{bmatrix} \begin{Bmatrix} f \\ 0 \\ 0 \end{Bmatrix} = \begin{Bmatrix} 2/3 \\ -1/3 \\ -1/3 \end{Bmatrix} \mathbf{f}$$

If we impose the statically determinate constraint on mass 1, Fig.2.6.b, the resulting flexibility matrix is

$$G_{iso} = \frac{1}{k} \begin{bmatrix} 0 & 0 & 0 \\ 0 & 1 & 1 \\ 0 & 1 & 2 \end{bmatrix}$$

leading to

$$PG_{iso}P^T = \frac{1}{9k} \begin{bmatrix} 5 & -1 & -4 \\ -1 & 2 & -1 \\ -4 & -1 & 5 \end{bmatrix}$$

The reader can easily check that other dummy constraints would lead to the same pseudo-static flexibility matrix (Problem 2.8).

## 2.6 Anti-resonances

Let us consider a diagonal term of the dynamic flexibility matrix:

$$G_{kk}(\omega) = \sum_{i=1}^m \frac{\phi_i^2(k)}{\mu_i \omega_i^2} D_i(\omega) + R_{kk} \quad (2.47)$$

where  $\phi_i^2(k)$  is the square of the modal amplitude at the d.o.f.  $k$ . This (scalar) FRF represents the ratio between the harmonic response of the d.o.f.  $k$  and the harmonic excitation applied to the same d.o.f. Such a configuration corresponds to a *collocated* system, where the actuator and the sensor are associated to the same d.o.f. If one assumes that the system is undamped, the FRF is purely real:

$$G_{kk}(\omega) = \sum_{i=1}^m \frac{\phi_i^2(k)}{\mu_i(\omega_i^2 - \omega^2)} + R_{kk} \quad (2.48)$$

All the residues are positive (square of the modal amplitude) and, as a result,  $G_{kk}(\omega)$  is a monotonously increasing function of  $\omega$ , which behaves as illustrated in Fig.2.7. The amplitude of the FRF goes from  $-\infty$  at the resonance frequencies  $\omega_i^+$  (corresponding to a pair of imaginary poles at  $s = \pm j\omega_i$ ) to  $+\infty$  at the next resonance frequency  $\omega_{i+1}^-$ . Since the function is continuous, in every interval, there is a frequency  $z_i$  such that  $\omega_i < z_i < \omega_{i+1}$  where the amplitude of the FRF vanishes, and there is one in every interval between two resonances. In structural dynamics, such frequencies are called *anti-resonances*; they correspond to purely imaginary zeros at  $\pm jz_i$ . Thus, *undamped collocated systems have alternating poles and zeros on the imaginary axis*. The pole / zero pattern is that of Fig.2.8.a. The

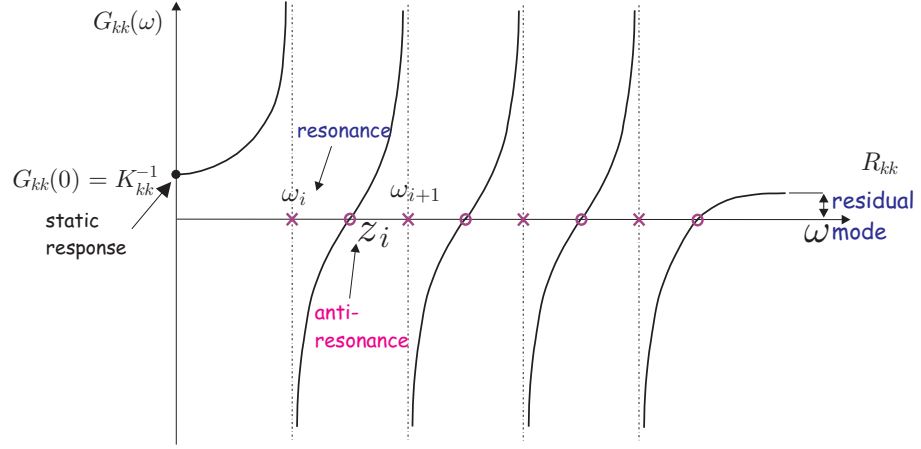


**Fig. 2.7.** Open-loop FRF of an undamped structure with a collocated actuator/sensor pair (no rigid body modes).

situation depicted in Fig.2.7 is that where there is no rigid body mode. In presence of rigid body modes, the FRF starts from  $-\infty$  at  $\omega = 0$  and there is an additional zero such that  $0 < z_1 < \omega_1$ . For a lightly damped structure, the poles and zeros are just moved a little in the left-half plane, but they are still *interlacing*, Fig.2.8.b.

If the undamped structure is excited harmonically by the actuator at the frequency of the transmission zero,  $z_i$ , the amplitude of the response of the collocated sensor vanishes. This means that the structure oscillates at the frequency  $z_i$  according to the shape shown in dotted line on Fig.2.10.b. We will establish in the next section that this shape, and the frequency

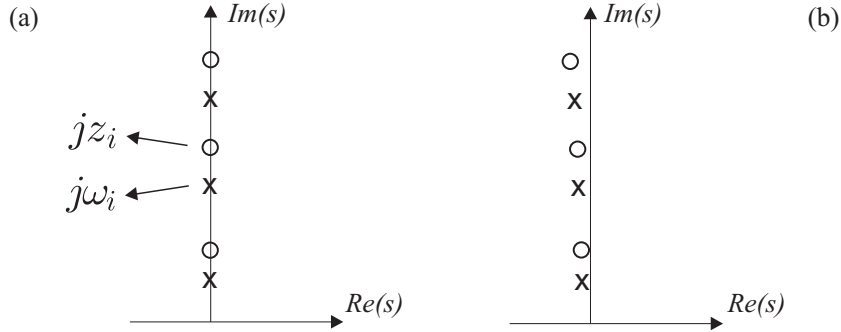


**Fig. 2.8.** Pole/Zero pattern of a structure with collocated (dual) actuator and sensor; (a) undamped; (b) lightly damped (only the upper half of the complex plane is shown, the diagram is symmetrical with respect to the real axis).

$z_i$ , are actually a mode shape and a natural frequency of the system obtained by constraining (blocking) the d.o.f.  $k$ . The natural frequencies of the constrained system depend on the d.o.f. where the constraint has been added.<sup>3</sup> However, from the foregoing discussion, for every component  $G_{kk}(\omega)$ , that is for every actuator/sensor configuration, there will be one and only one zero between two consecutive poles, and the interlacing property applies for any location of the collocated pair.

Referring once again to Fig.2.7, one easily sees that neglecting the residual mode in the modelling [ $R_{kk}$  in Equ.(2.48)] amounts to translating the FRF diagram vertically in such a way that its high frequency asymptote becomes tangent to the frequency axis. This produces a shift in the location of the transmission zeros to the right, and the last one even moves to infinity as the feedthrough (constant) component  $R_{kk}$  disappears from the FRF. Thus, neglecting the residual modes tends to overestimate the anti-resonance frequencies. The open-loop transfer function of a undamped structure with a collocated actuator/sensor pair can be written

$$G(s) = G_0 \frac{\prod_i (s^2/z_i^2 + 1)}{\prod_j (s^2/\omega_j^2 + 1)} \quad (\omega_i < z_i < \omega_{i+1}) \quad (2.49)$$

For a lightly damped structure, it reads

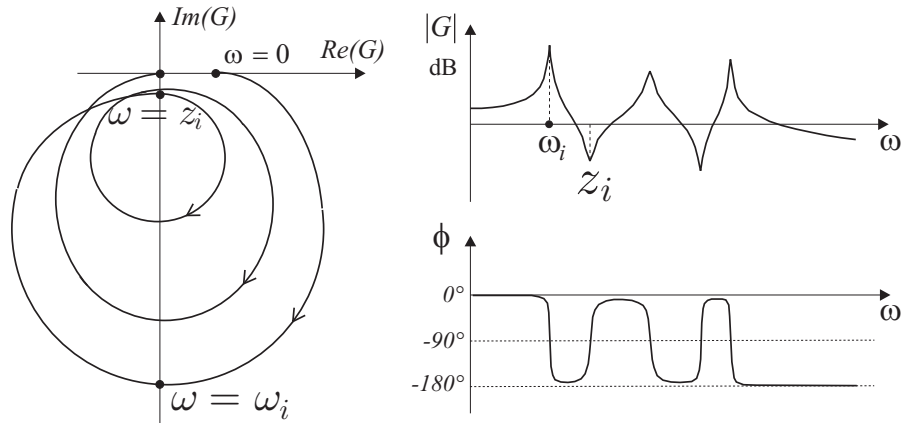


**Fig. 2.9.** Nyquist diagram and Bode plots of a lightly damped structure with collocated actuator and sensor.

<sup>3</sup> It is indeed well known in system theory that the open-loop poles are independent of the actuator and sensor configuration while the open-loop zeros do depend on it.

$$G(s) = G_0 \frac{\prod_i (s^2/z_i^2 + 2\xi_i s/z_i + 1)}{\prod_j (s^2/\omega_j^2 + 2\xi_j s/\omega_j + 1)} \quad (\omega_i < z_i < \omega_{i+1}) \quad (2.50)$$

The corresponding Bode and Nyquist plots are represented in Fig 2.9. Every imaginary pole at  $\pm j\omega_i$  introduces a  $180^\circ$  phase lag and every imaginary zero at  $\pm jz_i$  a  $180^\circ$  phase lead. In this way, the phase diagram is always contained between 0 and  $-180^\circ$ , as a consequence of the interlacing property. For the same reason, the Nyquist diagram consists of a set of nearly circles (one per mode), all contained in the third and fourth quadrants. Thus, the entire curve  $G(\omega)$  is below the real axis (the diameter of every circle is proportional to  $\xi_i^{-1}$ ).

### 2.6.1 Anti-resonances and constrained system

We now establish that the anti-resonances (transmission zeros) of the undamped system are the poles (natural frequencies) of the constrained system. Consider the undamped structure of Fig.2.10.a (a displacement sensor is assumed for simplicity). The governing equations are

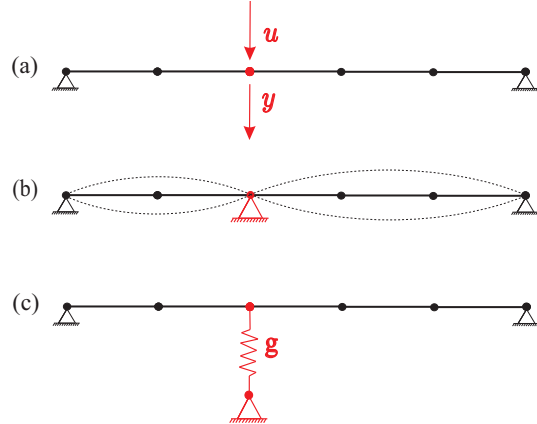


**Fig. 2.10.** (a) Structure with collocated actuator and sensor; (b) structure with additional constraint; (c) structure with additional stiffness along the controlled d.o.f.

*Structure:*

$$M\ddot{\mathbf{x}} + K\mathbf{x} = \mathbf{b} u \quad (2.51)$$

*Output sensor:*

$$y = \mathbf{b}^T \mathbf{x} \quad (2.52)$$

$u$  is the actuator input (scalar) and  $y$  is the sensor output (also scalar). The fact that the same vector  $\mathbf{b}$  appears in the two equations is due to collocation. For a stationary harmonic input at the actuator,  $u = u_0 e^{j\omega_0 t}$ ; the response is harmonic,  $\mathbf{x} = \mathbf{x}_0 e^{j\omega_0 t}$ , and the amplitude vector  $\mathbf{x}_0$  is solution of

$$(K - \omega_0^2 M) \mathbf{x}_0 = \mathbf{b} u_0 \quad (2.53)$$

The sensor output is also harmonic,  $y = y_0 e^{j\omega_0 t}$  and the output amplitude is given by

$$y_0 = \mathbf{b}^T \mathbf{x}_0 = \mathbf{b}^T (K - \omega_0^2 M)^{-1} \mathbf{b} u_0 \quad (2.54)$$

Thus, the antiresonance frequencies  $\omega_0$  are solutions of

$$\mathbf{b}^T (K - \omega_0^2 M)^{-1} \mathbf{b} = 0 \quad (2.55)$$

Now, consider the system with the additional stiffness  $g$  along the same d.o.f. as the actuator/sensor pair, Fig 2.10.c. The stiffness matrix of the modified system is  $K + g\mathbf{b}\mathbf{b}^T$ . The natural frequencies of the modified system are solutions of the eigenvalue problem

$$[K + g\mathbf{b}\mathbf{b}^T - \omega^2 M] \boldsymbol{\phi} = 0 \quad (2.56)$$

For all  $g$ , the solution  $(\omega, \boldsymbol{\phi})$  of the eigenvalue problem is such that

$$(K - \omega^2 M) \boldsymbol{\phi} + g\mathbf{b}\mathbf{b}^T \boldsymbol{\phi} = 0 \quad (2.57)$$

or

$$\mathbf{b}^T \boldsymbol{\phi} = -\mathbf{b}^T (K - \omega^2 M)^{-1} g\mathbf{b}\mathbf{b}^T \boldsymbol{\phi} \quad (2.58)$$

Since  $\mathbf{b}^T \boldsymbol{\phi}$  is a scalar, this implies that

$$\mathbf{b}^T (K - \omega^2 M)^{-1} \mathbf{b} = -\frac{1}{g} \quad (2.59)$$

Taking the limit for  $g \rightarrow \infty$ , one sees that the eigenvalues  $\omega$  satisfy

$$\mathbf{b}^T (K - \omega^2 M)^{-1} \mathbf{b} = 0 \quad (2.60)$$

which is identical to (2.55). Thus,  $\omega = \omega_0$ ; the imaginary zeros of the undamped collocated system, solutions of (2.55), are the poles of the constrained system (2.56) at the limit, when the stiffness  $g$  added along the actuation d.o.f. increases to  $\infty$ :

$$\lim_{g \rightarrow \infty} [(K + g\mathbf{b}\mathbf{b}^T) - \omega_0^2 M] \mathbf{x}_0 = 0 \quad (2.61)$$

This is equivalent to placing a kinematic constraint along the control d.o.f.

## 2.7 Natural frequencies of a $n$ -storey building\*

The construction of the mass and stiffness matrices of a building with 5 identical floors was examined in section 2.1. In this section we examine the more general case of a building with  $n$  identical floors and, rather than constructing the mass and stiffness matrices and solving the eigenvalue problem for a specific value of  $n$ , we seek an analytical solution to the difference equation, with appropriate boundary conditions.<sup>4</sup>

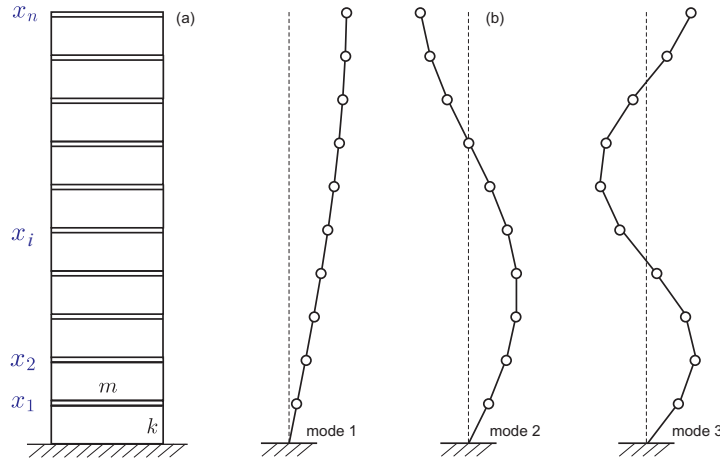


**Fig. 2.11.** (a) Model of a building with  $n$  identical floors; the floor is considered as a rigid slab of mass  $m$  and the columns are massless and clamped at both ends; the lateral stiffness of one floor is  $k$ . (b) Mode shapes.

The equation governing the motion of floor  $i$  is obtained by expressing the equilibrium between the inertia forces and the elastic restoring forces coming from the neighboring floors:

$$m\ddot{x}_i = -k(x_i - x_{i-1}) - k(x_i - x_{i+1})$$

or

$$-x_{i-1} + 2x_i - x_{i+1} = -\frac{m}{k}\ddot{x}_i \quad (2.62)$$

(which is essentially the equation of motion of a set of identical spring-mass systems attached in series). Assuming an harmonic motion,  $x_i = x_i e^{j\omega t}$ , and introducing the reduced frequency

---

<sup>4</sup> Reading the chapter on continuous systems is recommended before reading this section.

$$\mu^2 = \omega^2 \frac{m}{k} = \frac{\omega^2}{\omega_0^2} \quad (2.63)$$

( $\omega_0 = \sqrt{k/m}$  is the natural frequency of a single storey, Problem 1.3), the eigenvalue problem is

$$-x_{i-1} + 2x_i - x_{i+1} = \mu^2 x_i \quad (i = 1, \dots, n-1) \quad (2.64)$$

with the boundary conditions  $x_0 = 0$  (structure fixed at the base) and

$$x_n - x_{n-1} = \mu^2 x_n \quad (2.65)$$

at the free end. The difference equation (2.64) has a solution of the form  $x_i = A e^{zi}$  if  $z$  is solution of

$$-e^{-z} + (2 - \mu^2) - e^z = 0$$

or

$$\cosh z = 1 - \frac{\mu^2}{2}$$

(if  $z$  is solution,  $-z$  is also solution). Since the cosh of any real number is always larger than 1, there cannot be a solution with  $z$  real. If  $\mu^2 < 4$ , the solution is  $z = \pm j\lambda$ , with

$$\begin{aligned} \cos \lambda &= 1 - \frac{\mu^2}{2} & \text{or} & \sin^2 \frac{\lambda}{2} = \frac{\mu^2}{4} \\ \mu &= 2 \sin \frac{\lambda}{2} \end{aligned} \quad (2.66)$$

At this stage, the set of values possible for  $\lambda$  is still unknown. The general solution for the mode shape is

$$x_i = A e^{j\lambda i} + B e^{-j\lambda i} \quad \text{or} \quad x_i = C \sin \lambda i + D \cos \lambda i$$

Taking into account the boundary condition at the lower end,  $x_0 = 0$ ,  $D = 0$ . The eigenvalue is determined by enforcing the boundary condition (2.65) at the upper end of the structure:

$$\sin \lambda n - \sin \lambda(n-1) = \mu^2 \sin \lambda n$$

or

$$(1 - \mu^2) \sin \lambda n - \sin \lambda(n-1) = 0$$

which, after expanding  $\sin \lambda(n-1)$  and using (2.66), can be rewritten

$$2 \sin \frac{\lambda}{2} \cos(\lambda n + \frac{\lambda}{2}) = 0 \quad (2.67)$$

$\sin \frac{\lambda}{2} = 0$  is a trivial solution which corresponds to  $\mu = 0$ . The other solutions correspond to

$$\lambda_r n + \frac{\lambda_r}{2} = (2r - 1) \frac{\pi}{2} \quad (r = 1, 2, \dots, n)$$

or

$$\lambda_r = \frac{2r - 1}{2n + 1} \pi$$

Finally, using Equ.(2.66) and (2.63), one finds the natural frequencies:

$$\omega_r = 2\sqrt{\frac{k}{m}} \sin\left[\frac{(2r - 1)}{(2n + 1)} \frac{\pi}{2}\right] \quad (r = 1, 2, \dots, n) \quad (2.68)$$

The corresponding mode shape is

$$\mathbf{x}_r(i) = C \sin\left[i \frac{(2r - 1)}{(2n + 1)} \pi\right] \quad (2.69)$$

The first few mode shapes are illustrated in Fig.2.11.

## 2.8 Problems

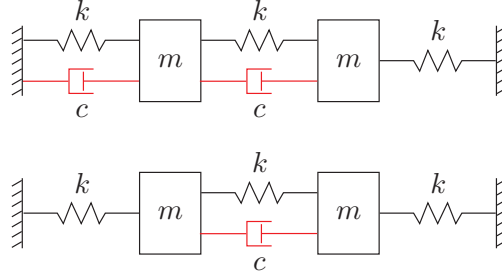


**Fig. 2.12.** Two d.o.f. lumped mass system with various damping configurations.

**P.2.1** For the various configurations shown in Fig.2.12, discuss the assumption of modal damping and calculate the modal damping ratios.

**P.2.2** Consider the system of Fig.2.13, consisting of two disks of polar moment of inertia  $J$  mounted on a shaft in three parts of identical torsional stiffness  $K_\theta$ . The system is supported by two bearings in  $A$  and

B. Write the equations governing the torsional vibration of the system and find the natural frequencies and the mode shapes for the following boundary conditions:

- (a) Clamped in A and B.
- (b) Free to rotate in A and B.
- (c) Clamped in A and free in B.

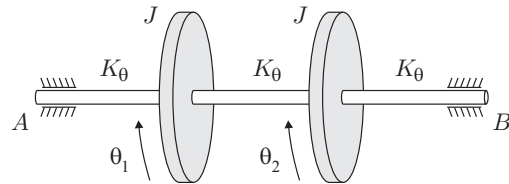


**Fig. 2.13.** Shaft with two disks.

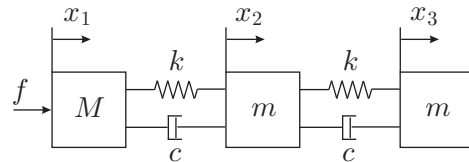


**Fig. 2.14.** Three mass system.

**P.2.3** Write the equations governing the vibration of the three-mass system of Fig.2.14. Find the mode shapes in the particular case  $M = m$ .

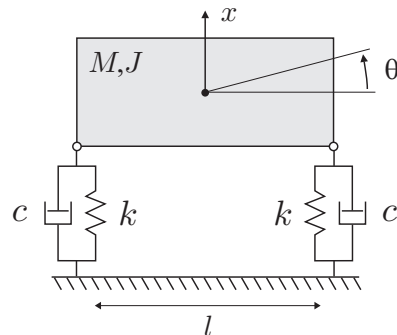


**Fig. 2.15.** Plane motion of a rigid body on a suspension.

**P.2.4** Write the equations governing the vibration of the suspension system of Fig.2.15. Find the natural frequencies, the modes and the modal damping ratios.

**P.2.5** Show that if  $\phi_i$  and  $\phi_j$  are mode shapes with the same natural frequency  $\omega_i$ ,  $a\phi_i + b\phi_j$  is also a mode shape with the same natural frequency, for any  $a$  and  $b$ .

**P.2.6** (a) Show that the projection matrix

$$A_k = \left[ I - \frac{\phi_k \phi_k^T M}{\phi_k^T M \phi_k} \right] \quad (2.70)$$

is such that

$$\begin{aligned} A_k \phi_k &= 0 \\ A_k \phi_i &= \phi_i \end{aligned} \quad (2.71)$$

$A_k$  projects any vector in the subspace orthogonal to  $\phi_k$ .

(b) What would be the matrix which projects any vector in the subspace orthogonal to  $\phi_k$  and  $\phi_l$ ?

**P.2.7** Sketch the evolution of the modal damping  $\xi_i$  with the modal frequency for the Rayleigh damping assumption (2.25).

**P.2.8** Consider the three mass system of section 2.5.2. Show that changing the dummy constraint to mass 2 does not change the pseudo-static flexibility matrix  $PG_{iso}P^T$ .

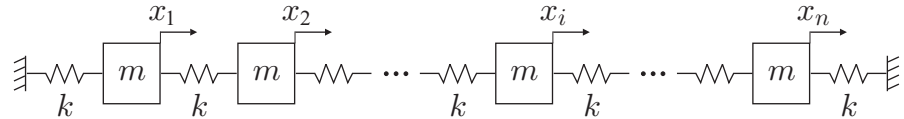


**Fig. 2.16.** Spring mass system with  $n$  identical masses  $m$  connected with  $n+1$  identical springs  $k$ .

**P.2.9** Consider the system of Fig.2.16, formed of  $n$  identical masses  $m$  connected with identical springs of stiffness  $k$ . Show that the natural frequencies of the system are given by

$$\omega_r = 2\sqrt{\frac{k}{m}} \cdot \sin\left[\frac{r\pi}{2(n+1)}\right] \quad (2.72)$$

and the corresponding mode shapes

$$x_r(i) = C \sin\left[i \frac{r\pi}{n+1}\right] \quad (2.73)$$

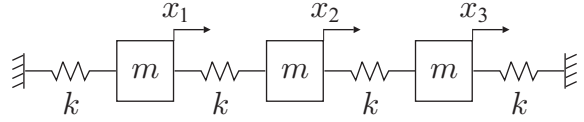


**Fig. 2.17.** Spring mass system with 3 identical masses  $m$  connected with 4 identical springs  $k$ .

[Hint: Solve the difference equation (2.64) with the boundary conditions  $x_0 = 0$ ,  $x_{n+1} = 0$ .]

**P.2.10** Consider the system of Fig.2.17, formed of three identical masses  $m$  connected with 4 identical springs of stiffness  $k$ . (a) Using the results of the previous problem, sketch the pole/zero pattern of the structure with a collocated actuator and sensor pair acting at the d.o.f. 1. (b) Do the same for an actuator and sensor pair acting at d.o.f. 2. Compare the two plots.

**P.2.11** Write the stiffness matrices of the systems of Fig.2.11 and Fig.2.16.

# 3

---

## Lagrangian dynamics

*Le bon sens est la chose la mieux répartie au monde, parce que nul ne se plaint de ne pas en avoir assez.*

Descartes, *Discours de la Méthode*, 1637

### 3.1 Introduction

Lagrangian dynamics has been motivated by the substitution of scalar quantities (energy and work) for vector quantities (force, momentum, torque, angular momentum) in classical vector dynamics. Generalized coordinates are substituted for physical coordinates, which allows a formulation independent of the reference frame. Systems are considered globally, rather than every component independently, with the advantage of eliminating the interaction forces (resulting from constraints) between the various elementary parts of the system. The choice of generalized coordinates is not unique.

The derivation of the variational form of the equations of dynamics from its vector counterpart (Newton's laws) is done through the principle of virtual work, extended to dynamics thanks to d'Alembert's principle, leading eventually to Hamilton's principle and the Lagrange equations for discrete systems.

Hamilton's *principle* is an alternative to Newton's laws and it can be argued that, as such, it is a fundamental law of physics which cannot be derived. We believe, however, that its form may not be immediately comprehensible to the unexperienced reader and that its derivation for a system of particles will ease its acceptance as an alternative formulation of dynamic equilibrium. Hamilton's principle is in fact more general than Newton's laws, because it can be generalized to distributed systems (governed by partial differential equations) and to electromechanical systems. It is also the starting point for the formulation of many numerical methods in dynamics, including the finite element method.

### 3.2 Generalized coordinates, kinematic constraints

A *kinematically admissible* motion denotes a spatial configuration that is always compatible with the geometric boundary conditions. The *generalized coordinates* are a set of coordinates that allow a full geometric description of the system with respect to a reference frame. This representation is not unique; Fig.3.1 shows two sets of generalized coordinates for the double pendulum in a plane; in the first case, the relative angles are adopted as generalized coordinates, while the absolute angles are taken in the second case. Note that the generalized coordinates do not always have a simple physical meaning such as a displacement or an angle; they may also represent the amplitude of an assumed mode in a distributed system, as is done extensively in the analysis of flexible structures.

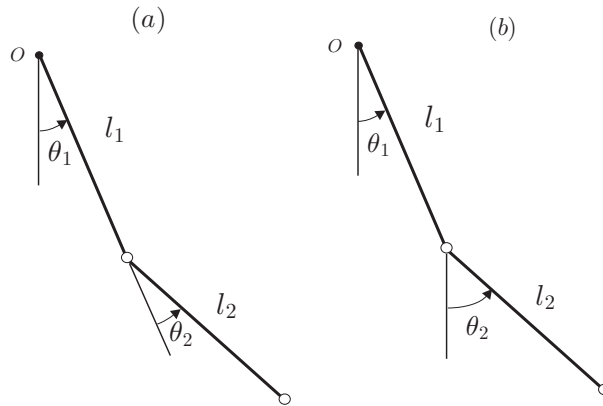


**Fig. 3.1.** Double pendulum in a plane (a) relative angles (b) absolute angles.

The number of degrees of freedom (d.o.f.) of a system is the minimum number of coordinates necessary to provide its full geometric description. If the number of generalized coordinates is equal to the number of d.o.f., they form a minimum set of generalized coordinates. The use of a minimum set of coordinates is not always possible, nor advisable; if their number exceeds the number of d.o.f., they are not independent and they are connected by kinematic constraints. If the constraint equations between the generalized coordinates  $q_i$  can be written in the form

$$f(q_1, \dots, q_n, t) = 0 \quad (3.1)$$

they are called *holonomic*. If the time does not appear explicitly in the constraints, they are called *scleronomous*.

$$f(q_1, \dots, q_n) = 0 \quad (3.2)$$

The algebraic constraints (3.1) or (3.2) can always be used to eliminate the redundant set of generalized coordinates and reduce the coordinates to a minimum set. This is no longer possible if the kinematic constraints are defined by a (non integrable) differential relation

$$\sum_i a_i dq_i + a_0 dt = 0 \quad (3.3)$$

or

$$\sum_i a_i dq_i = 0 \quad (3.4)$$

if the time is excluded; non integrable constraints such as (3.3) and (3.4) are called *non-holonomic*.

As an example of non-holonomic constraints, consider a vertical disk rolling without slipping on an horizontal plane (Fig.3.2). The system is fully characterized by four generalized coordinates, the location  $(x, y)$  of the contact point in the plane, and the orientation of the disk, defined by  $(\theta, \phi)$ . The reader can check that, if the appropriate path is used, the four generalized variables can be assigned *arbitrary* values (i.e. the disc can be moved to all points of the plane with an arbitrary orientation). However, the time derivatives of the coordinates are not independent, because they must satisfy the rolling conditions:

$$v = r\dot{\phi}$$

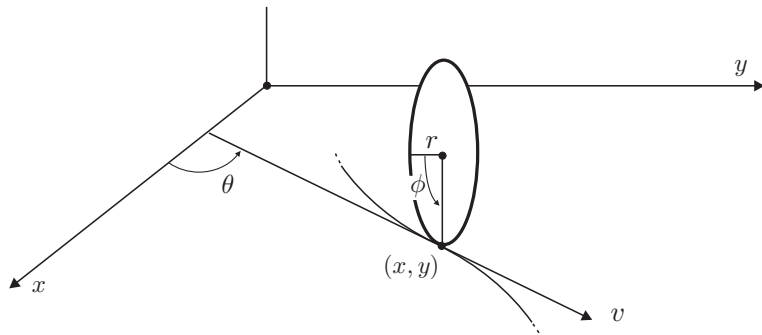


**Fig. 3.2.** Vertical disk rolling without slipping on an horizontal plane.

$$\dot{x} = v \cos \theta, \quad \dot{y} = v \sin \theta$$

combining these equations, we get the differential constraint equations :

$$dx - r \cos \theta d\phi = 0$$

$$dy - r \sin \theta d\phi = 0$$

which actually restrict the possible paths to go from one configuration to the other.

### 3.2.1 Virtual displacements

A *virtual displacement*, or more generally a virtual change of configuration, is an infinitesimal change of coordinates occurring *at constant time*, and consistent with the kinematic constraints of the system (but otherwise arbitrary). The notation  $\delta$  is used for the virtual changes of coordinates; they follow the same rules as the derivatives, except that time is not involved. It follows that, for a system with generalized coordinates  $q_i$  related by holonomic constraints (3.1) or (3.2), the admissible variations must satisfy

$$\delta f = \sum_i \frac{\partial f}{\partial q_i} \delta q_i = 0 \quad (3.5)$$

Note that the same form applies, whether  $t$  is explicitly involved in the constraints or not, because the virtual displacements are taken at constant time. For non-holonomic constraints (3.3) or (3.4), the virtual displacements must satisfy

$$\sum_i a_i \delta q_i = 0 \quad (3.6)$$

Comparing Equ.(3.3) and (3.6), we note that, if the time appears explicitly in the constraints, the virtual displacements are not possible displacements. The differential displacements  $dq_i$  are along a particular trajectory as it unfolds with time, while the virtual displacements  $\delta q_i$  measure the separation between two different trajectories at a given instant.

Consider a single particle constrained to move on a smooth surface

$$f(x, y, z) = 0$$

The virtual displacements must satisfy the constraint equation

$$\frac{\partial f}{\partial x}\delta x + \frac{\partial f}{\partial y}\delta y + \frac{\partial f}{\partial z}\delta z = 0$$

which is in fact the dot product of the gradient to the surface,

$$\text{grad}f = \nabla f = \left( \frac{\partial f}{\partial x}, \frac{\partial f}{\partial y}, \frac{\partial f}{\partial z} \right)^T$$

and the vector of virtual displacement  $\delta \mathbf{x} = (\delta x, \delta y, \delta z)^T$ :

$$\text{grad}f \cdot \delta \mathbf{x} = (\nabla f)^T \delta \mathbf{x} = 0$$

Since  $\nabla f$  is parallel to the normal  $n$  to the surface, this simply states that the virtual displacements belong to the plane tangent to the surface. Let us now consider the reaction force  $\mathbf{F}$  which constraints the particle to move along the surface. If we assume that the system is smooth and frictionless, the reaction force is also normal to the surface; it follows that

$$\mathbf{F} \cdot \delta \mathbf{x} = \mathbf{F}^T \delta \mathbf{x} = 0 \quad (3.7)$$

*the virtual work of the constraint forces on any virtual displacements is zero.* We will accept this as a general statement for a reversible system (without friction); note that it remains true if the surface equation depends explicitly on  $t$ , because the virtual displacements are taken at constant time.

### 3.3 Principle of virtual work

The principle of virtual work is a variational formulation of the static equilibrium of a mechanical system without friction. Consider a system of  $N$  particles with position vectors  $\mathbf{x}_i$ ,  $i = 1, \dots, N$ . Since the static equilibrium implies that the resultant  $\mathbf{R}_i$  of the force applied to each particle  $i$  is zero, each dot product  $\mathbf{R}_i \cdot \delta \mathbf{x}_i = 0$ , and

$$\sum_{i=1}^N \mathbf{R}_i \cdot \delta \mathbf{x}_i = 0$$

for all virtual displacements  $\delta \mathbf{x}_i$  compatible with the kinematic constraints.  $\mathbf{R}_i$  can be decomposed into the contribution of external forces applied  $\mathbf{F}_i$  and the constraint (reaction) forces  $\mathbf{F}'_i$

$$\mathbf{R}_i = \mathbf{F}_i + \mathbf{F}'_i$$

and the previous equation becomes

$$\sum \mathbf{F}_i \cdot \delta \mathbf{x}_i + \sum \mathbf{F}'_i \cdot \delta \mathbf{x}_i = 0$$

For a reversible system (without friction), Equ.(3.7) states that the virtual work of the constraint forces is zero, so that the second term vanishes, it follows that

$$\sum \mathbf{F}_i \cdot \delta \mathbf{x}_i = 0 \quad (3.8)$$

*The virtual work of the external applied forces on the virtual displacements compatible with the kinematics is zero.* The strength of this result comes from the fact that (i) the reaction forces have been removed from the equilibrium equation, (ii) the static equilibrium problem is transformed into kinematics, and (iii) it can be written in generalized coordinates:

$$\sum Q_k \cdot \delta q_k = 0 \quad (3.9)$$

where  $Q_k$  is the generalized force associated with the generalized coordinate  $q_k$ .

As an example of application, consider the one d.o.f. motion amplification mechanism of Fig.3.3. Its kinematics is governed by

$$x = 5a \sin \theta \quad y = 2a \cos \theta$$

It follows that

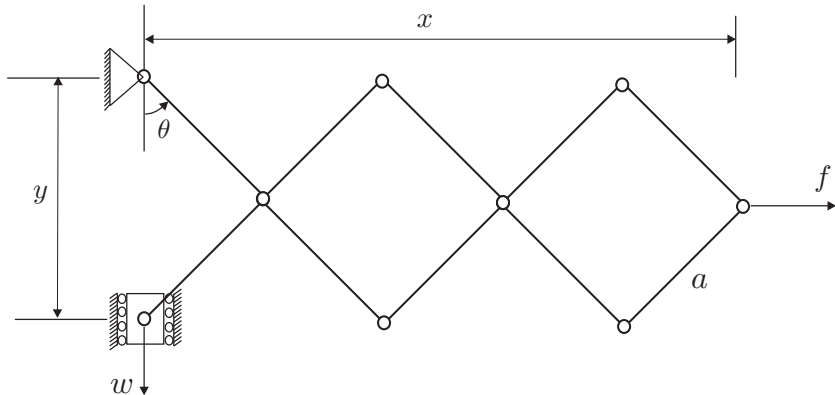


**Fig. 3.3.** Motion amplification mechanism.

$$\delta x = 5a \cos \theta \delta\theta \quad \delta y = -2a \sin \theta \delta\theta$$

The principle of virtual work reads

$$f \delta x + w \delta y = (f \cdot 5a \cos \theta - w \cdot 2a \sin \theta) \delta\theta = 0$$

for arbitrary  $\delta\theta$ , which implies that the static equilibrium forces  $f$  and  $w$  satisfy

$$f = w \frac{2}{5} \tan \theta$$

### 3.4 D'Alembert's principle

D'Alembert's principle extends the principle of virtual work to dynamics. It states that a problem of dynamic equilibrium can be transformed into a problem of static equilibrium by adding the inertia forces -  $m_i \ddot{\mathbf{x}}_i$  to the externally applied forces  $\mathbf{F}_i$  and constraints forces  $\mathbf{F}'_i$ .

Indeed, Newton's law implies that, for every particle,

$$\mathbf{R}_i = \mathbf{F}_i + \mathbf{F}'_i - m_i \ddot{\mathbf{x}}_i = 0$$

Following the same development as in the previous section, summing over all the particles and taking into account that the virtual work of the constraint forces is zero, one finds

$$\sum_{i=0}^N (\mathbf{F}_i - m_i \ddot{\mathbf{x}}_i) \cdot \delta \mathbf{x}_i = 0 \quad (3.10)$$

The sum of the applied external forces and the inertia forces is sometimes called the *effective force*. Thus, *the virtual work of the effective forces on the virtual displacements compatible with the constraints is zero*. This principle is most general; unfortunately, it is difficult to apply, because it still refers to vector quantities expressed in an inertial frame and, unlike the principle of virtual work, it cannot be translated directly into generalized coordinates. This will be achieved with Hamilton's principle in the next section.

If the time does not appear explicitly in the constraints, the virtual displacements are possible, and Equ.(3.10) is also applicable for the actual displacements  $d\mathbf{x}_i = \dot{\mathbf{x}}_i dt$

$$\sum_i \mathbf{F}_i \cdot d\mathbf{x}_i - \sum_i m_i \ddot{\mathbf{x}}_i \cdot \dot{\mathbf{x}}_i dt = 0$$

If the external forces can be expressed as the gradient of a potential  $V$  which does not depend explicitly on  $t$ ,  $\sum \mathbf{F}_i \cdot d\mathbf{x}_i = -dV$  (if  $V$  depends explicitly on  $t$ , the total differential includes a partial derivative with respect to  $t$ ). Such a force field is called *conservative*. The second term in the previous equation is the differential of the kinetic energy:

$$\sum_i m_i \ddot{\mathbf{x}}_i \cdot \dot{\mathbf{x}}_i dt = \frac{d}{dt} \left( \frac{1}{2} \sum_i m_i \dot{\mathbf{x}}_i \cdot \dot{\mathbf{x}}_i \right) dt = dT$$

It follows that

$$d(T + V) = 0$$

and

$$T + V = C^t \quad (3.11)$$

This is the law of *conservation of total energy*. Note that it is restricted to systems where (i) the potential energy does not depend explicitly on  $t$  and (ii) the kinematic constraints are independent of time.

### 3.5 Hamilton's principle

D'Alembert's principle is a complete formulation of the dynamic equilibrium; however, it uses the position coordinates of the various particles of the system, which are in general not independent; it cannot be formulated in generalized coordinates. On the contrary, Hamilton's principle expresses the dynamic equilibrium in the form of the stationarity of a definite integral of a scalar energy function. Thus, Hamilton's principle becomes independent of the coordinate system. Consider again Equ.(3.10); the first contribution

$$\delta W = \sum_i \mathbf{F}_i \cdot \delta \mathbf{x}_i$$

represents the virtual work of the applied external forces. The second contribution to Equ.(3.10) can be transformed using the identity

$$\ddot{\mathbf{x}}_i \cdot \delta \mathbf{x}_i = \frac{d}{dt} (\dot{\mathbf{x}}_i \cdot \delta \mathbf{x}_i) - \dot{\mathbf{x}}_i \cdot \delta \dot{\mathbf{x}}_i = \frac{d}{dt} (\dot{\mathbf{x}}_i \cdot \delta \mathbf{x}_i) - \delta \frac{1}{2} (\dot{\mathbf{x}}_i \cdot \dot{\mathbf{x}}_i)$$

where we have used the commutativity of  $\delta$  and  $(\cdot)$ . It follows that

$$\sum_{i=1}^N m_i \ddot{\mathbf{x}}_i \cdot \delta \mathbf{x}_i = \sum_{i=1}^N m_i \frac{d}{dt} (\dot{\mathbf{x}}_i \cdot \delta \mathbf{x}_i) - \delta T$$

where  $T$  is the kinetic energy of the system. Using this equation, we transform d'Alembert's principle (3.10) into

$$\delta W + \delta T = \sum_{i=0}^N m_i \frac{d}{dt} (\dot{\mathbf{x}}_i \cdot \delta \mathbf{x}_i)$$

The left hand side consists of scalar work and energy functions. The right hand side consists of a total time derivative which can be eliminated by integrating over some interval  $[t_1, t_2]$ , assuming that the system configuration is known at  $t_1$  and  $t_2$ , so that

$$\delta \mathbf{x}_i(t_1) = \delta \mathbf{x}_i(t_2) = 0 \quad (3.12)$$

Taking this into account, one gets

$$\int_{t_1}^{t_2} (\delta W + \delta T) dt = \sum_{i=1}^N m_i [\dot{\mathbf{x}}_i \cdot \delta \mathbf{x}_i]_{t_1}^{t_2} = 0$$

If some of the external forces are conservative,

$$\delta W = -\delta V + \delta W_{nc} \quad (3.13)$$

where  $V$  is the potential and  $\delta W_{nc}$  is the virtual work of the nonconservative forces. Thus, Hamilton's principle is expressed by the variational indicator (V.I.):

$$\text{V.I.} = \int_{t_1}^{t_2} [\delta(T - V) + \delta W_{nc}] dt = 0 \quad (3.14)$$

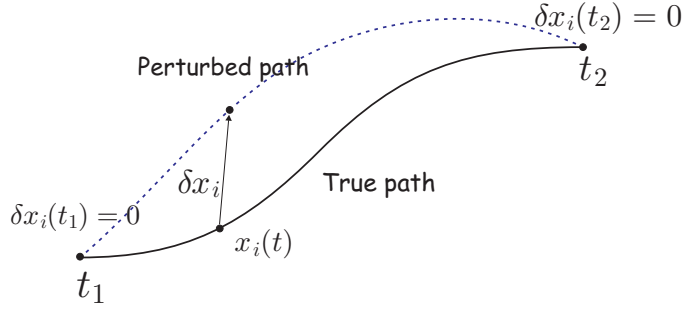
or

$$\text{V.I.} = \int_{t_1}^{t_2} [\delta L + \delta W_{nc}] dt = 0 \quad (3.15)$$

where

$$L = T - V \quad (3.16)$$

is the *Lagrangian* of the system. The statement of the dynamic equilibrium goes as follows: *The actual path is that which cancels the value of the variational indicator (3.14) or (3.15) with respect to all arbitrary*

**Fig. 3.4.** True and perturbed paths.

*variations of the path between two instants  $t_1$  and  $t_2$ , compatible with the kinematic constraints, and such that  $\delta\mathbf{x}_i(t_1) = \delta\mathbf{x}_i(t_2) = 0$ .*

Again, we stress that  $\delta x_i$  does not measure displacements on the true path, but the separation between the true path and a perturbed one at a given time (Fig.3.4).

Note that, unlike Equ.(3.11) which requires that the potential  $V$  does not depend explicitly on time, the virtual expression (3.13) allows  $V$  to depend on  $t$ , since the virtual variation is taken at constant time ( $\delta V = \nabla V \cdot \delta \mathbf{x}$ , while  $dV = \nabla V \cdot d\mathbf{x} + \partial V / \partial t \cdot dt$ ).

Hamilton's principle, that we derived here from d'Alembert's principle for a system of particles, is the most general statement of dynamic equilibrium, and it is, in many respects, more general than Newton's laws, because it applies to continuous systems and more. Some authors argue that, being a fundamental law of physics, it cannot be derived, just accepted. Thus we could have proceeded the opposite way: state Hamilton's principle, and show that it implies Newton's laws. It is a matter of taste, but also of history: 150 years separate Newton's Principia (1687) from Hamilton's principle (1835). From now on, we will consider Hamilton's principle as the fundamental law of dynamics.

Consider the plane pendulum of Fig.3.5; taking the altitude of the pivot  $O$  as reference, we find the Lagrangian

$$L = T - V = \frac{1}{2}m(l\dot{\theta})^2 + mgl \cos \theta$$

$$\delta L = ml^2\dot{\theta}\delta\dot{\theta} - mgl \sin \theta \delta\theta$$

Hamilton's principle states that the variational indicator (V.I).

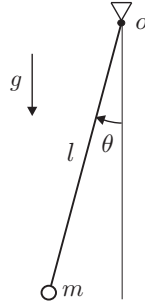


**Fig. 3.5.** Plane pendulum.

$$\text{V.I.} = \int_{t_1}^{t_2} [ml^2\dot{\theta}\delta\dot{\theta} - mgl \sin \theta \delta\theta] dt = 0$$

for all virtual variations  $\delta\theta$  such that  $\delta\theta(t_1) = \delta\theta(t_2) = 0$ . As always in variational calculus,  $\delta\dot{\theta}$  can be eliminated from the variational indicator by integrating by part over  $t$ . Using  $\dot{\theta}\delta\dot{\theta} = \frac{d}{dt}(\dot{\theta}\delta\theta) - \ddot{\theta}\delta\theta$  one gets

$$\text{V.I.} = [ml^2\dot{\theta}\delta\theta]_{t_1}^{t_2} - \int_{t_1}^{t_2} (ml^2\ddot{\theta} + mgl \sin \theta)\delta\theta dt = 0$$

for all virtual variations  $\delta\theta$  such that  $\delta\theta(t_1) = \delta\theta(t_2) = 0$ . Since the integral appearing in the second term must vanish for arbitrary  $\delta\theta$ , we conclude that

$$ml^2\ddot{\theta} + mgl \sin \theta = 0$$

which is the differential equation for the oscillation of the pendulum. The Lagrange's equations give a much quicker way of solving this type of problem.

### 3.6 Lagrange's equations

Hamilton's principle relies on scalar work and energy quantities; it does not refer to a particular coordinate system. The system configuration can be expressed in generalized coordinates  $q_i$ . If the generalized coordinates are independent, the virtual change of configuration can be represented by independent virtual variations of the generalized coordinates,  $\delta q_i$ . This allows us to transform the variational indicator (3.14) into a set of differential equations which are Lagrange's equations.

First, consider the case where the system configuration is described by a finite set of  $n$  independent generalized coordinates  $q_i$ . All the material points of the system follow

$$\mathbf{x}_i = \mathbf{x}_i(q_1, \dots, q_n; t) \quad (3.17)$$

We also allow an explicit dependency on time  $t$ , which is important for analyzing gyroscopic systems such as rotating machinery. The velocity of the material point  $i$  is given by

$$\dot{\mathbf{x}}_i = \sum_j \frac{\partial \mathbf{x}_i}{\partial q_j} \dot{q}_j + \frac{\partial \mathbf{x}_i}{\partial t} \quad (3.18)$$

where the matrix of partial derivatives  $\partial \mathbf{x}_i / \partial q_j$  has the meaning of a Jacobian. From Equ.(3.18), the kinetic energy can be written in the form

$$T = \frac{1}{2} \sum_i m_i \dot{\mathbf{x}}_i \cdot \dot{\mathbf{x}}_i = T_2 + T_1 + T_0 \quad (3.19)$$

where  $T_2$ ,  $T_1$  and  $T_0$  are respectively homogeneous functions of order 2,1 and 0 in the generalized velocities  $\dot{q}_j$ ; the coefficients of  $T_k$  depend on the partial derivatives  $\partial \mathbf{x}_i / \partial q_j$ , which are themselves functions of the generalized coordinates  $q_j$ . Note that without explicit dependency on  $t$ , the last term in (3.18) disappears and  $T = T_2$  (homogenous quadratic function of  $\dot{q}_j$ ). Being independent of  $\dot{q}_j$ , the term  $T_0$  appears as a potential; it is in general related to centrifugal forces, while the linear term  $T_1$  is responsible for the gyroscopic forces. The general form of the kinetic energy is

$$T = T(q_1, \dots, q_n, \dot{q}_1, \dots, \dot{q}_n; t) \quad (3.20)$$

The potential energy  $V$  does not depend on the velocity; it can be assumed to be of the general form

$$V = V(q_1, \dots, q_n; t) \quad (3.21)$$

From these two equations, it can be assumed that the most general form of the Lagrangian is

$$L = T - V = L(q_1, \dots, q_n, \dot{q}_1, \dots, \dot{q}_n; t) \quad (3.22)$$

Let us now examine the virtual work of the non-conservative forces; expressing the virtual displacement  $\delta \mathbf{x}_i$  in terms of  $\delta q_i$ , one finds

$$\delta W_{nc} = \sum_i \mathbf{F}_i \cdot \delta \mathbf{x}_i = \sum_i \sum_k \mathbf{F}_i \frac{\partial \mathbf{x}_i}{\partial q_k} \delta q_k = \sum_k Q_k \delta q_k \quad (3.23)$$

where

$$Q_k = \sum_i \mathbf{F}_i \frac{\partial \mathbf{x}_i}{\partial q_k} \quad (3.24)$$

$Q_k$  is the generalized force associated with the generalized variable  $q_k$ ; they are energetically conjugate (their product has the dimension of energy). Introducing Equ.(3.23) in Hamilton's principle (3.14), one finds

$$\begin{aligned} \text{V.I.} = \delta I &= \int_{t_1}^{t_2} [\delta L(q_1, \dots, q_n, \dot{q}_1, \dots, \dot{q}_n; t) + \sum Q_i \delta q_i] dt \\ &= \int_{t_1}^{t_2} [\sum_i (\frac{\partial L}{\partial q_i} \delta q_i + \frac{\partial L}{\partial \dot{q}_i} \delta \dot{q}_i) + \sum Q_i \delta q_i] dt \end{aligned}$$

and, upon integrating by part to eliminate  $\delta \dot{q}_i$ , using

$$\frac{\partial L}{\partial \dot{q}_i} \delta \dot{q}_i = \frac{d}{dt} \left( \frac{\partial L}{\partial \dot{q}_i} \delta q_i \right) - \frac{d}{dt} \left( \frac{\partial L}{\partial \dot{q}_i} \right) \delta q_i$$

one finds

$$\delta I = \sum_i [\frac{\delta L}{\delta \dot{q}_i} \delta q_i]_{t_1}^{t_2} - \int_{t_1}^{t_2} \sum_i [\frac{d}{dt} \left( \frac{\partial L}{\partial \dot{q}_i} \delta q_i \right) - \frac{\partial L}{\partial q_i} \delta q_i] dt = 0 \quad (3.25)$$

The first term vanishes because  $\delta q_i(t_1) = \delta q_i(t_2) = 0$ , and since the virtual variations are arbitrary ( $q_i$  are independent), one must have

$$\frac{d}{dt} \left( \frac{\partial L}{\partial \dot{q}_i} \right) - \frac{\partial L}{\partial q_i} = Q_i \quad i = 1, \dots, n \quad (3.26)$$

These are Lagrange's equations, their number is equal to the number  $n$  of independent coordinates. The generalized forces contain all the non-conservative forces; they are obtained from the principle of virtual work (3.23). Once the analytical expression of the Lagrangian in terms of the generalized coordinates has been found, Equ.(3.26) allows us to write the differential equations governing the motion in a straightforward way.

### 3.6.1 Vibration of a linear non-gyroscopic discrete system

The general form of the kinetic energy of a linear non-gyroscopic, discrete mechanical system is

$$T = \frac{1}{2} \dot{\mathbf{x}}^T M \dot{\mathbf{x}} \quad (3.27)$$

where  $\mathbf{x}$  is a set of generalized coordinates, and  $M$  is the mass matrix.  $M$  is symmetric and semi-positive definite, which translates the fact that any velocity distribution must lead to a non-negative value of the kinetic energy;  $M$  is strictly positive definite if all the coordinates have an inertia associated to them, so that it is impossible to find a velocity distribution such that  $T = 0$ . Similarly, the general form of the strain energy is

$$V = \frac{1}{2} \mathbf{x}^T K \mathbf{x} \quad (3.28)$$

where  $K$  is the stiffness matrix, also symmetric and semi-positive definite. A rigid body mode is a set of generalized coordinates with no strain energy in the system.  $K$  is strictly positive definite if the system does not have rigid body modes.

The Lagrangian of the system reads,

$$L = T - V = \frac{1}{2} \dot{\mathbf{x}}^T M \dot{\mathbf{x}} - \frac{1}{2} \mathbf{x}^T K \mathbf{x} \quad (3.29)$$

If, in addition, one assumes that the virtual work of the non-conservative external forces can be written  $\delta W_{nc} = \mathbf{f}^T \delta \mathbf{x}$ , applying the Lagrange equations (3.26), one gets the equation of motion

$$M \ddot{\mathbf{x}} + K \mathbf{x} = \mathbf{f} \quad (3.30)$$

### 3.6.2 Dissipation function

In the literature, it is customary to define the *dissipation function*  $D$  such that the dissipative forces are given by

$$Q_i = -\frac{\partial D}{\partial \dot{q}_i} \quad (3.31)$$

If this definition is used, Equ.(3.26) becomes

$$\frac{d}{dt} \left( \frac{\partial L}{\partial \dot{q}_i} \right) + \frac{\partial D}{\partial \dot{q}_i} - \frac{\partial L}{\partial q_i} = Q_i \quad (3.32)$$

where  $Q_i$  includes all the non-conservative forces which are not already included in the dissipation function. Viscous damping can be represented by a quadratic dissipation function. If one assumes

$$D = \frac{1}{2} \dot{\mathbf{x}}^T C \dot{\mathbf{x}} \quad (3.33)$$

in previous section, one gets the equation of motion

$$M\ddot{\mathbf{x}} + C\dot{\mathbf{x}} + K\mathbf{x} = \mathbf{f} \quad (3.34)$$

where  $C$  is the viscous damping matrix, also symmetric and semi-positive definite. We now examine a few examples of mechanical systems, to illustrate some of the features of the method.

### 3.6.3 Example 1: Pendulum with a sliding mass

Consider the pendulum of Fig.3.6.a where a mass  $m$  slides without friction on a massless rod in a constant gravity field  $g$ ; a linear spring of stiffness  $k$  connects the mass to the pivot  $O$  of the pendulum. This system has two d.o.f. and we select  $q_1$  (position of the mass along the bar) and  $q_2$  (angle of the pendulum) as the generalized coordinates. It is assumed that, when  $q_1 = 0$ , the spring force vanishes.

The kinetic energy is associated with the point mass  $m$ ; its velocity can be expressed in two orthogonal directions as in Fig.3.6.b; it follows that

$$T = \frac{1}{2}m(\dot{q}_1^2 + \dot{q}_2^2 q_1^2)$$

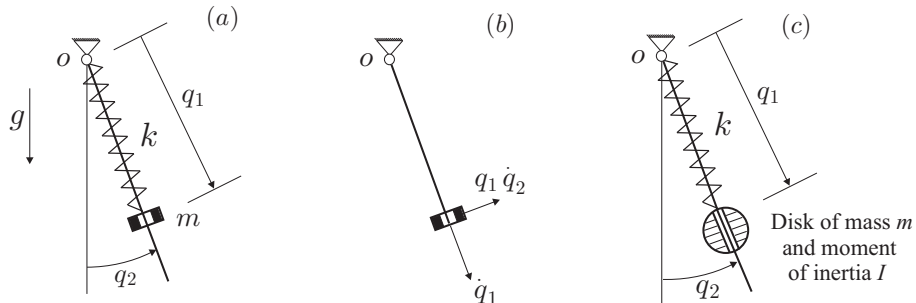


**Fig. 3.6.** Pendulum with a sliding mass attached with a spring. (a) and (b): Point mass. (c) Disk.

The potential energy reads

$$V = -m g q_1 \cos q_2 + \frac{1}{2} k q_1^2$$

The first contribution comes from gravity (the reference altitude has been taken at the pivot  $O$ ) and the second one is the strain energy in the spring (assumed unstretched when  $q_1 = 0$ ). The Lagrange equations are

$$\begin{aligned} \frac{d}{dt}(m q_1^2 \dot{q}_2) + m g q_1 \sin q_2 &= 0 \\ m \ddot{q}_1 - m q_1 \dot{q}_2^2 - m g \cos q_2 + k q_1 &= 0 \end{aligned}$$

If one assumes that the mass  $m$  is no longer a point mass, but a disk of moment of inertia  $I$  sliding along the massless rod [Fig.3.6.c], it contributes with an extra term to the kinetic energy, representing the kinetic energy of rotation of the disk (the kinetic energy of a rigid body is the sum of the kinetic energy of translation of the total mass lumped at the center of mass and the kinetic energy of rotation around the center of mass):

$$T = \frac{1}{2}m(\dot{q}_1^2 + \dot{q}_2^2 q_1^2) + \frac{1}{2}I\dot{q}_2^2$$

The disk has the same potential energy as the point mass. Furthermore, if the rod is uniform with a total mass  $M$  and a length  $l$ , its moment of inertia with respect to the pivot is

$$I_o = \int_0^l \varrho x^2 dx = \varrho l^3 / 3 = Ml^2 / 3$$

( $M = \varrho l$ ); the additional contribution to the kinetic energy is  $I_o \dot{q}_2^2 / 2$ . Note that, this includes the translational energy as well as the rotational energy of the rod, because the moment of inertia  $I_o$  refers to the fixed point at the pivot. The rod has also an additional contribution to the potential energy:  $-M g (l/2) \cos q_2$  (the center of mass is at mid length).

### 3.6.4 Example 2: Rotating pendulum

Consider the rotating pendulum of Figure 3.7.a. The point mass  $m$  is connected by a massless rod to a pivot which rotates about a vertical axis at constant velocity  $\Omega$ ; the system is in a vertical gravity field  $g$ . Because  $\Omega$  is constant, the system has a single d.o.f., with coordinate  $\theta$ . In order to write the kinetic energy, it is convenient to project the velocity

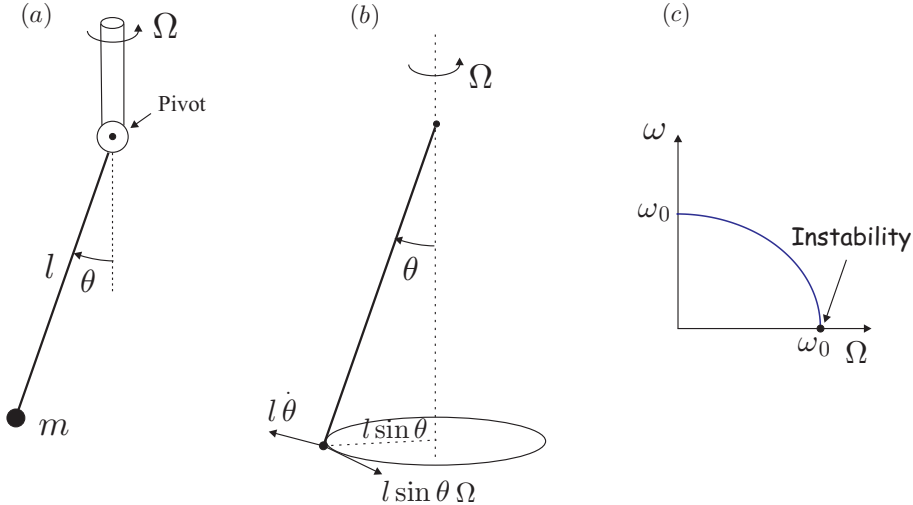


**Fig. 3.7.** Rotating pendulum.

of the point mass in the orthogonal frame shown in Fig.3.7.b. One axis is tangent to the circular trajectory when the pendulum rotates about the vertical axis with \$\theta\$ fixed, while the other one is tangent to the trajectory of the mass in the plane of the pendulum when it does not rotate about the vertical axis; the projected components are respectively \$l\Omega \sin \theta\$ and \$l\dot{\theta}\$. Being orthogonal, it follows that

$$T = \frac{m}{2} [(l\dot{\theta})^2 + (l\Omega \sin \theta)^2]$$

Note that the first term is quadratic in \$\dot{\theta}\$ [\${T}\_2\$ in (3.19)], while the second term is independent of \$\dot{\theta}\$ and appears as a potential of centrifugal forces [\${T}\_0\$ in (3.19)]. Taking the reference altitude at the pivot, the gravity potential is \$V = -gml \cos \theta\$ and

$$L = T - V = \frac{m}{2} [(l\dot{\theta})^2 + (l\Omega \sin \theta)^2] + gml \cos \theta$$

The corresponding Lagrange equation reads

$$ml^2\ddot{\theta} - ml^2\Omega^2 \sin \theta \cos \theta + mgl \sin \theta = 0$$

For small oscillations near \$\theta = 0\$, the equation can be simplified using the approximations \$\sin \theta \simeq \theta\$ and \$\cos \theta = 1\$; this leads to

$$\ddot{\theta} + \frac{g}{l}\theta - \Omega^2\theta = 0$$

Introducing  $\omega_0^2 = \frac{g}{l}$ , the pendulum frequency

$$\ddot{\theta} + (\omega_0^2 - \Omega^2) \theta = 0$$

One sees that the centrifugal force introduces a negative stiffness. Figure 3.7.c shows the evolution of the frequency of the small oscillations of the pendulum with  $\Omega$ ; the eigenvalues are solutions of the characteristic equation  $s^2 + (\omega_0^2 - \Omega^2) = 0$ ; the system is unstable beyond  $\Omega = \omega_0$ .

### 3.6.5 Example 3: Rotating spring mass system

A spring mass system is rotating in the horizontal plane at a constant velocity  $\Omega$ , Fig.3.8.a. The system has a single d.o.f., described by the coordinate  $u$  measuring the extension of the spring. The absolute velocity of the point mass  $m$  can be conveniently projected in the moving frame  $(x, y)$ ; the components are  $(\dot{u}, u\Omega)$ . It follows that

$$T = \frac{1}{2}m [\dot{u}^2 + (u\Omega)^2]$$

Once again, there is a quadratic contribution,  $T_2$ , and a contribution independent of the generalized velocity,  $T_0$  (potential of centrifugal force). It is not necessary to include the kinetic energy of the rotating mechanism, because it is constant, and will disappear when writing the Lagrange equation. Since the system is not subjected to gravity, the potential energy is associated with the extension of the spring; assuming that the spring force is equal to zero when  $u = 0$ ,

$$V = \frac{1}{2}ku^2$$

The Lagrangian reads

$$L = T - V = \frac{1}{2}m\dot{u}^2 - \frac{1}{2}(k - m\Omega^2)u^2$$

leading to the Lagrange equation

$$m\ddot{u} + (k - m\Omega^2)u = 0$$

or

$$\ddot{u} + (\omega_n^2 - \Omega^2)u = 0$$

after introducing  $\omega_n^2 = k/m$ . This equation is identical to the linearized form of the previous example; the eigenvalues are solutions of the characteristic equation  $s^2 + (\omega_n^2 - \Omega^2) = 0$ ; the system becomes unstable for  $\Omega > \omega_n$ .

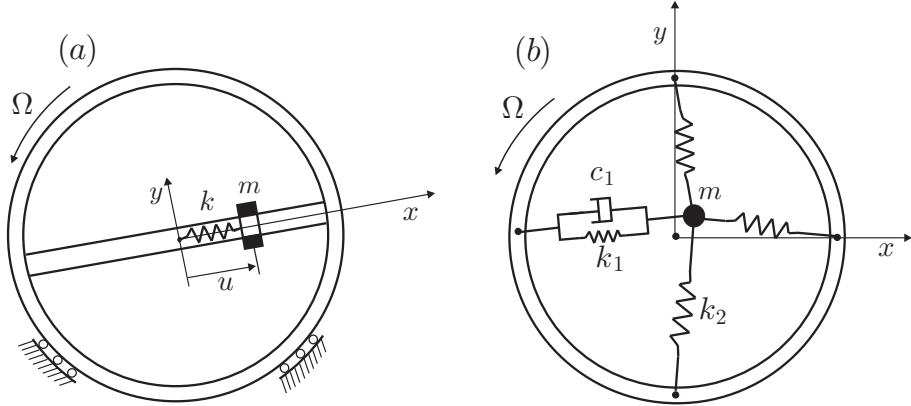


**Fig. 3.8.** Rotating spring-mass systems (a) Single axis (b) Two-axis with anisotropic stiffness. The frame  $Oxy$  is rotating at  $\Omega$ .

### 3.6.6 Example 4: Gyroscopic effects

Next, consider the system of Fig. 3.8.b, where the constraint along  $y = 0$  has been removed and replaced by another spring orthogonal to the previous one. This system has 2 d.o.f. with a stiffness  $k_1$  along  $Ox$  and  $k_2$  along  $Oy$ ;<sup>1</sup> it is fully described by the generalized coordinates  $x$  and  $y$ , the displacements along the moving axes rotating at constant speed  $\Omega$ . We assume small displacements and, in Fig. 3.8.b, the stiffness  $k_1$  and  $k_2$  represent the global stiffness along  $x$  and  $y$ , respectively. We assume viscous damping along  $x$ , with damping coefficient  $c_1$ . The absolute velocity in the rotating frame is  $(\dot{x} - \Omega y, \dot{y} + \Omega x)$ , leading to the kinetic energy of the point mass

$$T = \frac{1}{2}m [(\dot{x} - \Omega y)^2 + (\dot{y} + \Omega x)^2] \quad (3.35)$$

As in the previous example, we disregard the constant term associated with the rotation at constant speed of the supporting mechanism. Upon

<sup>1</sup> This system is in fact a model of the Jeffcott rotor with an anisotropic shaft; it will be reexamined in chapter 10.

expanding  $T$ , one gets

$$T = T_2 + T_1 + T_0$$

with

$$\begin{aligned} T_2 &= \frac{1}{2}m(\dot{x}^2 + \dot{y}^2) \\ T_1 &= m\Omega(x\dot{y} - \dot{x}y) \\ T_0 &= \frac{1}{2}m\Omega^2(x^2 + y^2) \end{aligned}$$

Note that a contribution  $T_1$  of the first order in the generalized velocities appears for the first time; it will be responsible for gyroscopic forces [the system of Fig.3.8.b is actually the simplest, where gyroscopic forces can be illustrated]. The potential  $V$  is associated with the extension of the springs; with the assumption of small displacements,

$$V = \frac{1}{2}k_1x^2 + \frac{1}{2}k_2y^2$$

The damping force can be handled either by the virtual work,  $\delta W_{nc} = -c_1\dot{x}\delta x$  or with the dissipation function (3.33). In this case,

$$D = \frac{1}{2}c_1\dot{x}^2$$

The Lagrange equations read

$$m\ddot{x} - 2m\Omega\dot{y} + c_1\dot{x} + k_1x - m\Omega^2x = 0$$

$$m\ddot{y} + 2m\Omega\dot{x} + k_2y - m\Omega^2y = 0$$

or, in matrix form, with  $\mathbf{q} = (x, y)^T$ ,

$$M\ddot{\mathbf{q}} + (C + G)\dot{\mathbf{q}} + (K - \Omega^2M)\mathbf{q} = 0 \quad (3.36)$$

where

$$M = \begin{bmatrix} m & 0 \\ 0 & m \end{bmatrix} \quad C = \begin{bmatrix} c_1 & 0 \\ 0 & 0 \end{bmatrix} \quad K = \begin{bmatrix} k_1 & 0 \\ 0 & k_2 \end{bmatrix}$$

are respectively the mass, damping and stiffness matrices, and

$$G = \begin{bmatrix} 0 & -2m\Omega \\ 2m\Omega & 0 \end{bmatrix} \quad (3.37)$$

is the anti-symmetric matrix of gyroscopic forces, which couples the motion in the two directions; its magnitude is proportional to the inertia ( $m$ )

and to the rotating speed  $\Omega$ . The contribution  $-\Omega^2 M$  is, once again, the centrifugal force. Note that, with the previous definitions of the matrices  $M, G, K$  and  $C$ , the various energy terms appearing in the Lagrangian can be written

$$\begin{aligned} T_2 &= \frac{1}{2} \dot{\mathbf{q}}^T M \dot{\mathbf{q}} \\ T_1 &= \frac{1}{2} \dot{\mathbf{q}}^T G \mathbf{q} \\ T_0 &= \frac{\Omega^2}{2} \mathbf{q}^T M \mathbf{q} \\ V &= \frac{1}{2} \mathbf{q}^T K \mathbf{q} \\ D &= \frac{1}{2} \dot{\mathbf{q}}^T C \dot{\mathbf{q}} \end{aligned}$$

Note that the modified potential

$$V^+ = V - T_0 = \frac{1}{2} \mathbf{q}^T (K - \Omega^2 M) \mathbf{q} \quad (3.38)$$

is no longer positive definite if  $\Omega^2 > k_1/m$  or  $k_2/m$ .

Let us examine this system a little further, in the particular case where  $k_1 = k_2 = k$  and  $c_1 = 0$ . If  $\omega_n^2 = k/m$ , the equations of motion become

$$\begin{aligned} \ddot{x} - 2\Omega \dot{y} + (\omega_n^2 - \Omega^2) x &= 0 \\ \ddot{y} + 2\Omega \dot{x} + (\omega_n^2 - \Omega^2) y &= 0 \end{aligned}$$

To analyze the stability of the system, let us assume a solution of the form  $x = X e^{st}$ ,  $y = Y e^{st}$ ; the corresponding eigenvalue problem is

$$\begin{bmatrix} s^2 + \omega_n^2 - \Omega^2 & -2\Omega s \\ 2\Omega s & s^2 + \omega_n^2 - \Omega^2 \end{bmatrix} \begin{Bmatrix} X \\ Y \end{Bmatrix} = 0$$

Nontrivial solutions of this homogenous system of equations require that the determinant be zero, leading to the characteristic equation

$$s^4 + 2s^2(\omega_n^2 + \Omega^2) + (\omega_n^2 - \Omega^2)^2 = 0$$

The roots of this equation are

$$s_1^2 = -(\omega_n - \Omega)^2, \quad s_2^2 = -(\omega_n + \Omega)^2$$

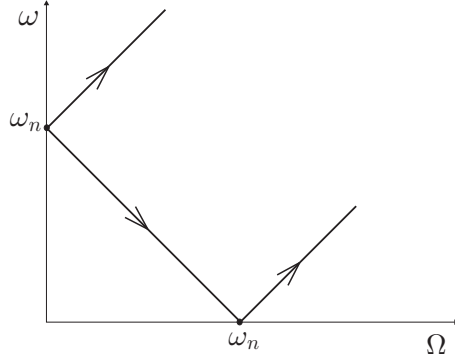


**Fig. 3.9.** Campbell diagram of the system of Fig.3.8.b, in the particular case  $k_1 = k_2$  and  $c_1 = 0$ .

Thus, the eigenvalues are all imaginary, for all values of  $\Omega$ . Figure 3.9 shows the evolution of the natural frequencies with  $\Omega$  (this plot is called *Campbell diagram*). We note that, in contrast with the previous example, the system does not become unstable beyond  $\Omega = \omega_n$ ; it is stabilized by the gyroscopic forces.

### 3.7 Lagrange's equations with constraints

Consider the case where the  $n$  generalized coordinates are not independent. In this case, the virtual changes of configuration  $\delta q_k$  must satisfy a set of  $m$  constraint equations of the form of Equ.(3.6):

$$\sum_k a_{lk} \delta q_k = 0 \quad l = 1, \dots, m \quad (3.39)$$

The number of degrees of freedom of the system is  $n - m$ . In Hamilton's principle (3.25), the variations  $\delta q_i$  are no longer arbitrary, because of Equ.(3.39), and the step leading from Equ.(3.25) to (3.26) is impossible. This difficulty can be solved by using *Lagrange multipliers*. The technique consists of adding to the variational indicator a linear combination of the constraint equations

$$\sum_{l=1}^m \lambda_l \left( \sum_{k=1}^n a_{lk} \delta q_k \right) = \sum_{k=1}^n \delta q_k \left( \sum_{l=1}^m \lambda_l a_{lk} \right) = 0 \quad (3.40)$$

where the Lagrange multipliers  $\lambda_l$  are unknown at this stage. Equation (3.40) is true for any set of  $\lambda_l$ . Adding to Equ.(3.25), one gets

$$\int_{t_1}^{t_2} \sum_{k=1}^n \left[ \frac{d}{dt} \left( \frac{\partial L}{\partial \dot{q}_k} \right) - \frac{\partial L}{\partial q_k} - Q_k - \sum_{l=1}^m \lambda_l a_{lk} \right] \delta q_k dt = 0$$

In this equation,  $n - m$  variations  $\delta q_k$  can be taken arbitrarily (the independent variables) and the corresponding expressions between brackets must vanish; the  $m$  terms left in the sum do not have independent variations  $\delta q_k$ , but we are free to select the  $m$  Lagrange multipliers  $\lambda_l$  to cancel them too. Overall, one gets

$$\frac{d}{dt} \left( \frac{\partial L}{\partial \dot{q}_k} \right) - \frac{\partial L}{\partial q_k} = Q_k + \sum_{l=1}^m \lambda_l a_{lk} \quad k = 1, \dots, n$$

The second term in the right hand side represents the generalized constraint forces, which are linear functions of the Lagrange multipliers. This set of  $n$  equations has  $n + m$  unknown (the generalized coordinates  $q_k$  and the Lagrange multipliers  $\lambda_l$ ). Combining with the  $m$  constraints equations, we obtain a set of  $n + m$  equations. For non-holonomic constraints of the form (3.3), the equations read

$$\sum_k a_{lk} dq_k + a_{l0} dt \quad l = 1, \dots, m \quad (3.41)$$

$$\frac{d}{dt} \left( \frac{\partial L}{\partial \dot{q}_k} \right) - \frac{\partial L}{\partial q_k} = Q_k + \sum_{l=1}^m \lambda_l a_{lk} \quad k = 1, \dots, n \quad (3.42)$$

with the unknown  $q_k, k = 1, \dots, n$  and  $\lambda_l, l = 1, \dots, m$ . If the system is holonomic, with constraints of the form (3.1), the equations become

$$g_l(q_1, q_2, \dots, q_n; t) = 0 \quad l = 1, \dots, m \quad (3.43)$$

$$\frac{d}{dt} \left( \frac{\partial L}{\partial \dot{q}_k} \right) - \frac{\partial L}{\partial q_k} = Q_k + \sum_{l=1}^m \lambda_l \frac{\partial g_l}{\partial q_k} \quad k = 1, \dots, n \quad (3.44)$$

This is a system of *algebro-differential* equations. This formulation is frequently met in multi-body dynamics.

## 3.8 Conservation laws

### 3.8.1 Jacobi integral

If the generalized coordinates are independent, the Lagrange equations constitute a set of  $n$  differential equations of the second order; their solution requires  $2n$  initial conditions describing the configuration and the

velocity at  $t = 0$ . In special circumstances, the system admits first integrals of the motion, which contain derivatives of the variables of one order lower than the order of the differential equations. The most celebrated of these first integrals is that of conservation of energy (3.11); it is a particular case of a more general relationship known as a *Jacobi integral*.

If the system is conservative ( $Q_k = 0$ ) and if the Lagrangian does not depend explicitly on time,

$$\frac{\partial L}{\partial t} = 0 \quad (3.45)$$

The total derivative of  $L$  with respect to time reads

$$\frac{dL}{dt} = \sum_{k=1}^n \frac{\partial L}{\partial q_k} \dot{q}_k + \sum_{k=1}^n \frac{\partial L}{\partial \dot{q}_k} \ddot{q}_k$$

On the other hand, from the Lagrange's equations (taking into account that  $Q_k = 0$ )

$$\frac{\partial L}{\partial q_k} = \frac{d}{dt} \left( \frac{\partial L}{\partial \dot{q}_k} \right)$$

Substituting into the previous equation, one gets

$$\frac{dL}{dt} = \sum_{k=1}^n \left[ \frac{d}{dt} \left( \frac{\partial L}{\partial \dot{q}_k} \right) \dot{q}_k + \frac{\partial L}{\partial \dot{q}_k} \ddot{q}_k \right] = \sum_{k=1}^n \frac{d}{dt} \left[ \left( \frac{\partial L}{\partial \dot{q}_k} \right) \dot{q}_k \right]$$

It follows that

$$\frac{d}{dt} \left[ \sum_{k=1}^n \left( \frac{\partial L}{\partial \dot{q}_k} \right) \dot{q}_k - L \right] = 0 \quad (3.46)$$

or

$$\sum_{k=1}^n \left( \frac{\partial L}{\partial \dot{q}_k} \right) \dot{q}_k - L = h = C^t \quad (3.47)$$

Recall that the Lagrangian reads

$$L = T - V = T_2 + T_1 + T_0 - V \quad (3.48)$$

where  $T_2$  is a homogenous quadratic function of  $\dot{q}_k$ ,  $T_1$  is homogenous linear in  $\dot{q}_k$ , and  $T_0$  and  $V$  do not depend on  $\dot{q}_k$ .

According to Euler's *theorem on homogeneous functions*, if  $T_n(x_i)$  is an homogeneous function of order  $n$  in some variables  $x_i$ , it satisfies the identity

$$\sum x_i \frac{\partial T_n(x_i)}{\partial x_i} = nT_n(x_i) \quad (3.49)$$

It follows from this theorem that

$$\sum \dot{q}_i \frac{\partial T_n}{\partial \dot{q}_i} = nT_n$$

and

$$\sum \left( \frac{\partial L}{\partial \dot{q}_k} \right) \dot{q}_k = \sum \left[ \frac{\partial (T_2 + T_1 + T_0)}{\partial \dot{q}_k} \right] \dot{q}_k = 2T_2 + T_1$$

and (3.47) can be rewritten

$$h = T_2 - T_0 + V = C^t \quad (3.50)$$

This result is known as the *Jacobi integral*, or also the *Painlevé integral*. If the kinetic energy is a homogeneous quadratic function of the velocity,  $T = T_2$  and  $T_0 = 0$ ; Equ.(3.50) becomes

$$T + V = C^t \quad (3.51)$$

which is the integral of *conservation of energy*. From the above discussion, it follows that it applies to conservative systems whose Lagrangian does not depend explicitly on time [Equ.(3.45)] and whose kinetic energy is a homogeneous quadratic function of the generalized velocities ( $T = T_2$ ). We have met this equation earlier [Equ.(3.11)], and it is interesting to relate the above conditions to the earlier ones: Indeed, (3.45) implies that the potential does not depend explicitly on  $t$ , and  $T = T_2$  implies that the kinematical constraints do not depend explicitly on  $t$  [see (3.18) and (3.19)].

### 3.8.2 Ignorable coordinate

Another first integral can be obtained if a generalized coordinate (say  $q_s$ ) does not appear explicitly in the Lagrangian of a conservative system (the Lagrangian contains  $\dot{q}_s$  but not  $q_s$ , so that  $\partial L / \partial q_s = 0$ ). Such a coordinate is called *ignorable*. From Lagrange's equation (3.26),

$$\frac{d}{dt} \left( \frac{\partial L}{\partial \dot{q}_s} \right) = \frac{\partial L}{\partial q_s} = 0$$

It follows that

$$p_s = \frac{\partial L}{\partial \dot{q}_s} = C^t$$

and, since  $V$  does not depend explicitly on the velocities, this can be rewritten

$$p_s = \frac{\partial L}{\partial \dot{q}_s} = \frac{\partial T}{\partial \dot{q}_s} = C^t \quad (3.52)$$

$p_s$  is the *generalized momentum conjugate to  $q_s$* .<sup>2</sup> Thus, *the generalized momentum associated with an ignorable coordinate is conserved*.

Note that the existence of the first integral (3.52) depends very much on the choice of coordinates, and that it may remain hidden if inappropriate coordinates are used. The ignorable coordinates are also called *cyclic*, because they often happen to be rotational coordinates.

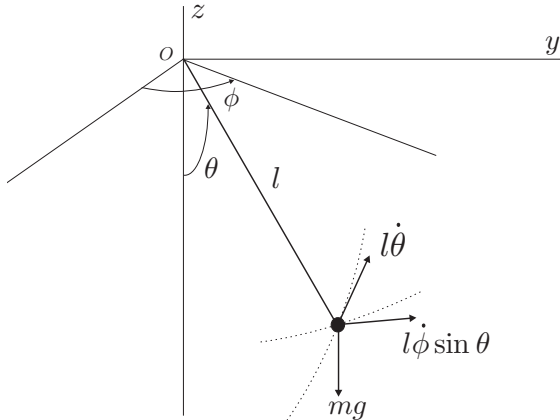


**Fig. 3.10.** The spherical pendulum.

---

<sup>2</sup> by analogy with the relation between the linear momentum,  $p = mv$ , with the kinetic energy,  $T = \frac{1}{2}mv^2$ , of a point mass:  $p = dT/dv$ .

### 3.8.3 Example: The spherical pendulum

To illustrate the previous paragraph, consider the spherical pendulum of Fig.3.10. Its configuration is entirely characterized by the two generalized coordinates  $\theta$  and  $\phi$ . the kinetic energy and the potential energy are respectively

$$T = \frac{1}{2}m[(l\dot{\theta})^2 + (\dot{\phi}l \sin \theta)^2]$$

$$V = -mgl \cos \theta$$

and the Lagrangian reads

$$L = T - V = \frac{1}{2}ml^2[\dot{\theta}^2 + (\dot{\phi} \sin \theta)^2] + mgl \cos \theta$$

The Lagrangian does not depend explicitly on  $t$ , nor on the coordinate  $\phi$ . The system is therefore eligible for the two first integrals discussed above. Since the kinetic energy is homogeneous quadratic in  $\dot{\theta}$  and  $\dot{\phi}$ , the conservation of energy (3.51) applies.

As for the ignorable coordinate  $\phi$ , the conjugate generalized momentum is

$$p_\phi = \partial T / \partial \dot{\phi} = ml^2 \dot{\phi} \sin^2 \theta = C$$

This equation simply states the conservation of the angular momentum about the vertical axis  $Oz$  (indeed, the moments about  $Oz$  of the external forces from the cable of the pendulum and the gravity vanish).

## 3.9 Prestresses, geometric strain energy

When a structure is prestressed, its natural frequencies are subject to changes. For example, the centrifugal force is a significant contributor to the total stiffness of an helicopter rotor blade and, similarly, large civil engineering structures have their natural frequencies lowered by the compression stresses due to the dead loads.<sup>3</sup> The tuning of a guitar string is done by adjusting its prestress. The prestresses are responsible of an additional contribution to the strain energy called the *geometric* strain energy. Its evaluation, however, is not easy and requires the introduction of the *Green strain tensor*.

---

<sup>3</sup> This is sometimes called the “P-Delta” effect.

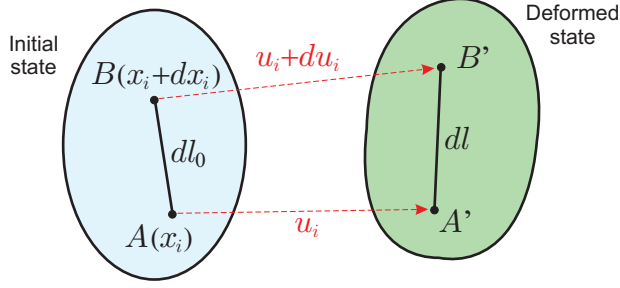


**Fig. 3.11.** Elastic body in the initial state and after deformation.

### 3.9.1 Green strain tensor

Consider the segment joining two points  $A : x_i$  and  $B : x_i + dx_i$  in the initial configuration (Fig. 3.11); the two points move to the position  $A' : x_i + u_i$  and  $B' : x_i + u_i + d(x_i + u_i)$  in the deformed configuration. If  $dl_0$  is the initial length of  $AB$  and  $dl$  the length of  $A'B'$ , the difference  $dl^2 - dl_0^2$  is

$$dl^2 - dl_0^2 = d(x_i + u_i)d(x_i + u_i) - dx_i \, dx_i$$

and, expanding  $du_i$  according to

$$du_i = \frac{\partial u_i}{\partial x_j} dx_j$$

it is readily established that

$$dl^2 - dl_0^2 = \left( \frac{\partial u_i}{\partial x_j} + \frac{\partial u_j}{\partial x_i} + \frac{\partial u_m}{\partial x_i} \frac{\partial u_m}{\partial x_j} \right) dx_i dx_j \quad (3.53)$$

The Green strain tensor is defined as

$$\varepsilon_{ij} = \frac{1}{2} \left( \frac{\partial u_i}{\partial x_j} + \frac{\partial u_j}{\partial x_i} + \frac{\partial u_m}{\partial x_i} \frac{\partial u_m}{\partial x_j} \right) \quad (3.54)$$

It is symmetric, and its linear part is the classical strain measure in linear elasticity; there is an additional quadratic part which accounts for large rotations.<sup>4</sup> Comparing the foregoing equations,

$$dl^2 - dl_0^2 = 2\varepsilon_{ij} dx_i dx_j \quad (3.55)$$

which shows that if  $\varepsilon_{ij} = 0$ , the length of the segment is indeed unchanged, even for large  $u_i$ . The Green strain tensor can be partitioned according to

---

<sup>4</sup> The sum is intended on the repeated index  $m$ .

$$\varepsilon_{ij} = \varepsilon_{ij}^{(1)} + \varepsilon_{ij}^{(2)} \quad (3.56)$$

where  $\varepsilon_{ij}^{(1)}$  is linear in the displacements, and  $\varepsilon_{ij}^{(2)}$  is quadratic.

To illustrate the Green tensor, let us examine the case of a straight bar (Fig.3.12.a) in the plane; the displacement field is  $u(x), v(x)$ . The Green strain measure  $\varepsilon_{xx}$  is given by

$$\varepsilon_{xx} = \frac{du}{dx} + \frac{1}{2}[(\frac{du}{dx})^2 + (\frac{dv}{dx})^2] \quad (3.57)$$

If the bar is subjected to a global rotation as a rigid body (Fig.3.12.b),

$$u(x) = -2x \sin \frac{\alpha}{2} \sin \frac{\alpha}{2} \quad v(x) = 2x \sin \frac{\alpha}{2} \cos \frac{\alpha}{2}$$

and

$$\varepsilon_{xx} = \frac{du}{dx} + \frac{1}{2}[(\frac{du}{dx})^2 + (\frac{dv}{dx})^2] = -2 \sin^2 \frac{\alpha}{2} + 2 \sin^4 \frac{\alpha}{2} + 2 \sin^2 \frac{\alpha}{2} \cos^2 \frac{\alpha}{2} = 0$$

Thus, there is no strain (in the sense of Green) associated with the rigid body rotation, which is what one expects; the linear part alone (first term) is different from 0 for finite  $\alpha$ .

If the axial deformations remain small with respect to the rotations,

$$\frac{du}{dx} \ll 1 \quad \text{and} \quad \frac{du}{dx} \ll \frac{dv}{dx}$$

Then, Equ.(3.57) can be simplified into

$$\varepsilon_{xx} \simeq \frac{du}{dx} + \frac{1}{2}(\frac{dv}{dx})^2 \quad (3.58)$$

This assumption is frequently done in nonlinear analysis: it accounts for the large rotations while assuming that the strains remain small.

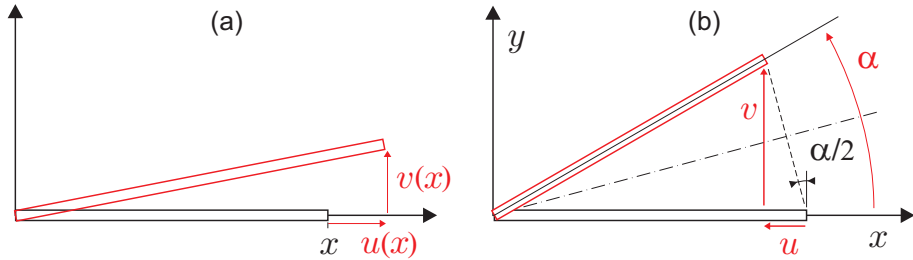


**Fig. 3.12.** (a) Bar deformed in the plane, including transverse displacements. (b) Bar subjected to a large rotation as a rigid body in the plane.

### 3.9.2 Geometric strain energy due to prestress

The constitutive equations of a linear elastic material are

$$\sigma_{ij} = c_{ijkl} \varepsilon_{kl} \quad (3.59)$$

where  $c_{ijkl}$  is the tensor of elastic constants. The strain energy density reads

$$U(\varepsilon_{ij}) = \int_0^{\varepsilon_{ij}} \sigma_{ij} d\varepsilon_{ij} \quad (3.60)$$

from which the constitutive equation may be rewritten

$$\sigma_{ij} = \frac{\partial U}{\partial \varepsilon_{ij}} \quad (3.61)$$

For a linear elastic material

$$U(\varepsilon_{ij}) = \frac{1}{2} c_{ijkl} \varepsilon_{ij} \varepsilon_{kl} \quad (3.62)$$

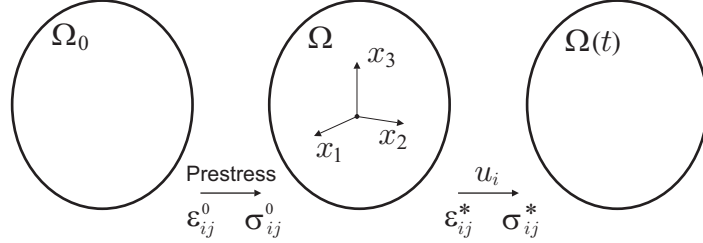


**Fig. 3.13.** Continuous system in a prestressed state.

Next, consider a continuous system in a prestressed state  $(\sigma_{ij}^0, \varepsilon_{ij}^0)$  independent of time, and then subjected to a dynamic motion involving additional stresses and strains  $(\sigma_{ij}^*, \varepsilon_{ij}^*)$ . The total stress and strain state is (Fig. 3.13)

$$\begin{aligned} \varepsilon_{ij} &= \varepsilon_{ij}^0 + \varepsilon_{ij}^* \\ \sigma_{ij} &= \sigma_{ij}^0 + \sigma_{ij}^* \end{aligned} \quad (3.63)$$

It is impossible to account for the strain energy associated with the pre-stress if the linear strain tensor is used. If the Green tensor is used,

$$\varepsilon_{ij}^* = \varepsilon_{ij}^{*(1)} + \varepsilon_{ij}^{*(2)} \quad (3.64)$$

it can be shown<sup>5</sup> that the strain energy can be written

$$V = V^* + V_g \quad (3.65)$$

where

$$V^* = \frac{1}{2} \int_{\Omega^*} c_{ijkl} \varepsilon_{ij}^* {}^{(1)} \varepsilon_{kl}^* {}^{(1)} d\Omega \quad (3.66)$$

is the additional strain energy due to the linear part of the deformation beyond the prestress (it is the unique term if there is no prestress), and

$$V_g = \int_{\Omega^*} \sigma_{ij}^0 \varepsilon_{ij}^* {}^{(2)} d\Omega \quad (3.67)$$

is the *geometric strain energy due to prestress* involving the prestressed state  $\sigma_{ij}^0$  and the quadratic part of the strain tensor. Unlike  $V^*$  which is always positive,  $V_g$  may be positive or negative, depending on the sign of the prestress. If  $V_g$  is positive, it tends to rigidify the system and to increase the resonance frequencies, as in the case of the centrifugal force in a rotor blade; the geometric strain energy softens the structure if it is negative, reducing the resonance frequencies, as in the case of the compression stresses due to the gravity loads in civil engineering structure. For a discrete system,  $V_g$  takes the general form of a quadratic function of the generalized coordinates describing the dynamic motion (we will see examples in later chapters)

$$V_g = \frac{1}{2} \mathbf{x}^T K_g \mathbf{x} \quad (3.68)$$

where  $K_g$  is the *geometric stiffness matrix*, no longer positive definite since  $V_g$  may be negative. If the geometric strain energy is included in the Lagrangian,

$$L = T - (V + V_g) = \frac{1}{2} \dot{\mathbf{x}}^T M \dot{\mathbf{x}} - \frac{1}{2} \mathbf{x}^T K \mathbf{x} - \frac{1}{2} \mathbf{x}^T K_g \mathbf{x} \quad (3.69)$$

applying the Lagrange equations (3.26), one gets the equation of motion

$$M \ddot{\mathbf{x}} + (K + K_g) \mathbf{x} = \mathbf{f} \quad (3.70)$$

Once again, it must be stressed that  $K_g$  is not positive definite and the geometric stiffness may either increase or decrease the resonance frequency of the structure, depending on the nature of the prestress. The natural frequencies are solutions of the eigenvalue problem

$$[(K + K_g) - \omega^2 M] \boldsymbol{\phi} = 0 \quad (3.71)$$

---

<sup>5</sup> see (Geradin & Rixen, 1997, p.149-152)

### 3.9.3 Buckling

The *buckling* occurs when the smallest natural frequency is reduced to  $\omega = 0$ . If a structure is subjected to a static loading  $\mathbf{f}_0$  leading to a prestress state  $\sigma_{ij}^0$  and a geometric stiffness matrix  $K_g(\sigma_{ij}^0)$ ; a proportional loading  $\lambda\mathbf{f}_0$  will lead to the stress state  $\lambda\sigma_{ij}^0$  and, according to Equ.(3.67), to a geometric stiffness matrix

$$K_g(\lambda\sigma_{ij}^0) = \lambda K_g(\sigma_{ij}^0)$$

The solution  $\lambda$  of the eigenvalue problem (corresponding to  $\omega = 0$ )

$$[K + \lambda K_g]\phi = 0 \quad (3.72)$$

gives the critical buckling amplification factor  $\lambda$  for the static load distribution defined by  $\mathbf{f}_0$ , and  $\phi$  is the corresponding buckling mode. A different load distribution  $\mathbf{f}_0$  will lead to a different amplification factor  $\lambda$  and a different buckling mode  $\phi$ .

### 3.10 Negative stiffness

The mechanism of Fig.3.14 is used to reduce the natural frequency of a spring-mass system in vibration isolation. The mass  $m$  is loaded laterally by a pair of loads  $P$  transmitted by the two bars  $AB$  and  $AC$  of length  $l$ ; the bars are horizontal in the equilibrium position and the two forces  $P$  act horizontally at  $B$  and  $C$  as indicated in the figure. The stiffness  $F/x$  of the mechanism near the equilibrium point may be evaluated by expressing the static equilibrium of point  $A$  with the theorem of virtual work. Considering the deformed configuration (Fig.3.14.b), it is easily established that

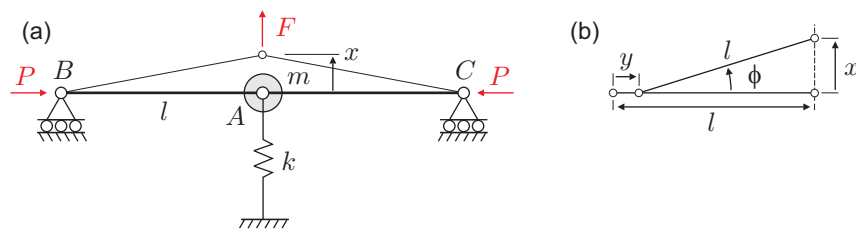


**Fig. 3.14.** (a) Mechanism used to reduce the stiffness of a spring  $k$ . (b) Deformed configuration.

$$y = l - \sqrt{l^2 - x^2}$$

leading to

$$\frac{dy}{dx} = \frac{x}{\sqrt{l^2 - x^2}}$$

It follows that the relationship between the virtual displacements  $\delta y$  and  $\delta x$  is

$$\delta y = \frac{x}{\sqrt{l^2 - x^2}} \delta x$$

Using the theorem of virtual work, the static equilibrium of point  $A$  is expressed by

$$2P.\delta y + F.\delta x - kx.\delta x = 0$$

or

$$\frac{2Px}{\sqrt{l^2 - x^2}} + F - kx = 0$$

Thus,

$$\frac{F}{x} = k - \frac{2P}{\sqrt{l^2 - x^2}}$$

and the static stiffness about the equilibrium point  $x = 0$  is

$$\left\{ \frac{F}{x} \right\}_{x=0} = k - \frac{2P}{l}$$

It follows that the natural frequency of the mechanism is

$$\omega_n = \sqrt{\frac{k}{m} - \frac{2P}{ml}}$$

### 3.11 Problems

**P.3.1** Assuming small displacements, write the equation governing the dynamics of the suspended mass of Fig.3.15. The spring is assumed to be unstressed for  $x = 0$ .

**P.3.2** Write the Lagrange equation governing the system of Fig.1.12.

**P.3.3** Write the Lagrange equations governing the system of Fig.2.1.

**P.3.4** Write the Lagrange equations governing the system of Fig.2.2.a.

**P.3.5** Write the Lagrangian of the system of Fig.2.13, for the various boundary conditions mentioned in problem 2.2.

**P.3.6** Write the Lagrangian for the small oscillations of the system of Fig.2.15.

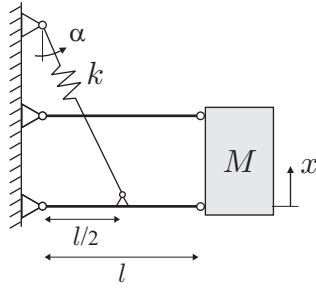


**Fig. 3.15.** Suspended mass (the angle  $\alpha$  may be assumed constant for small oscillations).

**P.3.7** Write the Lagrangian of the motion amplification mechanism of Fig.3.16; the system has two masses  $m_1$  and  $m_2$  placed as indicated in the figure, and the mass  $m_2$  is connected to a spring of stiffness  $k$  (assumed unstretched in the reference configuration). Evaluate the natural frequency for the small oscillations about a fixed configuration  $\theta$ .

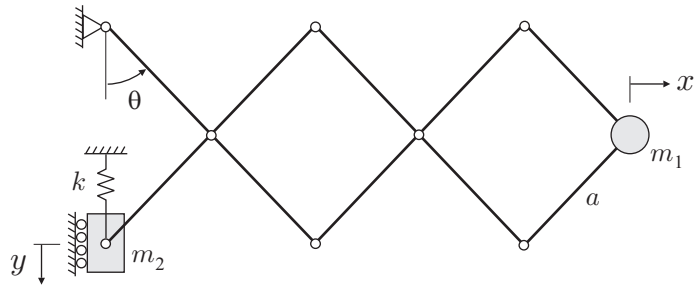
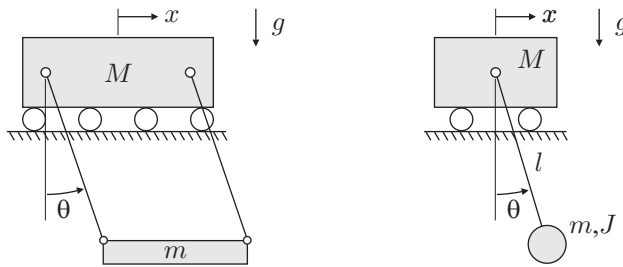


**Fig. 3.16.** Vibration of the motion amplification mechanism.

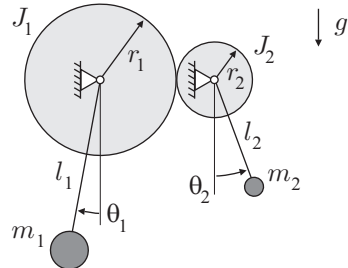
**P.3.8** Consider a cart of mass  $M$  free to move horizontally carrying a pendulum of length  $l$  and mass  $m$  and moment of inertia  $J$ . Write the Lagrangian of the system for the two configurations of Fig.3.17. Discuss.

**P.3.8** Consider the system of Fig.3.18, consisting of two pendulums connected by a pair of gears with pitch radius and moment of inertia of respectively  $r_1, J_1$  and  $r_2, J_2$  (the reduction ratio is  $r_1/r_2$ ). The system is in equilibrium when both pendulums are in vertical position. Write the Lagrangian and estimate the natural frequency for the small oscillations near the equilibrium position.

**P.3.9** Consider the system of Fig.3.19; it consists of a bar of mass  $M$  and moment of inertia  $J$ ; sliding without friction along two orthogonal surfaces

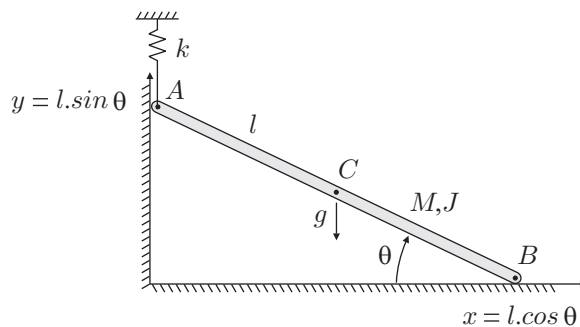


**Fig. 3.17.** Cart carrying a pendulum in two different configurations.



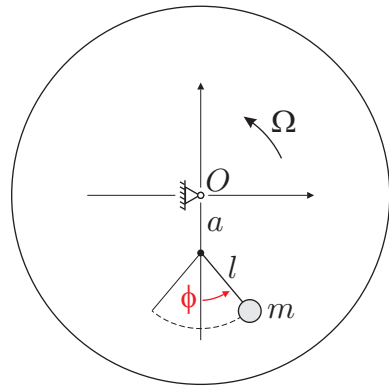
**Fig. 3.18.** System involving two pendulums connected by a gear.

with contacts at points *A* and *B*. The system is subjected to gravity and is attached by a vertical spring at point *A*; the spring is unstressed when  $\theta = 45^0$ . Write the Lagrangian of the system.



**Fig. 3.19.** Bar sliding on two orthogonal surfaces and attached with a spring.

**P.3.10** Consider the plane double pendulum of Fig.3.1, with point masses  $m_1$  and  $m_2$ . Write the Lagrangian of the system for the two choices of coordinates shown in the figure.

**Fig. 3.20.** Centrifugal pendulum.

**P.3.11** Centrifugal pendulum: Consider a disk rotating in the horizontal plane at the constant rotating speed  $\Omega$ . A pendulum of length  $l$  is attached at a distance  $a$  from the center of the disk (Fig. 3.20). Show that the small oscillations of the pendulum take place at the frequency

$$\omega_1 = \sqrt{\frac{a}{l}} \cdot \Omega \quad (3.73)$$

This result leads to an interesting family of vibration absorbers, because once tuned, the centrifugal pendulum vibration absorber is tuned for all values of the spin velocity (see Chapter 11).

---

## Continuous systems

*Le motif seul fait le mérite des actions des hommes, et le désintéressement y met la perfection.*

La Bruyère, *Les Caractères*, 1688

This chapter consists of a brief introduction to the continuous systems described by partial differential equations. It begins with the plane vibration of a beam without shear, the vibration of a string, and the axial vibration of a bar. The end of this chapter considers the bending vibration of rectangular and circular plates and the response of rotationally periodic structures to rotating forces.

### 4.1 Planar vibration of a beam (Euler-Bernoulli)

Consider the transverse deformation of a beam vibrating in a plane (Fig.4.1.a). The beam has a symmetric cross section of area  $A$  and moment of inertia  $I$ ; the mass density is  $\varrho$  and the Young modulus is  $E$ . It is subjected to a distributed load  $p(x, t)$ ; the transverse displacement is  $v(x, t)$ . The free body diagram of a small slice  $dx$  of the beam is shown in Fig.4.1.b, with all the forces acting on the two cross sections. According to classical notations,  $M$  and  $S$  represent respectively the bending moment and the shear force acting on left side, while  $M + dM$  and  $S + dS$  are those acting on the right side. The inertia load  $-\varrho A \ddot{v} dx$  is applied to the center of mass of the small element, in the direction opposing the motion. The vertical equilibrium reads:

$$S + p(x, t)dx - (S + dS) - \varrho A \ddot{v} dx = 0$$

or

$$\frac{dS}{dx} = -\varrho A \ddot{v} + p(x, t) \quad (4.1)$$

The rotational equilibrium (moment about the point  $P$  on the left side of Fig.4.1.b, positive clockwise; the rotational inertia is neglected.)

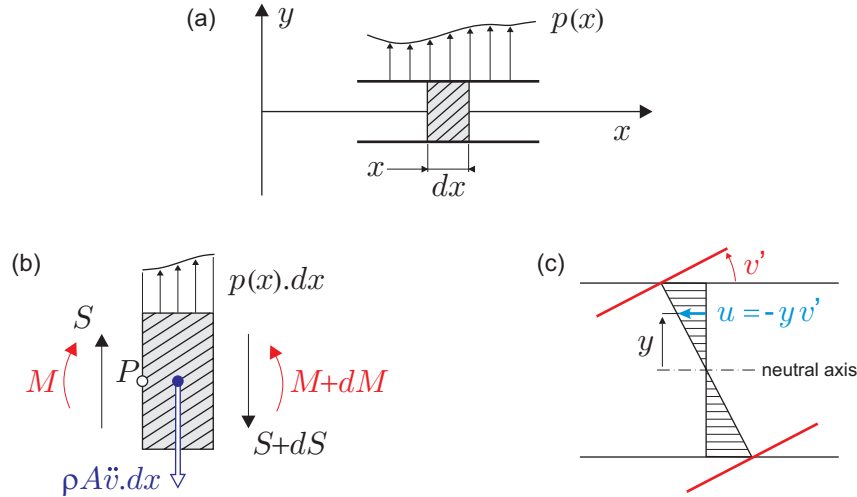


**Fig. 4.1.** (a) Transverse vibration of a beam; the transverse displacement is  $v(x, t)$ . (b) Free body diagram of a slice  $dx$  of the beam. (c) Euler-Bernoulli kinematic assumption.

$$M + (S + dS)dx + (\rho A \ddot{v} - p)dx.dx/2 - (M + dM) = 0$$

and, if one neglects the second order terms  $dS.dx$  and  $(dx)^2$ ,

$$\frac{dM}{dx} = S \quad (4.2)$$

These are the equilibrium equations. The kinematic assumptions of the Euler-Bernoulli theory of beam are that (i) the plane cross section of the beam remains plane after deformation, and normal to the neutral axis (no shear strain); (ii) there is no stretching of the neutral axis, and (iii) the loading acts in the plane  $(x, y)$  which is a plane of symmetry, so that the beam remains in the same plane after deformation.

The vertical displacement, common to all points in the same cross section is  $v(x)$ . Since the cross section remains plane and orthogonal to the neutral axis, the axial displacements vary linearly with the distance to the neutral axis:

$$u(x, y) = -y \frac{dv}{dx} = -y v'(x) \quad (4.3)$$

Every fiber in the beam is assumed to be in a uniaxial state of stress and strain:

$$\varepsilon_x = \frac{\partial u}{\partial x} = -y v''(x) \quad \sigma_x = E \varepsilon_x \quad (4.4)$$

In absence of axial loading,

$$\int_A \sigma_x dA = 0$$

which states that the neutral fiber is at the geometrical center of the cross section. Taking into account that a positive bending moment induces negative stresses above the neutral axis, the bending moment reads

$$M = - \int_A \sigma_x y dA = E v''(x) \int_A y^2 dA = EI v''(x) \quad (4.5)$$

where

$$I = \int_A y^2 dA$$

is the moment of inertia of the cross section.  $EI$  is called the *bending stiffness*. Combining Equ.(4.1)and (4.2),

$$\frac{d^2 M}{dx^2} = -\rho A \ddot{v} + p(x, t)$$

and, using Equ.(4.5), one gets the partial differential equation governing the vibration of the beam

$$(EI v'')'' + \rho A \ddot{v} = p(x, t) \quad (4.6)$$

It is of the second order in time and of the fourth order in space. Before discussing the boundary conditions, let us examine how this equation may be derived from Hamilton's principle.

#### 4.1.1 Hamilton's principle

Consider Figure 4.2; according to Hamilton's principle, the virtual displacements  $\delta v(x, t)$  satisfy the geometric (kinematic) boundary conditions and are such that the configuration is fixed at the limit times  $t_1$  and  $t_2$ :

$$\delta v(x, t_1) = \delta v(x, t_2) = 0 \quad (4.7)$$

The first step is to evaluate the Lagrangian. The strain energy resulting from the uniaxial stress state defined by Equ.(4.4) is

$$V(\varepsilon_{ij}) = \frac{1}{2} \int_V E \varepsilon_x^2 dV = \frac{1}{2} \int_0^L \int_A E (v'')^2 y^2 dA dx$$

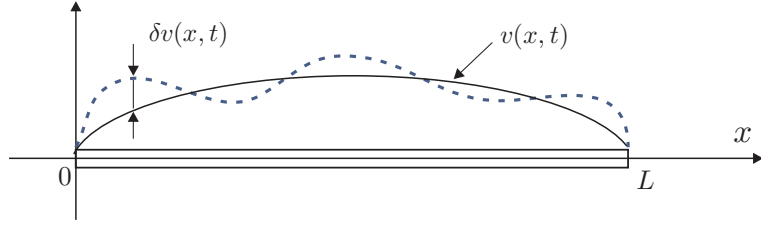


**Fig. 4.2.** Transverse vibration of a beam;  $\delta v(x, t)$  is a virtual displacement compatible with the boundary conditions and such that  $\delta v(x, t_1) = \delta v(x, t_2) = 0$ .

or

$$V = \frac{1}{2} \int_0^L EI(v'')^2 dx \quad (4.8)$$

If one includes only the translational inertia, the kinetic energy is

$$T = \frac{1}{2} \int_0^L \varrho A(\dot{v})^2 dx \quad (4.9)$$

The virtual work of the non-conservative forces is associated with the distributed load:

$$\delta W_{nc} = \int_0^L p \delta v dx \quad (4.10)$$

From (4.8) and (4.9),

$$\delta V = \int_0^L EIv''\delta v'' dx \quad \text{and} \quad \delta T = \int_0^L \varrho A\dot{v}\delta\dot{v} dx$$

As in the previous chapter,  $\delta\dot{v}$  can be eliminated by integrating by parts over  $t$ , using  $\dot{v}\delta\dot{v} = \frac{d}{dt}(\dot{v}\delta v) - \ddot{v}\delta v$ , and similarly,  $\delta v''$  can be eliminated by integrating twice by parts over  $x$ ; one gets

$$\begin{aligned} \delta V &= \int_0^L EIv''\delta v'' dx = [EIv''\delta v']_0^L - \int_0^L (EIv'')'\delta v' dx \\ &= [EIv''\delta v']_0^L - [(EIv'')'\delta v]_0^L + \int_0^L (EIv'')''\delta v dx \end{aligned}$$

and similarly

$$\int_{t_1}^{t_2} \delta T dt = \int_{t_1}^{t_2} dt \int_0^L \varrho A\dot{v}\delta\dot{v} dx = [\int_0^L \varrho A\dot{v}\delta v dx]_{t_1}^{t_2} - \int_{t_1}^{t_2} dt \int_0^L \varrho A\ddot{v}\delta v dx$$

The expression in brackets vanishes because of (4.7). Substituting the above expressions in Hamilton's principle, one gets

$$\int_{t_1}^{t_2} dt \{ -[EIv''\delta v']_0^L + [(EIv'')'\delta v]_0^L + \int_0^L [-(EIv'')'' - \varrho A\ddot{v} + p]\delta v dx \} = 0 \quad (4.11)$$

This variational indicator must vanish for all arbitrary variations  $\delta v$  compatible with the kinematic constraints and satisfying (4.7). This implies that, because  $\delta v$  is arbitrary within the beam  $[0, L]$ , the dynamic equilibrium is governed by the following partial differential equation

$$(EIv'')'' + \varrho A\ddot{v} = p \quad (4.12)$$

Besides, cancelling the terms within brackets in Equ.(4.11), we find that the following conditions must be fulfilled at  $x = 0$  and  $x = L$ ,

$$EIv''.\delta v' = 0 \quad (4.13)$$

$$(EIv'')'.\delta v = 0 \quad (4.14)$$

The first equation expresses that, at both ends, one must have either  $\delta v' = 0$ , which is the case if the rotation is fixed, or  $EIv'' = 0$ , which means that the bending moment is equal to 0. Similarly, the second one implies that at both ends, either  $\delta v = 0$ , which is the case if the displacement is fixed, or  $(EIv'')' = 0$ , which means that the shear force is equal to 0.  $\delta v = 0$  and  $\delta v' = 0$  are kinematic (geometric) boundary conditions;  $EIv'' = 0$  and  $(EIv'')' = 0$  are sometimes called *natural* boundary conditions, because they come naturally from the variational principle. A *free end* allows arbitrary  $\delta v$  and  $\delta v'$ ; this implies  $EIv'' = 0$  and  $(EIv'')' = 0$ . A *clamped end* implies that  $\delta v = 0$  and  $\delta v' = 0$ . A *pinned end* implies that  $\delta v = 0$ , but  $\delta v'$  is arbitrary; it follows that  $EIv'' = 0$ . Note that the kinematic and the natural boundary conditions are energetically conjugate: displacement and shear force, rotation and bending moment.

## 4.2 Beam with axial prestress

If the beam is subjected to an axial preload  $N$ , the axial force interacts with the lateral displacement to produce an additional term in the moment equilibrium equation (Fig.4.3). The moment associated with the axial loading is  $N dv = Nv'dx$  ( $N$  positive in traction). It follows that the moment equilibrium equation (moment about the point  $P$ ) reads

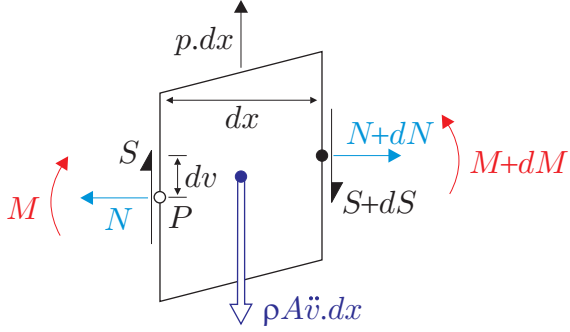


**Fig. 4.3.** Free body diagram of the beam in presence of an axial preload  $N$ .

$$M + (S + dS)dx + (N + dN)dv + (\rho A \ddot{v} - p)dx \cdot dx/2 - (M + dM) = 0$$

and, if one neglects the second order terms,

$$Sdx + Nv'dx - dM = 0$$

$$S = \frac{dM}{dx} - Nv' \quad (4.15)$$

Using this equation instead of Eq.(4.2) and pursuing the same development, one gets the partial differential equation governing the vibration of a prestressed beam:

$$(EI v'')'' - (Nv')' + \rho A \ddot{v} = p(x, t) \quad (4.16)$$

This equation may be obtained alternatively from Hamilton's principle by including the geometric strain energy in the Lagrangian. Using the strain measure (3.58), the nonlinear part of the axial strain is

$$\varepsilon_{xx}^{*(2)} = \frac{1}{2} \left( \frac{dv}{dx} \right)^2$$

and the prestress is  $\sigma_{xx}^0 = N/A$ . It follows that the geometric strain energy is

$$V_g = \int_{\Omega^*} \sigma_{ij}^0 \varepsilon_{ij}^{*(2)} d\Omega = \frac{1}{2} \int_0^L \frac{N}{A} \left( \frac{dv}{dx} \right)^2 A dx = \frac{1}{2} \int_0^L N(v')^2 dx \quad (4.17)$$

Repeating the developments of the previous section, there is an additional term

$$\delta V_g = \int_0^L Nv' \delta v' dx$$

Integrating by parts and using  $Nv'\delta v' = (Nv'\delta v)' - (Nv')'\delta v$ , one finds

$$\delta V_g = [Nv'\delta v]_0^L - \int_0^L (Nv')'\delta v \, dx$$

and Equ.(4.11) becomes in this case

$$\begin{aligned} & \int_{t_1}^{t_2} dt \{ -[EIv''\delta v']_0^L + [(EIv'')'\delta v]_0^L - [Nv'\delta v]_0^L \\ & + \int_0^L [-(EIv'')'' - \varrho A\ddot{v} + p + (Nv')']\delta v \, dx \} = 0 \end{aligned} \quad (4.18)$$

Since the virtual displacement  $\delta v$  is arbitrary, this implies that the dynamic equilibrium within the beam is governed by Equ.(4.16). The boundary conditions must satisfy:

$$EIv''.\delta v' = 0 \quad (4.19)$$

$$[(EIv'')' - Nv'].\delta v = 0 \quad (4.20)$$

This last equation expresses the static equilibrium between the axial force and the shear force at a free tip. We will return to this problem at the end of this chapter when we analyze the static buckling of a uniform beam.

### 4.3 Free vibration of a beam

The free vibration of a (Euler Bernoulli) beam without axial load is governed by Equ.(4.12) (with  $p = 0$ ). If the beam is uniform,

$$EI v^{IV} + \varrho A \ddot{v} = 0 \quad (4.21)$$

A non trivial harmonic solution  $v(x, t) = V(x)e^{j\omega t}$  exists if  $V(x)$  and  $\omega$  satisfy the eigenvalue problem

$$EI V(x)^{IV} - \omega^2 \varrho A V(x) = 0 \quad (4.22)$$

Introducing the non-dimensional quantities  $\eta = V(x)/L$  and  $\xi = x/L$ , using

$$V(x)^{IV} = \frac{d^4 V}{dx^4} = \frac{L d^4 \eta}{L^4 d\xi^4} = \frac{1}{L^3} \frac{d^4 \eta}{d\xi^4}$$

we get

$$\frac{d^4\eta}{d\xi^4} - \frac{\omega^2 \rho A L^4}{EI} \eta = 0 \quad (4.23)$$

or

$$\eta^{IV} - \mu^4 \eta = 0 \quad (4.24)$$

after introducing the non-dimensional frequency

$$\mu^4 = \frac{\omega^2 \rho A L^4}{EI} \quad (4.25)$$

The characteristic equation of this ordinary differential equation is

$$z^4 - \mu^4 = 0$$

with four solutions:

$$z = \pm \mu \quad z = \pm j\mu$$

and the general solution has the form:

$$\eta = C_1 e^{\mu\xi} + C_2 e^{-\mu\xi} + C_3 e^{j\mu\xi} + C_4 e^{-j\mu\xi} \quad (4.26)$$

where  $C_1, \dots, C_4$  are constants which depend on the four boundary conditions, two at each end. These can be kinematic  $\eta = 0$  (blocked displacement),  $\eta' = 0$  (blocked rotation), or *natural*,  $\eta'' = 0$  (no bending moment) or  $\eta''' = 0$  (no shear force); they must satisfy the requirements of (4.13) and (4.14).

### 4.3.1 Decoupling the boundary conditions

Solving for the constants  $C_1, \dots, C_4$  involves the solution of a system of four equations with four unknowns. However, the solution of the problem may be considerably simplified if, instead of using the exponential functions of Equ.(4.26), one uses linear combinations of them defined as follows

$$\begin{aligned} s_1(\mu\xi) &= 1/2[\sin(\mu\xi) + \sinh(\mu\xi)] \\ c_1(\mu\xi) &= 1/2[\cos(\mu\xi) + \cosh(\mu\xi)] \\ s_2(\mu\xi) &= 1/2[-\sin(\mu\xi) + \sinh(\mu\xi)] \\ c_2(\mu\xi) &= 1/2[-\cos(\mu\xi) + \cosh(\mu\xi)] \end{aligned} \quad (4.27)$$

Note that all these functions vanish at the origin  $\xi = 0$  except  $c_1$  and their derivatives are related by

$$\begin{aligned} s'_1 &= \mu c_1 & s_1(0) &= 0 \\ c'_1 &= \mu s_2 & c_1(0) &= 1 \\ s'_2 &= \mu c_2 & s_1(0) &= 0 \\ c'_2 &= \mu s_1 & c_2(0) &= 0 \end{aligned} \quad (4.28)$$

The general solution (4.26) may be written alternatively

$$\eta = As_1(\mu\xi) + Bc_1(\mu\xi) + Cs_2(\mu\xi) + Dc_2(\mu\xi) \quad (4.29)$$

so that the derivatives with respect to  $\xi$  are respectively

$$\begin{aligned} \eta' &= \mu[Ac_1(\mu\xi) + Bs_2(\mu\xi) + Cc_2(\mu\xi) + Ds_1(\mu\xi)] \\ \eta'' &= \mu^2[As_2(\mu\xi) + Bc_2(\mu\xi) + Cs_1(\mu\xi) + Dc_1(\mu\xi)] \\ \eta''' &= \mu^3[Ac_2(\mu\xi) + Bs_1(\mu\xi) + Cc_1(\mu\xi) + Ds_2(\mu\xi)] \end{aligned} \quad (4.30)$$

Note that the relationship between the constants  $A, B, C, D$  and the value of  $\eta$  and its derivatives at  $\xi = 0$  is totally decoupled

$$\begin{aligned} \eta(0) &= B \\ \eta'(0) &= \mu A \\ \eta''(0) &= \mu^2 D \\ \eta'''(0) &= \mu^3 C \end{aligned} \quad (4.31)$$

which allows a considerable simplification of the problem, as we can see in the following examples.

### 4.3.2 Simply supported beam

Consider the simply supported beam of Fig.4.4; it is pinned at both ends, so that the displacement  $v = 0$  and the bending moment  $M = 0$  (or equivalently  $v'' = 0$ ) vanish at both ends. Thus, we have  $\eta(0) = 0$  and  $\eta''(0) = 0$ ; it follows from the foregoing equation that  $B = 0$  and  $D = 0$ . Expressing the boundary conditions at  $\xi = 1$ ,  $\eta(\mu) = 0$  and  $\eta''(\mu) = 0$  one gets the following system of equations

$$\begin{bmatrix} s_1(\mu) & s_2(\mu) \\ s_2(\mu) & s_1(\mu) \end{bmatrix} \begin{Bmatrix} A \\ C \end{Bmatrix} = 0 \quad (4.32)$$

In order to have a solution, the determinant must vanish:

$$s_1^2(\mu) - s_2^2(\mu) = 0$$

or

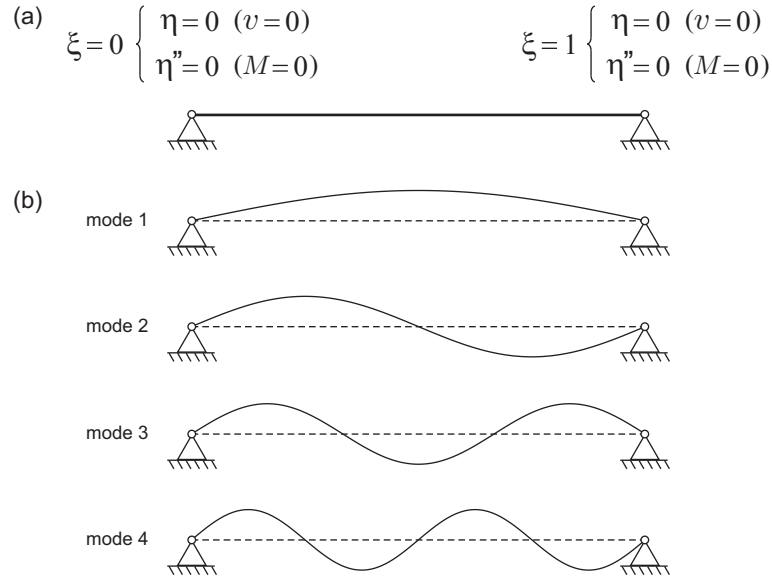


**Fig. 4.4.** Simply supported beam. (a) boundary conditions. (b) Mode shapes.

$$\sin \mu \cdot \sinh \mu = 0 \quad (4.33)$$

The solution  $\mu = 0$  would lead to  $\eta = 0$ . The non trivial solutions are  $\mu = k\pi$  for which  $s_1(\mu) = s_2(\mu) = \sinh \mu$ , thus leading to

$$A + C = 0$$

or  $A = -C$ . Substituting this (and  $B = D = 0$ ) in (4.29), one finds

$$\eta = A[s_1(\mu\xi) - s_2(\mu\xi)] = A \sin \mu\xi = A \sin k\pi\xi$$

The natural frequencies are obtained by substituting  $\mu = k\pi$  in Equ.(4.25). Finally, the natural frequencies and the mode shapes are

$$\omega_k = k^2 \sqrt{\frac{\pi^4 EI}{\rho A L^4}} \quad V_k(x) = V_0 \sin \frac{k\pi x}{L} \quad (k = 1, \dots, \infty) \quad (4.34)$$

As for all distributed systems, there is an infinite set of modes; the first four mode shapes are displayed in Fig.4.4.b. The natural frequencies vary with the square of the order  $k$  of the mode and the inverse of the square of the length  $L$ .

### 4.3.3 Free-free beam

Consider a uniform beam in free-free support conditions; the boundary conditions are  $S = M = 0$  at both ends,  $\xi = 0$  and  $\xi = 1$ . Thus,  $\eta''(0) = 0$  and  $\eta'''(0) = 0$  and, according to (4.31),  $D = C = 0$ . Expressing the boundary conditions at  $\xi = 1$ ,  $\eta''(1) = 0$  and  $\eta'''(1) = 0$ , one gets

$$\begin{bmatrix} s_2(\mu) & c_2(\mu) \\ c_2(\mu) & s_1(\mu) \end{bmatrix} \begin{Bmatrix} A \\ B \end{Bmatrix} = 0 \quad (4.35)$$

The eigenvalues cancel the determinant

$$s_2(\mu)s_1(\mu) - c_2^2(\mu) = 0$$

$$\cosh \mu \cos \mu = 1$$

or

$$\cos \mu = \frac{1}{\cosh \mu} \quad (4.36)$$

This equation is illustrated in Fig.4.5. The eigenvalues correspond to the crossing between the two curves. Once the value of  $\mu$  is obtained, the natural frequency may be computed from (4.25). Note that the two curves are tangent to each other at the origin, leading to a double root at  $\mu = 0$ . Substituting in Equ.(4.24), one gets  $\eta^{IV} = 0$ , meaning that

$$\eta = a\xi^3 + b\xi^2 + c\xi + d$$

and, taking into account the boundary conditions  $\eta''(1) = \eta'''(1) = 0$ ,  $a = b = 0$ , and the solution is

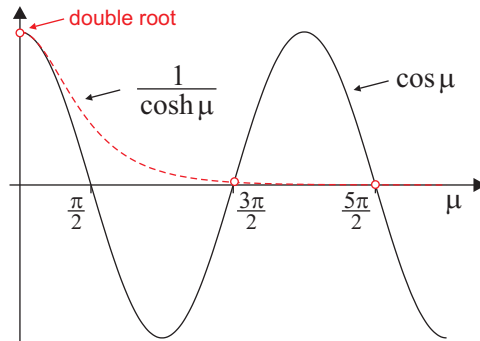


**Fig. 4.5.** Free-free beam. The solutions of the equation  $\cos \mu = (\cosh \mu)^{-1}$  are the eigenvalues of the problem.

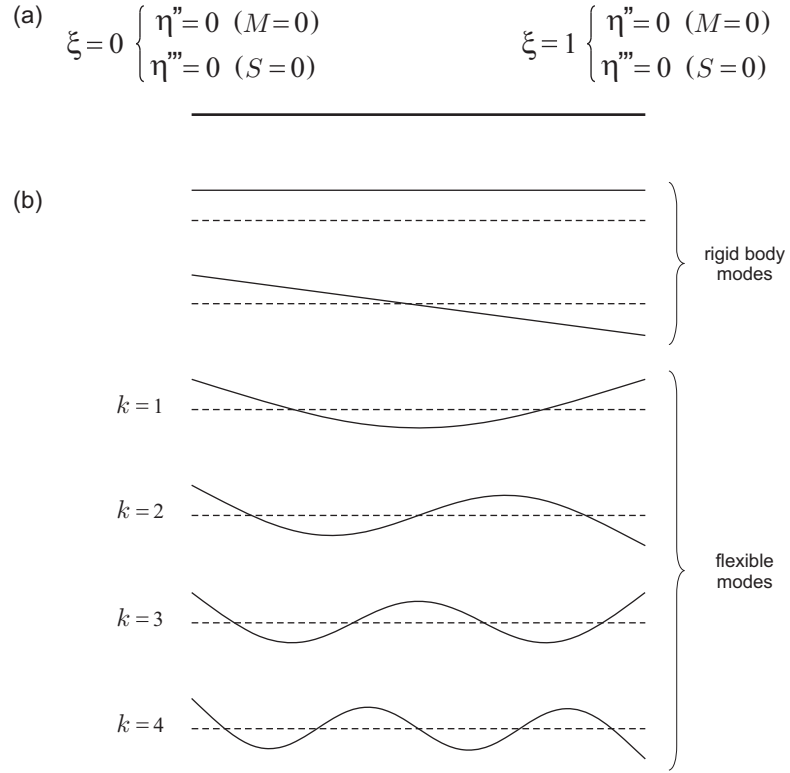


**Fig. 4.6.** Free-free beam. (a) Boundary conditions. (b) Mode shapes (rigid body modes and flexible modes).

$$\eta = c\xi + d$$

It consists of a family of two rigid body modes (there are two free parameters  $c$  and  $d$ ).

On the other hand, the function  $(\cosh \mu)^{-1}$  decreases extremely fast, so that the solution converges quite quickly towards its asymptotic value

$$\mu_k \simeq \frac{(2k+1)\pi}{2} \quad (k \gg 1)$$

For small values of  $k$ , a better estimate can be obtained by an *asymptotic method* whereby a first order correction  $\varepsilon_k$  is added to the asymptotic value:

$$\mu_k \simeq \frac{(2k+1)\pi}{2} + \varepsilon_k \quad (4.37)$$

Introducing into the characteristic equation (4.36) and expanding,

$$\begin{aligned} & [\cosh \frac{(2k+1)\pi}{2} \cosh \varepsilon_k + \sinh \frac{(2k+1)\pi}{2} \sinh \varepsilon_k] \\ & \cdot [\cos \frac{(2k+1)\pi}{2} \cos \varepsilon_k - \sin \frac{(2k+1)\pi}{2} \sin \varepsilon_k] = 1 \end{aligned}$$

Taking into account that  $\cos \frac{(2k+1)\pi}{2} = 0$ ,  $\sin \frac{(2k+1)\pi}{2} = (-1)^k$ , and using the approximations  $\cosh \varepsilon_k \simeq 1$ ,  $\sinh \varepsilon_k \simeq \varepsilon_k$  and  $\sin \varepsilon_k \simeq \varepsilon_k$ , this becomes

$$[\cosh \frac{(2k+1)\pi}{2} + \varepsilon_k \sinh \frac{(2k+1)\pi}{2}](-1)^{k+1} \varepsilon_k = 1$$

and finally, keeping only the first order term in  $\varepsilon_k$  in the left hand side,

$$\varepsilon_k \simeq \frac{(-1)^{k+1}}{\cosh \frac{(2k+1)\pi}{2}} \quad (k \geq 1) \quad (4.38)$$

The first order correction is alternately positive and negative, and decreases rapidly with  $k$ . For a given eigenvalue  $\mu$  the mode shape is obtained from anyone of the equation (4.35); from the first one we get:

$$As_2(\mu) + Bc_2(\mu) = 0 \Rightarrow B = -\frac{s_2(\mu)}{c_2(\mu)}A$$

leading to the mode shape

$$\eta(\xi) = A[s_1(\mu\xi) - \frac{s_2(\mu)}{c_2(\mu)}c_1(\mu\xi)] \quad (4.39)$$

The first few modes are represented in Fig.4.6.

#### 4.4 Orthogonality relationships

We now establish, as we did for discrete systems in Chapter 2, the orthogonality relationships between the mode shapes. Consider two modes with distinct frequencies; mode  $i$  satisfies

$$(EI v_i'')'' - \varrho A \omega_i^2 v_i = 0$$

Multiplying by  $v_j$  and integrating over the length of the beam, one gets

$$\int_0^L [v_j(EI v_i'')'' - \varrho A \omega_i^2 v_j v_i] dx = 0$$

We then integrate by parts twice, in order to distribute evenly the spatial derivatives over  $v_i$  and  $v_j$ :

$$\int_0^L v_j (EI v_i'')'' dx = [(EI v_i'')' v_j]_0^L - [EI v_i'' v_j']_0^L + \int_0^L EI v_i'' v_j'' dx$$

The two expressions in brackets vanish, because of the boundary conditions [at each end of the beam, either  $EIv'' = 0$  or  $v' = 0$ , and similarly  $(EIv'')' = 0$  or  $v = 0$ ]; substituting into the previous equation, one gets

$$\int_0^L EI v_i'' v_j'' dx = \omega_i^2 \int_0^L \varrho A v_j v_i dx$$

Similarly, permuting  $i$  and  $j$ , one gets

$$\int_0^L EI v_j'' v_i'' dx = \omega_j^2 \int_0^L \varrho A v_i v_j dx$$

and, subtracting these two equations,

$$0 = (\omega_i^2 - \omega_j^2) \int_0^L \varrho A v_i v_j dx$$

Thus, if  $\omega_i \neq \omega_j$ , one must have

$$\int_0^L \varrho A v_i v_j dx = 0 \quad (4.40)$$

This is the first orthogonality relationship: the mode shapes corresponding to distinct frequencies are orthogonal with respect to the mass distribution ( $\varrho A$  is the mass per unit length). Returning to the previous equation, it follows also that

$$\int_0^L EI v_i'' v_j'' dx = 0 \quad (4.41)$$

The mode shapes are also orthogonal with respect to the stiffness distribution ( $EI$  is the bending stiffness). By analogy with Equ.(2.8) and (2.9), these equations are conveniently written

$$\int_0^L \varrho A v_i v_j dx = \mu_i \delta_{ij} \quad (4.42)$$

$$\int_0^L EI v_i'' v_j'' dx = \mu_i \omega_i^2 \delta_{ij} \quad (4.43)$$

where  $\delta_{ij}$  is the Kronecker delta ( $\delta_{ij} = 1$  if  $i = j$ ,  $\delta_{ij} = 0$  if  $i \neq j$ ),  $\mu_i$  is the *modal mass* (also called generalized mass) of mode  $i$ . From the foregoing equations,

$$\omega_i^2 = \frac{\int_0^L EI (v_i'')^2 dx}{\int_0^L \varrho A v_i^2 dx} \quad (4.44)$$

This result should be compared to Equ.(2.10). We will return to it when we study the *Rayleigh quotient*. The discussion of section 2.2.3 about multiple eigenvalues applies also here.

## 4.5 Modal decomposition

We now return to the general equation (4.12) and perform a modal decomposition according to

$$v(x, t) = \sum_{i=1}^{\infty} z_i(t) v_i(x) \quad (4.45)$$

where  $v_i(x)$  are the mode shapes and the modal amplitudes  $z_i(t)$  form an infinite set of modal coordinates. Substituting into (4.12), one finds

$$\sum_{i=1}^{\infty} z_i(t) (EI v_i'')'' + \sum_{i=1}^{\infty} \ddot{z}_i(t) \varrho A v_i(x) = p \quad (4.46)$$

Upon multiplying by  $v_k$  and integrating over the beam length,

$$\sum_{i=1}^{\infty} z_i(t) \int_0^L v_k (EI v_i'')'' dx + \sum_{i=1}^{\infty} \ddot{z}_i(t) \int_0^L \varrho A v_k v_i dx = \int_0^L v_k p dx$$

After integrating by parts the first term, as in the previous section, it is rewritten

$$\sum_{i=1}^{\infty} z_i(t) \int_0^L EI v_i'' v_k'' dx + \sum_{i=1}^{\infty} \ddot{z}_i(t) \int_0^L \varrho A v_k v_i dx = \int_0^L v_k p dx$$

and, upon using the orthogonality conditions (4.40) (4.41), one finds a set of decoupled equations:

$$\mu_k (\ddot{z}_k + \omega_k^2 z_k) = \int_0^L v_k p dx \quad (4.47)$$

which is identical to (2.23). This equation states that every mode behaves like a single d.o.f. oscillator of mass  $\mu_k$  and frequency  $\omega_k$ ; the generalized force is once again the work of the external distributed force  $p$  on the mode  $v_k$ . A point force  $F(t)$  applied at  $x_0$  is represented by  $p(x,t) = F(t)\delta(x - x_0)$  where  $\delta(x)$  is the Dirac function such that

$$\delta(x) = 0 \quad (x \neq 0) \quad \text{and} \quad \int \delta(x) dx = 1 \quad (4.48)$$

so that the work is  $F(t).v_k(x_0)$ . The modal damping can be added as in (2.23). The displacement at a point  $x_1$  along the beam is

$$v(x_1) = \sum_{k=1}^{\infty} z_k(t)v_k(x_1)$$

Using (4.47) and duplicating what we did in section 2.5, the FRF between a point force excitation at  $x_0$  and the displacement at  $x_1$  reads

$$G(\omega) = \sum_{i=1}^{\infty} \frac{v_k(x_0)v_k(x_1)}{\mu_k\omega_k^2} \cdot D_k(\omega) \quad (4.49)$$

with  $D_k(\omega)$  being the dynamic amplification factor of mode  $k$ , given by (2.30). What has been said about truncating the modal expansion in section 2.5 applies fully here and will not be reproduced.

## 4.6 Vibration of a string

The transverse stiffness of a taut string comes entirely from the axial preload  $T_0$  (uniform along the string). The governing equation can be obtained by expressing the equilibrium in the transverse direction, Fig.4.7. The vertical projection of the string tension is related to the slope of the

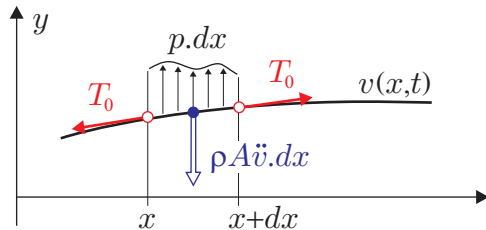


**Fig. 4.7.** Vibration of a string, free body diagram of a segment  $dx$ .

string, which is  $v'(x)$  at  $x$ , and  $v'(x) + dv' = v'(x) + v''dx$  at  $x + dx$ . The vertical equilibrium reads

$$\varrho A \ddot{v} dx = p dx - T_0 v' + T_0(v' + v''dx)$$

This leads to the partial differential equation

$$\varrho A \ddot{v} - T_0 v'' = p \quad (4.50)$$

It is of the second order, both in time and in space. Note that this equation can be obtained from that of a preloaded beam, Equ.(4.16), by cancelling the bending stiffness  $EI$  and taking a uniform axial preload  $N = T_0$ . The free vibration of a string is governed by

$$\varrho A \ddot{v} - T_0 v'' = 0$$

A solution of the form  $v(x, t) = V(x)e^{j\omega t}$  exists if  $V(x)$  and  $\omega$  satisfy the eigenvalue problem

$$V'' + \frac{\omega^2 \varrho A}{T_0} V = 0 \quad (4.51)$$

The characteristic equation is

$$z^2 + \frac{\omega^2 \varrho A}{T_0} = 0 \quad \Rightarrow \quad z = \pm j\omega \sqrt{\frac{\varrho A}{T_0}}$$

The general solution is

$$V(x) = A \sin(\omega \sqrt{\frac{\varrho A}{T_0}} x) + B \cos(\omega \sqrt{\frac{\varrho A}{T_0}} x) \quad (4.52)$$

Assuming that the string is pinned at  $x = 0$  and  $x = L$ , the boundary condition  $V(0) = 0$  enforces  $B = 0$  and  $V(L) = 0$  provides the equation governing the eigenvalues:

$$\sin(\omega \sqrt{\frac{\varrho A}{T_0}} L) = 0 \quad \Rightarrow \quad \omega \sqrt{\frac{\varrho A}{T_0}} L = k\pi$$

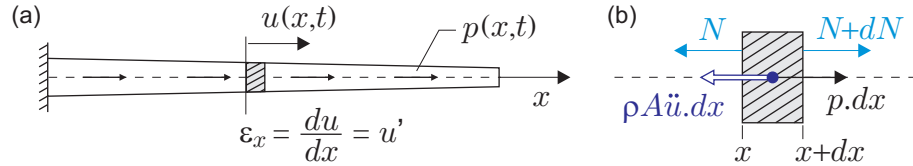
The mode shape is obtained by back substituting this frequency in Equ.(4.52); one finds

$$\omega_k = k \frac{\pi}{L} \sqrt{\frac{T_0}{\varrho A}} \quad V_k(x) = A \sin \frac{k\pi x}{L} \quad (k = 1, \dots, \infty) \quad (4.53)$$

The natural frequencies vary linearly with the order  $k$  of the mode and with the inverse of the length  $L$ ; thus, halving the length doubles the frequency.<sup>1</sup> The mode shapes are identical to those of a simply supported beam, Fig.4.4.

---

<sup>1</sup> one octave higher; this fact is well known to all musicians.

Fig. 4.8. (a) Vibration of a bar. (b) Free body diagram of a segment  $dx$ .

### 4.7 Axial vibration of a bar

A beam vibrates in the transverse direction; a bar vibrates in the axial direction with a uniform strain in every cross section. Once again, the governing equation may be obtained either from the equilibrium of a segment of the bar, or from Hamilton's principle.

Consider the free body diagram of Fig.4.8,  $N(x)$  is the axial force acting on the left side of the segment and  $N(x)+dN$  is that acting on the right side; the distributed force is  $p dx$  and the inertia force is  $-\rho A \ddot{u} dx$ . The equilibrium equation is

$$N + \rho A \ddot{u} dx = p dx + N + dN$$

or

$$\rho A \ddot{u} = p + \frac{dN}{dx}$$

Since the bar is in a uniaxial stress state,  $N = AE\varepsilon_x = AE(du/dx) = AEu'$ ; substituting in the previous equation, one gets the partial differential equation

$$\rho A \ddot{u} - (AEu')' = p \quad (4.54)$$

It is of the second order, both in time and in space.

This equation may also be derived from Hamilton's principle, by using the appropriate expressions for the strain energy and the kinetic energy:

$$V = \frac{1}{2} \int_0^L AE \varepsilon_x^2 dx = \frac{1}{2} \int_0^L AE(u')^2 dx \quad (4.55)$$

$$T = \frac{1}{2} \int_0^L \rho A(\dot{u})^2 dx \quad (4.56)$$

The virtual work of the non-conservative forces is associated with the distributed load  $p$

$$\delta W_{nc} = \int_0^L p \delta u dx \quad (4.57)$$

Substituting the above expressions into Hamilton's principle and integrating by parts to eliminate  $\delta\dot{u}$  and  $\delta u'$ , one gets<sup>2</sup>

$$\int_{t_1}^{t_2} dt \{ -[AEu'\delta u]_0^L + \int_0^L [(AEu')' - \varrho A\ddot{u} + p]\delta u \, dx \} = 0 \quad (4.58)$$

Since the variational indicator must vanish for arbitrary variations  $\delta u$ , the second term of the integral implies (4.54). The term within brackets must also vanish at both ends

$$AEu'\delta u = 0$$

which means that either the displacement is fixed (and  $\delta u = 0$ ), or the axial force  $AEu'$  must be zero, meaning a free end.

#### 4.7.1 Free vibration

The free vibration of a bar with uniform cross section is governed by

$$AEu'' - \varrho A\ddot{u} = 0$$

A solution of the form  $u(x, t) = U(x)e^{j\omega t}$  exists if  $U(x)$  and  $\omega$  satisfy the eigenvalue problem

$$U'' + \frac{\omega^2 \varrho}{E} U = 0 \quad (4.59)$$

The characteristic equation is

$$z^2 + \frac{\omega^2 \varrho}{E} = 0 \quad \Rightarrow \quad z = \pm j\omega \sqrt{\frac{\varrho}{E}} = \pm j\frac{\omega}{c}$$

where

$$c = \sqrt{\frac{E}{\varrho}} \quad (4.60)$$

is the speed of sound in the bar. The general solution is

$$U(x) = C_1 \sin \frac{\omega x}{c} + C_2 \cos \frac{\omega x}{c}$$

At this point, one must enforce the boundary conditions. If the bar is fixed at  $x = 0$ ,  $C_2 = 0$  and, assuming that it is free at  $x = L$ , the strain must vanish:

---

<sup>2</sup> The developments are very similar to those of section 4.1.1 and are omitted.

$$U'(L) = C_1 \frac{\omega}{c} \cos \frac{\omega L}{c} = 0$$

leading to

$$\frac{\omega L}{c} = \frac{(2k-1)\pi}{2}$$

Finally,

$$\omega_k = \frac{(2k-1)\pi}{2} \left( \frac{c}{L} \right) \quad U_k(x) = C_1 \sin \left[ \frac{(2k-1)\pi}{2} \left( \frac{x}{L} \right) \right] \quad (k = 1, \dots, \infty) \quad (4.61)$$

#### 4.8 Static buckling of a beam\*

In this section, we return to the beam with axial prestress. The free vibration is governed by

$$(EI v'')'' - (Nv')' + \varrho A \ddot{v} = 0$$

with the boundary conditions (4.19) and (4.20). The solution of the eigenvalue problem is slightly more cumbersome than when  $N = 0$ , because the boundary conditions cannot be decoupled as we did in section 4.3.1. A complete solution of this problem may be found in [Shaker, 1975]; approximate solutions will be considered in the next chapter with the Rayleigh-Ritz method.

The equation governing the static buckling of a beam is obtained from the previous equation by removing the inertia term:

$$(EI v'')'' - (Nv')' = 0 \quad (4.62)$$

where the axial preload  $N$  is positive in traction. If the bending stiffness  $EI$  and the compression load  $N(x) = -P$  are uniform along the beam,

$$EI v^{IV} + Pv'' = 0 \quad (4.63)$$

Using once again the non-dimensional quantities  $\eta = v(x)/L$  and  $\xi = x/L$ , using

$$v(x)^{IV} = \frac{d^4 v}{dx^4} = \frac{1}{L^3} \frac{d^4 \eta}{d\xi^4} \quad v(x)'' = \frac{d^2 v}{dx^2} = \frac{1}{L} \frac{d^2 \eta}{d\xi^2}$$

one gets

$$\eta^{IV} + \frac{PL^2}{EI} \eta'' = 0$$

or

$$\eta^{IV} + \mu^2 \eta'' = 0 \quad (4.64)$$

with

$$\mu^2 = \frac{PL^2}{EI} \quad (4.65)$$

The characteristic equation is

$$z^4 + \mu^2 z^2 = 0$$

with the solutions

$$z = 0 \quad z = \pm j\mu$$

( $z = 0$  is a double root) and the general solution has the form

$$\eta(\xi) = A \sin \mu\xi + B \cos \mu\xi + C + D\xi \quad (4.66)$$

#### 4.8.1 Simply supported beam

The boundary conditions are such that

$$\eta(0) = 0 \quad \eta''(0) = 0 \quad \eta(1) = 0 \quad \eta''(1) = 0$$

The first two conditions enforce  $B = C = 0$ ; the two conditions at  $\xi = 1$  enforce  $D = 0$  and  $\sin \mu = 0$ , leading to  $\mu = k\pi$ . Thus,

$$\eta(\xi) = A \sin \mu\xi \quad (4.67)$$

and the critical buckling load, corresponding to  $k = 1$ , is

$$\frac{PL^2}{EI} = \pi^2$$

or

$$P_{cr} = \frac{\pi^2 EI}{L^2} \quad (4.68)$$

This is the well known Euler critical buckling load. The corresponding buckling mode is

$$\eta(\xi) = A \sin \pi\xi = A \sin \frac{\pi x}{L} \quad (4.69)$$

It is represented in Fig.4.9.a.

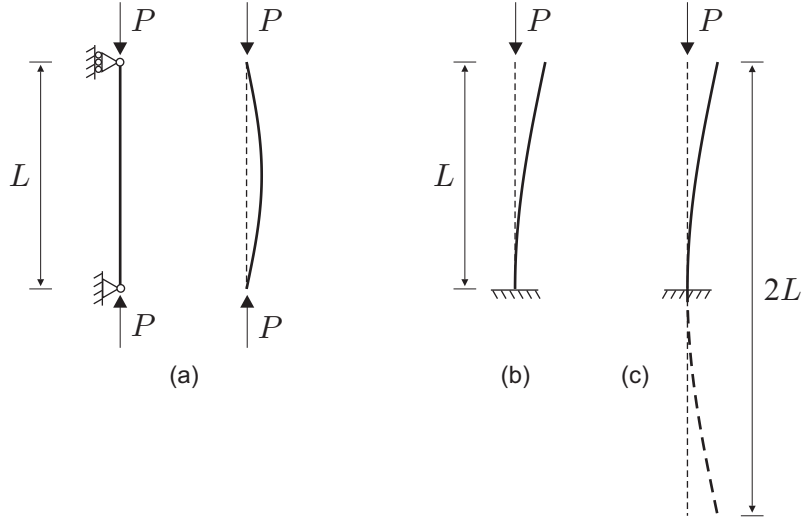


**Fig. 4.9.** (a) Simply supported beam with uniform axial compression load  $P$  and shape of the first buckling mode. (b) Clamped-free beam with uniform axial compression load  $P$  and shape of the first buckling mode beam. (c) Relation between the buckling of a clamped-free beam and that of a simply supported beam of double length.

#### 4.8.2 Clamped-free beam

As a second example, consider the clamped-free beam (Fig.4.9.b); the boundary conditions derive from Equ.(4.19) and (4.20): At the clamped end,

$$\eta(0) = \eta'(0) = 0$$

and at the free end,

$$\eta''(1) = 0, \quad \eta'''(1) = -\mu^2 \eta'(1)$$

The last condition enforces  $D = 0$ ;  $\eta'(0) = 0$  enforces  $A = 0$ ;  $\eta(0) = 0$  enforces  $B + C = 0$  and  $\eta''(1) = 0$  leads to  $\cos \mu = 0$ . It follows that the eigenvalues are  $\mu = (2k - 1)\pi/2$ . Thus, the critical load of the first buckling mode is

$$\frac{PL^2}{EI} = \left(\frac{\pi}{2}\right)^2$$

or

$$P_{cr} = \frac{\pi^2 EI}{4L^2} \quad (4.70)$$

and the corresponding buckling mode is

$$\eta(\xi) = C(1 - \cos \mu\xi) = C(1 - \cos \frac{\pi\xi}{2}) \quad (4.71)$$

It is represented in Fig.4.9.b. Note that the critical buckling load is that of a simply supported beam of double length, and this can be deduced from symmetry considerations, as illustrated in Fig.4.9.c.

## 4.9 Bending vibration of thin plates\*

### 4.9.1 Kirchhoff plate

According to the Kirchhoff theory of plates, a straight line normal to the midplane remains straight and normal to the midplane in the deformed state. If the midplane undergoes a displacement  $u_0, v_0, w_0$ , a point located on the same normal at a distance  $z$  from the midplane undergoes the displacements (Fig.4.10)

$$\begin{aligned} u &= u_0 - z \frac{\partial w_0}{\partial x} \\ v &= v_0 - z \frac{\partial w_0}{\partial y} \\ w &= w_0 \end{aligned} \quad (4.72)$$

In this study, it is assumed that the mid plane is not stretched (no membrane strains), so that  $u_0 = 0$  and  $v_0 = 0$ . It follows that the strains are only related to bending (and twisting):

$$\boldsymbol{\varepsilon} = \begin{Bmatrix} \varepsilon_x \\ \varepsilon_y \\ \gamma_{xy} \end{Bmatrix} = \begin{Bmatrix} \partial u / \partial x \\ \partial v / \partial y \\ \partial u / \partial y + \partial v / \partial x \end{Bmatrix} = -z \begin{Bmatrix} \partial^2 w / \partial x^2 \\ \partial^2 w / \partial y^2 \\ 2 \partial^2 w / \partial x \partial y \end{Bmatrix} = z \boldsymbol{\kappa} \quad (4.73)$$

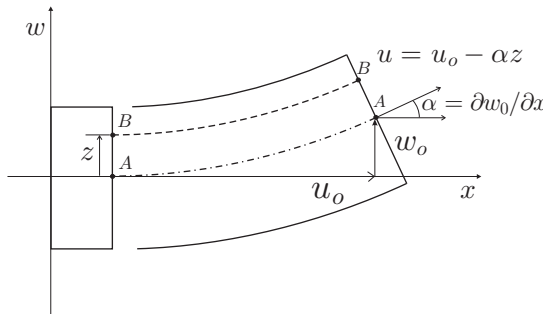


**Fig. 4.10.** Kinematics of a Kirchhoff plate.

where the subscript  $_0$  has been dropped.  $\kappa$  is the vector of curvatures; the third component represents twisting. For an isotropic elastic material, the strains in the  $(x, y)$  plane are related to the stresses by

$$\begin{aligned}\varepsilon_x &= \frac{1}{E}[\sigma_x - \nu(\sigma_y + \sigma_z)] \\ \varepsilon_y &= \frac{1}{E}[\sigma_y - \nu(\sigma_x + \sigma_z)] \\ \gamma_{xy} &= \tau_{xy}/G = \frac{2(1+\nu)}{E}\tau_{xy}\end{aligned}\quad (4.74)$$

If one assumes that  $\sigma_z = 0$  (plane stress),

$$\begin{Bmatrix} \varepsilon_x \\ \varepsilon_y \\ \gamma_{xy} \end{Bmatrix} = \frac{1}{E} \begin{bmatrix} 1 & -\nu & 0 \\ -\nu & 1 & 0 \\ 0 & 0 & 2(1+\nu) \end{bmatrix} \begin{Bmatrix} \sigma_x \\ \sigma_y \\ \tau_{xy} \end{Bmatrix} \quad (4.75)$$

This equation can be inverted into

$$\boldsymbol{\sigma} = \begin{Bmatrix} \sigma_x \\ \sigma_y \\ \tau_{xy} \end{Bmatrix} = \frac{E}{1-\nu^2} \begin{bmatrix} 1 & \nu & 0 \\ \nu & 1 & 0 \\ 0 & 0 & \frac{1-\nu}{2} \end{bmatrix} \begin{Bmatrix} \varepsilon_x \\ \varepsilon_y \\ \gamma_{xy} \end{Bmatrix} = H\varepsilon \quad (4.76)$$

These are the constitutive equations for plane stresses. They can be integrated through the thickness of the plate and, combining with the strain-curvature relationship (4.73), one finds the moment-curvature relationship:

$$\mathbf{M} = \begin{Bmatrix} M_x \\ M_y \\ M_{xy} \end{Bmatrix} = \int_{-h/2}^{h/2} z \begin{Bmatrix} \sigma_x \\ \sigma_y \\ \tau_{xy} \end{Bmatrix} dz = D \begin{bmatrix} 1 & \nu & 0 \\ \nu & 1 & 0 \\ 0 & 0 & \frac{1-\nu}{2} \end{bmatrix} \boldsymbol{\kappa} \quad (4.77)$$

where  $D$  is the flexural rigidity, defined by

$$D = \frac{Eh^3}{12(1-\nu^2)} \quad (4.78)$$

The Lagrangian is now developed. The strain energy density is

$$\frac{1}{2} \boldsymbol{\sigma}^T \boldsymbol{\varepsilon} = \frac{1}{2} \boldsymbol{\varepsilon}^T H \boldsymbol{\varepsilon} \quad (4.79)$$

The strain energy is obtained by integrating over the volume of the plate,

$$V = \frac{1}{2} \int_S dS \int_{-h/2}^{h/2} \boldsymbol{\varepsilon}^T H \boldsymbol{\varepsilon} dz = \frac{1}{2} \int_S D \boldsymbol{\kappa}^T \begin{bmatrix} 1 & \nu & 0 \\ \nu & 1 & 0 \\ 0 & 0 & \frac{1-\nu}{2} \end{bmatrix} \boldsymbol{\kappa} dS \quad (4.80)$$

and, upon substituting the vector of curvatures  $\kappa$  from Equ.(4.73),

$$V = \frac{1}{2} \int_S D \left\{ \left( \frac{\partial^2 w}{\partial x^2} + \frac{\partial^2 w}{\partial y^2} \right)^2 - 2(1-\nu) \left[ \frac{\partial^2 w}{\partial x^2} \cdot \frac{\partial^2 w}{\partial y^2} - \left( \frac{\partial^2 w}{\partial x \partial y} \right)^2 \right] \right\} dS \quad (4.81)$$

This form of  $V$  corresponds to Equ.(4.8) for an Euler-Bernoulli beam. Similarly, if one considers only the translational inertia, the kinetic energy reads

$$T = \frac{1}{2} \int_V \varrho \dot{w}^2 dV = \frac{1}{2} \int_S m \dot{w}^2 dS \quad (4.82)$$

where  $m$  is the areal density (in kg/m<sup>2</sup>). If one assumes that the external load is a distributed force  $p$  acting normally to the plate (i.e. a pressure, in N/m<sup>2</sup>), the virtual work of the external loads is

$$\delta W_{nc} = \int_S p \delta w dS \quad (4.83)$$

Once the analytical expressions of the potential, the kinetic energy and the virtual work of the external forces have been derived, the partial differential equation may be established from Hamilton's principle; however, the derivation is significantly more complicated than for a beam and it will be skipped here.<sup>3</sup> The partial differential equation governing the transverse vibration of a thin plate without prestress is

$$D \nabla^4 w + m \ddot{w} = p \quad (4.84)$$

where  $\nabla^4 = \Delta^2$  is the double Laplacian operator. The *nabla* operator  $\nabla$  and the Laplacian operator  $\Delta$  are respectively (in Cartesian coordinates)

$$\nabla = \left( \frac{\partial}{\partial x}, \frac{\partial}{\partial y} \right)^T \quad (4.85)$$

$$\Delta = \left[ \frac{\partial^2}{\partial x^2} + \frac{\partial^2}{\partial y^2} \right] \quad (4.86)$$

Note the perfect similarity with Equ.(4.21) governing the vibration of beams, with  $D$  being substituted to  $EI$  and  $\nabla$  to  $\partial/\partial x$ . Equation (4.84) may be solved analytically for some simple geometries; two of them are examined below.

---

<sup>3</sup> see, for example, Geradin & Rixen, 1997, p.221.

### 4.9.2 Free vibration of a simply supported rectangular plate

The governing equation of the free vibration is

$$D \nabla^4 w + m \ddot{w} = 0 \quad (4.87)$$

A non trivial harmonic solution  $w = W(x, y)e^{j\omega t}$  exists if  $W(x, y)$  and  $\omega$  satisfy the eigenvalue problem

$$(\nabla^4 - \beta^4)W = 0 \quad (4.88)$$

where

$$\beta^4 = \frac{m\omega^2}{D} \quad (4.89)$$

This equation may be factored into

$$(\nabla^2 + \beta^2)(\nabla^2 - \beta^2)W = 0 \quad (4.90)$$

The complete solution of this equation is given by the superposition  $W = W_1 + W_2$  of the solutions  $W_1$  and  $W_2$  of the equations

$$\begin{aligned} (\nabla^2 + \beta^2)W_1 &= 0 \\ (\nabla^2 - \beta^2)W_2 &= 0 \end{aligned} \quad (4.91)$$

The general solutions are respectively

$$\begin{aligned} W_1 &= A_1 \cos \alpha x \cos \gamma y + B_1 \sin \alpha x \cos \gamma y \\ &\quad + C_1 \cos \alpha x \sin \gamma y + D_1 \sin \alpha x \sin \gamma y \end{aligned} \quad (4.92)$$

$$\begin{aligned} W_2 &= A_2 \cosh \alpha x \cosh \gamma y + B_2 \sinh \alpha x \cosh \gamma y \\ &\quad + C_2 \cosh \alpha x \sinh \gamma y + D_2 \sinh \alpha x \sinh \gamma y \end{aligned}$$

with

$$\alpha^2 + \gamma^2 = \beta^2 \quad (4.93)$$

At any point of the rectangular contour, the boundary conditions must be as follows:

- (1) the shear force or the vertical displacement must be zero.
- (2) the bending moment or the slope normal to the contour must be zero.

For the particular case of a simply supported rectangular plate of size  $(a, b)$ , this becomes

$$\begin{aligned} w &= 0 \quad \text{and} \quad \frac{\partial^2 w}{\partial x^2} = 0 \quad \text{at} \quad x = 0 \quad \text{and} \quad x = a \\ w &= 0 \quad \text{and} \quad \frac{\partial^2 w}{\partial y^2} = 0 \quad \text{at} \quad y = 0 \quad \text{and} \quad y = b \end{aligned} \quad (4.94)$$

Using these conditions, the general form of the eigen modes of the rectangular plate is

$$W(x, y) = A \sin \alpha x \sin \gamma y \quad (4.95)$$

with the additional conditions

$$\sin \alpha a = 0 \quad \text{and} \quad \sin \gamma b = 0 \quad (4.96)$$

Thus, the eigenvalues are

$$\alpha_i = \frac{i\pi}{a}, \quad \gamma_k = \frac{k\pi}{b}, \quad i, k = 1, 2, \dots, \infty$$

Using (4.93) and (4.89), the corresponding frequencies are given by

$$\omega_{ik} = \pi^2 \sqrt{\frac{D}{m}} \left[ \left( \frac{i}{a} \right)^2 + \left( \frac{k}{b} \right)^2 \right] \quad (4.97)$$

A few mode shapes are shown in Fig.4.11; the natural frequencies and the mode shapes have two indexes;  $i$  refer to the waviness in the direction  $x$  and  $k$  to the waviness in the direction  $y$ . The number of nodal lines (where the amplitude is zero) are respectively  $i - 1$  along  $x$  and  $k - 1$  along  $y$ . Table 4.1 gives the ratio  $\omega_{ik}/\omega_{11}$  for the first few modes; notice that the modal density (i.e. the number of modes in a given frequency band) of plates is significantly larger than that of beams (the natural frequencies of a simply supported beam was found to follow  $\omega_k/\omega_1 = k^2$ ).

$\frac{\omega_{ik}}{\omega_{11}}$	$i$				
	1	2	3	4	5
$k$	1	1	1.6	2.6	4
	2	3.4	4	5	6.4
	3	7.4	8	9	10.4
	4	13	13.6	14.6	16
	5	20.2	20.8	21.8	23.2
					25

**Table 4.1.** Simply supported rectangular plate with  $a = 2b$ ; ratio  $\omega_{ik}/\omega_{11}$  for increasing values of  $i$  and  $k$ .

#### 4.9.3 Free vibration of a clamped circular plate

For a circular plate (of radius  $a$ ), it is convenient to use the polar coordinates  $(r, \theta)$ . Equation (4.87) still applies, with the Laplacian operator expressed in polar coordinates:

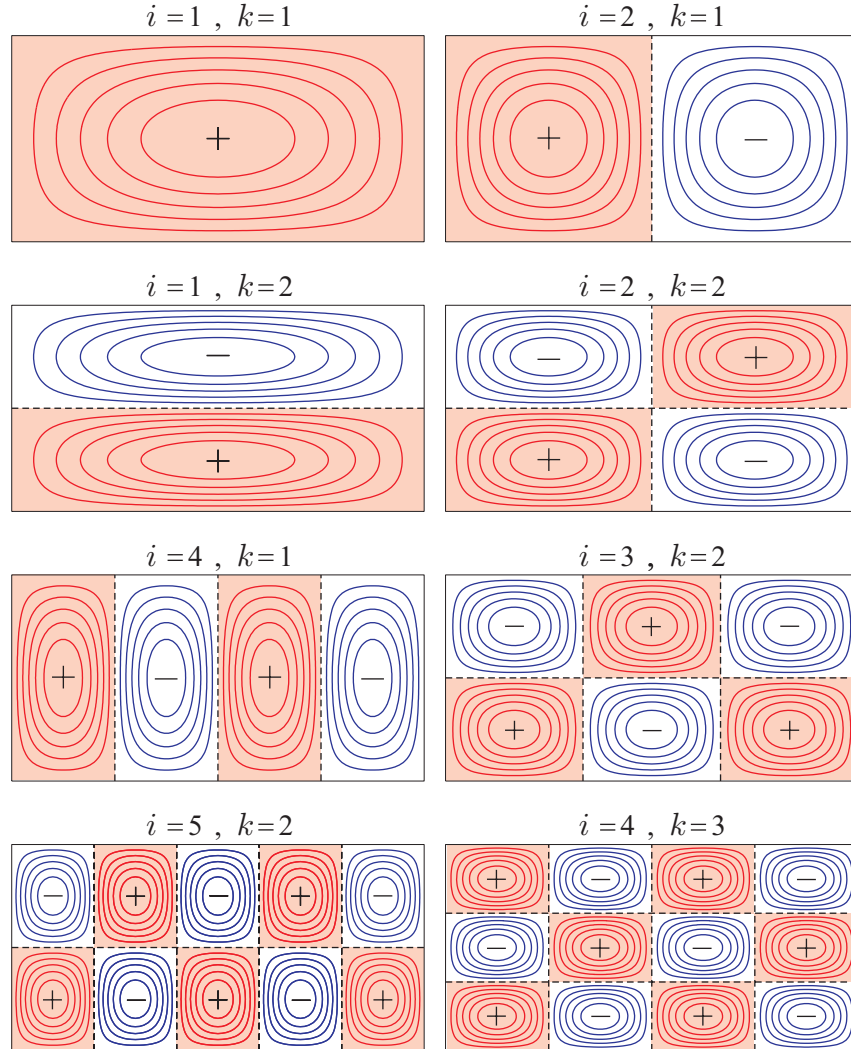


**Fig. 4.11.** Level lines of a few mode shapes of a simply supported rectangular plate with  $a = 2b$ . The nodal lines are in dotted lines.

$$\nabla^2 = \frac{\partial^2}{\partial r^2} + \frac{1}{r} \frac{\partial}{\partial r} + \frac{1}{r^2} \frac{\partial^2}{\partial \theta^2} \quad (4.98)$$

If the plate is clamped, the boundary conditions along the contour are

$$w = 0, \quad \frac{\partial w}{\partial r} = 0 \quad \text{at } r = a \quad (4.99)$$

Once again, a non trivial harmonic solution  $w = W(r, \theta)e^{j\omega t}$  exists if  $W(r, \theta)$  and  $\omega$  satisfy the eigenvalue problem (4.90)

$$(\nabla^2 + \beta^2)(\nabla^2 - \beta^2)W = 0$$

The complete solution is given by the superposition  $W = W_1 + W_2$  of the solutions of (4.91); assuming Fourier components in  $\theta$ ,

$$W(r, \theta) = \sum_{n=0}^{\infty} W_n(r) \cos n\theta + \sum_{n=1}^{\infty} W_n^*(r) \sin n\theta \quad (4.100)$$

Since the boundary conditions are axisymmetric, the terms involving the  $\sin n\theta$  are not needed. Substituting into Equ.(4.91) yields

$$\frac{d^2 W_{n1}(r)}{dr^2} + \frac{1}{r} \frac{dW_{n1}(r)}{dr} - \left( \frac{n^2}{r^2} - \beta^2 \right) W_{n1} = 0 \quad (4.101)$$

$$\frac{d^2 W_{n2}(r)}{dr^2} + \frac{1}{r} \frac{dW_{n2}(r)}{dr} - \left( \frac{n^2}{r^2} + \beta^2 \right) W_{n2} = 0 \quad (4.102)$$

These are Bessel's equations with solutions

$$\begin{aligned} W_{n1} &= A_n J_n(\beta r) + B_n Y_n(\beta r) \\ W_{n2} &= C_n I_n(\beta r) + D_n K_n(\beta r) \end{aligned} \quad (4.103)$$

where  $J_n(\beta r)$  and  $Y_n(\beta r)$  are Bessel functions of the first and second kinds, and  $I_n(\beta r)$  and  $K_n(\beta r)$  are modified Bessel functions of the first and second kinds, respectively;  $A_n, \dots, D_n$  are constants depending on the boundary conditions. The terms in  $Y_n(\beta r)$  and  $K_n(\beta r)$  must be discarded, because they are singular at  $r = 0$  (they would lead to infinite deflections); it follows that  $B_n = D_n = 0$ . The general solution is reduced to the sum of modes

$$W_n(r, \theta) = [A_n J_n(\beta r) + C_n I_n(\beta r)] \cos n\theta \quad (n = 0, \dots, \infty) \quad (4.104)$$

Since the plate is clamped at  $r = a$ , the boundary conditions (4.99) lead to the system of equations

$$\begin{bmatrix} J_n(\lambda) & I_n(\lambda) \\ J'_n(\lambda) & I'_n(\lambda) \end{bmatrix} \begin{Bmatrix} A_n \\ C_n \end{Bmatrix} = 0 \quad (4.105)$$

where the primes indicate the derivative with respect to the argument and  $\lambda = \beta a$ . The values of  $\lambda$  which cancel the determinant are the eigenvalues of the problem; using recursive properties of the Bessel's functions, one can show that they are solutions of

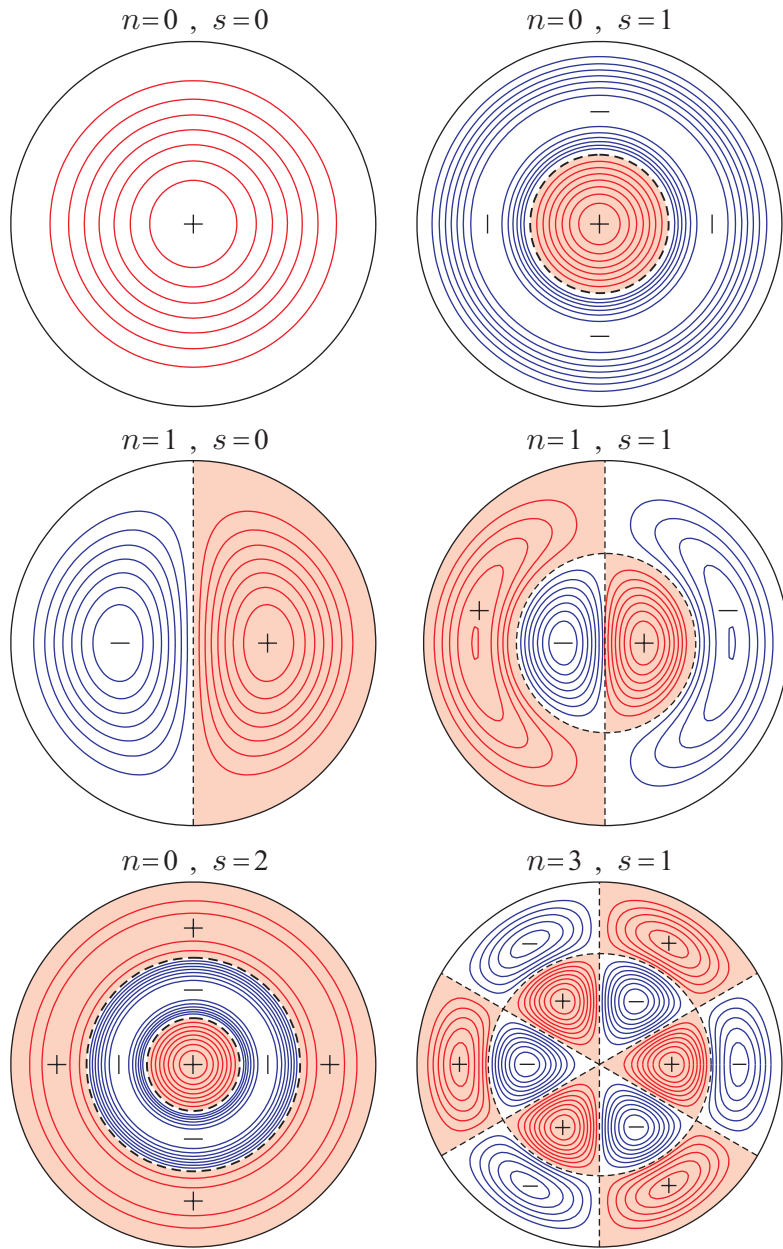


**Fig. 4.12.** Level lines of a few mode shapes of a circular plate clamped on the outer edge.  $n$  is the number of nodal diameters and  $s$  is the number of nodal circles. The nodal lines are in dotted lines.

$$J_n(\lambda)I_{n+1}(\lambda) + I_n(\lambda)J_{n+1}(\lambda) = 0 \quad (4.106)$$

Thus, for any number of nodal diameters  $n$ , there is a set of solutions corresponding to an increasing number of nodal circles  $s$ .<sup>4</sup> Once  $\lambda_{ns}$  has been determined, the natural frequency is obtained from Equ.(4.89):

$$\omega_{ns} = \beta_{ns}^2 \sqrt{\frac{D}{m}} = \frac{\lambda_{ns}^2}{a^2} \cdot \sqrt{\frac{D}{m}} \quad (4.107)$$

For every eigenvalue  $\lambda$ , the first equation (4.105) provides

$$C_n = -\frac{J_n(\lambda)}{I_n(\lambda)} A_n$$

and the mode shape corresponding to  $n$  nodal diameters and  $s$  nodal circles is

$$W_{ns}(r, \theta) = A_n [J_n(\beta r) - \frac{J_n(\beta a)}{I_n(\beta a)} I_n(\beta r)] \cos n\theta \quad (4.108)$$

where  $\beta = \lambda_{ns}/a$  (the subscript  $ns$  is dropped from  $\beta$  for clarity). A few mode shapes are shown in Fig.4.12.

#### 4.9.4 Rotating modes

Since the disk is axisymmetric, the modes occur by pairs, with the same natural frequency: If  $W_{ns}(r, \theta) = W_{ns}(r) \cos n\theta$  is a mode shape of natural frequency  $\omega_{ns}$  (with  $n$  nodal diameters and  $s$  nodal circles),  $W_{ns}^*(r, \theta) = W_{ns}(r) \sin n\theta$  is also a mode shape, with the same natural frequency  $\omega_{ns}$ ;  $W_{ns}^*$  is simply rotated by  $\pi/2$  with respect to  $W_{ns}$ . If these modes are excited equally at  $\omega$  with a phase shift of  $\pi/2$ , their combined response may be written

$$W(r, \theta, t) = W_{ns}(r)(\cos n\theta \cos \omega t + \sin n\theta \sin \omega t)$$

or

$$W(r, \theta, t) = W_{ns}(r) \cos(n\theta - \omega t) \quad (4.109)$$

The result is a traveling wave with  $n$  nodal diameters turning in the positive direction (progressive wave) with a velocity  $\omega/n$ . The situation is similar for any axisymmetric boundary conditions: the mode shapes have the form

---

<sup>4</sup> The values of  $\lambda_{ns}$  are tabulated in Leissa, 1969.

$$\begin{aligned} W_{ns}(r, \theta) &= W_{ns}(r) \cos n\theta \\ W_{ns}^*(r, \theta) &= W_{ns}(r) \sin n\theta \end{aligned} \quad (4.110)$$

with different radial shapes  $W_{ns}(r)$  and different natural frequencies (depending on the boundary conditions).

#### 4.10 Response of a disk to a rotating point force\*

The response of *rotationally periodic structures* (such as circular saws, bladed turbine disks) to rotating forces is important in the analysis of rotating machines. These structures possess the notable feature that their mode shapes are harmonic in the circumferential direction, which makes them very similar to axisymmetric structures. In this section, we examine the response of a disk with axisymmetric boundary conditions to a rotating point force and analyze the conditions under which a rotating force is able to excite resonances (Wildheim, 1979).

The general response of a disk may be written

$$W(r, \theta, t) = \sum_{n=0}^{\infty} \sum_{s=0}^{\infty} W_{ns}(r) [c_{ns}(t) \cos n\theta + s_{ns}(t) \sin n\theta] \quad (4.111)$$

where  $W_{ns}(r)$  is the mode shape with  $n$  nodal diameters and  $s$  nodal circles, and  $c_{ns}(t)$  and  $s_{ns}(t)$  are the modal amplitudes of respectively the cosine mode and the sine mode (with the same frequency  $\omega_{ns}$ ).

##### 4.10.1 Constant rotating point force

Let us first consider a constant point force  $F$  applied at  $r = R$  and rotating at the angular speed  $\Omega$ :

$$f(r, \theta, t) = F\delta(\theta - \Omega t)\delta(r - R) \quad (4.112)$$

where  $\delta$  is the Dirac function; the generalized forces in modal coordinates, equal to the work of the point force on the cosine modes,  $p_{ns}(t)$  and the sine modes,  $q_{ns}(t)$  are respectively

$$p_{ns}(t) = \int_0^a \int_0^{2\pi} f(r, \theta, t) W_{ns}(r) \cos n\theta dr d\theta$$

$$p_{ns}(t) = \int_0^a \int_0^{2\pi} F \delta(\theta - \Omega t) \delta(r - R) W_{ns}(r) \cos n\theta dr d\theta$$

$$p_{ns}(t) = FRW_{ns}(R) \cos n\Omega t \quad (4.113)$$

and

$$\begin{aligned} q_{ns}(t) &= \int_0^a \int_0^{2\pi} f(r, \theta, t) W_{ns}(r) \sin n\theta dr d\theta \\ q_{ns}(t) &= FRW_{ns}(R) \sin n\Omega t \end{aligned} \quad (4.114)$$

Neglecting the damping, the modal coordinates [respectively  $c_{ns}(t)$  and  $s_{ns}(t)$ ] are governed by

$$\begin{aligned} \mu_{ns} \ddot{c}_{ns} + \mu_{ns} \omega_{ns}^2 c_{ns} &= p_{ns} = FRW_{ns}(R) \cos n\Omega t \\ \mu_{ns} \ddot{s}_{ns} + \mu_{ns} \omega_{ns}^2 s_{ns} &= p_{ns} = FRW_{ns}(R) \sin n\Omega t \end{aligned} \quad (4.115)$$

where  $\mu_{ns}$  is the modal mass. If the modes are normalized in such a way that  $RW_{ns}(R)/\mu_{ns} = 1$ , these equations become

$$\begin{aligned} \ddot{c}_{ns} + \omega_{ns}^2 c_{ns} &= F \cos n\Omega t \\ \ddot{s}_{ns} + \omega_{ns}^2 s_{ns} &= F \sin n\Omega t \end{aligned} \quad (4.116)$$

The steady state modal response is harmonic:

$$c_{ns}(t) = \frac{F \cos n\Omega t}{\omega_{ns}^2 - (n\Omega)^2}, \quad s_{ns}(t) = \frac{F \sin n\Omega t}{\omega_{ns}^2 - (n\Omega)^2}$$

From (4.111), the global response reads

$$W(r, \theta, t) = \sum_{n=0}^{\infty} \sum_{s=0}^{\infty} W_{ns}(r) \frac{F}{\omega_{ns}^2 - (n\Omega)^2} (\cos n\Omega t \cos n\theta + \sin n\Omega t \sin n\theta)$$

or

$$W(r, \theta, t) = \sum_{n=0}^{\infty} \sum_{s=0}^{\infty} W_{ns}(r) \frac{F \cos n(\theta - \Omega t)}{\omega_{ns}^2 - (n\Omega)^2} \quad (4.117)$$

The forced response of the various modes has the character of a traveling wave, whose amplitude is magnified in the vicinity of the resonance

$$\omega_{ns} = n\Omega \quad (4.118)$$

where  $n$  is the number of nodal diameters of the mode.

#### 4.10.2 Harmonic rotating point force

If the forcing function is harmonic of frequency  $\omega_f$ , in addition to rotating at  $\Omega$ ,

$$f(r, \theta, t) = F \cos \omega_f t. \delta(\theta - \Omega t) \delta(r - R) \quad (4.119)$$

The generalized modal forces become

$$\begin{aligned} p_{ns}(t) &= FRW_{ns}(R) \cos n\Omega t. \cos \omega_f t \\ q_{ns}(t) &= FRW_{ns}(R) \sin n\Omega t. \cos \omega_f t \end{aligned} \quad (4.120)$$

Normalizing according to  $RW_{ns}(R)/\mu_{ns} = 1$  as in the previous case, the modal forces may be written as the superposition of two forcing functions, respectively at  $n\Omega + \omega_f$  and  $n\Omega - \omega_f$

$$\begin{aligned} p_{ns}(t) &= \frac{F}{2} [\cos(n\Omega + \omega_f)t + \cos(n\Omega - \omega_f)t] \\ q_{ns}(t) &= \frac{F}{2} [\sin(n\Omega + \omega_f)t + \sin(n\Omega - \omega_f)t] \end{aligned} \quad (4.121)$$

The modal responses are

$$\begin{aligned} c_{ns} &= \frac{F}{2} \left[ \frac{\cos(n\Omega + \omega_f)t}{\omega_{ns}^2 - (n\Omega + \omega_f)^2} + \frac{\cos(n\Omega - \omega_f)t}{\omega_{ns}^2 - (n\Omega - \omega_f)^2} \right] \\ s_{ns} &= \frac{F}{2} \left[ \frac{\sin(n\Omega + \omega_f)t}{\omega_{ns}^2 - (n\Omega + \omega_f)^2} + \frac{\sin(n\Omega - \omega_f)t}{\omega_{ns}^2 - (n\Omega - \omega_f)^2} \right] \end{aligned} \quad (4.122)$$

After substituting in Equ.(4.111) and resolving the products of cosine and sine functions with trigonometric identities, the global response reads

$$W(r, \theta, t) = \sum_{n,s} W_{ns}(r) \frac{F}{2} \left[ \frac{\cos n[\theta - (\Omega + \frac{\omega_f}{n})t]}{\omega_{ns}^2 - (n\Omega + \omega_f)^2} + \frac{\cos n[\theta - (\Omega - \frac{\omega_f}{n})t]}{\omega_{ns}^2 - (n\Omega - \omega_f)^2} \right] \quad (4.123)$$

which appears also as a combination of traveling waves whose amplitudes are magnified in the vicinity of the resonances defined by

$$\omega_{ns} = |\pm n\Omega \pm \omega_f| \quad (4.124)$$

This relation defines the resonance conditions which must be avoided in the operation of the system.

## 4.11 Problems

**P.4.1** Solve the eigenvalue problem for the vibration of a uniform beam without preload with the following boundary conditions:

- (a) Clamped-free [ $\mu_1 = 1.875$ ,  $\mu_2 = 4.694$ ,  $\mu_n \approx (2n - 1)\pi/2$ ]
- (b) Clamped-clamped [ $\mu_1 = 4.73$ ,  $\mu_2 = 7.853$ ,  $\mu_n \approx (2n + 1)\pi/2$ ]

**P.4.2** Solve the eigenvalue problem of a uniform bar with free-free boundary conditions.

**P.4.3** Derive the partial differential equation governing the vibration of a string from Hamilton's principle. [Hint: The strain energy is entirely due to the preload  $T_0$ .]



## Rayleigh-Ritz method

*La sagesse a ses excès et n'a pas moins besoin de modération que la folie.*

Montaigne, *Essais*, 1572-1588

### 5.1 introduction

The partial differential equations of structural dynamics are difficult to solve, except for very simple configurations; a few of them were examined in the previous chapter. For more complicated systems, approximate solutions are sought, by transforming the partial differential equation into a system of second order ordinary differential equations which carry the dominant (low frequency) behavior of the system. This process is called *discretization* and the number of ordinary differential equations is the number of degrees of freedom (d.o.f.) of the discretized system. If the method is well conditioned and convergent, the degree of approximation will improve with the number of degrees of freedom and the error can be made arbitrarily small in a limited frequency band.

In this chapter, we consider a *global* method of approximation known as the Rayleigh-Ritz method;<sup>1</sup> the method relies on the selection of global shape functions which satisfy the global boundary conditions; it is very elegant and works very well for rather simple structures where a set of shape functions is not too difficult to guess. Once the shape functions have been selected, the various energies involved in the problem are expressed in terms of a finite set of generalized variables and introduced in the Lagrange equations. With a good choice of shape functions, the convergence is very quick; however, when the structure is more complicated, global shape functions become almost impossible to guess and the method is difficult to use. The problem can be solved by using *finite elements*, as discussed later.

---

<sup>1</sup> It is also called “global assumed modes method”.

For simplicity, the method is presented here for structures with one spatial coordinate; however, there is no restriction and the method applies identically to structures with several spatial coordinates ( $x$  simply becomes a vector). The mathematical developments are reduced to the strict minimum, to focus on the physical aspects.

## 5.2 Shape functions

In the Rayleigh-Ritz method, the global displacement field  $u(x, t)$  is approximated according to a finite expansion with  $n$  d.o.f.

$$u(x, t) = \sum_{i=1}^n \psi_i(x) q_i(t) \quad (5.1)$$

where the  $q_i(t)$  are the generalized variables and  $\psi_i(x)$  are a set of *shape functions*, *linearly independent* and *complete*, and satisfying the global kinematic boundary conditions of the problem.

By *linearly independent*, it is meant that one cannot find a set of coefficients  $a_k \neq 0$  such that  $\sum a_k \psi_k(x) = 0$ . Shape functions which are not linearly independent do not enlarge the space spanned by the approximation.

The set of functions  $\psi_i(x)$  is *complete* if the error  $\varepsilon_n$  in the approximation of any function  $f(x)$  satisfying the same boundary conditions,

$$\varepsilon_n = \|f(x) - \sum_{i=1}^n \psi_i(x) a_i\| \quad (5.2)$$

can be made arbitrarily small by increasing the number of terms  $n$  in the approximation:

$$\lim_{n \rightarrow \infty} \varepsilon_n = 0$$

In Equ.(5.2),  $\|\cdot\|$  stands for some *norm* measuring the distance between the function  $f(x)$  and its approximation. The most frequent norm is the quadratic norm:

$$\|u\|_2 = (u, u)^{1/2} \quad (5.3)$$

where  $(u, v)$  is the *inner product* between the two functions  $u$  and  $v$ :  $(u, v)$  is a real number satisfying the following properties

- (a) Symmetric :  $(u, v) = (v, u)$
- (b) Homogeneous :  $(\alpha u, v) = \alpha(u, v)$
- (c) Additive :  $(u_1 + u_2, v) = (u_1, v) + (u_2, v)$
- (d) Positive definite :  $(u, u) > 0$  for all  $u \neq 0$

A simple example is

$$(u, v) = \int_{\Omega} uv d\Omega \quad (5.5)$$

where the integral extends over the complete domain  $\Omega$  where the functions are defined. There can also be a positive weight  $w(\Omega)$  included in the integral.

To illustrate the necessity of a *complete* set of shape functions, consider a continuous function  $f(x)$  defined on  $[0, L]$  and such that  $f(0) = 0$  and  $f(L) = 0$ . The harmonic functions

$$\psi_i(x) = \sin \frac{i\pi x}{L} \quad i = 1, 2, \dots, n \quad (5.6)$$

satisfy the boundary conditions and constitute a complete set of  $n$  admissible shape functions. On the contrary, assume that one of the harmonic components is missing, for example that for  $i = 2$ ; the set of admissible functions

$$\sin \frac{\pi x}{L}, \sin \frac{3\pi x}{L}, \sin \frac{4\pi x}{L}, \dots$$

is not complete, because the contribution associated with any component in  $\sin(2\pi x/L)$  present in  $f(x)$  cannot be matched by increasing the number of terms in the expansion.

The case of *orthogonal functions* is particularly interesting, because the coefficients of the expansion can be determined independently. A set of functions  $u_i(x)$  is *orthogonal with respect to an inner product operator*  $(u, v)$  if

$$(u_i, u_j) = \|u_i\|^2 \delta_{ij} \quad (5.7)$$

where  $\delta_{ij}$  is the Kronecker delta ( $\delta_{ij} = 1$  if  $i = j$ ,  $\delta_{ij} = 0$  if  $i \neq j$ ). In this case, the coefficients  $\alpha_k$  of the expansion

$$f(x) = \sum_{i=1}^n \alpha_i u_i(x) \quad (5.8)$$

are determined independently according to

$$\alpha_k = \frac{(u_k, f)}{(u_k, u_k)} \quad (5.9)$$

The harmonic functions (5.6)(which are in fact the well known Fourier series expansion) are orthogonal with respect to the inner product (5.5):

$$\int_0^L \sin \frac{i\pi x}{L} \cdot \sin \frac{j\pi x}{L} dx = \frac{L}{2} \delta_{ij}$$

The methodology is now explained with a few examples.

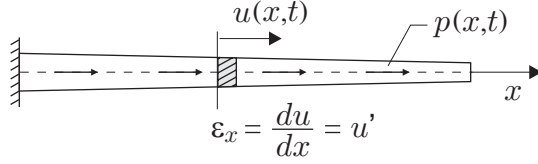


Fig. 5.1. Axial vibration of a bar.

### 5.3 Axial vibration of a bar

Consider the bar of cross section  $A(x)$  with an axial distributed load  $p(x)$ , Fig. 5.1. The strain is uniform across the section,  $\varepsilon_x = u'$  and the strain energy reads

$$V = \frac{1}{2} \int_0^L EA(u')^2 dx \quad (5.10)$$

If the axial displacement is approximated according to (5.1), the axial strain can be written

$$u'(x, t) = \sum_{i=1}^n \psi'_i(x) q_i(t) \quad (5.11)$$

Substituting into the strain energy,

$$\begin{aligned} V &= \frac{1}{2} \int_0^L EA \left[ \sum_{i=1}^n \psi'_i(x) q_i(t) \right] \left[ \sum_{j=1}^n \psi'_j(x) q_j(t) \right] dx \\ V &= \frac{1}{2} \sum_{i=1}^n \sum_{j=1}^n \left[ \int_0^L EA \psi'_i(x) \psi'_j(x) dx \right] q_i(t) q_j(t) \end{aligned}$$

or

$$V = \frac{1}{2} \mathbf{q}^T K \mathbf{q} \quad (5.12)$$

where  $\mathbf{q} = (q_1, \dots, q_n)^T$  is the vector of generalized coordinates and  $K$  is the *stiffness matrix* of the discretized system:

$$K_{ij} = \int_0^L EA \psi'_i(x) \psi'_j(x) dx \quad (5.13)$$

$K$  is symmetric and positive definite (by construction, since  $V > 0$  for all  $u$  such that  $u' \neq 0$ ;  $K$  is semi-positive definite if rigid body displacements are allowed).

Similarly, the velocity  $\dot{u}$  is uniform in the cross section and the kinetic energy reads

$$T = \frac{1}{2} \int_0^L \varrho A \dot{u}^2 dx \quad (5.14)$$

If the axial displacement is approximated according to (5.1), the axial velocity can be written

$$\dot{u}(x, t) = \sum_{i=1}^n \psi_i(x) \dot{q}_i(t) \quad (5.15)$$

Substituting into the kinetic energy,

$$T = \frac{1}{2} \int_0^L \varrho A \left[ \sum_{i=1}^n \psi_i(x) \dot{q}_i(t) \right] \left[ \sum_{j=1}^n \psi_j(x) \dot{q}_j(t) \right] dx$$

$$T = \frac{1}{2} \sum_{i=1}^n \sum_{j=1}^n \left[ \int_0^L \varrho A \psi_i(x) \psi_j(x) dx \right] \dot{q}_i(t) \dot{q}_j(t)$$

or

$$T = \frac{1}{2} \dot{\mathbf{q}}^T M \dot{\mathbf{q}} \quad (5.16)$$

where  $\dot{\mathbf{q}} = (\dot{q}_1, \dots, \dot{q}_n)^T$  is the vector of generalized velocities and  $M$  is the *mass matrix* of the discretized system:

$$M_{ij} = \int_0^L \varrho A \psi_i(x) \psi_j(x) dx \quad (5.17)$$

$M$  is symmetric and positive definite (by construction, since  $T > 0$ ).

Finally, the virtual displacements can be expressed in terms of the generalized variables:

$$\delta u(x, t) = \sum_{i=1}^n \psi_i(x) \delta q_i \quad (5.18)$$

and the virtual work of the non conservative forces  $p$  reads

$$\delta W_{nc} = \int_0^L p \delta u dx = \sum_{i=1}^n \delta q_i \left[ \int_0^L p(x, t) \psi_i(x) dx \right] = \mathbf{f}^T \delta \mathbf{q} \quad (5.19)$$

where  $\mathbf{f}(t) = (f_1, \dots, f_n)^T$  is the vector of generalized forces:

$$f_i = \int_0^L p(x, t) \psi_i(x) dx \quad (5.20)$$

$f_i$  is in fact the work of the distributed load on the shape function  $\psi_i(x)$ .

In summary, the Rayleigh-Ritz approximation transforms the infinite dimensional problem into a problem with  $n$  degrees of freedom [ $\mathbf{q} = (q_1, \dots, q_n)^T$ ], with the following expressions

$$\begin{aligned} V &= \frac{1}{2} \mathbf{q}^T K \mathbf{q} \\ T &= \frac{1}{2} \dot{\mathbf{q}}^T M \dot{\mathbf{q}} \\ L &= T - V = \frac{1}{2} \dot{\mathbf{q}}^T M \dot{\mathbf{q}} - \frac{1}{2} \mathbf{q}^T K \mathbf{q} \\ \delta W_{nc} &= \mathbf{f}^T \delta \mathbf{q} \end{aligned} \quad (5.21)$$

From Lagrange's equations

$$\frac{d}{dt} \left( \frac{\partial L}{\partial \dot{\mathbf{q}}} \right) - \frac{\partial L}{\partial \mathbf{q}} = \mathbf{f} \quad (5.22)$$

one gets the governing equation which was already discussed in section 3.6.1:

$$M \ddot{\mathbf{q}} + K \mathbf{q} = \mathbf{f} \quad (5.23)$$

#### 5.4 Planar vibration of a beam

Consider the planar vibration of a beam with the Euler-Bernoulli kinematic assumption discussed in section 4.1, Fig.5.2. The uniaxial bending strain is related to the transverse displacement according to Equ.(4.3) and (4.4)

$$u(x, y) = -y \frac{dv}{dx} = -y v'(x) \quad \varepsilon_x = \frac{\partial u}{\partial x} = -y v''(x)$$

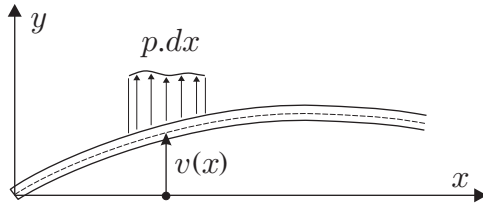


Fig. 5.2. Planar vibration of a beam.

It follows that the strain energy reads

$$V = \frac{1}{2} \int_{\Omega} E\varepsilon_x^2 dx = \frac{1}{2} \int_0^L [E(v'')^2 \int_A y^2 dA] dx = \frac{1}{2} \int_0^L EI(v'')^2 dx \quad (5.24)$$

The kinetic energy and the virtual work of the non conservative forces are respectively

$$T = \frac{1}{2} \int_0^L \varrho A(\dot{v})^2 dx, \quad \delta W_{nc} = \int_0^L p \delta v dx \quad (5.25)$$

In the Rayleigh-Ritz methods, the transverse displacement field  $v(x, t)$  is approximated according to a finite expansion with  $n$  d.o.f.

$$v(x, t) = \sum_{i=1}^n \psi_i(x) q_i(t) \quad (5.26)$$

where the shape functions  $\psi_i(x)$  satisfy the global boundary conditions. It follows that

$$v''(x, t) = \sum_{i=1}^n \psi''_i(x) q_i(t) \quad (5.27)$$

Substituting into the strain energy,

$$\begin{aligned} V &= \frac{1}{2} \int_0^L EI \left[ \sum_{i=1}^n \psi''_i(x) q_i(t) \right] \left[ \sum_{j=1}^n \psi''_j(x) q_j(t) \right] dx \\ V &= \frac{1}{2} \sum_{i=1}^n \sum_{j=1}^n \left[ \int_0^L EI \psi''_i(x) \psi''_j(x) dx \right] q_i(t) q_j(t) \end{aligned}$$

or

$$V = \frac{1}{2} \mathbf{q}^T K \mathbf{q} \quad (5.28)$$

where  $\mathbf{q} = (q_1, \dots, q_n)^T$  is the vector of generalized coordinates and  $K$  is the *stiffness matrix* of the discretized system:

$$K_{ij} = \int_0^L EI \psi''_i(x) \psi''_j(x) dx \quad (5.29)$$

$K$  is symmetric and positive definite (by construction, since  $V > 0$  for all  $v(x)$  such that  $v'' \neq 0$ ;  $K$  is semi-positive definite if rigid body displacements are allowed).

Similarly, the transverse velocity can be written

$$\dot{v}(x, t) = \sum_{i=1}^n \psi_i(x) \dot{q}_i(t) \quad (5.30)$$

Substituting into the kinetic energy,

$$T = \frac{1}{2} \int_0^L \varrho A \left[ \sum_{i=1}^n \psi_i(x) \dot{q}_i(t) \right] \left[ \sum_{j=1}^n \psi_j(x) \dot{q}_j(t) \right] dx$$

$$T = \frac{1}{2} \sum_{i=1}^n \sum_{j=1}^n \left[ \int_0^L \varrho A \psi_i(x) \psi_j(x) dx \right] \dot{q}_i(t) \dot{q}_j(t)$$

or

$$T = \frac{1}{2} \dot{\mathbf{q}}^T M \dot{\mathbf{q}} \quad (5.31)$$

where  $\dot{\mathbf{q}} = (\dot{q}_1, \dots, \dot{q}_n)^T$  is the vector of generalized velocities and  $M$  is the *mass matrix* of the discretized system:

$$M_{ij} = \int_0^L \varrho A \psi_i(x) \psi_j(x) dx \quad (5.32)$$

$M$  is symmetric and positive definite (by construction, since  $T > 0$ ).

Finally, the virtual displacements can be expressed in terms of the generalized variables:

$$\delta v(x, t) = \sum_{i=1}^n \psi_i(x) \delta q_i \quad (5.33)$$

and the virtual work of the non conservative forces  $p$  reads

$$\delta W_{nc} = \int_0^L p \delta v dx = \sum_{i=1}^n \delta q_i \left[ \int_0^L p(x, t) \psi_i(x) dx \right] = \mathbf{f}^T \delta \mathbf{q} \quad (5.34)$$

where  $\mathbf{f}(t) = (f_1, \dots, f_n)^T$  is the vector of generalized forces:

$$f_i = \int_0^L p(x, t) \psi_i(x) dx \quad (5.35)$$

$f_i$  is the work of the distributed load on the shape function  $\psi_i(x)$ .

Thus, the developments follow closely those of the axial vibration of a bar, leading to the same general form (5.21) for the various energy terms involved in the Lagrange equation, leading to the same governing equation (5.23) with the appropriate definition of the stiffness and mass matrices.

Comparing the elements of the mass and stiffness matrices with the orthogonality relationships (4.40) and (4.41), one sees that, if the shape functions  $\psi_i(x)$  are chosen to be the mode shapes  $v_i(x)$  corresponding to the same boundary conditions, both matrices become diagonal, leading to a set of decoupled equations.

### 5.4.1 Damping

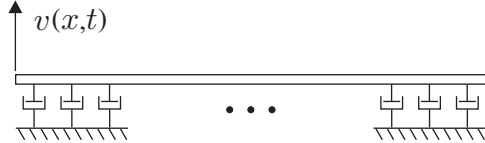


**Fig. 5.3.** Planar vibration of a beam with distributed damping,  $p(x, t) = -\xi(x)\dot{v}(x, t)$ .

Consider the distributed damping (Fig.5.3) generating the distributed force

$$p(x, t) = -\xi(x)\dot{v}(x, t) \quad (5.36)$$

with  $\xi(x) > 0$ . Using Equ.(5.30) and (5.33),

$$\begin{aligned} \delta W_{nc} &= \int_0^L p \delta v dx = \int_0^L [-\xi(x) \sum_{i=1}^n \psi_i(x) \dot{q}_i(t)] [\sum_{j=1}^n \psi_j(x) \delta q_j] dx \\ \delta W_{nc} &= - \sum_{i=1}^n \sum_{j=1}^n \dot{q}_i(t) \delta q_j [\int_0^L \xi(x) \psi_i(x) \psi_j(x) dx] = -\delta \mathbf{q}^T C \dot{\mathbf{q}} \end{aligned} \quad (5.37)$$

with the damping matrix  $C$  defined as

$$C_{ij} = \int_0^L \xi(x) \psi_i(x) \psi_j(x) dx \quad (5.38)$$

( $C$  is symmetric and positive definite). It follows that the generalized damping forces read

$$\mathbf{f} = -C \dot{\mathbf{q}} \quad (5.39)$$

### 5.4.2 Beam with axial load

Because of the axial load, there is an additional contribution due to the geometric strain energy; it is given by (4.17)

$$V_g = \frac{1}{2} \int_0^L N(v')^2 dx \quad (5.40)$$

where  $N$  is positive in traction. From (5.26),

$$v'(x, t) = \sum_{i=1}^n \psi'_i(x) q_i(t) \quad (5.41)$$

$$\begin{aligned} V_g &= \frac{1}{2} \int_0^L N \left[ \sum_{i=1}^n \psi'_i(x) q_i(t) \right] \left[ \sum_{j=1}^n \psi'_j(x) q_j(t) \right] dx \\ V_g &= \frac{1}{2} \sum_{i=1}^n \sum_{j=1}^n \left[ \int_0^L N \psi'_i(x) \psi'_j(x) dx \right] q_i(t) q_j(t) \end{aligned}$$

or

$$V_g = \frac{1}{2} \mathbf{q}^T K_g \mathbf{q} \quad (5.42)$$

$$(K_g)_{ij} = \int_0^L N \psi'_i(x) \psi'_j(x) dx \quad (5.43)$$

The novelty here is that the geometric stiffness matrix  $K_g$  is not positive definite, because  $N$  may be positive or negative. The global stiffness matrix is  $K + K_g$ .

#### 5.4.3 Simply supported beam with uniform axial load

As an example, consider the simply supported beam with uniform axial load  $N = -P$  (Fig.4.9.a). The first natural frequency is evaluated with a single term approximation

$$v(x, t) = q(t) \cdot \sin \frac{\pi x}{L} \quad (5.44)$$

where the shape function  $\psi(x) = \sin \frac{\pi x}{L}$  satisfies the kinematic boundary conditions  $x(0) = 0$  and  $x(L) = 0$ . From (5.29), (5.43) and (5.32), one gets:

$$\begin{aligned} K &= \int_0^L EI (\psi'')^2 dx = EI \left(\frac{\pi}{L}\right)^4 \int_0^L \sin^2 \frac{\pi x}{L} dx = \frac{EI\pi^4}{2L^3} \\ K_g &= - \int_0^L P (\psi')^2 dx = -P \left(\frac{\pi}{L}\right)^2 \int_0^L \cos^2 \frac{\pi x}{L} dx = -\frac{P\pi^2}{2L} \end{aligned}$$

$$M = \int_0^L \varrho A \psi^2 dx = \varrho A \int_0^L \sin^2 \frac{\pi x}{L} dx = \frac{\varrho A L}{2}$$

and the equation of motion is

$$\frac{\varrho A L}{2} \ddot{q} + \left[ \frac{EI\pi^4}{2L^3} - \frac{P\pi^2}{2L} \right] q = 0$$

or

$$\varrho A L \ddot{q} + \frac{EI\pi^4}{L^3} \left[ 1 - \frac{P}{P_{cr}} \right] q = 0 \quad (5.45)$$

where  $P$  is positive in compression and  $P_{cr}$  is Euler's critical buckling load (4.68). Thus, the natural frequency is

$$\omega_1 = \sqrt{\frac{EI\pi^4}{\varrho A L^4}} \cdot \sqrt{1 - \frac{P}{P_{cr}}} \quad (5.46)$$

This result is in fact the analytical solution of the eigenvalue problem

$$EI v^{IV} + Pv'' - \varrho A \omega^2 v = 0$$

as can be checked by substitution. This is because the selected shape function happens to be the first mode shape of the problem. This illustrates that the Rayleigh-Ritz method gives the best possible approximation within the space defined by the assumed shape functions. Equation (5.46) defines the buckling load as the compression load which reduces the first natural frequency to zero.

## 5.5 Rayleigh quotient

### 5.5.1 Continuous beam

According to Equ.(4.44), the mode shape  $v_i(x)$  and the natural frequency  $\omega_i$  of a beam satisfy

$$\omega_i^2 = \frac{\int_0^L EI (v_i'')^2 dx}{\int_0^L \varrho A v_i^2 dx} \quad (5.47)$$

In this section, we study a more general form called the *Rayleigh quotient*:

$$R(v) = \frac{\int_0^L EI (v'')^2 dx}{\int_0^L \varrho A v^2 dx} \quad (5.48)$$

where  $v(x)$  is any displacement field compatible with the kinematics of the problem.  $R(v)$  is a functional, because every function  $v(x)$  leads to a scalar value  $R(v) \geq 0$  (by construction). If  $v(x)$  is expanded in the mode shapes according to

$$v(x) = \sum_{k=1}^{\infty} c_k v_k(x) \quad (5.49)$$

the denominator of  $R(v)$  can be written

$$\begin{aligned} \int_0^L \varrho A v^2 dx &= \int_0^L \varrho A \left[ \sum_{i=1}^{\infty} c_i v_i(x) \right] \left[ \sum_{j=1}^{\infty} c_j v_j(x) \right] dx \\ &= \sum_{i=1}^{\infty} \sum_{j=1}^{\infty} c_i c_j \left\{ \int_0^L \varrho A v_i v_j dx \right\} = \sum_{i=1}^{\infty} \mu_i c_i^2 \end{aligned}$$

after using the orthogonality condition (4.40). Similarly, using the second orthogonality condition (4.43), the numerator of  $R(v)$  can be written

$$\int_0^L EI (v'')^2 dx = \dots = \sum_{i=1}^{\infty} \mu_i \omega_i^2 c_i^2$$

leading to

$$R(v) = \frac{\sum_{i=1}^{\infty} \mu_i \omega_i^2 c_i^2}{\sum_{i=1}^{\infty} \mu_i c_i^2} = \frac{\mu_1 \omega_1^2 c_1^2 + \mu_2 \omega_2^2 c_2^2 + \mu_3 \omega_3^2 c_3^2 + \dots}{\mu_1 c_1^2 + \mu_2 c_2^2 + \mu_3 c_3^2 + \dots} \quad (5.50)$$

Thus, if the modes are ordered by increasing frequencies,

$$R(v) \geq \omega_1^2 \quad (5.51)$$

It follows that any approximate solution obtained with the Rayleigh-Ritz method will provide an estimate by excess of the first natural frequency  $\omega_1$ . Similarly, if the function  $v(x)$  belongs to the subspace orthogonal to mode 1,  $c_1 = 0$  and  $R(v) \geq \omega_2^2$ , and etc... The Rayleigh quotient is a very general concept which extends far beyond the beam theory; next section considers a general discrete non-gyroscopic system.

### 5.5.2 Discrete system

According to Equ.(2.10), the mode shape  $\phi_i$  and the corresponding frequency  $\omega_i$  of a discrete non-gyroscopic system satisfy

$$\omega_i^2 = \frac{\phi_i^T K \phi_i}{\phi_i^T M \phi_i} \quad (5.52)$$

The general form of the Rayleigh quotient for a discrete system is:

$$R(\mathbf{x}) = \frac{\mathbf{x}^T K \mathbf{x}}{\mathbf{x}^T M \mathbf{x}} \quad (5.53)$$

where  $\mathbf{x}$  is a vector of generalized displacements compatible with the kinematics of the problem (i.e. satisfying the kinematic boundary conditions).  $R(\mathbf{x})$  is a functional, because for every function  $\mathbf{x}$  ( $\mathbf{x}$  is a function of the space coordinates), it has a scalar value ( $\geq 0$ , because of the properties of  $K$  and  $M$ ). Observe that the numerator is twice the strain energy associated with the displacement field  $\mathbf{x}$ , and the denominator looks very similar to twice the kinetic energy, except that  $\mathbf{x}$  appears instead of  $\dot{\mathbf{x}}$ ; for an harmonic vibration,  $\mathbf{x} = \mathbf{x}_0 e^{j\omega t}$  and  $\dot{\mathbf{x}} = j\omega \mathbf{x}_0 e^{j\omega t}$ , so that  $R(\mathbf{x})$  has indeed the dimension of a frequency squared,  $\omega^2$ .

### 5.5.3 Principle of stationarity

We now establish that the Rayleigh quotient is stationary in the vicinity of the natural frequencies  $\omega_k$  of the system, and that an error of the first order on the mode shape  $\phi_k$  leads to an error of the second order on  $\omega_k^2$ .

To demonstrate this, let

$$\mathbf{x} = \phi_k + \varepsilon \mathbf{y}$$

where  $\mathbf{y}$  is the shape of the error, and the small scalar  $\varepsilon$  fixes the amplitude.  $R(\mathbf{x})$  being homogeneous in  $\mathbf{x}$ , the amplitude may be normalized in such a way that

$$\mathbf{x}^T M \mathbf{x} = \phi_k^T M \phi_k \quad (5.54)$$

Since

$$\mathbf{x}^T M \mathbf{x} = \phi_k^T M \phi_k + 2\varepsilon \mathbf{y}^T M \phi_k + \varepsilon^2 \mathbf{y}^T M \mathbf{y}$$

It follows that

$$\mathbf{y}^T M \phi_k = -\frac{\varepsilon}{2} \mathbf{y}^T M \mathbf{y}$$

On the other hand, since  $\phi_k$  satisfies the eigenvalue problem

$$K \phi_k - \omega_k^2 M \phi_k = 0 \quad (5.55)$$

it follows that

$$\mathbf{y}^T K \phi_k = \omega_k^2 \mathbf{y}^T M \phi_k = -\frac{\varepsilon}{2} \omega_k^2 \mathbf{y}^T M \mathbf{y}$$

We will use this result to evaluate the numerator of  $R(\mathbf{x})$ :

$$\mathbf{x}^T K \mathbf{x} = \phi_k^T K \phi_k + 2\varepsilon \mathbf{y}^T K \phi_k + \varepsilon^2 \mathbf{y}^T K \mathbf{y} = \phi_k^T K \phi_k + \varepsilon^2 \mathbf{y}^T (K - \omega_k^2 M) \mathbf{y}$$

Thus,

$$R(\mathbf{x}) = \frac{\mathbf{x}^T K \mathbf{x}}{\mathbf{x}^T M \mathbf{x}} = \omega_k^2 + \varepsilon^2 \frac{\mathbf{y}^T (K - \omega_k^2 M) \mathbf{y}}{\phi_k^T M \phi_k} \quad (5.56)$$

One sees that, in the vicinity of  $\mathbf{x} = \phi_k$ , the error on  $R(\mathbf{x})$  with respect to  $\omega_k^2$  is a function of  $\varepsilon^2$ , which means that  $R(\mathbf{x})$  is indeed stationary; however, the matrix  $K - \omega_k^2 M$  is not positive definite and one cannot say that  $R(\mathbf{x})$  is minimum. The matrix of second derivative

$$\frac{K - \omega_k^2 M}{\phi_k^T M \phi_k} \quad (5.57)$$

is called the *Hessian* matrix of the Rayleigh quotient near the stationary point  $\omega_k$ . If the error shape  $\mathbf{y}$  is expanded into the modes:

$$\mathbf{y} = \sum \alpha_i \phi_i \quad (5.58)$$

The error associated with the Rayleigh quotient may be written

$$\delta\omega^2 = R(\mathbf{x}) - \omega_k^2 = \varepsilon^2 \sum_{i,j} \alpha_i \alpha_j \frac{\phi_i^T (K - \omega_k^2 M) \phi_j}{\phi_k^T M \phi_k}$$

and, taking into account the orthogonality conditions (2.8) and (2.9),

$$\delta\omega^2 = R(\mathbf{x}) - \omega_k^2 = \varepsilon^2 \sum_i \alpha_i^2 \frac{\mu_i}{\mu_k} (\omega_i^2 - \omega_k^2) \quad (5.59)$$

Since the  $\mu_i$  are all positive, this equation indicates that the frequencies below  $\omega_k$  have a negative contribution while the frequencies above  $\omega_k$  contribute positively. If the error  $\mathbf{y}$  is restricted to the space orthogonal to the  $k-1$  first modes,  $\alpha_i = 0$  ( $i = 1, \dots, k-1$ ); then  $\delta\omega^2 \geq 0$  and the Rayleigh quotient constitutes a true minimum. The above property leads naturally to a recursive search of eigenvalues and eigenvectors based on the Rayleigh quotient.

### 5.5.4 Recursive search of eigenvectors

From the previous section, the eigenvectors  $\phi_k$  and eigenvalues  $\omega_k$  can be obtained as solution of

$$\min_{\mathbf{x}} R(\mathbf{x}) = \frac{\mathbf{x}^T K \mathbf{x}}{\mathbf{x}^T M \mathbf{x}} \quad (5.60)$$

for all  $\mathbf{x}$  in the subspace orthogonal to mode 1 to  $k-1$ :

$$\mathbf{x}^T M \phi_i = 0, \quad (i = 1, \dots, k-1) \quad (5.61)$$

(the first mode is the absolute minimum). It remains to examine how to project a vector in the space orthogonal to one or several modes  $\phi_i$ . The coefficient  $\alpha_i$  of the expansion

$$\mathbf{x} = \sum_{i=1}^n \alpha_i \phi_i \quad (5.62)$$

can be determined independently because of the orthogonality condition (2.8):

$$\alpha_k = \frac{\phi_k^T M \mathbf{x}}{\phi_k^T M \phi_k} \quad (5.63)$$

The projection in the subspace orthogonal to  $\phi_k$  is obtained by removing the contribution along  $\phi_k$ ,

$$\begin{aligned} \mathbf{x} - \alpha_k \phi_k &= \mathbf{x} - \frac{\phi_k^T M \mathbf{x}}{\phi_k^T M \phi_k} \phi_k \\ &= \mathbf{x} - \frac{\phi_k \phi_k^T M}{\phi_k^T M \phi_k} \mathbf{x} = [I - \frac{\phi_k \phi_k^T M}{\phi_k^T M \phi_k}] \mathbf{x} \end{aligned}$$

Thus, the projection matrix

$$A_k = [I - \frac{\phi_k \phi_k^T M}{\phi_k^T M \phi_k}] \quad (5.64)$$

is such that

$$\begin{aligned} A_k \phi_k &= 0 \\ A_k \phi_i &= \phi_i \quad (i \neq k) \end{aligned} \quad (5.65)$$

It projects an arbitrary vector in the subspace orthogonal to  $\phi_k$ . In order to eliminate a set of modes, one can apply successively the various projection matrices. Taking into account the orthogonality condition (2.8),

one finds that the matrix projecting a vector in a subspace orthogonal to modes 1 to  $m$  is

$$A_m^* = \prod_{k=1}^m A_k = \prod_{k=1}^m [I - \frac{\phi_k \phi_k^T M}{\phi_k^T M \phi_k}] = [I - \sum_{k=1}^m \frac{\phi_k \phi_k^T M}{\phi_k^T M \phi_k}] \quad (5.66)$$

Thus, the eigenvectors  $\phi_{k+1}$  and eigenvalues  $\omega_{k+1}$  can be obtained as solution of minimum without constraint

$$\min_{\mathbf{x}} R(\mathbf{x}) = \frac{\mathbf{x}^T [A_k^{*T} K A_k^*] \mathbf{x}}{\mathbf{x}^T [A_k^{*T} M A_k^*] \mathbf{x}} \quad (5.67)$$

## 5.6 Building with gravity loads

### 5.6.1 Single storey building

In order to further illustrate the Rayleigh-Ritz method and the Rayleigh principle, consider the vibration of a single story building with massless columns (Fig.5.4). This system is analyzed in Problem 1.3 in absence of gravity loads; using standard results of beam theory, the stiffness of the equivalent spring-mass system is  $k = 24EI/l^3$ . In this section, we reconsider this problem including the gravity loads, and we estimate the natural frequency of the system with the Rayleigh-Ritz method, assuming that the columns deform according to

$$\psi(x) = \frac{1}{2}(1 - \cos \frac{\pi x}{l}) \quad (5.68)$$

The transverse displacement along the beam is  $w(x, t) = q(t)\psi(x)$  where  $q(t)$  is the horizontal displacement of the mass  $m$ . From Equ.(5.29), the bending stiffness due to one column is

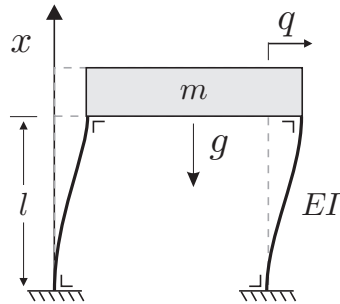


**Fig. 5.4.** Single storey building with gravity loads.

$$k_1 = \int_0^l EI[\psi''(x)]^2 dx = \frac{\pi^4}{8} \frac{EI}{l^3}$$

The total bending stiffness of the two columns is

$$k = 2k_1 = \frac{\pi^4}{4} \frac{EI}{l^3} = 24.35 \frac{EI}{l^3}$$

Thus, the stiffness is slightly larger ( $24.35 > 24$ ) than that obtained in Problem 1.3 which was based on  $\psi(x) = 3x^2/l^2 - 2x^3/l^3$  (the exact static solution which is also appropriate in dynamics since the columns are massless). As a result, the natural frequency  $\omega_1 = \sqrt{k/m}$  is overestimated, as expected from the Rayleigh quotient.

Let us now include the gravity loads. The geometric stiffness of one column is given by Equ.(5.43), with  $N = -mg/2$  being the compression load in one column:

$$k_{g1} = -\frac{mg}{2} \int_0^l [\psi'(x)]^2 dx = \frac{-mg\pi^2}{16l}$$

The total geometric stiffness is

$$k_g = 2k_{g1} = \frac{-mg\pi^2}{8l} \quad (5.69)$$

Finally, the total geometric stiffness (bending + geometric) is

$$\begin{aligned} k_t &= k + k_g = \frac{\pi^4}{4} \frac{EI}{l^3} + \frac{-mg\pi^2}{8l} = \frac{\pi^4}{4} \frac{EI}{l^3} \left[ 1 - \frac{mg l^2}{2\pi^2 EI} \right] \\ k_t &= \frac{\pi^4}{4} \frac{EI}{l^3} \left( 1 - \frac{mg}{P_{cr}} \right) \end{aligned} \quad (5.70)$$

where  $P_{cr}$  is the critical buckling load of the system,<sup>2</sup>  $P_{cr} = 2(\pi^2 EI/l^2)$

Once  $k_t$  has been obtained, the natural frequency is given by  $\omega_1^* = \sqrt{k_t/m}$ , leading, once again, to

$$\omega_1^* = \omega_1 \sqrt{1 - \frac{mg}{P_{cr}}} \quad (5.71)$$

where  $\omega_1$  is the natural frequency without gravity loads; this result is very similar to (5.46).

---

<sup>2</sup> The buckling load of one column is equal to that of a pinned-pinned beam with the same length and the same properties, and the buckling mode happens to be the assumed shape (5.68).

### 5.6.2 Building with $n$ -identical floors

Using the results of the foregoing section, it is easy to build the equivalent spring-mass model of a  $n$ -storey building (Fig.5.5). The geometric stiffness of a floor is a linear function of the axial load applied to the columns, and the columns below floor  $i$  have to support the  $n + 1 - i$  floors above it, which leads to a geometric stiffness  $k_g^i = (n + 1 - i)k_g$ , where  $k_g$  is the geometric stiffness of the single storey building, given by (5.69); the stiffness  $k$  due to the bending of the column is identical for every floor.

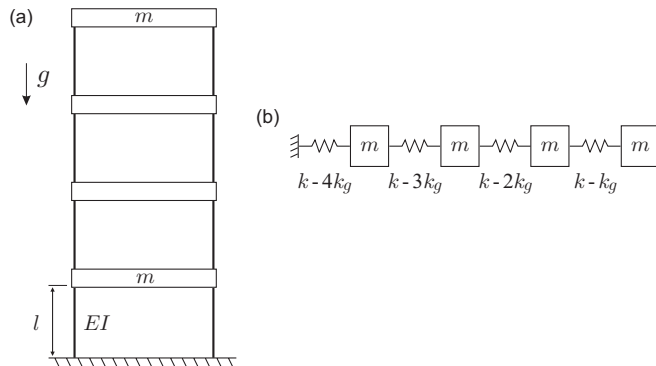


**Fig. 5.5.** (a) Building with 4 identical floors including the geometric stiffness. (b) Spring-mass model.

## 5.7 Problems

**P.5.1** Consider a clamped-free beam loaded axially with a uniform compression load  $P$  (Fig.4.9.b). Find an approximate solution for the first natural frequency, assuming that

- (a)  $\psi(x) = x^2$
- (b)  $\psi(x) = 1 - \cos(\pi x / 2L)$

Comment on the influence of the shape function  $\psi(x)$  on the result.

**P.5.2** Consider a clamped-free beam subjected to gravity loads (Fig.5.6)

$$N_0(x) = -g\varrho A(L - x)$$

Evaluate  $\omega_1$  with the Rayleigh-Ritz method, assuming  $\psi(x) = x^2$ .

**P.5.3** Consider the out of plane vibration of a uniform clamped-free beam rotating with a uniform velocity  $\Omega$  (Fig.5.7).

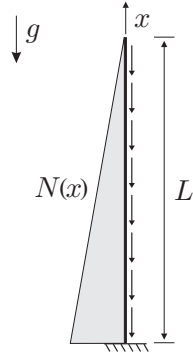


**Fig. 5.6.** Clamped-free beam subjected to gravity loads. The axial preload varies linearly from 0 at the tip to  $-\varrho g A L$  at the base.

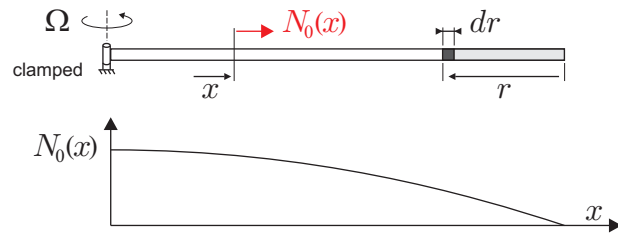


**Fig. 5.7.** Clamped-free beam rotating with a uniform velocity  $\Omega$ .

(a) Show that the tension preload  $N_0(x)$  due to the centrifugal force is given by

$$N_0(x) = \int_0^{L-x} \varrho A \Omega^2 (L-r) dr = \frac{\varrho A \Omega^2}{2} (L^2 - x^2)$$

(b) Evaluate  $\omega_1$  assuming a shape function  $\psi(x) = x^2$ .

**P.5.4** Consider the vibration of a taut string under tension  $T_0$  (Fig. 5.8). Find an approximation to the first natural frequency using the Rayleigh-Ritz method, with the following shape functions:

- (a)  $\psi(x) = x(L-x)$
- (b)  $\psi(x) = \sin(\pi x/L)$

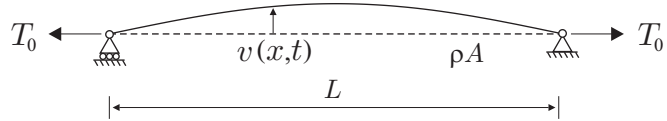


**Fig. 5.8.** Taut string.

Comment on the influence of the shape function  $\psi(x)$  on the result. [Hint: The strain energy is entirely due to the preload  $T_0$ .]

**P.5.5** Consider a uniform beam supported at both ends by elastic supports of stiffness  $K_\theta$  (Fig.5.9). Find an approximation of the first natural frequency. Comment on the quality of the approximation for various values of  $K_\theta$ .

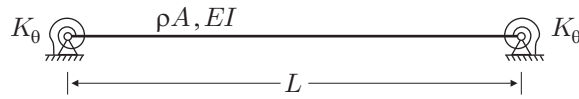


**Fig. 5.9.** Uniform beam with elastic supports.

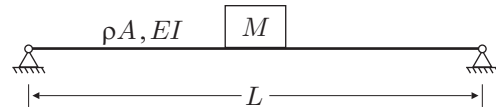


**Fig. 5.10.** Simply supported uniform beam with a lumped mass in the middle.

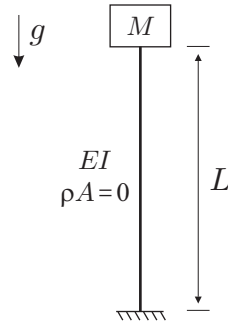


**Fig. 5.11.** Massless vertical beam supporting a mass  $M$  in a gravity field  $g$ .

**P.5.6** Consider a simply supported uniform beam with a lumped mass  $M$  in the middle (Fig.5.10). Find an approximation for the first natural frequency. Comment on the quality of the approximation for various values of the ratio  $M/\rho AL$ .

**P.5.7** Consider a mass  $M$  supported by a massless vertical beam with uniform stiffness  $EI$  and clamped at the bottom (Fig.5.11). The mass is subjected to a gravity field  $g$ . Propose at least two shape functions

to estimate the first natural frequency using the Rayleigh-Ritz method. Explain your choice. Compare the approximations and comment.

**P.5.8** Consider the in-plane rotation of a rigid main body with a flexible appendage represented by a beam of uniform mass per unit length  $\varrho A$  (Fig. 5.12). Let  $\theta$  be the (small) angle of rotation and  $J_0$  be the moment of inertia of the main body. Using a decomposition

$$w(x) = \theta x + \sum_i \phi_i(x) z_i$$

where  $\phi_i(x)$  are the constrained flexible modes, show that the Lagrangian reads

$$L = T - V = \frac{1}{2} J \dot{\theta}^2 - \sum_i \Gamma_i \dot{z}_i \dot{\theta} + \frac{1}{2} \sum_i \mu_i \dot{z}_i^2 - \frac{1}{2} \sum_i \mu_i \Omega_i^2 z_i^2$$

where  $\mu_i$  and  $\Omega_i$  are the modal masses and the natural frequencies of the constrained modes of the flexible appendages,

$$J = J_0 + \int_0^L \varrho A x^2 dx$$

is the total moment of inertia, and  $\Gamma_i$  are the modal participation factors of the flexible modes

$$\Gamma_i = \int_0^L \varrho A \phi_i x dx$$

[ $\Gamma_i$  is the work done on mode  $i$  of the flexible appendages by the inertia forces associated with a unit angular acceleration of the main body].

Show that the equations of motion read

$$J \ddot{\theta} - \sum_{i=1}^m \Gamma_i \ddot{z}_i = T_0$$

$$\mu_i \ddot{z}_i + \mu_i \Omega_i^2 z_i - \Gamma_i \ddot{\theta} = 0 \quad i = 1, \dots, m$$

where  $T_0$  is the torque applied to the main body,

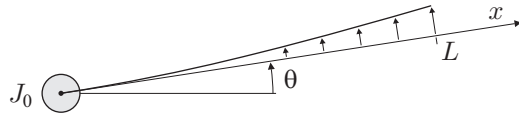


**Fig. 5.12.** In-plane rotation of a rigid body with a flexible beam of uniform mass distribution;  $w(x) = \theta x + \sum_i \phi_i(x) z_i$ .



# 6

## Finite elements

*Notre folie, à nous autres, est de croire que toute la nature, sans exception, est destinée à nos usages,...*

Fontenelle, *Entretiens sur la pluralité des mondes*, 1686

### 6.1 Introduction

The Rayleigh-Ritz method was introduced in chapter 5; it is also called the *global assumed modes method*, because the discretization is achieved by decomposition of the global displacements in a set of global shape functions  $\psi_i(x)$  defined on the whole domain (Fig.6.1.a). The method is very powerful for simple structures where appropriate shape functions may be guessed from intuition, but the functions become difficult to choose when the structure is complex. Besides, since the shape functions must satisfy the global kinematic boundary conditions, a new set of functions must be used for new boundary conditions. This difficulty is overcome by

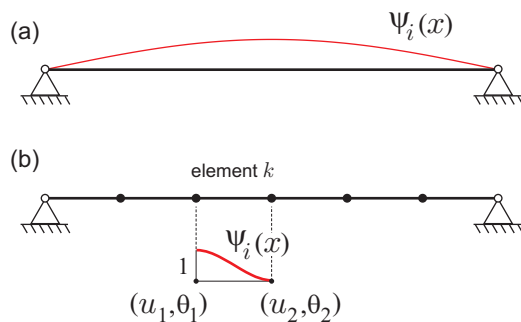


**Fig. 6.1.** Comparison between the Rayleigh-Ritz method and the finite element method. (a) In the Rayleigh-Ritz method, the shape functions  $\psi_i(x)$  are defined globally and must satisfy the kinematic boundary conditions. (b) In the finite element method, the shape functions are defined within the element, in such a way that the generalized coordinates are the nodal displacements  $u_i$  and rotations  $\theta_i$  of the element.

the finite element (FE) method which is a *local* assumed modes method (Fig.6.1.b): The structure is divided into *elements* which are connected at the *nodes*, and the shape functions  $\psi_i(x)$  are selected in such a way that the displacements  $u_i$  and the rotations  $\theta_i$  at the nodes are the generalized coordinates. Thus, all the elements of the same family use the same shape functions and their stiffness and mass matrices have all the same form, that can be computed a-priori from a few geometric and material parameters. The global stiffness and mass matrices are assembled in a second step from the topology of the structure, and finally the boundary conditions are enforced.

The first part of this chapter consists only of a brief introduction to the construction of the stiffness and mass matrices from finite elements; the discussion will be limited to bars and beams in the plane. The reader will refer to the many good textbooks for a comprehensive treatment of the finite element method. The second part of the chapter is devoted to the methods for model reduction (Guyan method and Craig-Bampton method), which aim at reducing the number of generalized coordinates while preserving the accuracy in the prediction of the low frequency modes of the structure.

The finite element method is very mature and commercial FE softwares have user interfaces which simplify considerably the input of the complex geometries as well as the display of the output results.

## 6.2 Formulation for a plane truss

The finite element method is an energy method, just as the Rayleigh-Ritz method; the element stiffness and mass matrices are obtained by expressing the strain energy and the kinetic energy in terms of the generalized coordinates (which are in this case the nodal displacements and rotations) with the assumed kinematics. Contrary to the Rayleigh-Ritz method, the shape functions (assumed modes) are selected once and for all.

### 6.2.1 Bar element

A bar can only deform axially. Figure 6.2 shows a bar element of length  $l$ , with uniform cross section  $A$  and density  $\varrho$  and Young modulus  $E$ . It is assumed that the axial displacements within the element are related to the nodal displacements by

$$u(x, t) = \psi_1(x)u_1(t) + \psi_2(x)u_2(t) \quad (6.1)$$

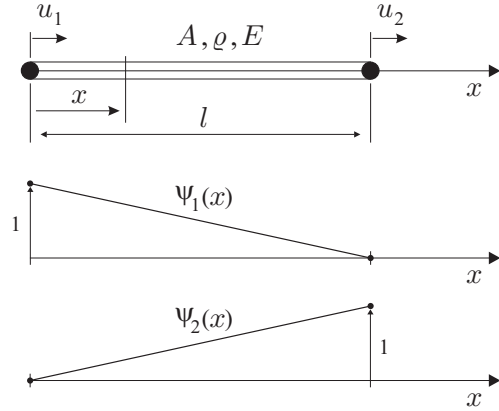


**Fig. 6.2.** Bar element in the plane: The generalized coordinates are the axial displacements at the extremities of the element. The shape functions are respectively  $\psi_1(x) = 1 - x/l$  and  $\psi_2(x) = x/l$ .

where

$$\psi_1(x) = 1 - x/l \quad \text{and} \quad \psi_2(x) = x/l \quad (6.2)$$

It follows from the kinematic assumption that the axial strain is uniform within the element:

$$u'(x, t) = \psi'_1(x)u_1(t) + \psi'_2(x)u_2(t) = \frac{u_2 - u_1}{l} \quad (6.3)$$

Proceeding as in section 5.3 for the Rayleigh-Ritz method, the strain energy in the element is

$$\begin{aligned} V_e &= \frac{1}{2} \int_0^l EA(u')^2 dx \\ V_e &= \frac{1}{2} \int_0^l EA \left[ \sum_{i=1}^2 \psi'_i(x)u_i(t) \right] \left[ \sum_{j=1}^2 \psi'_j(x)u_j(t) \right] dx \\ V_e &= \frac{1}{2} \sum_{i=1}^2 \sum_{j=1}^2 \left[ \int_0^l EA \psi'_i(x)\psi'_j(x) dx \right] u_i(t)u_j(t) \end{aligned} \quad (6.4)$$

or

$$V_e = \frac{1}{2} \mathbf{u}_e^T K_e \mathbf{u}_e \quad (6.5)$$

where  $\mathbf{u}_e = (u_1, u_2)^T$  is the vector of generalized coordinates (the nodal displacements along the axis of the element) and the elements of the stiffness matrix are

$$K_e^{ij} = \int_0^l EA \psi'_i(x) \psi'_j(x) dx \quad (6.6)$$

$$K_e = \frac{AE}{l} \begin{bmatrix} 1 & -1 \\ -1 & 1 \end{bmatrix} \quad (6.7)$$

Similarly, the kinetic energy in the element is written

$$T_e = \frac{1}{2} \int_0^l \varrho A \dot{u}^2 dx \quad (6.8)$$

$$T_e = \frac{1}{2} \int_0^l \varrho A \left[ \sum_{i=1}^2 \psi_i(x) \dot{u}_i(t) \right] \left[ \sum_{j=1}^2 \psi_j(x) \dot{u}_j(t) \right] dx$$

$$T_e = \frac{1}{2} \sum_{i=1}^2 \sum_{j=1}^2 \left[ \int_0^l \varrho A \psi_i(x) \psi_j(x) dx \right] \dot{u}_i(t) \dot{u}_j(t)$$

$$T_e = \frac{1}{2} \dot{\mathbf{u}}_e^T M_e \dot{\mathbf{u}}_e \quad (6.9)$$

where  $\dot{\mathbf{u}}_e = (\dot{u}_1, \dot{u}_2)^T$  is the vector of generalized velocities and  $M_e$  is the mass matrix of the element:

$$M_e^{ij} = \int_0^l \varrho A \psi_i(x) \psi_j(x) dx \quad (6.10)$$

$M_e$  is symmetric and positive definite (by construction, since  $T_e > 0$ ).

$$M_e = \frac{\varrho Al}{6} \begin{bmatrix} 2 & 1 \\ 1 & 2 \end{bmatrix} \quad (6.11)$$

Equations (6.7) and (6.11) are the generic forms of the mass and stiffness matrices of a planar bar element with uniform cross section. The form of these matrices is fixed and they depend on the geometry ( $A$  and  $l$ ) as well as the material properties ( $\varrho$  and  $E$ ). An element with variable cross section may be derived by allowing the cross section to vary linearly between  $A_1$  and  $A_2$  along the bar (Problem 6.1).

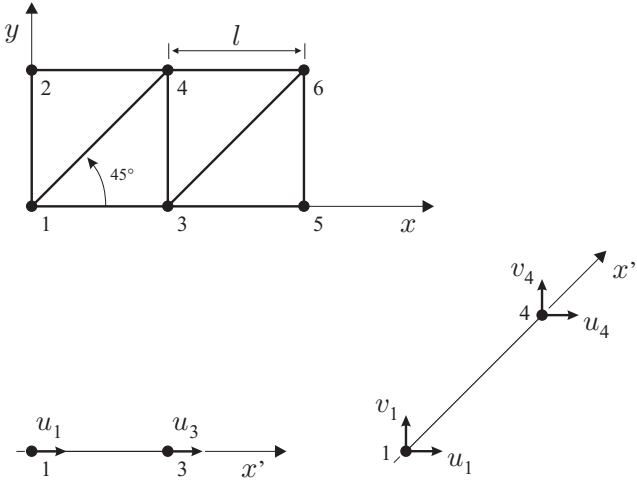


**Fig. 6.3.** Plane truss assembled from bars with uniform cross section.

### 6.2.2 Truss structure

The step of constructing the global stiffness and mass matrices from the element matrices is called *assembly*. Consider the plane truss of Fig.6.3; it consists of 2 identical bays formed by bars of the same material and the same cross section (the horizontal and vertical bars have a length  $l$  while the diagonal ones have a length  $l\sqrt{2}$ ). The truss has 6 nodes with two d.o.f. each, the displacements ( $u_i, v_i$ ) along the global coordinate system. The global stiffness and mass matrices are constructed by expressing that the total energy (strain and kinetic) is the sum of the energy stored in individual bars. To do this, one needs to relate the local coordinates of every element to the global coordinates, taking into account the topology of the structure. This is done by a localization matrix  $L_e$  such that

$$\mathbf{u}_e = L_e \mathbf{u} \quad (6.12)$$

Each element has its own localization matrix; in the case of the truss of Fig.6.3, there are 12 generalized coordinates  $\mathbf{u} = (u_1, v_1, u_2, v_2, \dots)^T$  (the node displacements in the global coordinate system) and the dimension of  $L_e$  is therefore  $2 \times 12$ . It is obtained by projecting the end displacements of each bar along the axis of the element. For the element connecting nodes 1 and 3, the localization matrix reads

$$L_e = \begin{bmatrix} 1 & 0 & 0 & 0 & 0 & 0 & \dots \\ 0 & 0 & 0 & 0 & 1 & 0 & \dots \end{bmatrix}$$

which indicate that the first coordinate of the element is the first global d.o.f. of the truss and that the second coordinate of the element is the fifth global d.o.f. of the truss. Similarly the localization matrix of the element connecting nodes 1 and 4, which is at  $45^0$  in the global coordinate system is

$$L_e = \begin{bmatrix} \sqrt{2}/2 & \sqrt{2}/2 & 0 & 0 & 0 & 0 & 0 & 0 & \dots \\ 0 & 0 & 0 & 0 & 0 & 0 & \sqrt{2}/2 & \sqrt{2}/2 & \dots \end{bmatrix}$$

Note that the localization matrices are sparsely populated and do not have to be constructed explicitly to assemble the mass and stiffness matrices. The global matrices are obtained by expressing that the total energy is the sum of the energy contained in all the elements:

$$V = \frac{1}{2} \mathbf{u}^T K \mathbf{u} = \sum_e \left[ \frac{1}{2} \mathbf{u}_e^T K_e \mathbf{u}_e \right] = \frac{1}{2} \sum_e \mathbf{u}^T L_e^T K_e L_e \mathbf{u} \quad (6.13)$$

leading to the global stiffness matrix

$$K = \sum_e L_e^T K_e L_e \quad (6.14)$$

and similarly

$$T = \frac{1}{2} \dot{\mathbf{u}}^T M \dot{\mathbf{u}} = \sum_e \left[ \frac{1}{2} \dot{\mathbf{u}}_e^T M_e \dot{\mathbf{u}}_e \right] = \frac{1}{2} \dot{\mathbf{u}}^T L_e^T M_e L_e \dot{\mathbf{u}} \quad (6.15)$$

leading to the global mass matrix

$$M = \sum_e L_e^T M_e L_e \quad (6.16)$$

In Equ.(6.14) and (6.16), the element matrices  $K_e$  and  $M_e$  are given respectively by Equ.(6.7) and (6.11), with appropriate values of  $A$ ,  $E$  and  $l$  for each element.

### 6.3 Planar structure made of beams

In this section, we consider the simplest case of a planar structure whose deformations are assumed to be in pure bending. The discussion parallels that of section 5.4; only the transverse motion  $v(x, t)$  is considered, and the kinematics is assumed to follow the Euler-Bernoulli assumption (section 4.1). The strain energy and the kinetic energy are given respectively by

$$V = \frac{1}{2} \int_0^l EI(v'')^2 dx \quad \text{and} \quad T = \frac{1}{2} \int_0^l \varrho A(\dot{v})^2 dx, \quad (6.17)$$

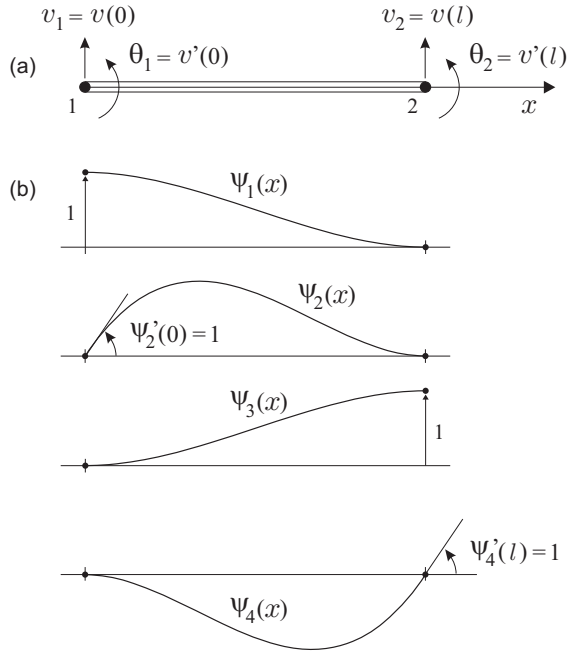


**Fig. 6.4.** Planar beam element in pure bending. (a) Generalized variables  $\mathbf{u}_e = (v_1, \theta_1, v_2, \theta_2)^T$ . (b) Shape functions  $\psi_i(x)$ .

### 6.3.1 Beam element

In the finite element of beam in pure bending, the axial extension is ignored and the generalized coordinates are the transverse displacements and the rotations at the two end nodes,  $\mathbf{u}_e = (v_1, \theta_1, v_2, \theta_2)^T$  (Fig.6.4). The transverse displacements along the beam are assumed of the form

$$v(x, t) = v_1(t)\psi_1(x) + \theta_1(t)\psi_2(x) + v_2(t)\psi_3(x) + \theta_2(t)\psi_4(x) \quad (6.18)$$

where the shape functions are polynomials of the third order:<sup>1</sup>

$$\begin{aligned} \psi_1(x) &= 1 - 3x^2/l^2 + 2x^3/l^3 \\ \psi_2(x) &= x - 2x^2/l + x^3/l^2 \\ \psi_3(x) &= 3x^2/l^2 - 2x^3/l^3 \\ \psi_4(x) &= x^3/l^2 - x^2/l \end{aligned} \quad (6.19)$$

which satisfy the following conditions (Fig.6.4.b):

<sup>1</sup> Observe that these shape functions are such that any rigid body motion such that  $\theta_1 = \theta_2$  and  $v_2 = v_1 + \theta_1 l$  will lead to a linear distribution of the transverse displacements:  $v(x) = v_1 + \theta_1 x$ .

$$\begin{aligned}\psi_1(0) &= 1 & \psi'_1(0) &= 0 & \psi_1(l) &= 0 & \psi'_1(l) &= 0 \\ \psi_2(0) &= 0 & \psi'_2(0) &= 1 & \psi_2(l) &= 0 & \psi'_2(l) &= 0 \\ \psi_3(0) &= 0 & \psi'_3(0) &= 0 & \psi_3(l) &= 1 & \psi'_3(l) &= 0 \\ \psi_4(0) &= 0 & \psi'_4(0) &= 0 & \psi_4(l) &= 0 & \psi'_4(l) &= 1\end{aligned}$$

Proceeding as in the previous section, the strain energy of the element is written

$$V_e = \frac{1}{2} \int_0^l EI(v'')^2 dx = \frac{1}{2} \mathbf{u}_e^T K_e \mathbf{u}_e \quad (6.20)$$

where

$$K_e^{ij} = \int_0^l EI \psi_i''(x) \psi_j''(x) dx \quad (6.21)$$

$$K_e = \frac{EI}{l^3} \begin{bmatrix} 12 & 6l & -12 & 6l \\ 6l & 4l^2 & -6l & 2l^2 \\ -12 & -6l & 12 & -6l \\ 6l & 2l^2 & -6l & 4l^2 \end{bmatrix} \quad (6.22)$$

and similarly for the kinetic energy

$$T_e = \frac{1}{2} \int_0^l \varrho A(\dot{v})^2 dx = \frac{1}{2} \dot{\mathbf{u}}_e^T M_e \dot{\mathbf{u}}_e \quad (6.23)$$

where

$$M_e^{ij} = \int_0^l \varrho A \psi_i(x) \psi_j(x) dx \quad (6.24)$$

$$M_e = \frac{\varrho Al}{420} \begin{bmatrix} 156 & 22l & 54 & -13l \\ 22l & 4l^2 & 13l & -3l^2 \\ 54 & 13l & 156 & -22l \\ -13l & -3l^2 & -22l & 4l^2 \end{bmatrix} \quad (6.25)$$

The mass matrix is again symmetric and positive definite; it is called *consistent*, because it is based on the same shape functions as the stiffness matrix. However, in many applications, the finite element decomposition is governed by the accuracy of the representation of the structural stiffness, rather than by the accuracy of the representation of the mass distribution, and it may be convenient to use a simpler representation of the inertia forces with a *lumped mass* model. One such a representation is obtained by ignoring the inertia associated with the rotations and lumping half of the mass of the element at the translational d.o.f. at both ends;

the kinetic energy of the element is in this case  $T_e = \frac{1}{2}(\rho Al/2)[\dot{v}_1^2 + \dot{v}_2^2]$ , leading to

$$M_e = \frac{\rho Al}{2} \begin{bmatrix} 1 & 0 & 0 & 0 \\ 0 & 0 & 0 & 0 \\ 0 & 0 & 1 & 0 \\ 0 & 0 & 0 & 0 \end{bmatrix} \quad (6.26)$$

The error associated with the use of a lumped mass model is illustrated in Fig.6.6; in many applications, this representation will be sufficient. Note, however, that  $M_e$  is no longer positive definite, because no inertia is associated with the rotational d.o.f.

### 6.3.2 Beam structure

Consider the structure formed of two elements of planar beam of equal length (Fig.6.5); the global coordinate vector is  $\mathbf{u} = (v_1, \theta_1, v_2, \theta_2, v_3, \theta_3)^T$ . The localization matrices of the two elements are respectively

$$L_1 = \begin{bmatrix} 1 & 0 & 0 & 0 & 0 & 0 \\ 0 & 1 & 0 & 0 & 0 & 0 \\ 0 & 0 & 1 & 0 & 0 & 0 \\ 0 & 0 & 0 & 1 & 0 & 0 \end{bmatrix}$$

and

$$L_2 = \begin{bmatrix} 0 & 0 & 1 & 0 & 0 & 0 \\ 0 & 0 & 0 & 1 & 0 & 0 \\ 0 & 0 & 0 & 0 & 1 & 0 \\ 0 & 0 & 0 & 0 & 0 & 1 \end{bmatrix}$$

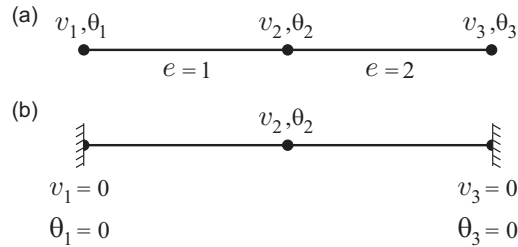


**Fig. 6.5.** Beam structure formed of two finite elements. (a) Global d.o.f. (b) Clamped-clamped boundary conditions.

The global stiffness is constructed according to Equ.(6.14), with the appropriate form of  $L_e$  and the element matrix; one finds easily

$$K = \frac{EI}{l^3} \left[ \begin{array}{cccc|cc} 12 & 6l & -12 & 6l & 0 & 0 \\ 6l & 4l^2 & -6l & 2l^2 & 0 & 0 \\ -12 & -6l & 12 + 12 & -6l + 6l & -12 & 6l \\ 6l & 2l^2 & -6l + 6l & 4l^2 + 4l^2 & -6l & 2l^2 \\ \hline 0 & 0 & -12 & -6l & 12 & -6l \\ 0 & 0 & 6l & 2l^2 & -6l & 4l^2 \end{array} \right] \quad (6.27)$$

where  $l$  is the length of one element. The contributions from the two finite elements to the global stiffness matrix has been highlighted and the contributions to the central block of the matrix have been written explicitly for clarity. Similarly, the global mass matrix is constructed according to Equ.(6.16):

$$M = \frac{\rho Al}{420} \left[ \begin{array}{cccc|cc} 156 & 22l & 54 & -13l & 0 & 0 \\ 22l & 4l^2 & 13l & -3l^2 & 0 & 0 \\ 54 & 13l & 156 + 156 & -22l + 22l & 54 & -13l \\ -13l & -3l^2 & -22l + 22l & 4l^2 + 4l^2 & 13l & -3l^2 \\ \hline 0 & 0 & 54 & 13l & 156 & -22l \\ 0 & 0 & -13l & -3l^2 & -22l & 4l^2 \end{array} \right] \quad (6.28)$$

### 6.3.3 Boundary conditions

Both  $K$  and  $M$  are  $6 \times 6$  matrices, because there are 6 d.o.f. in the model. The next step consists of enforcing the boundary conditions associated with the supports of the structure. If the d.o.f.  $\mathbf{u}$  are partitioned into the those which remain free  $\mathbf{u}_1$  and those associated with the supports where  $\mathbf{u}_2 = 0$ ,  $\mathbf{u}^T = (\mathbf{u}_1^T, \mathbf{u}_2^T)$ , the strain energy may be written

$$\begin{aligned} V &= \frac{1}{2}(\mathbf{u}_1^T, \mathbf{u}_2^T) \begin{bmatrix} K_{11} & K_{12} \\ K_{12}^T & K_{22} \end{bmatrix} \begin{Bmatrix} \mathbf{u}_1 \\ \mathbf{u}_2 \end{Bmatrix} \\ &= \mathbf{u}_1^T K_{11} \mathbf{u}_1 + 2\mathbf{u}_1^T K_{12} \mathbf{u}_2 + \mathbf{u}_2^T K_{22} \mathbf{u}_2 \\ &= \mathbf{u}_1^T K_{11} \mathbf{u}_1 \end{aligned}$$

since  $\mathbf{u}_2 = 0$ . Thus, the global stiffness matrix after enforcing the boundary conditions consists of the sub-matrix  $K_{11}$  relative to the d.o.f. which remain free. It is obtained by elimination of all the lines and columns

corresponding to the d.o.f. of supports. A similar result is obtained for the mass matrix by considering the kinetic energy.

To illustrate this, consider the example of Fig.6.5.b where the beam is clamped at both ends. There are only 2 d.o.f. which remain free ( $v_2, \theta_2$ ) and, after deleting the lines and columns corresponding to the blocked d.o.f. in the stiffness and mass matrices, one gets

$$K = \frac{EI}{l^3} \begin{bmatrix} 24 & 0 \\ 0 & 8l^2 \end{bmatrix} \quad M = \frac{\rho Al}{420} \begin{bmatrix} 312 & 0 \\ 0 & 8l^2 \end{bmatrix} \quad (6.29)$$

The corresponding eigenvalue problem,  $[K - \omega_i^2 M] \phi_i = 0$  reads:

$$\left\{ \frac{EI}{l^3} \begin{bmatrix} 24 & 0 \\ 0 & 8l^2 \end{bmatrix} - \omega_i^2 \frac{\rho Al}{420} \begin{bmatrix} 312 & 0 \\ 0 & 8l^2 \end{bmatrix} \right\} \phi_i = 0 \quad (6.30)$$

and, upon introducing the reduced eigenvalue<sup>2</sup>

$$\lambda_i = \frac{\rho Al^4}{420EI} \omega_i^2 = \frac{\mu_i^4}{420.2^4}$$

it becomes

$$\begin{bmatrix} 24 - 312\lambda_i & 0 \\ 0 & 8l^2(1 - \lambda_i) \end{bmatrix} \phi_i = 0 \quad (6.31)$$

The first eigenvalue is  $\lambda_1 = \frac{24}{312}$  corresponding to  $\mu_1^4 = 517$ , which is quite close, and slightly larger than to the analytical result  $\mu_1^4 = 500.5$  from the solution of the partial differential equation (Problem 4.1). The corresponding mode shape involves only the d.o.f. of translation  $v_2$ . Similarly, the second eigenvalue is  $\lambda_2 = 1$ , corresponding to  $\mu_2^4 = 6720$  which is much larger than the analytical prediction  $\mu_2^4 = 3803$ ; the corresponding mode shape is a pure rotation  $\theta_2$ .

#### 6.3.4 Convergence

Although extremely simple, the foregoing example illustrates important properties the finite element method: (i) It tends to *overestimate* the

---

<sup>2</sup> In section 4.3 devoted to the analysis of continuous beams, the reduced eigenvalue was defined as

$$\mu^4 = \frac{\rho AL^4}{EI} \omega^2$$

where  $L$  is the length of the beam; in this case,  $L = 2l$ .

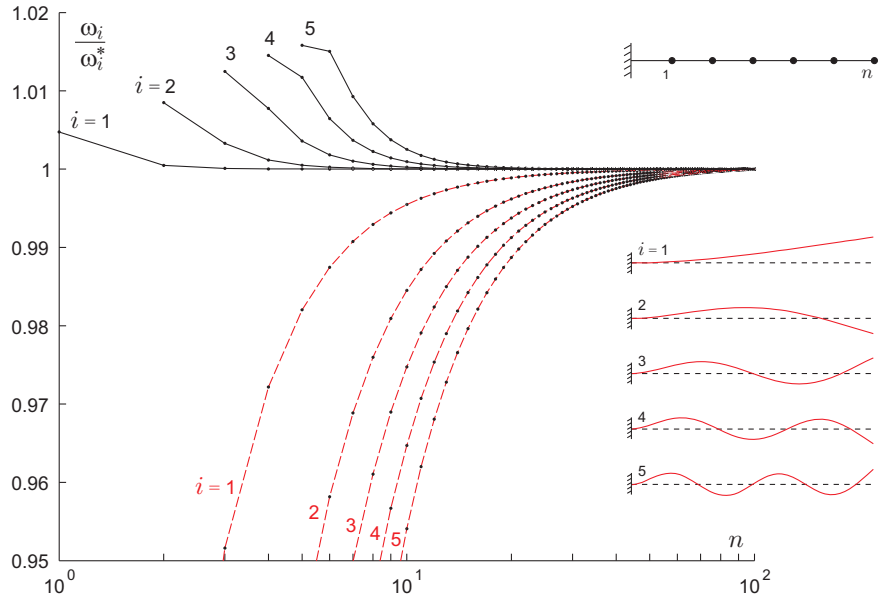


**Fig. 6.6.** Convergence analysis: Uniform clamped-free beam; evolution of the natural frequencies  $\omega_i$  normalized to the analytical values  $\omega_i^*$  as a function of the number  $n$  of elements in the model. Full line: Consistent mass matrix with convergence from above. Dashed lines: Lumped mass model which converges from below.

natural frequencies. As the number of elements increases, the natural frequencies of the low order modes obtained with a consistent mass model converge from above towards the analytical results. This is in fact a consequence of the Rayleigh quotient as discussed in section 5.5. (ii) For a given discretization, the error on the natural frequency of higher modes increases rapidly, and achieving a reasonable accuracy requires a number of d.o.f. significantly larger than the index of the highest mode of interest. This is illustrated in Figure 6.6 for a uniform clamped-free beam; the figure shows the evolution of the first five natural frequencies with the number  $n$  of elements (the number of d.o.f. is  $2n$ ). In the figure, the full lines refer to the consistent mass model (6.25), which converge from above; the dashed lines correspond to the lumped mass model (6.26); they converge more slowly, and from below.

Note also that the mode shapes of higher orders depend on the discretization and have no or little physical meaning. The best way to become familiar with the finite element method is to run computations with a commercial FE code; performing convergence analysis on simple cases

will give some feeling about the convergence properties and the accuracy which is possible to achieve (Problem 6.2).

### 6.3.5 Geometric stiffness of a planar beam element

When a beam is subjected to an axial load  $N$ , there is an additional contribution to the geometric strain energy:

$$V_g = \frac{1}{2} \int_0^L N(v')^2 dx \quad (6.32)$$

where  $N$  is positive in traction. The geometric strain energy in a beam element subject to a constant axial force is expressed in the form

$$V_{ge} = \frac{1}{2} \int_0^l N(v')^2 dx = \frac{1}{2} \mathbf{u}_e^T K_{ge} \mathbf{u}_e \quad (6.33)$$

where  $\mathbf{u}_e = (v_1, \theta_1, v_2, \theta_2)^T$  and the elements of the geometric stiffness matrix are given by

$$K_{ge}^{ij} = N \int_0^l \psi_i'(x) \psi_j'(x) dx \quad (6.34)$$

Using the shape functions (6.19), one finds

$$K_{ge} = \frac{N}{30l} \begin{bmatrix} 36 & 3l & -36 & 3l \\ 3l & 4l^2 & -3l & -l^2 \\ -36 & -3l & 36 & -3l \\ 3l & -l^2 & -3l & 4l^2 \end{bmatrix} \quad (6.35)$$

In order to illustrate the geometric stiffness, let us consider once again the single storey building with gravity loads (Fig.5.4). Each of the two massless columns can be modeled by a single finite element (the shape functions are statically exact regarding the transverse displacements of the column); there is a single d.o.f., the horizontal displacement  $q$  at the top (rotation  $\theta = 0$  at the top). The stiffness corresponding to a single column is obtained from Equ.(6.22):

$$k_1 = 12 \frac{EI}{l^3}$$

The geometric stiffness of one column corresponds to a compression load of half the floor weight,  $-mg/2$ , leading to

$$k_{g1} = -\frac{mg}{2} \cdot \frac{36}{30l} = \frac{-6mg}{10l}$$

Overall, the total stiffness for the two columns is

$$k_t = 2(k_1 + k_{g1}) = \frac{24EI}{l^3} [1 - \frac{mgl^2}{20EI}] \quad (6.36)$$

This result must be compared with (5.70) obtained by assuming the shape function (5.68) corresponding to the buckling mode of the column.<sup>3</sup>

To account for the geometric stiffness of a structure made of beams, the analysis must proceed in two steps: (i) The first step consists of a static analysis under the external constant loads, to evaluate the static axial loads  $N_e$  applied to all the beam elements. (ii) The geometric stiffness matrix of every element is computed from Equ.(6.35) and added to the stiffness matrix (6.22) coming from the bending strain energy.

#### 6.4 Guyan reduction

As already mentioned, the size of a discretized model obtained by finite elements is essentially governed by the representation of the stiffness of the structure. For complicated geometries, it may become very large, especially with automated mesh generators. Before solving the eigenvalue problem, it may be advisable to reduce the size of the model by condensing the degrees of freedom with little or no inertia and which are not used to apply external forces, or equipped with a sensor to measure the structural response. The degrees of freedom to be condensed, denoted  $\mathbf{x}_2$  in what follows, are often referred to as *slaves*; those kept in the reduced model are called *masters* and are denoted  $\mathbf{x}_1$ .

To begin with, consider the undamped forced vibration of a structure where the slaves  $\mathbf{x}_2$  are not excited and have no inertia; the governing equation is

$$\begin{bmatrix} M_{11} & 0 \\ 0 & 0 \end{bmatrix} \begin{Bmatrix} \ddot{\mathbf{x}}_1 \\ \ddot{\mathbf{x}}_2 \end{Bmatrix} + \begin{bmatrix} K_{11} & K_{12} \\ K_{21} & K_{22} \end{bmatrix} \begin{Bmatrix} \mathbf{x}_1 \\ \mathbf{x}_2 \end{Bmatrix} = \begin{Bmatrix} \mathbf{f}_1 \\ 0 \end{Bmatrix} \quad (6.37)$$

or

$$M_{11}\ddot{\mathbf{x}}_1 + K_{11}\mathbf{x}_1 + K_{12}\mathbf{x}_2 = \mathbf{f}_1 \quad (6.38)$$

---

<sup>3</sup> This model leads to a buckling load of  $P_{cr} = 20EI/l^2$ , instead of the analytical value of  $P_{cr} = 2\pi^2EI/l^2$  obtained in section 5.6.1 when using the analytical buckling shape as shape function.

$$K_{21}\mathbf{x}_1 + K_{22}\mathbf{x}_2 = 0 \quad (6.39)$$

According to the second equation, the slaves  $\mathbf{x}_2$  are completely determined by the masters  $\mathbf{x}_1$ :

$$\mathbf{x}_2 = -K_{22}^{-1}K_{21}\mathbf{x}_1 \quad (6.40)$$

Substituting into Equ.(6.38), we find the reduced equation

$$M_{11}\ddot{\mathbf{x}}_1 + (K_{11} - K_{12}K_{22}^{-1}K_{21})\mathbf{x}_1 = \mathbf{f}_1 \quad (6.41)$$

which involves only  $\mathbf{x}_1$ . Note that in this case, the reduced equation has been obtained without approximation.

The idea in the so-called *Guyan reduction* is to assume that the master-slave relationship (6.40) applies even if the degrees of freedom  $\mathbf{x}_2$  have some inertia (i.e. when the sub-matrix  $M_{22} \neq 0$ ), or have forces applied to them. Thus, one *assumes* the following transformation

$$\mathbf{x} = \begin{Bmatrix} \mathbf{x}_1 \\ \mathbf{x}_2 \end{Bmatrix} = \begin{bmatrix} I \\ -K_{22}^{-1}K_{21} \end{bmatrix} \mathbf{x}_1 = L \mathbf{x}_1 \quad (6.42)$$

The reduced mass and stiffness matrices are obtained by substituting the above transformation into the kinetic and strain energy:

$$\begin{aligned} \mathcal{T} &= \frac{1}{2}\dot{\mathbf{x}}^T M \dot{\mathbf{x}} = \frac{1}{2}\dot{\mathbf{x}}_1^T L^T M L \dot{\mathbf{x}}_1 = \frac{1}{2}\dot{\mathbf{x}}_1^T \hat{M} \dot{\mathbf{x}}_1 \\ \mathcal{U} &= \frac{1}{2}\mathbf{x}^T K \mathbf{x} = \frac{1}{2}\mathbf{x}_1^T L^T K L \mathbf{x}_1 = \frac{1}{2}\mathbf{x}_1^T \hat{K} \mathbf{x}_1 \end{aligned}$$

with

$$\hat{M} = L^T M L \quad \hat{K} = L^T K L \quad (6.43)$$

The second equation produces  $\hat{K} = K_{11} - K_{12}K_{22}^{-1}K_{21}$  as in Equ.(6.41). If external loads are applied to  $\mathbf{x}_2$ , the reduced loads are obtained by equating the virtual work

$$\delta \mathbf{x}^T \mathbf{f} = \delta \mathbf{x}_1^T L^T \mathbf{f} = \delta \mathbf{x}_1^T \hat{\mathbf{f}}_1$$

or

$$\hat{\mathbf{f}}_1 = L^T \mathbf{f} = \mathbf{f}_1 - K_{12}K_{22}^{-1} \mathbf{f}_2 \quad (6.44)$$

Finally, the reduced equation of motion reads

$$\hat{M}\ddot{\mathbf{x}}_1 + \hat{K}\mathbf{x}_1 = \hat{\mathbf{f}}_1 \quad (6.45)$$

Usually, it is not necessary to consider the damping matrix in the reduction, because it is rarely known explicitly at this stage. The Guyan reduction can be performed automatically in commercial finite element packages, the selection of masters and slaves being made by the user. In the selection process the following aspects should be kept in mind:

- The degrees of freedom without inertia and applied load can be condensed without affecting the accuracy.
- Translational degrees of freedom carry more information than rotational ones. In selecting the masters, preference should be given to translations, especially if large modal amplitudes are expected (Problem 6.4).
- The error in the natural frequencies  $\omega_i$  and the mode shape  $\phi_i$  associated with the Guyan reduction is an increasing function of the ratio

$$\frac{\omega_i^2}{\nu_1^2} \quad (6.46)$$

where  $\nu_1$  is the first natural frequency of the constrained system, where all the degrees of freedom  $\mathbf{x}_1$  (masters) have been blocked [ $\nu_1$  is the smallest solution of  $\det(K_{22} - \nu^2 M_{22}) = 0$ ]. Therefore, the quality of a Guyan reduction is strongly related to the natural frequencies of the constrained system and  $\nu_1$  should be kept far above the frequency band  $\omega_b$  where the model is expected to be accurate. If this is not the case, the model reduction can be improved by the Craig-Bampton reduction discussed below after the example.

#### 6.4.1 Examples

Consider the clamped-free beam of Fig.6.7, modeled with a single finite element. The stiffness and mass matrices are respectively

$$K = \frac{EI}{l^3} \begin{bmatrix} 12 & -6l \\ -6l & 4l^2 \end{bmatrix} \quad M = \frac{\rho Al}{420} \begin{bmatrix} 156 & -22l \\ -22l & 4l^2 \end{bmatrix} \quad (6.47)$$

Introducing the reduced eigenvalue

$$\lambda = \frac{\omega^2 \rho Al^4}{420 EI} = \frac{\mu^4}{420}$$

the eigenvalue problem reads

$$\det \begin{bmatrix} 12 - 156\lambda & -6l - 22l\lambda \\ -6l - 22l\lambda & 4l^2(1 - \lambda) \end{bmatrix} = 0$$

The solutions are:  $\mu_1^4 = 420\lambda_1 = 12.48$  which should be compared to the analytical solution  $\mu_1^4 = 12.36$  (Problem 4.1) and  $\mu_2^4 = 420\lambda_2 = 1209.6$ , to be compared with the analytical solution  $\mu_2^4 = 485.48$ . Once again, one observes that the first natural frequency is slightly overestimated, but quite close to the analytical value in spite of the small size of the model, while the second natural frequency is grossly overestimated. With this simple model, we now compare two different Guyan reductions; in the first one,  $u_2$  is the master and  $\theta_2$  is the slave; in the second one,  $\theta_2$  is the master and  $u_2$  is the slave.

**Reduction 1:  $\theta_2$  is the slave.** In this case, the coordinates  $u_2$  and  $\theta_2$  are related by the equation formed with the second row of the stiffness matrix:

$$-6lu_2 + 4l^2\theta_2 = 0 \quad \Rightarrow \quad \theta_2 = \frac{3}{2l}u_2$$

This is the exact ratio between  $u_2$  and  $\theta_2$  for a beam loaded statically by a point force at the tip (Fig.6.7.b).<sup>4</sup> The transformation matrix (6.42) is in this case

$$\begin{Bmatrix} u_2 \\ \theta_2 \end{Bmatrix} = \begin{Bmatrix} 1 \\ 3/2l \end{Bmatrix} u_2 = Lu_2$$

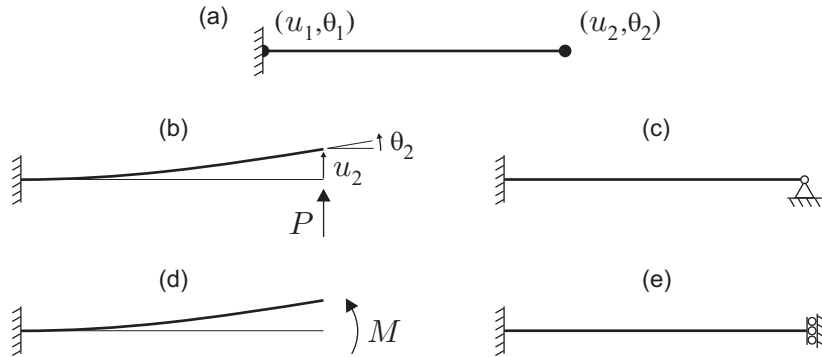


**Fig. 6.7.** (a) Clamped-free beam modelled with a single finite element. (b) Clamped beam loaded statically by a point force at the tip;  $\theta_2 = \frac{Pl^2}{2EI}$  and  $u_2 = \frac{Pl^3}{3EI}$ ;  $\theta_2 = \frac{3}{2l}u_2$ . (c) Clamped-pinned beam corresponding to  $u_2$  blocked. (d) Clamped beam loaded statically by a torque at the tip;  $\theta_2 = \frac{Ml}{EI}$  and  $u_2 = \frac{Ml^2}{2EI}$ ;  $\theta_2 = \frac{2}{l}u_2$ . (e) Beam clamped at the left end and guided at the right end, corresponding to  $\theta_2$  blocked.

<sup>4</sup> The finite element method provides the best solution in the family of possible shape functions; in this case, the third order polynomials contain the analytical solution.

It follows that

$$\hat{M} = L^T M L = \frac{99\varrho Al}{420}, \quad \hat{K} = L^T K L = \frac{3EI}{l^3}$$

The reduced system is governed by

$$\frac{99\varrho Al}{420} \ddot{u}_2 + \frac{3EI}{l^3} u_2 = 0$$

and the natural frequency is

$$\omega_1^2 = \frac{3 \times 420}{99} \frac{EI}{\varrho Al^4} \quad \Rightarrow \quad \mu_1^4 = \frac{3 \times 420}{99} = 12.73$$

Thus, comparing the analytical result, the two d.o.f. model and the reduced model, one finds

$$\mu_1^4 = 12.36 \text{ (analytical)} < 12.48 \text{ (2 d.o.f.)} < 12.73 \text{ (reduction 1)}$$

The natural frequency  $\nu_1$  of the constrained system when the master d.o.f. is blocked is obtained by eliminating the first line and the first column of the element matrices (6.47); one finds easily

$$\nu_1^2 = \frac{4l^2 EI}{l^3} / \frac{4l^2 \varrho Al}{420} = 420 \frac{EI}{\varrho Al^4} \quad \Rightarrow \quad \frac{\omega_1^2}{\nu_1^2} = \frac{1}{33}$$

A small value of this ratio indicates the good quality of the reduction.

**Reduction 2:  $u_2$  is the slave.** In this case, the coordinates  $u_2$  and  $\theta_2$  are related by the equation formed with the first row of the stiffness matrix:

$$12u_2 - 6l\theta_2 = 0 \quad \Rightarrow \quad \theta_2 = \frac{2}{l}u_2$$

This is the exact ratio between  $u_2$  and  $\theta_2$  for a beam loaded statically by a torque applied at the tip (Fig.6.7.d). The transformation matrix (6.42) is in this case<sup>5</sup>

$$\begin{Bmatrix} u_2 \\ \theta_2 \end{Bmatrix} = \begin{Bmatrix} 1 \\ 2/l \end{Bmatrix} u_2 = Lu_2$$

It follows that

$$\hat{M} = L^T M L = \frac{84\varrho Al}{420}, \quad \hat{K} = L^T K L = \frac{4EI}{l^3}$$

---

<sup>5</sup> It does not matter which variable of  $u_2$  and  $\theta_2$  is kept in the final model; the choice of  $u_2$  as slave coordinate was made when the first row of the stiffness matrix was adopted.

The reduced system is governed by

$$\frac{84\varrho Al}{420}\ddot{u}_2 + \frac{4EI}{l^3}u_2 = 0$$

and the natural frequency is

$$\omega_1^2 = \frac{4 \times 420}{84} \frac{EI}{\varrho Al^4} \quad \Rightarrow \quad \mu_1^4 = \frac{4 \times 420}{84} = 20$$

Thus, comparing the analytical result, the two d.o.f. model and the reduced models, one finds

$$12.36 \text{ (anal.)} < 12.48 \text{ (2 d.o.f.)} < 12.73 \text{ (red. 1)} < 20 \text{ (red. 2)}$$

which is much worse than the previous case. This is because the choice of  $\theta_2$  as the master coordinate was a bad choice. This is confirmed by the calculation of the natural frequency  $\nu_1$  of the constrained system when the master d.o.f. ( $\theta_2$ ) is blocked; it is obtained by eliminating the second line and the second column of the element matrices (6.47); one finds easily

$$\nu_1^2 = \frac{12EI}{l^3} / \frac{156\varrho Al}{420} = 32.3 \frac{EI}{\varrho Al^4} \quad \Rightarrow \quad \frac{\omega_1^2}{\nu_1^2} = \frac{20}{32.3}$$

which is no longer small compared to 1. This example confirms that the translational d.o.f. are more important than the rotational ones.

**Table 6.1.** Comparison of various Guyan reductions for the clamped-free beam of Fig.6.8. Natural frequencies  $\omega_i$  reduced with respect to the analytical result  $\omega_1^*$ .  $\nu_1$  is the natural frequency of the first constrained mode (when all the masters are blocked). The first line shows the analytical results.

Masters	$N$ d.o.f.	$\omega_1/\omega_1^*$	$\omega_2/\omega_1^*$	$\omega_3/\omega_1^*$	$\omega_4/\omega_1^*$	$\nu_1/\omega_1^*$
Analytical solution	$\infty$	1.	6.267	17.55	34.39	-
$u_i, \theta_i$ ( $i = 1, \dots, 6$ )	12	1.00	6.27	17.58	34.61	-
$u_i$ ( $i = 1, \dots, 6$ )	6	1.00	6.27	17.61	34.93	115
$\theta_i$ ( $i = 1, \dots, 6$ )	6	1.00	6.51	19.28	41.17	9.30
$u_2, \theta_2, u_4, \theta_4, u_6, \theta_6$	6	1.00	6.29	17.77	40.01	58.2
$u_2, u_4, u_6$	3	1.00	6.32	17.82	-	27.34
$\theta_2, \theta_4, \theta_6$	3	1.02	7.41	30.41	-	4.66

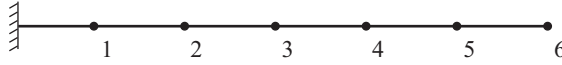


**Fig. 6.8.** Clamped-free beam modeled with 6 finite elements of equal length.

To further illustrate the choice of the masters in the Guyan reduction, consider the clamped-free beam of Fig. 6.8; it is modeled with 6 finite elements of equal length. Table 6.1 compares the reduced natural frequencies  $\omega_i/\omega_1^*$  for  $i = 1$  to 4, for the various Guyan reductions ( $\omega_1^*$  is the analytical solution for mode 1). The results indicate clearly the superiority of the translations over rotations in the reduction process.

## 6.5 Craig-Bampton reduction

Consider the finite element model

$$\begin{bmatrix} M_{11} & M_{12} \\ M_{21} & M_{22} \end{bmatrix} \begin{Bmatrix} \ddot{\mathbf{x}}_1 \\ \ddot{\mathbf{x}}_2 \end{Bmatrix} + \begin{bmatrix} K_{11} & K_{12} \\ K_{21} & K_{22} \end{bmatrix} \begin{Bmatrix} \mathbf{x}_1 \\ \mathbf{x}_2 \end{Bmatrix} = \begin{Bmatrix} \mathbf{f}_1 \\ 0 \end{Bmatrix} \quad (6.48)$$

where the degrees of freedom have been partitioned into the masters  $\mathbf{x}_1$  and the slaves  $\mathbf{x}_2$ . The masters include all the d.o.f. with a specific interest in the problem: those where disturbance and control loads are applied, where sensors are located and where the performance is evaluated. The slaves include all the other d.o.f. which have no particular interest in the problem and are ready for elimination.

The *Craig-Bampton reduction* is conducted in two steps. First, a Guyan reduction is performed according to the static relationship (6.40). In a second step, the constrained system is considered:

$$M_{22}\ddot{\mathbf{x}}_2 + K_{22}\mathbf{x}_2 = 0 \quad (6.49)$$

(obtained by setting  $\mathbf{x}_1 = 0$  in the foregoing equation). Let us assume that the eigen modes of this system constitute the column of the matrix  $\Psi_2$ , and that they are normalized according to  $\Psi_2^T M_{22} \Psi_2 = I$ . We then perform the change of coordinates

$$\begin{Bmatrix} \mathbf{x}_1 \\ \mathbf{x}_2 \end{Bmatrix} = \begin{bmatrix} I & 0 \\ -K_{22}^{-1}K_{21} & \Psi_2 \end{bmatrix} \begin{Bmatrix} \mathbf{x}_1 \\ \boldsymbol{\alpha} \end{Bmatrix} = T \begin{Bmatrix} \mathbf{x}_1 \\ \boldsymbol{\alpha} \end{Bmatrix} \quad (6.50)$$

Comparing with (6.42), one sees that the solution has been enriched with a set of fixed boundary modes of modal amplitude  $\boldsymbol{\alpha}$ . Using the transformation matrix  $T$ , the mass and stiffness matrices are obtained as in the previous section:

$$\hat{M} = T^T M T \quad \hat{K} = T^T K T \quad (6.51)$$

leading to

$$\begin{bmatrix} \hat{M}_{11} & \hat{M}_{12} \\ \hat{M}_{21} & I \end{bmatrix} \begin{Bmatrix} \ddot{\mathbf{x}}_1 \\ \ddot{\boldsymbol{\alpha}} \end{Bmatrix} + \begin{bmatrix} \hat{K}_{11} & 0 \\ 0 & \Omega^2 \end{bmatrix} \begin{Bmatrix} \mathbf{x}_1 \\ \boldsymbol{\alpha} \end{Bmatrix} = \begin{Bmatrix} \mathbf{f}_1 \\ 0 \end{Bmatrix} \quad (6.52)$$

In this equation, the stiffness matrix is block diagonal, with  $\hat{K}_{11} = K_{11} - K_{12}K_{22}^{-1}K_{21}$  being the Guyan stiffness matrix and  $\Omega^2 = \Psi_2^T K_{22} \Psi_2$  being a diagonal matrix with entries equal to the square of the natural frequencies of the fixed boundary modes. Similarly,  $\hat{M}_{11} = M_{11} - M_{12}K_{22}^{-1}K_{21} - K_{12}K_{22}^{-1}M_{21} + K_{12}K_{22}^{-1}M_{22}K_{22}^{-1}K_{21}$  is the Guyan mass matrix [the same as that given by (6.43)].  $\hat{K}_{11}$  and  $\hat{M}_{11}$  are fully populated but do not depend on the set of constrained modes  $\Psi_2$ . The off-diagonal term of the mass matrix is given by  $\hat{M}_{12} = (M_{12} - K_{12}K_{22}^{-1}M_{22})\Psi_2$ . Since all the external loads are applied to the master d.o.f., the right hand side of this equation is unchanged by the transformation. The foregoing equation may be used with an increasing number of constrained modes (increasing the size of  $\boldsymbol{\alpha}$ ), until the model provides an appropriate representation of the system in the requested frequency band.

## 6.6 Problems

**P.6.1** Write the mass and stiffness matrices of a plane bar element with variable cross section varying linearly from  $A_1$  to  $A_2$ .

**P.6.2** Convergence: Consider a simply supported beam with uniform properties and its FE model consisting of  $n$  elements of equal length. Plot a diagram of the evolution of the error of the natural frequency of the first five modes with the number of elements in the model. [The exact natural frequencies are given by Equ.(4.34)].

**P.6.3** Lumped mass vs. consistent mass: Consider a simply supported beam with uniform properties. Compare the natural frequencies predicted by two F.E. models involving the same number of elements, one using a consistent mass matrix, and one using a lumped mass model corresponding to Equ.(6.26). Comment the results.

**P.6.4** Guyan reduction: Build a FE model of a uniform clamped-free beam with 10 elements of equal size. Evaluate the accuracy of the model for the first 4 modes (the analytical results are given in Problem 4.1 ). Suggest one or several Guyan reductions which provide an estimate of the first 4 natural frequencies with an error of less than 1%. Comment the results.

**P.6.5**  $n$ -storey building with geometric stiffness: Using the results of section 6.3, build a spring-mass model of a building made of  $n$  identical floors and massless columns, including the gravity loads. Compare with section 5.6.

---

## Seismic excitation

*On ne vit point assez pour profiter de ses fautes.*

La Bruyère, *Les Caractères*, 1688

### 7.1 Introduction

By seismic response, it is meant that the excitation comes from the motion of the support(s). This includes civil structures during an earthquake, a spacecraft excited by the launcher vibrations, a precision machine excited by the floor vibrations. More specific information about earthquakes will be discussed in Chapter 9. The seismic response has some special features which need to be treated with care. This chapter develops the equations governing the motion of a structure subjected to a support acceleration; the case of a single axis excitation is considered first; the case of multiple supports is considered next.

### 7.2 Equation of motion for a single axis excitation

Consider a linear structure subjected to a point force  $f$  and a single-axis seismic excitation of acceleration  $\ddot{x}_0$  (Fig.7.1.a). The system may be considered as placed on a fictitious shaking table excited by an (unknown) reaction force  $f_0$  (Fig.7.1.b).

Hamilton's principle states that the variational indicator :

$$\int_{t_1}^{t_2} (\delta L + \delta W_{nc}) dt = \int_{t_1}^{t_2} [\delta(T - V) + \delta W_{nc}] dt = 0 \quad (7.1)$$

vanishes for arbitrary virtual variations of the path between two instants  $t_1$  and  $t_2$  compatible with the kinematics, and such that the configuration is fixed at  $t_1$  and  $t_2$ . In this equation,  $T$  is the kinetic energy,  $V$  the strain energy and  $\delta W_{nc}$  is the virtual work associated with the non-conservative forces (the external force  $f$  and the support reaction  $f_0$  in this case).

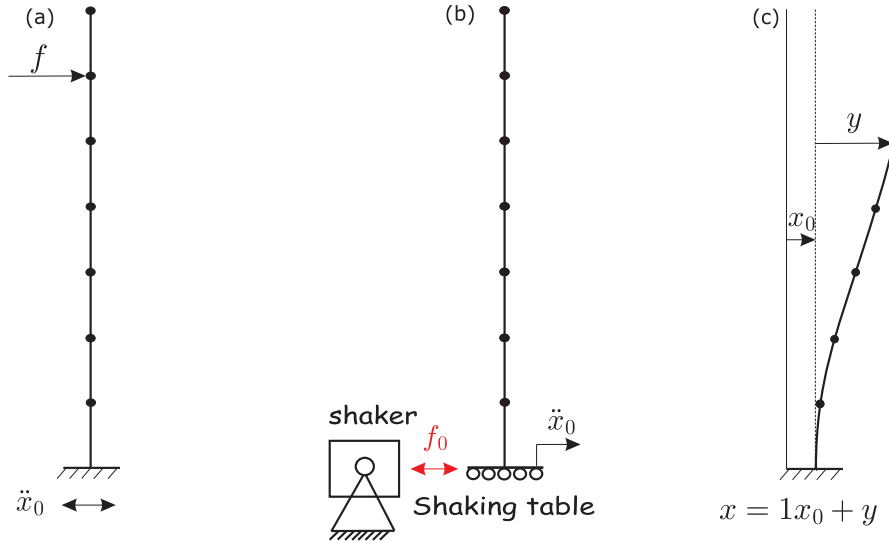


**Fig. 7.1.** (a) Structure subjected to a single-axis support excitation (b) Fictitious shaking table representation highlighting the reaction force  $f_0$  (c) Partition of the global displacement into rigid body motion and flexible motion relative to the base.

If one decomposes the global displacements  $\mathbf{x}$  (generalized displacements including translational as well as rotational degrees of freedom, d.o.f.) into the rigid body mode and the flexible motion relative to the base (Fig.7.1.c).

$$\mathbf{x} = \mathbf{1}x_0 + \mathbf{y} \quad (7.2)$$

where  $x_0$  is the support motion,  $\mathbf{1}$  is the unit rigid body mode (all translational d.o.f. along the axis of excitation are equal to 1 and the rotational d.o.f. are equal to 0). The virtual displacements satisfy

$$\delta\mathbf{x} = \mathbf{1}\delta x_0 + \delta\mathbf{y} \quad (7.3)$$

where  $\delta x_0$  is arbitrary and  $\delta\mathbf{y}$  satisfies the clamped boundary conditions at the base. Let  $\mathbf{b}$  be the influence vector of the external loading  $f$  (for a point force,  $\mathbf{b}$  contains all 0 except 1 at the d.o.f. where the load is applied), so that  $\mathbf{b}^T\mathbf{x}$  is the generalized displacement of the d.o.f. where  $f$  is applied. The various energy terms involved in Hamilton's principle are respectively

$$T = \frac{1}{2}\dot{\mathbf{x}}^T M \dot{\mathbf{x}} \quad V = \frac{1}{2}\mathbf{y}^T K \mathbf{y} \quad (7.4)$$

$$\delta W_{nc} = f_0\delta x_0 + f\mathbf{b}^T\delta\mathbf{x} = (f_0 + f\mathbf{b}^T\mathbf{1})\delta x_0 + f\mathbf{b}^T\delta\mathbf{y} \quad (7.5)$$

One notices that the kinetic energy depends on the absolute velocity while the strain energy depends on the flexible motion alone, that is the motion relative to the base. For a point force,  $\mathbf{b}^T \mathbf{1} = 1$ . Substituting into the variational indicator, one finds

$$\int_{t_1}^{t_2} [\dot{\mathbf{x}}^T M \delta \dot{\mathbf{x}} - \mathbf{y}^T K \delta \mathbf{y} + (f_0 + f) \delta x_0 + f \mathbf{b}^T \delta \mathbf{y}] dt = 0 \quad (7.6)$$

and, upon integrating the first term by parts, taking into account that  $\delta \mathbf{x}(t_1) = \delta \mathbf{x}(t_2) = 0$ ,

$$\int_{t_1}^{t_2} [(-\ddot{\mathbf{x}}^T M \mathbf{1} + f_0 + f) \delta x_0 - (\ddot{\mathbf{x}}^T M + \mathbf{y}^T K - f \mathbf{b}^T) \delta \mathbf{y}] dt = 0 \quad (7.7)$$

for arbitrary  $\delta x_0$  and  $\delta \mathbf{y}$ . It follows that

$$M \ddot{\mathbf{x}} + K \mathbf{y} = \mathbf{b} f \quad (7.8)$$

$$f_0 = \mathbf{1}^T M \ddot{\mathbf{x}} - f \quad (7.9)$$

The presence of  $f$  in the right side of this equation is necessary to achieve static equilibrium; it is often ignored in the formulation.

Combining (7.2) with (7.8), one gets the classical equation expressed in relative coordinates

$$M \ddot{\mathbf{y}} + K \mathbf{y} = -M \mathbf{1} \ddot{x}_0 + \mathbf{b} f \quad (7.10)$$

Also combining with (7.8), (7.9) can be rewritten alternatively

$$f_0 = -\mathbf{1}^T K \mathbf{y} \quad (7.11)$$

The first term in the right hand side of (7.10) is simply the inertia forces associated with a rigid body acceleration  $\ddot{x}_0$  of the support. The structural damping has been ignored for simplicity; if a viscous damping is assumed on the relative coordinates  $\mathbf{y}$ , a contribution  $C \dot{\mathbf{y}}$  is added to the left hand side of (7.10), leading to

$$M \ddot{\mathbf{y}} + C \dot{\mathbf{y}} + K \mathbf{y} = -M \mathbf{1} \ddot{x}_0 + \mathbf{b} f \quad (7.12)$$

Equ.(7.11) becomes

$$f_0 = -\mathbf{1}^T (K \mathbf{y} + C \dot{\mathbf{y}}) \quad (7.13)$$

From now on, we will assume  $f = 0$  to focus on the response to the support acceleration.

### 7.2.1 Modal coordinates

Let  $\omega_1, \dots, \omega_n$  and  $\Phi = (\phi_1, \dots, \phi_n)$  be respectively the natural frequencies and the mode shapes of the structure clamped at its base (no base motion), solution of the homogeneous equation

$$M\ddot{\mathbf{y}} + K\mathbf{y} = 0 \quad (7.14)$$

They satisfy the eigenvalue problem

$$(K - \omega_i^2 M)\phi_i = 0 \quad (7.15)$$

and the orthogonality conditions (2.11) and (2.12)

$$\Phi^T M \Phi = \text{diag}(\mu_i) \quad (7.16)$$

$$\Phi^T K \Phi = \text{diag}(\mu_i \omega_i^2) \quad (7.17)$$

Once again, a modal damping is assumed, so that Equ.(2.20) applies

$$\Phi^T C \Phi = \text{diag}(2\xi_i \mu_i \omega_i) \quad (7.18)$$

Now, let us consider equation (7.12) again

$$M\ddot{\mathbf{y}} + C\dot{\mathbf{y}} + K\mathbf{y} = -M\mathbf{1}\ddot{x}_0 \quad (7.19)$$

and let us perform a change of variables from physical coordinates  $\mathbf{y}$  (motion relative to the base) to modal coordinates  $\mathbf{z}$  according to

$$\mathbf{y} = \Phi \mathbf{z} \quad (7.20)$$

$\mathbf{z}$  is the vector of modal amplitudes. Substituting into the foregoing equation, left multiplying by  $\Phi^T$  and using the orthogonality relationships, one gets a set of decoupled equations

$$\mu_i \ddot{z}_i + 2\xi_i \mu_i \omega_i \dot{z}_i + \mu_i \omega_i^2 z_i = -\phi_i^T M \mathbf{1} \ddot{x}_0 \quad (7.21)$$

$$\Gamma_i = -\phi_i^T M \mathbf{1} \quad (7.22)$$

is known as the *modal participation factor* of mode  $i$ , it is simply the work on mode  $i$  of the inertia forces associated with a unit acceleration of the support. We define the vector of modal participation factors (modal participation vector)  $\boldsymbol{\Gamma} = (\Gamma_1, \Gamma_2, \dots, \Gamma_i, \dots)^T$  as

$$\boldsymbol{\Gamma} = -\Phi^T M \mathbf{1} \quad (7.23)$$

### 7.2.2 Support reaction, dynamic mass

Now let us consider the reaction force  $f_0$  due to the seismic motion  $\ddot{x}_0$ . From (7.9) and (7.2)

$$\begin{aligned} f_0 &= \mathbf{1}^T M \ddot{\mathbf{x}} = \mathbf{1}^T M (\mathbf{1} \ddot{x}_0 + \ddot{\mathbf{y}}) \\ &= \mathbf{1}^T M \mathbf{1} \ddot{x}_0 + \mathbf{1}^T M \Phi \ddot{\mathbf{z}} \\ f_0 &= m_T \ddot{x}_0 - \mathbf{I}^T \ddot{\mathbf{z}} \end{aligned} \quad (7.24)$$

where (7.23) has been used and  $m_T = \mathbf{1}^T M \mathbf{1}$  is the total mass of the system. The fact that  $m_T$  is the total mass of the system can be seen from the expression of the kinetic energy (7.4): if a rigid body velocity  $\dot{\mathbf{x}} = \mathbf{1} \dot{x}_0$  is applied, the total kinetic energy is

$$\frac{1}{2} \dot{\mathbf{x}}^T M \dot{\mathbf{x}} = \frac{1}{2} \dot{x}_0^T \mathbf{1}^T M \mathbf{1} \dot{x}_0 = \frac{1}{2} m_T \dot{x}_0^2 \quad (7.25)$$

The *dynamic mass* of the system is defined as the ratio between the complex amplitude of the harmonic force applied to the shaker,  $F_0$  and the amplitude of the acceleration of the shaking table,  $\ddot{X}_0$ , for every excitation frequency :

$$\ddot{x}_0 = \ddot{X}_0 e^{j\omega t} \quad f_0 = F_0 e^{j\omega t} \quad \mathbf{z} = \mathbf{Z} e^{j\omega t} \quad (7.26)$$

Assuming no damping for simplicity, the relationship between the amplitude  $\ddot{X}_0$  and  $\mathbf{Z}$  follows from (7.21):

$$Z_i = \frac{\Gamma_i}{\mu_i(\omega_i^2 - \omega^2)} \ddot{X}_0 \quad (7.27)$$

Combining with (7.24), the dynamic mass reads

$$\frac{F_0}{\ddot{X}_0} = m_T + \sum_{i=1}^n \frac{\Gamma_i^2}{\mu_i} \left( \frac{\omega^2}{\omega_i^2 - \omega^2} \right) \quad (7.28)$$

Before discussing this result, let us consider the alternative formulation based on (7.11); using (7.15) one gets

$$f_0 = -\mathbf{1}^T K \Phi \mathbf{z} = -\mathbf{1}^T M \Phi \text{diag}(\omega_i^2) \mathbf{z} = \mathbf{I}^T \text{diag}(\omega_i^2) \mathbf{z} \quad (7.29)$$

and combining with (7.27), one finds

$$\frac{F_0}{\ddot{X}_0} = \sum_{i=1}^n \frac{\Gamma_i^2}{\mu_i} \left( \frac{\omega_i^2}{\omega_i^2 - \omega^2} \right) \quad (7.30)$$

Comparing (7.28) and (7.30) at  $\omega = 0$ , one finds that

$$m_T = \sum_{i=1}^n \frac{\Gamma_i^2}{\mu_i} \quad (7.31)$$

where the sum extends to all the modes.  $\Gamma_i^2/\mu_i$  is called the *effective modal mass* of mode  $i$ ; it represents the part of the total mass which is associated with mode  $i$  for this particular type of excitation (defined by the vector  $\mathbf{1}$ ). Equations (7.28) and (7.30) are equivalent if all the modes are included in the modal expansion. However, if equation (7.30) is truncated after  $m < n$  modes, the modal mass of the high frequency mode is simply ignored, making this result statically incorrect. A quasi-static correction can be applied, by assuming that the high frequency modes respond in a quasi-static manner (i.e. as for  $\omega = 0$ ); this leads to

$$\frac{F_0}{\ddot{X}_0} \simeq \sum_{i=1}^m \frac{\Gamma_i^2}{\mu_i} \left( \frac{\omega_i^2}{\omega_i^2 - \omega^2} \right) + \sum_{i=m+1}^n \frac{\Gamma_i^2}{\mu_i} \quad (7.32)$$

and upon using (7.31),

$$\frac{F_0}{\ddot{X}_0} = \sum_{i=1}^m \frac{\Gamma_i^2}{\mu_i} \left( \frac{\omega_i^2}{\omega_i^2 - \omega^2} \right) + m_T - \sum_{i=1}^m \frac{\Gamma_i^2}{\mu_i} = m_T + \sum_{i=1}^m \frac{\Gamma_i^2}{\mu_i} \left( \frac{\omega^2}{\omega_i^2 - \omega^2} \right) \quad (7.33)$$

Thus, one recovers the truncated form of (7.28), which is statically correct. If the damping is included, the equation becomes

$$\frac{F_0(\omega)}{\ddot{X}_0(\omega)} = m_T + \sum_{i=1}^m \frac{\Gamma_i^2}{\mu_i} \left( \frac{\omega^2}{\omega_i^2 + 2j\xi_i\omega_i\omega - \omega^2} \right) \quad (7.34)$$

It can be truncated after the  $m$  modes which belong to the bandwidth of the excitation *without any error on the static mass*.

### 7.3 Example: $n$ -storey building

Consider the building constituted of  $n$  identical floors already analyzed in section 2.7 (Fig.2.11). The natural frequencies and mode shapes are given by

$$\omega_r = 2\sqrt{\frac{k}{m}} \sin\left[\frac{(2r-1)\pi}{(2n+1)2}\right] \quad (r = 1, 2, \dots, n) \quad (7.35)$$

$$\phi_r(i) = C \sin[i \frac{(2r-1)}{(2n+1)} \pi] \quad (7.36)$$

where  $m$  and  $k$  are the mass and the stiffness of a single floor ( $C$  is an arbitrary constant).<sup>1</sup> The first few mode shapes are illustrated in Fig.2.11. The mass matrix of the system is  $M = mI_n$ ; the unit rigid body mode associated with the support motion is  $\mathbf{1} = (1, 1, \dots, 1)^T$ , because all the d.o.f. are translations. It follows that the modal participation factors are

$$\Gamma_r = -\phi_r^T M \mathbf{1} = -m \sum_{i=1}^n \phi_r(i) \quad (7.37)$$

The generalized mass is

$$\mu_r = \phi_r^T M \phi_r = m \sum_{i=1}^n \phi_r^2(i) \quad (7.38)$$

The effective modal mass of mode  $r$  is

$$\frac{\Gamma_r^2}{\mu_r} = m \frac{[\sum_{i=1}^n \phi_r(i)]^2}{\sum_{i=1}^n \phi_r^2(i)} \quad (7.39)$$

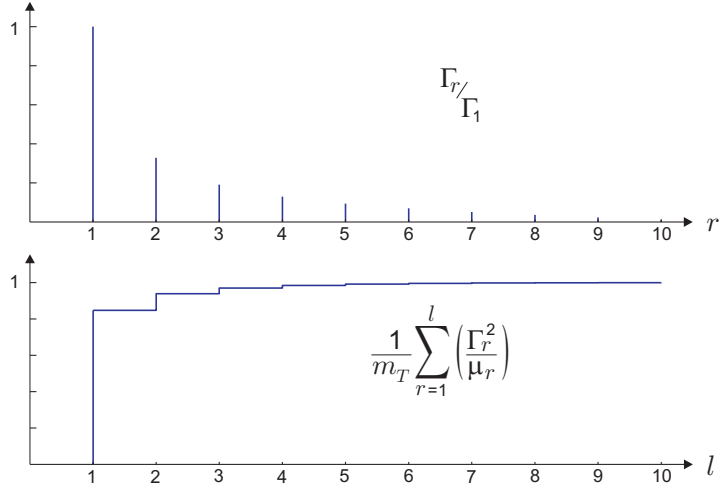


**Fig. 7.2.** (a) Evolution of the modal participation factor  $|\Gamma_r/\Gamma_1|$  with the order  $r$  of the mode. (b) Cumulated effective modal mass  $\frac{1}{m_T} \sum_{r=1}^l (\Gamma_r^2 / \mu_r)$ . The amplitude of the steps correspond to the effective modal mass of individual modes.

<sup>1</sup> In Equ.(7.36),  $r$  refers to the mode and  $i$  to the floor.

Recall that  $\sum_{r=1}^n \Gamma_r^2 / \mu_r = n.m = m_T$ , the total mass of the system. Figure 7.2 shows the evolution of the modal participation factor  $|\Gamma_r/\Gamma_1|$ , the cumulated effective modal mass (normalized to the total mass)  $\frac{1}{m_T} \sum_{r=1}^l \Gamma_r^2 / \mu_r$ ; the modal participation factor and the effective modal mass decrease rapidly with the order of the mode.

## 7.4 Multi-axis excitation\*

In many situations, the structure is excited along several axes and, if there are several supports (consider, for example, a pipeline connecting different buildings), the excitation may differ from one support to the next, which brings the issue of differential displacements. Let us partition the d.o.f. between the restrained d.o.f.  $\mathbf{x}_0$ , attached to the supports and the unrestrained d.o.f.  $\mathbf{x}_1$ ; the motion  $\mathbf{x}_0$  is prescribed. If one neglects the structural damping (it will be included later, in modal coordinates), the equation of motion reads

$$\begin{bmatrix} M_{11} & M_{10} \\ M_{01} & M_{00} \end{bmatrix} \begin{Bmatrix} \ddot{\mathbf{x}}_1 \\ \ddot{\mathbf{x}}_0 \end{Bmatrix} + \begin{bmatrix} K_{11} & K_{10} \\ K_{01} & K_{00} \end{bmatrix} \begin{Bmatrix} \mathbf{x}_1 \\ \mathbf{x}_0 \end{Bmatrix} = \begin{Bmatrix} 0 \\ \mathbf{f}_0 \end{Bmatrix} \quad (7.40)$$

where  $\mathbf{f}_0$  is the vector of support reactions. Partitioning this equation, one finds

$$M_{11}\ddot{\mathbf{x}}_1 + K_{11}\mathbf{x}_1 = -M_{10}\ddot{\mathbf{x}}_0 - K_{10}\mathbf{x}_0 \quad (7.41)$$

$$\mathbf{f}_0 = M_{01}\ddot{\mathbf{x}}_1 + M_{00}\ddot{\mathbf{x}}_0 + K_{01}\mathbf{x}_1 + K_{00}\mathbf{x}_0 \quad (7.42)$$

In these equations,  $\mathbf{x}_1$  are the absolute displacements (or rotation) of the unrestrained d.o.f. and  $\mathbf{x}_0$  are the absolute displacements of the support d.o.f.. In a way similar to (7.2), we partition the absolute displacements according to

$$\mathbf{x}_1 = \mathbf{y} + \mathbf{x}_1^{qs} \quad (7.43)$$

where  $\mathbf{x}_1^{qs}$  is the *quasi-static* response due to the support displacements, solution of  $K_{11}\mathbf{x}_1^{qs} = -K_{10}\mathbf{x}_0$

$$\mathbf{x}_1^{qs} = -K_{11}^{-1}K_{10}\mathbf{x}_0 = T_{qs}\mathbf{x}_0 \quad (7.44)$$

and  $\mathbf{y}$  is the dynamic response of the unrestrained d.o.f. (the subscript 1 is omitted for the dynamic response which concerns only the unrestrained d.o.f.). In the foregoing equation,  $T_{qs}$  is the quasi-static transmission matrix; its  $i^{th}$  column gives the absolute quasi-static displacements resulting from a displacement with a unit amplitude being given to the  $i^{th}$  support

d.o.f. (all the others being 0). For a statically determinate structure,  $T_{qs}$  comes from rigid body kinematics; for a single-axis excitation,  $T_{qs} = \mathbf{1}$  and Equ.(7.2) is recovered. The dynamic response  $\mathbf{y}$  satisfies homogeneous (zero) boundary conditions at the support d.o.f.. Substituting

$$\mathbf{x}_1 = T_{qs}\mathbf{x}_0 + \mathbf{y} \quad (7.45)$$

into Equ.(7.41), one finds

$$M_{11}\ddot{\mathbf{y}} + K_{11}\mathbf{y} = -(M_{11}T_{qs} + M_{10})\ddot{\mathbf{x}}_0 \quad (7.46)$$

which is the counterpart of Equ.(7.10) (with no external force  $f$  in this case).

#### 7.4.1 Modal coordinates

In the same way as in section 7.2.1, the dynamic response may be expanded into the modes shapes of the structure clamped at its base. Let  $\omega_1, \dots, \omega_n$  and  $\Phi = (\phi_1, \dots, \phi_n)$  be respectively the natural frequencies and the mode shapes of the structure clamped at its base (no base motion,  $\mathbf{x}_0 = 0$ ), solution of the homogeneous equation

$$M_{11}\ddot{\mathbf{y}} + K_{11}\mathbf{y} = 0 \quad (7.47)$$

They satisfy the eigenvalue problem

$$(K_{11} - \omega_i^2 M_{11})\phi_i = 0 \quad (7.48)$$

and the orthogonality conditions

$$\Phi^T M_{11} \Phi = \text{diag}(\mu_i) \quad (7.49)$$

$$\Phi^T K_{11} \Phi = \text{diag}(\mu_i \omega_i^2) \quad (7.50)$$

Now, let us consider equation (7.46) again and let us perform a change of variables from physical coordinates  $\mathbf{y}$  (motion relative to the base) to modal coordinates  $\mathbf{z}$  according to

$$\mathbf{y} = \Phi \mathbf{z} \quad (7.51)$$

Taking into account the orthogonality conditions, one finds easily a set of decoupled equations

$$\mu \ddot{\mathbf{z}} + \mu \Omega^2 \mathbf{z} = -\Phi^T (M_{11}T_{qs} + M_{10})\ddot{\mathbf{x}}_0 = \Gamma \ddot{\mathbf{x}}_0 \quad (7.52)$$

where  $\mu = \text{diag}(\mu_i)$  is the diagonal matrix of the generalized masses and  $\Omega = \text{diag}(\omega_i)$  is the diagonal matrix of the natural frequencies and

$$\Gamma = -\Phi^T(M_{11}T_{qs} + M_{10}) \quad (7.53)$$

is the *modal participation matrix*. The size of  $\Gamma$  is  $m \times n_s$ , where  $m$  is the number of modes and  $n_s$  is the number of independent excitations. In  $\Gamma_{ij}$ ,  $i$  refer to the mode and  $j$  refers to the support<sup>2</sup>;  $\Gamma_{ij}$  is the work done on mode  $i$  by the inertia forces associated with the quasi-static acceleration produced by a unit acceleration applied to the component  $j$  of the support acceleration  $\ddot{\mathbf{x}}_0$ . This is a generalization of the modal participation vector defined earlier for a single axis excitation. Note that the term  $M_{10}$  coupling the unrestrained d.o.f. and the support d.o.f. disappears for a lumped mass system; it is usually small and it is frequently neglected. The above equation neglects the damping; if modal damping is assumed according to (7.18), Equ.(7.52) becomes

$$\mu \ddot{\mathbf{z}} + 2\xi\mu\Omega\dot{\mathbf{z}} + \mu\Omega^2\mathbf{z} = -\Phi^T(M_{11}T_{qs} + M_{10})\ddot{\mathbf{x}}_0 = \Gamma\ddot{\mathbf{x}}_0 \quad (7.54)$$

where  $\xi = \text{diag}(\xi_i)$  is the diagonal matrix of modal damping factor. As usual, the normal modes may be normalized according to  $\mu_i = 1$  if appropriate ( $\mu = I$ ). In the particular case of a single-axis excitation,  $\ddot{x}_0$  is a scalar and the modal participation becomes a column vector  $\boldsymbol{\Gamma}$  and the equation is reduced to (7.22).

To transform the equation in the frequency domain, we assume harmonic functions

$$\ddot{\mathbf{x}}_0 = \ddot{\mathbf{X}}_0 e^{j\omega t} \quad \mathbf{z} = \mathbf{Z} e^{j\omega t} \quad (7.55)$$

The relationship between the complex amplitudes  $\mathbf{Z}$  and  $\ddot{\mathbf{X}}_0$  is

$$\mathbf{Z} = H_m(\omega)\boldsymbol{\Gamma} \ddot{\mathbf{X}}_0 \quad (7.56)$$

where

$$H_m(\omega) = \text{diag}\left[\frac{1}{\mu_i(\omega_i^2 - \omega^2 + 2j\xi_i\omega\omega_i)}\right] \quad (7.57)$$

This relation holds also between the Fourier transforms of respectively the modal amplitudes and the support acceleration vector.

---

<sup>2</sup> If several supports have the same motion, they can be treated as a single support.

### 7.4.2 Support reactions

As already pointed out for a single axis excitation, one must be careful in the formulation of the support reactions, if one wants to obtain an expression which remains statically correct after modal truncation. Examining the single-axis case again, one sees that this was achieved when starting from the inertia forces, Equ.(7.9), while a quasi-static correction for the high frequency modes was necessary when starting from the elastic restoring forces (7.11). We proceed in a similar way in the case of a multi-axis excitation, and eliminate the elastic restoring term  $K_{01}\mathbf{x}_1$  from Equ.(7.42) using Equ.(7.41):

$$\mathbf{x}_1 = -K_{11}^{-1}(K_{10}\mathbf{x}_0 + M_{10}\ddot{\mathbf{x}}_0 + M_{11}\ddot{\mathbf{x}}_1)$$

$$K_{01}\mathbf{x}_1 = T_{qs}^T(K_{10}\mathbf{x}_0 + M_{10}\ddot{\mathbf{x}}_0 + M_{11}\ddot{\mathbf{x}}_1)$$

Upon substituting into Equ.(7.42) and using the identity  $T_{qs}^T K_{10} = K_{01} T_{qs}$ , one gets

$$\mathbf{f}_0 = (M_{01} + T_{qs}^T M_{11})\ddot{\mathbf{x}}_1 + (M_{00} + T_{qs}^T M_{10})\ddot{\mathbf{x}}_0 + (K_{00} + K_{01} T_{qs})\mathbf{x}_0 \quad (7.58)$$

which contains only the acceleration vector  $\ddot{\mathbf{x}}_1$  and no longer the displacements  $\mathbf{x}_1$ . This equation is the multi-support counterpart of Equ.(7.24); the second term represents the inertia forces of the support d.o.f. (that were included in  $m_T$  in the single-axis case) and the third term represents the forces induced by the differential displacements. Using

$$\ddot{\mathbf{x}}_1 = T_{qs}\ddot{\mathbf{x}}_0 + \Phi\ddot{\mathbf{z}} \quad (7.59)$$

to transform into modal coordinates, one finds

$$\mathbf{f}_0 = \hat{M}_{00}\ddot{\mathbf{x}}_0 - I^T\ddot{\mathbf{z}} + (K_{00} + K_{01} T_{qs})\mathbf{x}_0 \quad (7.60)$$

with

$$\hat{M}_{00} = M_{00} + M_{01} T_{qs} + T_{qs}^T M_{10} + T_{qs}^T M_{11} T_{qs} \quad (7.61)$$

$\hat{M}_{00}$  is the *Guyan mass matrix*, defined in chapter 6, with  $\mathbf{x}_0$  as master d.o.f.: If all the d.o.f. are assumed to be related quasi-statically to the support d.o.f.,  $\mathbf{x}_0$ ,

$$\begin{Bmatrix} \mathbf{x}_1 \\ \mathbf{x}_0 \end{Bmatrix} = \begin{bmatrix} T_{qs} \\ I \end{bmatrix} \mathbf{x}_0 \quad (7.62)$$

the total kinetic energy may be written

$$T = \frac{1}{2}(\dot{\mathbf{x}}_1^T, \dot{\mathbf{x}}_0^T) \begin{bmatrix} M_{11} & M_{10} \\ M_{01} & M_{00} \end{bmatrix} \begin{Bmatrix} \dot{\mathbf{x}}_1 \\ \dot{\mathbf{x}}_0 \end{Bmatrix} = \frac{1}{2}\dot{\mathbf{x}}_0^T \hat{M}_{00} \dot{\mathbf{x}}_0 \quad (7.63)$$

If all supports move in the same direction,  $\dot{\mathbf{x}}_0 = \mathbf{1}_i v$  where  $\mathbf{1}_i$  indicates the direction of motion and  $v$  is the magnitude of the velocity; the total kinetic energy is in this case

$$\frac{1}{2}\dot{\mathbf{x}}_0^T \hat{M}_{00} \dot{\mathbf{x}}_0 = \frac{1}{2}\mathbf{1}_i^T \hat{M}_{00} \mathbf{1}_i v^2 = \frac{1}{2}m_T v^2$$

where  $m_T$  is the total mass of the system; thus, for any direction  $\mathbf{1}_i$  defining a global motion of the supports, one has

$$m_T = \mathbf{1}_i^T \hat{M}_{00} \mathbf{1}_i \quad (7.64)$$

Equation (7.60) is the multi-axis counterpart of Equ.(7.24); the last term is associated with the differential displacements (it does not exist for a single axis excitation). The modal amplitudes are solution of Equ.(7.54) in the time domain or (7.56) in the frequency domain. Upon substituting (7.56), one finds the FRF matrix of the support reaction vector

$$\mathbf{F}_0 = [\hat{M}_{00} + \omega^2 \Gamma^T H_m(\omega) \Gamma] \ddot{\mathbf{x}}_0 + (K_{00} + K_{01} T_{qs}) \mathbf{x}_0 \quad (7.65)$$

This is the counterpart of (7.34), with the addition of the differential displacements, which vanish if all supports have the same motion. If all supports move along some direction defined by the vector  $\mathbf{1}_r$ ,  $\ddot{\mathbf{x}}_0 = \mathbf{1}_r \ddot{x}_0$ ; if the force vector  $\mathbf{F}_0$  is projected along the same direction,  $\mathbf{1}_r^T \mathbf{F}_0$ , the dynamic mass along the direction  $\mathbf{1}_r$  is given by

$$\begin{aligned} \frac{\mathbf{1}_r^T \mathbf{F}_0}{\ddot{x}_0} &= \mathbf{1}_r^T [\hat{M}_{00} + \omega^2 \Gamma^T H_m(\omega) \Gamma] \mathbf{1}_r \\ \frac{\mathbf{1}_r^T \mathbf{F}_0}{\ddot{x}_0} &= m_T + \omega^2 (\Gamma \mathbf{1}_r)^T H_m(\omega) \Gamma \mathbf{1}_r \end{aligned} \quad (7.66)$$

This formula is identical to (7.34);  $\Gamma \mathbf{1}_r$  is the vector of modal participation factors along the direction  $\mathbf{1}_r$ .

## 7.5 Cascade analysis

When the systems are very complicated, as for example a nuclear power plant, there is a need to simplify the analysis. If the secondary structures

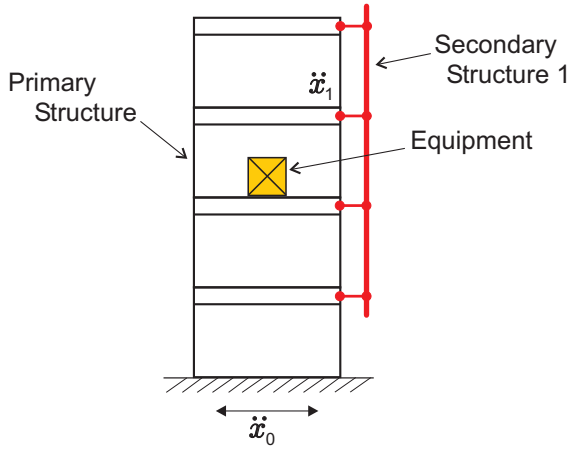


**Fig. 7.3.** Cascade Analysis: The primary structure is analyzed first and the absolute accelerations at the support points of the secondary structure,  $\ddot{x}_1$ , are calculated. In a second step, the secondary response is analyzed with a full model of the secondary structure (which can be complex, depending on the equipment) and the excitation computed at step one.

and equipments are much lighter than the primary structure, their influence on the response of the primary structure is negligible. In this case, it is legitimate, and often advisable, to perform the analysis in two steps: the primary structure is analyzed first<sup>3</sup> and the absolute accelerations are calculated at the support points of the secondary structure (Fig. 7.3); this acceleration field is then used as input acceleration to analyze the secondary structure, with a full model. From (7.45), the absolute acceleration is given by

$$\ddot{\mathbf{x}}_1 = T_{qs} \ddot{\mathbf{x}}_0 + \Phi \ddot{\mathbf{z}} \quad (7.67)$$

where  $\ddot{\mathbf{z}}$  is governed by (7.54) in the time domain. In the frequency domain, the Fourier transforms of the absolute acceleration vectors  $\ddot{\mathbf{X}}_1(\omega)$  and  $\ddot{\mathbf{X}}_0(\omega)$  are related by

$$\ddot{\mathbf{X}}_1(\omega) = [T_{qs} - \omega^2 \Phi H_m(\omega) \Gamma] \ddot{\mathbf{X}}_0(\omega) \quad (7.68)$$

For a single support excitation,  $T_{qs} = \mathbf{1}$ ,  $\ddot{x}_0$  is a scalar and  $\Gamma$  is a vector; the foregoing result becomes

$$\ddot{\mathbf{X}}_1(\omega) = [\mathbf{1} - \omega^2 \Phi H_m(\omega) \Gamma] \ddot{\mathbf{X}}_0(\omega) \quad (7.69)$$

or

---

<sup>3</sup> with an approximate model of the secondary structure if needed.

$$\ddot{\mathbf{X}}_1(\omega) = [\mathbf{1} - \sum_{i=1}^n \frac{\omega^2 \Gamma_i}{\mu_i(\omega_i^2 - \omega^2 + 2j\xi_i \omega \omega_i)} \phi_i] \ddot{X}_0(\omega) \quad (7.70)$$

## 7.6 Problems

**P.7.1** The following empirical formula relates the first natural period  $T_1 = 2\pi/\omega_1$  of vibration of a building to the number  $n$  of stories :

$$T_1 = 0.1n \quad (7.71)$$

[Newmark and Rosenblueth, p.421]. Show that the linear variation of the natural period with the number of floors is consistent with the  $n$ -storey building model examined in section 7.3, by showing that

$$T_1 = 2\pi/\omega_1 \simeq 4n\sqrt{m/k}$$

**P.7.2** Consider a shear frame with  $n = 10$  identical floors with  $m = 10^5$  kg and  $k = 16 \times 10^7$  N/m and a uniform modal damping of  $\xi_i = 0.01$ . (a) Evaluate the dynamic mass of the frame,  $F_0(\omega)/\ddot{X}_0(\omega)$ . (b) Evaluate the dynamic amplification of the acceleration on the upper floor,  $\ddot{X}_{10}(\omega)/\ddot{X}_0(\omega)$ .

**P.7.3** Consider a spring mass system with  $n = 10$  masses, organized according to Fig.2.16, with  $k = 1$  and  $m = 1$ . It is assumed that the two extremities move identically with the same acceleration  $\ddot{x}_0$ , so that the system may be regarded as having a single support. Calculate the modal participation factors and the effective modal masses of the various modes. Plot the cumulated effective modal mass in a figure similar to Fig.7.2. [Hint: The natural frequencies and the mode shapes are given by Equ.(2.72) and (2.73).]

**P.7.4** Consider the same system as in the previous problem, but the motion of the two extremities is independent; the seismic excitation is now defined by the excitation vector  $(\ddot{x}_0, \ddot{x}_{n+1})^T$ . Calculate the quasi-static transmission matrix  $T_{qs}$  and the modal participation matrix  $\Gamma$ .

## Random vibration

*Toute explication lucide m'a toujours convaincu, toute politesse m'a conquise, tout bonheur m'a presque toujours rendu sage.*

Marguerite Yourcenar, *Mémoires d'Hadrien*, 1951

### 8.1 Introduction

Many vibration problems are associated with machines operating in a random environment: wind on tall buildings and bridges, sea waves on off-shore platforms and ships, earthquakes on civil engineering structures, launch acceleration on spacecrafts, acoustic fatigue on aircraft panels, etc... This chapter gives a brief introduction to the main concepts in random vibration. It is assumed that the structure is known and deterministic, and therefore not subject to random variations of its characteristics. This chapter is restricted to linear structures under stationary excitation. The problem is solved conveniently in the frequency domain, because the input-output relationships for linear structures, which are expressed by convolutions in the time domain, can be expressed as simple products in the frequency domain.

It is assumed that the reader has been exposed to an introductory course in statistics and random processes, and that he is familiar with the concepts of random variable, probability density function, expectation, variance, the Gaussian distribution, etc...

### 8.2 Stationary random process

A random process  $x(\theta, t)$  is a parameterized family of random variables:  $\theta$  defines the sample (in the sample space), that is the outcome of the random experiment, and  $t$  is the parameter (assumed to be the time in this case). For a fixed  $\theta$ ,  $x(\theta, t)$  is a function of time; for a fixed  $t$ , it

is a random variable. A random process is stationary if its probability structure and all its statistics are invariant with respect to a time shift. This implies in particular that the *average*  $\mu = E[x(t)]$  is independent of  $t$ .<sup>1</sup>

### 8.3 Correlation function and power spectral density

The most important statistical information about a random process is contained in the *autocorrelation function*:  $\phi(t_1, t_2) = E[x(t_1)x^*(t_2)]$ , where  $x^*(t)$  is the complex conjugate of  $x(t)$  (most of the processes considered here will be real, except when explicitly stated). For a stationary process, it depends only on the delay  $\tau = t_1 - t_2$  between the two instants; it is denoted  $R_{xx}(\tau)$

$$R_{xx}(\tau) = E[x(t + \tau)x^*(t)] \quad (8.1)$$

For  $\tau = 0$ ,  $R_{xx}(0) = E[x^2]$  is the *mean square* value (MS). When the process is considered with respect to its mean,

$$\Gamma_{xx}(\tau) = E[\{x(t + \tau) - \mu\}\{x(t) - \mu\}] \quad (8.2)$$

$\Gamma_{xx}(\tau)$  is called the *autocovariance* function. If the process has a zero mean,  $\mu = 0$ , there is no difference between the autocorrelation function and the autocovariance. For  $\tau = 0$ ,  $\sigma^2 = \Gamma_{xx}(0)$  is the *variance* of the process (the square of the standard deviation  $\sigma$ ). It is the most important statistical information about the magnitude of the process (together with the mean), but it does not give any information about its frequency content, which is contained in the function  $R_{xx}(\tau)$ . The cross-correlation between two random processes  $x(t)$  and  $y(t)$  is defined by

$$R_{xy}(\tau) = E[x(t + \tau)y^*(t)] \quad (8.3)$$

where  $y^*(t)$  is the complex conjugate of  $y(t)$ .

A typical autocorrelation function of a stationary random process is represented in Fig.8.1. The correlation functions enjoy the property of symmetry which, for a real stationary process, reads

---

<sup>1</sup>  $E[.]$  stands for the mathematical expectation,

$$E[x] = \int_{-\infty}^{\infty} x p(x) dx$$

where  $p(x)$  is the probability density function of the random variable  $x$ .

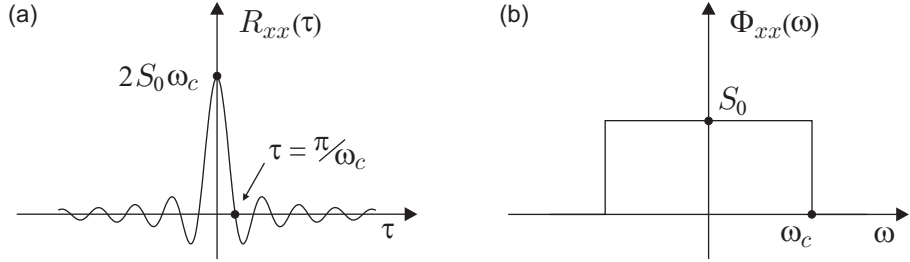


**Fig. 8.1.** Ideal low pass process. (a) Autocorrelation:  $R_{xx}(\tau) = 2S_0(\sin \omega_c \tau)/\tau$  is symmetric and has its maximum at  $\tau = 0$ . (b) PSD:  $\Phi_{xx}(\omega) = S_0$  ( $|\omega| \leq \omega_c$ ). Note that the wider  $\Phi_{xx}(\omega)$  in the frequency domain, the shorter  $R_{xx}(\tau)$  in the time domain, as a consequence of the duality of the Fourier transform.

$$R_{xx}(\tau) = R_{xx}(-\tau) \quad (8.4)$$

$$R_{xy}(\tau) = R_{yx}(-\tau)$$

They satisfy the following inequalities

$$[R_{xx}(0)R_{yy}(0)]^{1/2} \geq |R_{xy}(\tau)| \quad \text{and} \quad R_{xx}(0) \geq |R_{xx}(\tau)| \quad (8.5)$$

and the autocorrelation is such that it has a *non-negative Fourier transform*:

$$\Phi_{xx}(\omega) = \frac{1}{2\pi} \int_{-\infty}^{\infty} R_{xx}(\tau) e^{-j\omega\tau} d\tau \geq 0 \quad (8.6)$$

$\Phi_{xx}(\omega)$  is the *power spectral density* (PSD) of the stationary process  $x(t)$ . The autocorrelation function being an even function of  $\tau$ ,  $\Phi_{xx}(\omega)$  is real and even function of  $\omega$ . The inverse relationship is obtained by the inverse Fourier transform,

$$R_{xx}(\tau) = \int_{-\infty}^{\infty} \Phi_{xx}(\omega) e^{j\omega\tau} d\omega \quad (8.7)$$

from which the relationship between the mean square (MS) value and the PSD is established:

$$E[x^2] = R_{xx}(0) = \int_{-\infty}^{\infty} \Phi_{xx}(\omega) d\omega \quad (8.8)$$

Thus, the PSD provides a frequency decomposition of the MS value of the process. The unit of  $\Phi_{xx}$  is: (unit of  $x$ )<sup>2</sup> × sec/rad.

Additionally, it is easy to show (Problem 8.1) that

$$R_{\dot{x}\dot{x}}(\tau) = R'_{xx}(\tau) \quad (8.9)$$

and

$$R_{\dot{x}\dot{x}}(\tau) = -R''_{xx}(\tau) \quad (8.10)$$

If the process is differentiable [i.e. if the derivative  $\dot{x}(t)$  exists], the second derivative  $R''_{xx}(0)$  is finite, and  $R'_{xx}(0) = 0$  by symmetry. It follows that

$$R_{\dot{x}\dot{x}}(0) = 0 \quad (8.11)$$

Thus, the process is *orthogonal to its first derivative* (evaluated at the same time). If the process is not differentiable,  $R'_{xx}(\tau)$  may be discontinuous at the origin, where  $R''_{xx}(\tau)$  does not exist.

### 8.3.1 PSD estimation from time histories

The definition of the PSD given above is an abstract one, which is not suitable for estimation from a set of samples (time histories) of the process. Consider the integral of finite duration  $T$ :

$$X(\omega, T) = \int_{-T/2}^{T/2} x(t)e^{-j\omega t} dt \quad (8.12)$$

(which is in fact the Fourier transform of the process which has been passed into a rectangular window of duration  $T$ ). Since  $x(t)$  is a random process,  $X(\omega, T)$  is also a random process. It can be shown that, under mild conditions,

$$\lim_{T \rightarrow \infty} \frac{1}{2\pi T} E[|X(\omega, T)|^2] = \Phi_{xx}(\omega) \quad (8.13)$$

This formula<sup>2</sup> is the starting point for the evaluation of the PSD from a set of sample time histories  $x_i(t)$ , using the Fast Fourier Transform (FFT) to compute  $X_i(\omega, T)$ ; if  $n$  samples of duration  $T$  are considered, an estimate of the PSD is given by

$$\hat{\Phi}_{xx}(\omega) = \frac{1}{2\pi n T} \sum_{i=1}^n |X_i(\omega, T)|^2 \quad (8.14)$$

---

<sup>2</sup> Similarly, for the cross PSD,

$$\Phi_{xy}(\omega) = \frac{1}{2\pi} \int_{-\infty}^{\infty} R_{xy}(\tau)e^{-j\omega\tau} d\tau = \lim_{T \rightarrow \infty} \frac{1}{2\pi T} E[X(\omega, T)Y^*(\omega, T)]$$

### 8.3.2 Cumulative mean square response

The PSD function  $\Phi_{xx}(\omega)$  is defined over  $-\infty < \omega < \infty$ ; however, since it is an even function of  $\omega$ , for practical applications, one may consider a one sided PSD  $\bar{\Phi}_x(\omega)$  defined over  $0 \leq \omega < \infty$ , such that

$$E[x^2] = R_{xx}(0) = \int_0^\infty \bar{\Phi}_x(\omega) d\omega \quad (8.15)$$

Obviously,  $\bar{\Phi}_x(\omega) = 2\Phi_{xx}(\omega)$ . As we will see shortly, the PSD functions of the response of lightly damped structures to broadband excitations tend to be strongly peaked at the resonance frequencies of the structure (Fig.8.2). In order to estimate the various modal contributions to the global response, it is very convenient to examine the *cumulative mean square response*:

$$\sigma_x^2(\omega) = \int_\omega^\infty \bar{\Phi}_x(\nu) d\nu \quad (8.16)$$

A typical diagram is shown in Fig.8.2; it is a decreasing function of  $\omega$  starting from the MS value at  $\omega = 0$ ; the magnitude of the steps at the various resonance frequencies corresponds to the contribution of this mode in the overall MS response. This diagram is very convenient to identify the critical modes affecting the global response of the structure.

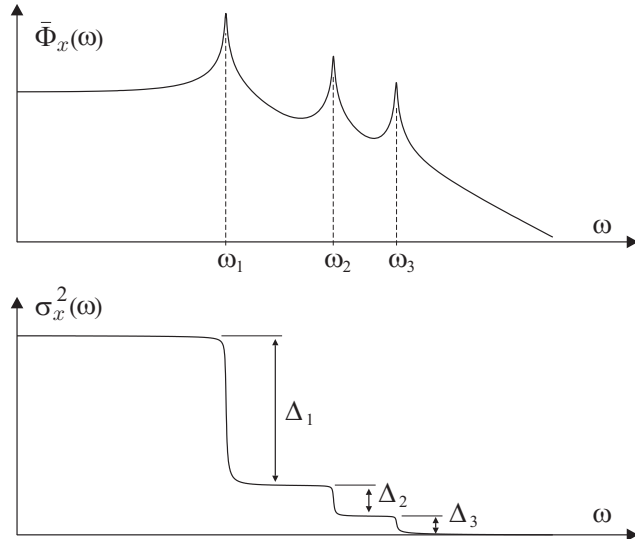


**Fig. 8.2.** Typical PSD function of a lightly damped structure ( $\omega$  is usually in log scale) and corresponding curve of the cumulative MS  $\sigma_x^2(\omega) = \int_\omega^\infty \bar{\Phi}_x(\nu) d\nu$ .  $\Delta_i$  is the contribution of mode  $i$  to the MS response.

### 8.3.3 Gaussian process

The justification of the frequent assumption that a random process is Gaussian is associated with the *central limit theorem* which establishes that, under mild conditions, the distribution of the sum of a large number of independent random variables tend to be Gaussian. The key word here is *independent*; the probability distribution of the individual random variables is not important. In nature, many phenomena may be regarded as resulting from the superposition of a large number of independent events,<sup>3</sup> which justifies the assumption (often confirmed by practice).

The main feature of Gaussian random processes is that they are *fully characterized by their statistics of the second order* [i.e. mean  $\mu$  and autocorrelation function  $R_{xx}(\tau)$  or equivalently the power spectral density  $\Phi_{xx}(\omega)$ ]. As a result, two Gaussian random variables which are uncorrelated are also independent.

### 8.3.4 White noise

A white noise is a stationary random process with uniform PSD (Fig.8.3):

$$\Phi_{xx}(\omega) = \Phi_0 \quad -\infty < \omega < \infty \quad (8.17)$$

The corresponding autocorrelation function is a Dirac function<sup>4</sup>

$$R_{xx}(\tau) = 2\pi\Phi_0\delta(\tau) \quad (8.18)$$

One sees immediately that the area under the PSD curve is infinite, which means that the MS value of such a process would be infinite. Although it is not physically realizable, the white noise process is a convenient approximation to analyze systems: When the actual excitation has a correlation time much shorter than the time constant of the system, it is legitimate to approximate the excitation by a white noise. We will see shortly a powerful approximation for the response of a linear oscillator to a wide band excitation.

---

<sup>3</sup> The wind results from a multitude of pressure gradients distributed randomly at the surface of the earth, or a seismic acceleration may be considered as resulting from a large number of micro slips along the fault line, each one being the source of a random wave.

<sup>4</sup> Observe, once again, the duality of the Fourier transform: infinitely long in the frequency domain means infinitely short in the time domain.

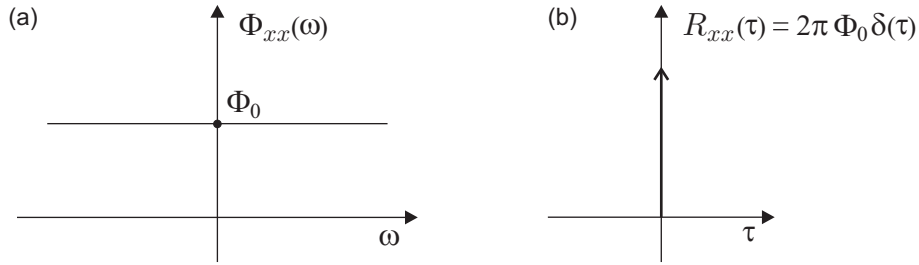


**Fig. 8.3.** White noise process: (a) The PSD is uniform for all frequencies. (b) Auto-correlation function.

#### 8.4 Stationary response of a SISO linear system

Consider the single-input single-output (SISO) linear system of impulse response  $h(t)$  [or equivalently the FRF  $H(\omega)$ ], excited by the random function  $x(t)$ . The response  $y(t)$  of the system is governed by the convolution integral (1.11)

$$y(t) = \int_0^\infty h(t - \tau)x(\tau)d\tau \quad (8.19)$$

It is straightforward to establish that the cross correlation  $R_{yx}(\tau) = E[y(t + \tau)x(t)]$  is given by the convolution integral (Problem 8.2)

$$R_{yx}(\tau) = \int_0^\infty h(\xi)R_{xx}(\tau - \xi)d\xi \quad (8.20)$$

and that the autocorrelation function  $R_{yy}(\tau) = E[y(t + \tau)y(t)]$  is given by the *correlation integral*

$$R_{yy}(\tau) = \int_0^\infty h(\xi)R_{yx}(\tau + \xi)d\xi \quad (8.21)$$

These two formulae are not particularly useful, but taking their Fourier transform, one gets the fundamental input-output relationship in the frequency domain for a SISO system:

$$\Phi_{yx}(\omega) = H(\omega)\Phi_{xx}(\omega) \quad (8.22)$$

$$\Phi_{yy}(\omega) = H^*(\omega)\Phi_{yx}(\omega) = |H(\omega)|^2\Phi_{xx}(\omega) \quad (8.23)$$

Note that  $\Phi_{yx}(\omega)$  and  $H(\omega)$  are complex quantities; they contain amplitude and phase information, while  $\Phi_{xx}(\omega)$  and  $\Phi_{yy}(\omega)$  are positive real quantities and do not contain phase information. Also observe that the

output at one frequency depends only on the input and the FRF of the system at that frequency; there is *no transfer of energy between distinct frequencies*. If the excitation has no energy in some frequency band, the response will not contain energy in the same frequency band.

#### 8.4.1 Random response of a linear oscillator

Consider the linear oscillator subjected to a seismic excitation of acceleration  $\ddot{x}_0$  (Fig. 8.4). The relative response  $y = x - x_0$  is governed by the equation

$$m\ddot{x} + c\dot{x} + ky = 0$$

(the damping and spring restoring forces depend on the relative motion while the inertia force depends on the absolute acceleration); this can be written alternatively

$$m\ddot{y} + c\dot{y} + ky = -m\ddot{x}_0$$

With the classical notations  $\omega_n^2 = k/m$  and  $2\xi\omega_n = c/m$ , it is rewritten

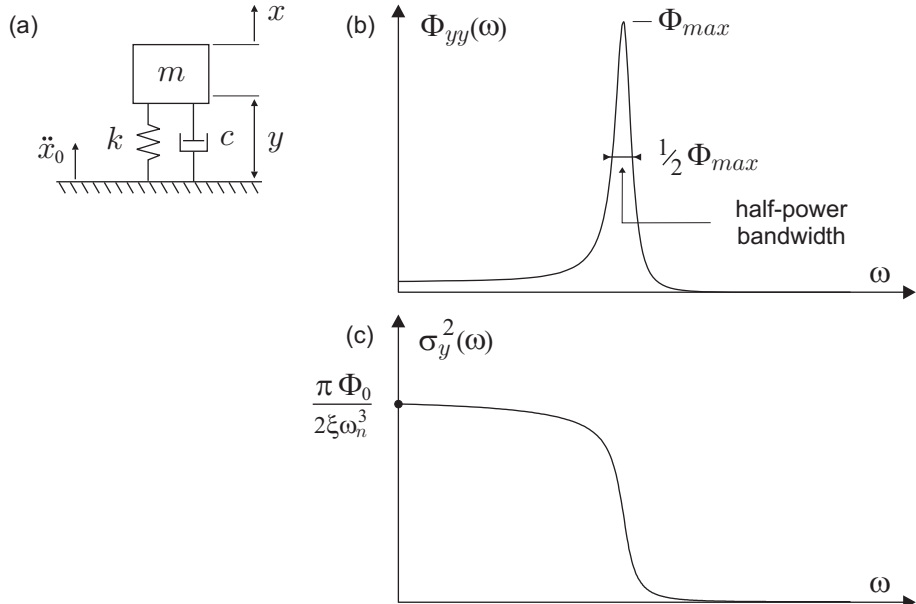


**Fig. 8.4.** (a) Linear oscillator subjected to a seismic excitation of acceleration  $\ddot{x}_0$ . (b) PSD of the relative displacement  $y = x - x_0$ ; the half-power bandwidth is  $2\xi\omega_n$ . (c) Cumulative MS response.

$$\ddot{y} + 2\xi\omega_n\dot{y} + \omega_n^2 y = -\ddot{x}_0 \quad (8.24)$$

Note that the relative displacement is independent of the mass of the system. The FRF between the seismic acceleration and the relative displacement reads

$$H(\omega) = \frac{y}{\ddot{x}_0} = \frac{-1}{(\omega_n^2 - \omega^2) + 2j\xi\omega\omega_n} \quad (8.25)$$

It follows from the previous section that, if the seismic excitation is a white noise  $\Phi_0$ , the PSD of the relative displacement is

$$\Phi_{yy}(\omega) = \Phi_0 |H(\omega)|^2 = \frac{\Phi_0}{(\omega_n^2 - \omega^2)^2 + 4\xi^2\omega^2\omega_n^2} \quad (8.26)$$

It is strongly peaked in the vicinity of the resonance frequency (Fig.8.4.b). The mean square response is given by

$$\sigma^2 = m_0 = R_{yy}(0) = \int_{-\infty}^{\infty} \Phi_{yy}(\omega) d\omega = \frac{\pi\Phi_0}{2\xi\omega_n^3} \quad (8.27)$$

The cumulative MS plot is shown in Fig.8.4.c. The main contribution to the MS response comes from the vicinity of the resonance frequency, in a frequency band equal to the bandwidth of the oscillator  $2\xi\omega_n$  (half power bandwidth).<sup>5</sup> The analytical expression of the cumulative MS response is

$$\sigma_y^2(\omega) = \int_{\omega}^{\infty} \bar{\Phi}_y(\nu) d\nu = \frac{\pi\Phi_0}{2\xi\omega_n^3} [1 - I(\frac{\omega}{\omega_n}, \xi)] \quad (8.28)$$

where

$$\begin{aligned} I(\frac{\omega}{\omega_n}, \xi) &= \frac{1}{\pi} \arctan[\frac{2\xi(\frac{\omega}{\omega_n})}{1 - (\frac{\omega}{\omega_n})^2}] \\ &+ \frac{\xi}{2\pi\sqrt{1 - \xi^2}} \cdot \ln[\frac{1 + (\frac{\omega}{\omega_n})^2 + 2\sqrt{1 - \xi^2}(\frac{\omega}{\omega_n})}{1 + (\frac{\omega}{\omega_n})^2 - 2\sqrt{1 - \xi^2}(\frac{\omega}{\omega_n})}] \end{aligned} \quad (8.29)$$

$I(\frac{\omega}{\omega_n}, \xi)$  is a monotonically increasing function of  $\omega/\omega_n$  with values between 0 and 1 (Fig.8.5); the change in the vicinity of the resonance frequency is faster for lower damping ratios.

---

<sup>5</sup> The *half power bandwidth* is defined as the width of the spectral density diagram when  $\Phi_{yy} = \frac{1}{2}\Phi_{max}$  (Fig.8.4.b).

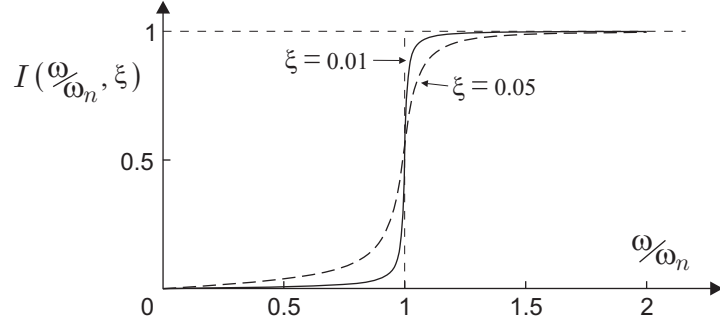


Fig. 8.5.  $I(\frac{\omega}{\omega_n}, \xi)$  for various damping values.

#### 8.4.2 White noise approximation

The fact that most of the contribution to the mean square response comes from the vicinity of the resonance suggests that, in more complex situations where the seismic excitation is not a white noise, but its spectral density  $\Phi_0(\omega_n)$  has significant values and varies smoothly in the vicinity of the resonance  $\omega_n$ , the following approximation may be used:

$$\begin{aligned}\sigma_y^2 = m_0 = R_{yy}(0) &= \int_{-\infty}^{\infty} \Phi_{yy}(\omega) d\omega = \int_{-\infty}^{\infty} \Phi_0(\omega) |H(\omega)|^2 d\omega \\ &\simeq \Phi_0(\omega_n) \int_{-\infty}^{\infty} |H(\omega)|^2 d\omega = \frac{\pi \Phi_0(\omega_n)}{2\xi \omega_n^3}\end{aligned}\quad (8.30)$$

This is the so-called *white noise approximation*; the broadband excitation of PSD  $\Phi_0(\omega)$  is replaced by an equivalent white noise  $\Phi_0(\omega_n)$  with the same spectral density at  $\omega_n$ .

#### 8.4.3 Band limited white noise excitation

Consider the band limited white noise (Fig.8.6)

$$\Phi_0(\omega) = \Phi_0 \quad (\omega_1 \leq |\omega| \leq \omega_2) \quad (8.31)$$

The power spectral density of the oscillator response reads

$$\Phi_{yy}(\omega) = \frac{\Phi_0}{(\omega_n^2 - \omega^2)^2 + 4\xi^2\omega^2\omega_n^2} \quad (\omega_1 \leq |\omega| \leq \omega_2) \quad (8.32)$$

and the variance (MS) is given by

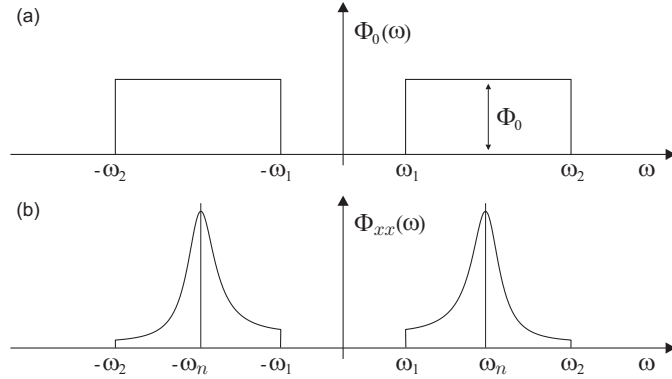


**Fig. 8.6.** (a) Band limited white noise excitation. (b) Oscillator response.

$$\sigma^2 = m_0 = \frac{\pi\Phi_0}{2\xi\omega_n^3} [I\left(\frac{\omega_2}{\omega_n}, \xi\right) - I\left(\frac{\omega_1}{\omega_n}, \xi\right)] \quad (8.33)$$

where  $I\left(\frac{\omega}{\omega_n}, \xi\right)$  is given by (8.29). For the more general case of an oscillator subjected to an arbitrary PSD, a numerical procedure may be developed by decomposing the excitation into a sum of band limited white noise processes on adjacent intervals  $[\omega_i, \omega_{i+1}]$ , and for each of them, the above formula can be used (Problem 8.3).

#### 8.4.4 Kanai-Tajimi spectrum

In earthquake engineering, it is frequently assumed that the ground acceleration at one point can be modelled by the absolute acceleration response of an oscillator excited by a white noise. The natural frequency  $\omega_g$  and the damping ratio  $\xi_g$  are selected to fit the local ground conditions. From Equ.(8.25), the FRF between the seismic excitation and the absolute acceleration is given by

$$H(\omega) = \frac{\ddot{x}}{\ddot{x}_0} = 1 + \frac{\ddot{y}}{\ddot{x}_0} = 1 + \frac{\omega^2}{(\omega_g^2 - \omega^2) + 2j\xi_g\omega\omega_g} = \frac{\omega_g^2 + 2j\xi_g\omega\omega_g}{(\omega_g^2 - \omega^2) + 2j\xi_g\omega\omega_g}$$

leading to the PSD

$$\Phi_g(\omega) = \Phi_0 \frac{1 + 4\xi_g^2(\omega^2/\omega_g^2)}{(1 - \omega^2/\omega_g^2)^2 + 4\xi_g^2(\omega^2/\omega_g^2)} \quad (8.34)$$

### 8.5 Spectral moments, Rice formulae, central frequency

Since the FRF between a process  $x(t)$  and its time derivatives  $\dot{x}(t)$  and  $\ddot{x}(t)$  are respectively  $j\omega$  and  $-\omega^2$ , the PSD of  $\dot{x}(t)$  and  $\ddot{x}(t)$  are given respectively by

$$\Phi_{\dot{x}\dot{x}}(\omega) = \omega^2 \Phi_{xx}(\omega) \quad \Phi_{\ddot{x}\ddot{x}}(\omega) = \omega^4 \Phi_{xx}(\omega) \quad (8.35)$$

The spectral moments of a stationary random process  $x(t)$  are defined by

$$m_0 = \sigma_x^2 = \int_{-\infty}^{\infty} \Phi_{xx}(\omega) d\omega \quad (8.36)$$

$$m_2 = \sigma_{\dot{x}}^2 = \int_{-\infty}^{\infty} \omega^2 \Phi_{xx}(\omega) d\omega \quad (8.37)$$

$$m_4 = \sigma_{\ddot{x}}^2 = \int_{-\infty}^{\infty} \omega^4 \Phi_{xx}(\omega) d\omega \quad (8.38)$$

provided that these integrals exist ( $m_0$  does not exist for a white noise, or  $m_4$  does not exist for the response of an oscillator to a white noise).

For a zero-mean stationary Gaussian process  $x(t)$ , one can show that the average number per unit of time of zero up-crossings (with a positive slope, marked by  $\circ$  in Fig.8.7), called *central frequency*, is given by (*Rice formula*)

$$\nu_0 = \frac{\omega_0}{2\pi} = \frac{1}{2\pi} \left( \frac{m_2}{m_0} \right)^{1/2} = \frac{1}{2\pi} \frac{\sigma_{\dot{x}}}{\sigma_x} \quad (8.39)$$

For the response of a linear oscillator to a white noise,

$$m_0 = \frac{\pi \Phi_0}{2\xi \omega_n^3} \quad m_2 = \frac{\pi \Phi_0}{2\xi \omega_n} \quad (8.40)$$

and the central frequency is identical to the natural frequency of the oscillator:

$$\omega_0 = \omega_n \quad (8.41)$$

Similarly, the zero crossings of the time derivative  $\dot{x}(t)$  correspond to the extrema of the process. The average number of maxima per unit of time is given by

$$\nu_1 = \frac{\omega_1}{2\pi} = \frac{1}{2\pi} \left( \frac{m_4}{m_2} \right)^{1/2} = \frac{1}{2\pi} \frac{\sigma_{\ddot{x}}}{\sigma_{\dot{x}}} \quad (8.42)$$

By continuity, there must be at least one maximum between two zero up-crossings; thus  $\nu_1 \geq \nu_0$  (Fig.8.7); a wide band process has several maxima

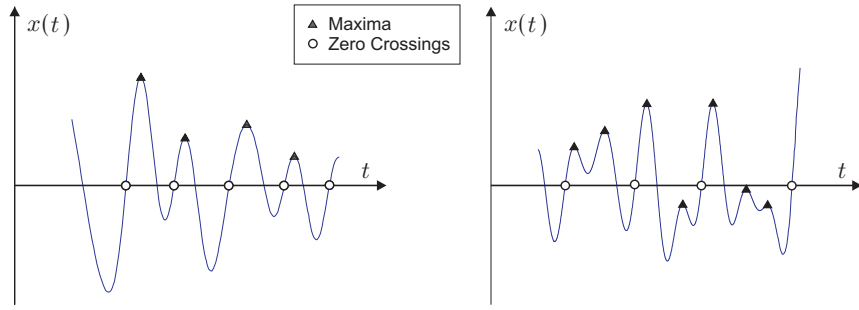


**Fig. 8.7.** Zero crossings and maxima. (a) Narrow band process ( $\nu_1 \simeq \nu_0$ ). (b) Wide band process: there are several maxima between two successive zero crossings ( $\nu_1 \gg \nu_0$ ).

between two successive zero up-crossings ( $\nu_1 \gg \nu_0$ ), while  $\nu_1 \simeq \nu_0$  for a narrow band process.

The ratio

$$0 \leq \left(\frac{\nu_0}{\nu_1}\right)^2 = \frac{m_2^2}{m_0 m_4} \leq 1 \quad (8.43)$$

may be considered as a measure of the bandwidth of the process;<sup>6</sup> it is close to 1 for a narrow band process and decreases as the bandwidth increases.

## 8.6 Envelope of a narrow band process

A narrow band process (Fig.8.8) has its power distribution concentrated in the vicinity of its central frequency. A sample of such a process behaves like an harmonic function with slowly varying amplitude and frequency; the envelope (Fig.8.8.b) may be considered as a slowly varying curve connecting the extrema of the process. A formal definition can be obtained by considering the process in the phase plane ( $x, \dot{x}/\omega_0$ ) (Fig.8.8.c), where the image point of an harmonic motion moves clockwise along a circle at constant angular velocity  $\omega_0$ ; the radius of this circle is the amplitude of the harmonic function. Similarly, the image point of a sample of a narrow band process consists of a smooth curve rotating clockwise at a frequency varying slowly about the central frequency  $\omega_0$ ; the distance to the origin of the image point also varies slowly, and passes through the extrema each time the image point crosses the  $x$  axis. The envelope  $a(t)$  of a narrow band process may be defined as the radius of the image point of the

<sup>6</sup>  $m_4$  is often difficult to compute in practice, but  $\nu_1$  and  $\nu_0$  can easily be estimated from a sample record, by counting the maxima and the zero up-crossings.

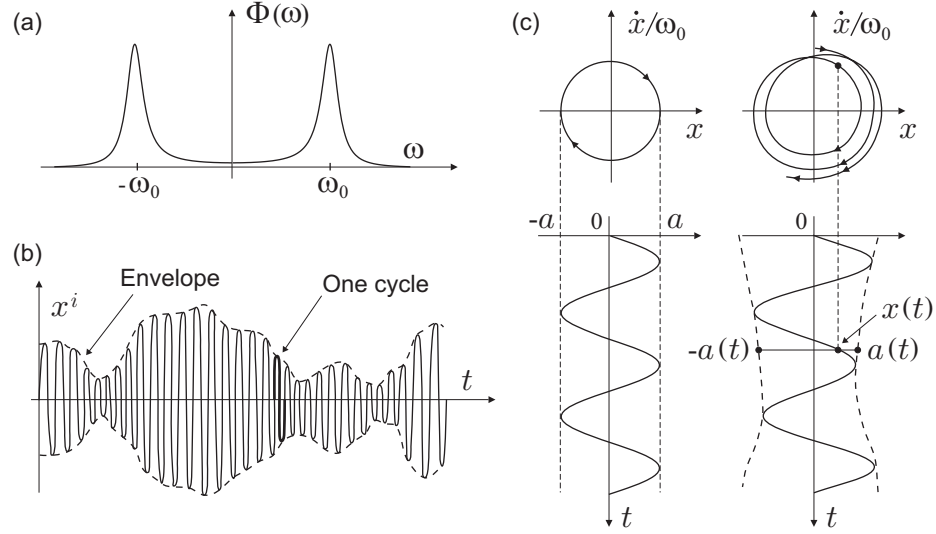


**Fig. 8.8.** Definition of the envelope of a narrow band process. (a) Power spectral density. (b) Typical sample. (c) Trajectory in the phase plane of an harmonic function (left) and of a narrow band process (right).

process in the phase plane (Crandall & Mark):

$$a^2(t) = x^2(t) + \frac{\dot{x}^2(t)}{\omega_0^2} \quad (8.44)$$

If the process  $x(t)$  is Gaussian of zero mean, it follows from (8.11) that  $x(t)$  and  $\dot{x}(t)$  are independent (at the same instant  $t$ ) and that the joint distribution of  $x(t)$  and  $\dot{x}(t)$  reads

$$p_{x\dot{x}}(x, t; \dot{x}, t) = \frac{1}{2\pi\sigma_x\sigma_{\dot{x}}} \exp\left[-\frac{1}{2}\left(\frac{x^2}{\sigma_x^2} + \frac{\dot{x}^2}{\sigma_{\dot{x}}^2}\right)\right] \quad (8.45)$$

with  $\sigma_{\dot{x}} = \omega_0\sigma_x$ . One can show (Problem 8.5) that the probability distribution of the envelope  $a(t)$  defined by (8.44) is the *Rayleigh distribution*

$$p_a(a) = \frac{a}{\sigma_x^2} \exp\left(-\frac{a^2}{2\sigma_x^2}\right) \quad (a > 0) \quad (8.46)$$

It is represented in Fig. 8.9. The MS value of the envelope is

$$E[a^2] = \int_0^\infty a^2 p_a(a) da = 2\sigma_x^2$$

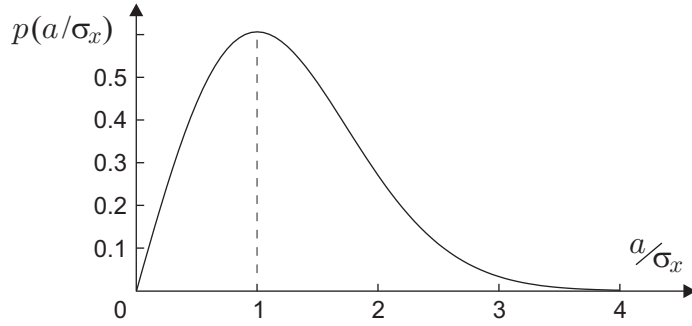


Fig. 8.9. Rayleigh distribution of the envelope  $a(t)$ .

## 8.7 FRF estimation and coherence function

Consider a linear time-invariant SISO system. The input output relationships in the frequency domain are

$$\Phi_{yx}(\omega) = H(\omega) \Phi_{xx}(\omega) \quad (8.47)$$

$$\Phi_{yy}(\omega) = H^*(\omega) \Phi_{yx}(\omega) = H(\omega) \Phi_{xy}(\omega) = |H(\omega)|^2 \Phi_{xx}(\omega) \quad (8.48)$$

The cross PSD  $\Phi_{yx}(\omega)$  is a complex quantity while the PSD  $\Phi_{xx}(\omega)$  and  $\Phi_{yy}(\omega)$  are real functions. These formulae provide the following estimates of the FRF from measured input and output PSDs (section 8.3.1):

$$H_1(\omega) = \frac{\Phi_{yx}(\omega)}{\Phi_{xx}(\omega)} \quad (8.49)$$

$$H_2(\omega) = \frac{\Phi_{yy}(\omega)}{\Phi_{xy}(\omega)} \quad (8.50)$$

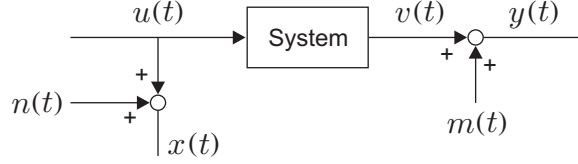
If the system is perfectly linear and the measurements are not contaminated by noise, these estimators provide identical results and the *coherence function*, defined by

$$0 \leq \gamma_{xy}^2 = \frac{|\Phi_{xy}(\omega)|^2}{\Phi_{xx}(\omega) \Phi_{yy}(\omega)} \leq 1 \quad (8.51)$$

would be equal to

$$\gamma_{xy}^2 = \frac{H_1(\omega)}{H_2(\omega)} = 1$$

In practice, however, the measured signals  $x(t)$  and  $y(t)$  differ from the actual ones  $u(t)$  and  $v(t)$

**Fig. 8.10.** SISO system with measurement noise.

$$x(t) = u(t) + n(t)$$

$$y(t) = v(t) + m(t) \quad (8.52)$$

where  $n(t)$  is the input noise and  $m(t)$  is the output noise (Fig.8.10). If one assumes that they are statistically independent of each other and independent of  $u(t)$  and  $v(t)$ ,

$$\Phi_{un}(\omega) = \Phi_{vn}(\omega) = \Phi_{nm}(\omega) = 0$$

It follows that

$$\Phi_{xx}(\omega) = \Phi_{uu}(\omega) + \Phi_{nn}(\omega)$$

$$\Phi_{yy}(\omega) = \Phi_{vv}(\omega) + \Phi_{mm}(\omega)$$

$$\Phi_{xy}(\omega) = \Phi_{uv}(\omega)$$

This leads to

$$H_1(\omega) = \frac{\Phi_{vu}(\omega)}{\Phi_{uu}(\omega) + \Phi_{nn}(\omega)} \quad (8.53)$$

$$H_2(\omega) = \frac{\Phi_{vv}(\omega) + \Phi_{mm}(\omega)}{\Phi_{uv}(\omega)} \quad (8.54)$$

$$\gamma_{xy}^2 = \frac{|\Phi_{xy}(\omega)|^2}{\Phi_{xx}(\omega)\Phi_{yy}(\omega)} = \frac{|\Phi_{uv}(\omega)|^2}{[\Phi_{uu}(\omega) + \Phi_{nn}(\omega)][\Phi_{vv}(\omega) + \Phi_{mm}(\omega)]} \leq \gamma_{uv}^2 \quad (8.55)$$

Thus,  $H_2$  is insensitive to an uncorrelated noise at the input while  $H_1$  is insensitive to an uncorrelated noise at the output and, as a result, is unbiased in the case of multiple uncorrelated inputs which appear as an output noise. In practice, the input PSD  $\Phi_{uu}(\omega)$  is controllable to a large extent, while  $\Phi_{vv}(\omega)$  depends on the system to identify. As a result, the estimator  $H_1$  is often superior to  $H_2$ , except in the vicinity of the resonances, where the power level of the excitation drops to a lower value, increasing the noise to signal ratio  $\Phi_{nn}(\omega)/\Phi_{uu}(\omega)$ . Similarly,  $H_1$  will be preferred in the vicinity of the anti-resonance where the response level becomes very small, increasing the noise to signal ratio  $\Phi_{mm}(\omega)/\Phi_{vv}(\omega)$ .

Because of this, the coherence function  $\gamma_{xy}^2$  is usually significantly lower than 1 near the resonances and the anti-resonances of the FRF, even for good testing conditions and if the structure behaves linearly.

For the linear system of Fig.8.10, since  $\Phi_{uy}(\omega) = \Phi_{uv}(\omega) = H(\omega)\Phi_{uu}(\omega)$ , the coherence function between the actual input  $u$  and the measured output  $y$  may be written

$$\gamma_{uy}^2(\omega) = \frac{|H(\omega)|^2\Phi_{uu}(\omega)}{|H(\omega)|^2\Phi_{uu}(\omega) + \Phi_{mm}(\omega)} \quad (8.56)$$

where the uncorrelated noise  $m(t)$  includes the system nonlinearities, the other sources of excitation as well as the output measurement noise. This formula states that, *for every frequency  $\omega$ , the coherence function  $\gamma_{uy}^2$  represents the fraction of the output PSD resulting from the input*. Any system nonlinearity, unwanted source of excitation or measurement noise will contribute to reducing the coherence function which can be regarded as a measure of the *causality* between the input and the output of the system. The signal to noise ratio is given by

$$\frac{\text{Signal}}{\text{Noise}} = \frac{|H(\omega)|^2\Phi_{uu}(\omega)}{\Phi_{mm}(\omega)} = \frac{\gamma_{uy}^2(\omega)}{1 - \gamma_{uy}^2(\omega)} \quad (8.57)$$

## 8.8 Random response of MIMO systems

In the time domain, the input output relationship of a linear MIMO system is

$$\mathbf{x}(t) = \int_{-\infty}^{\infty} h(t - \tau) \mathbf{f}(\tau) d\tau \quad (8.58)$$

where  $h(t)$  is the impulse response matrix.  $h_{kl}(t)$  is the time response of the d.o.f.  $k$  to a unit impulse applied to d.o.f.  $l$ . In the frequency domain, the relationship is

$$\mathbf{X}(\omega) = H(\omega)\mathbf{F}(\omega) \quad (8.59)$$

where  $H(\omega)$  is the FRF matrix.  $H_{kl}(\omega)$  gives the complex amplitude of the harmonic response of d.o.f.  $k$  to an harmonic excitation of unit amplitude  $e^{j\omega t}$  at d.o.f.  $l$ .  $H_{kl}(\omega)$  is the Fourier transform of  $h_{kl}(t)$ . These relations are general and apply to any linear system; in the particular case of a linear structure, the FRF  $H(\omega)$  is the dynamic flexibility matrix, given by (2.27) or (2.28). The stationary random excitation may be defined by the correlation matrix

$$R_f(\tau) = E[\mathbf{f}(t + \tau)\mathbf{f}^T(t)] \quad (8.60)$$

which satisfies  $R_f(\tau) = R_f^T(-\tau)$ , or the PSD matrix

$$\Phi_f(\omega) = \frac{1}{2\pi} \int_{-\infty}^{\infty} R_f(\tau) e^{-j\omega\tau} d\tau \quad (8.61)$$

which is Hermitian,  $\Phi_{lk}(\omega) = \Phi_{kl}^*(\omega)$ . The input output relationship between the stationary excitation and the stationary response is given by

$$\Phi_x(\omega) = H(\omega)\Phi_f(\omega)H^*(\omega) \quad (8.62)$$

where  $H^*(\omega)$  is the conjugate transpose (Hermitian) of  $H(\omega)$ . This relation is very general, with the only restriction that the system must be *linear*. For a SISO system, it becomes (8.23). Equation (8.62) is formally very simple, but the physical meaning of  $R_f(\tau)$  and  $\Phi_f(\omega)$  is not at all simple and will be discussed below. Before this, however, let us particularize to the structural response in modal coordinate.

### 8.8.1 Response in modal coordinates

Rather than using directly the dynamic flexibility matrix, it is convenient to compute the response in several steps:

- Compute the modal excitation PSD matrix: The vector of modal excitation is given by  $\mathbf{p} = \Psi^T \mathbf{f}$  where  $\Psi = (\phi_1, \dots, \phi_i, \dots, \phi_m)$  is the matrix of the mode shapes.<sup>7</sup> Note that, in most applications, the physical excitation process is low pass (e.g. an earthquake accelerogram does not have energy content above 30 Hz). As a result, only a few modes contribute significantly to the global response and the size of the vector  $\mathbf{p}$  is usually much smaller than the size of  $\phi_i$ . It follows from the previous equation that

$$\Phi_p(\omega) = \Psi^T \Phi_f(\omega) \Psi \quad (8.63)$$

- Compute the PSD of modal response: From Equ.(2.23), the FRF between the modal excitation and the modal response is

$$\mathbf{z} = \text{diag}\left\{\frac{1}{\mu_i(\omega_i^2 - \omega^2 + 2j\xi_i\omega_i\omega)}\right\} \mathbf{p} = H_m(\omega) \mathbf{p} \quad (8.64)$$

It follows that

$$\Phi_z(\omega) = H_m(\omega)\Phi_p(\omega)H_m^*(\omega) \quad (8.65)$$

---

<sup>7</sup> the notation  $\Psi$  is used instead of the more traditional  $\Phi$ , because  $\Phi$  is used for the power spectral densities, also according to tradition.

- Finally, if the response quantity (a displacement or a stress component) is a linear function of the modal amplitudes,  $r = \mathbf{b}^T \mathbf{z}$ , the PSD of the response is

$$\Phi_r(\omega) = \mathbf{b}^T \Phi_z(\omega) \mathbf{b} \quad (8.66)$$

Both  $\Phi_p(\omega)$  and  $\Phi_z(\omega)$  are Hermitian, of size  $m$ , the number of modes retained in the analysis. The procedure is computationally simple, once  $\Phi_f(\omega)$  has been properly defined.

The situation is slightly more complex to calculate the support reaction produced by a seismic excitation. From Equ.(7.24),

$$f_0 = m_T \ddot{x}_0 - \boldsymbol{\Gamma}^T \ddot{\mathbf{z}} \quad (8.67)$$

where  $\mathbf{z}$  is governed by Equ.(7.21):

$$\mu_i \ddot{z}_i + 2\xi_i \mu_i \omega_i \dot{z}_i + \mu_i \omega_i^2 z_i = \Gamma_i \ddot{x}_0$$

or, with the notation of Equ.(8.64),

$$\mathbf{z} = H_m(\omega) \boldsymbol{\Gamma} \ddot{x}_0 \quad (8.68)$$

Substituting into (8.67), one gets the transmissibility between the support acceleration and the support reaction

$$f_0 = [m_T + \omega^2 \boldsymbol{\Gamma}^T H_m(\omega) \boldsymbol{\Gamma}] \ddot{x}_0 = H_{f_0}(\omega) \ddot{x}_0 \quad (8.69)$$

which is a scalar function in the case of a single axis excitation (recall that the modal expansion may be truncated to a small number  $m$  of modes without any error on the static mass). From (8.23),

$$\Phi_{f_0}(\omega) = |H_{f_0}(\omega)|^2 \Phi_{\ddot{x}_0}(\omega) \quad (8.70)$$

### 8.8.2 Correlation and PSD matrices

The correlation matrix  $R_f(\tau)$  and the PSD matrix  $\Phi_f(\omega)$

$$R_f(\tau) = \begin{bmatrix} R_{11}(\tau) & R_{12}(\tau) & \cdots \\ R_{21}(\tau) & R_{22}(\tau) & \cdots \\ R_{31}(\tau) & \cdots & \cdots \end{bmatrix} \quad \Phi_f(\omega) = \begin{bmatrix} \Phi_{11}(\omega) & \Phi_{12}(\omega) & \cdots \\ \Phi_{21}(\omega) & \Phi_{22}(\omega) & \cdots \\ \Phi_{31}(\omega) & \cdots & \cdots \end{bmatrix} \quad (8.71)$$

define the spatial and temporal structure of the random excitation vector  $\mathbf{f}$  (Fig.8.11). The correlation matrix is such that  $R_{ij}(\tau) = R_{ji}(-\tau)$  and

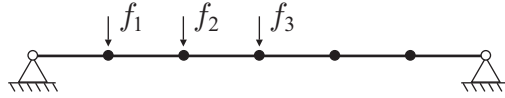


**Fig. 8.11.** Structure with multiple excitations.

the PSD matrix satisfies  $\Phi_{ij}(\omega) = \Phi_{ji}^*(\omega)$ . The diagonal terms define the excitation at one point and the off-diagonal terms describes the statistical relationship between the excitations at neighboring points. Consider the two extreme cases: (i) If the components  $f_i$  are uncorrelated (or equivalently independent if the process is Gaussian), both  $R_f(\tau)$  and  $\Phi_f(\omega)$  are diagonal, all off-diagonal terms being 0. (ii) If the components  $f_i$  are all identical, as for example in the case of a uniform pressure in a regular mesh, all the components of  $R_f(\tau)$  and  $\Phi_f(\omega)$  are identical. In more general situations, the correlation between the components  $f_i$  tends to decrease with the distance.

The physical excitation process is often a continuous pressure field  $p(x, y, z, t)$  and the discretized excitation vector is constructed by lumping the excitation at a regular mesh (Fig. 8.12) which forms a subset of the structural nodes used in the discretization.<sup>8</sup> This assumes that the pressure is uniform and fully correlated over one element of the excitation mesh; this procedure produces a good approximation provided that the size  $\delta$  of the excitation mesh is small compared to (i) the wavelength of the modes contributing significantly to the response and (ii) the correlation length of the excitation process (i.e. the distance over which the correlation drops significantly). These two conditions should guarantee a good representation of the modal excitation (8.63).

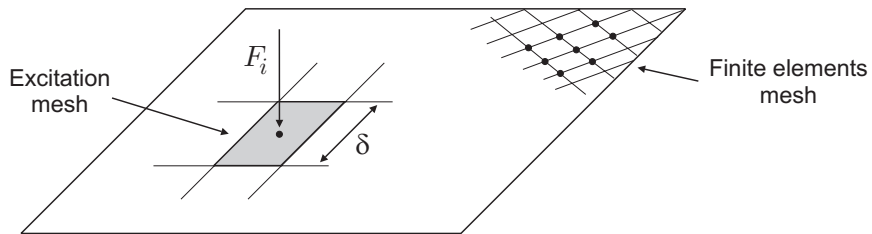


**Fig. 8.12.** Regular excitation mesh and finite element mesh. The size  $\delta$  of the excitation mesh should be small compared to (i) the wavelength of the modes contributing significantly to the response and (ii) the correlation length of the excitation process.

<sup>8</sup> The finite element mesh is usually governed by a good representation of the stiffness of the structure.

The statistics of a random pressure field are described by the correlation function  $R_p(\mathbf{x}_1, \mathbf{x}_2, \tau)$ , or alternatively by the PSD function  $\Phi_p(\mathbf{x}_1, \mathbf{x}_2, \omega)$ , where  $\mathbf{x}_1$  and  $\mathbf{x}_2$  refer to two points in space [ $R_p$  and  $\Phi_p$  are related by Equ.(8.6)]. If the pressure field is *homogeneous*, they depend only on the separation between the two points,  $\mathbf{x}_1 - \mathbf{x}_2$ , and the PSD function may be written

$$\Phi_p(\mathbf{x}_1 - \mathbf{x}_2, \omega) = \Phi_p(\omega) \cdot \mathcal{C}(\mathbf{x}_1 - \mathbf{x}_2, \omega) \quad (8.72)$$

where  $\Phi_p(\omega)$  describes the pressure distribution at one point and the *co-spectrum*  $\mathcal{C}(\mathbf{x}_1 - \mathbf{x}_2, \omega)$  describes the spatial coherence between the pressure excitation at two points located  $\mathbf{x}_1 - \mathbf{x}_2$  apart.

In many physical phenomena such as turbulent flows, the pressure fluctuations are due to the transport of eddies in the flow and the PSD is a decreasing function of the ratio

$$\frac{|\mathbf{x}_1 - \mathbf{x}_2|}{\lambda}$$

where  $\lambda$  is the characteristic size of the eddies. If the flow velocity is  $U_c$ , the typical period of a disturbance associated with an eddy of size  $\lambda$  is  $\lambda/U_c$  (time necessary for the eddy to pass at one point); the pressure fluctuation will therefore be felt at the frequency  $\omega \sim U_c/\lambda$ . Combining with the previous relationship, one finds that the dependency with respect to the space and frequency should take the form

$$\frac{|\mathbf{x}_1 - \mathbf{x}_2| \cdot \omega}{U_c} \quad (8.73)$$

which is the *Strouhal number*; this non-dimensional number appears in most unsteady fluid dynamics problems.

### 8.8.3 Boundary layer noise

The correlation function of the pressure field in a boundary layer flow has the form

$$R(x, y, \tau) = R_0(\tau - x/U_c) e^{-\alpha_1|x|} e^{-\alpha_2|y|} \quad (8.74)$$

where  $R_0(\tau)$  is the autocorrelation function at one point,  $U_c$  is the flow velocity, assumed along the coordinate  $x$ , and  $x$  and  $y$  are the distances between the points, respectively in the streamwise and the transverse directions. The two exponential functions account for the reduction of the

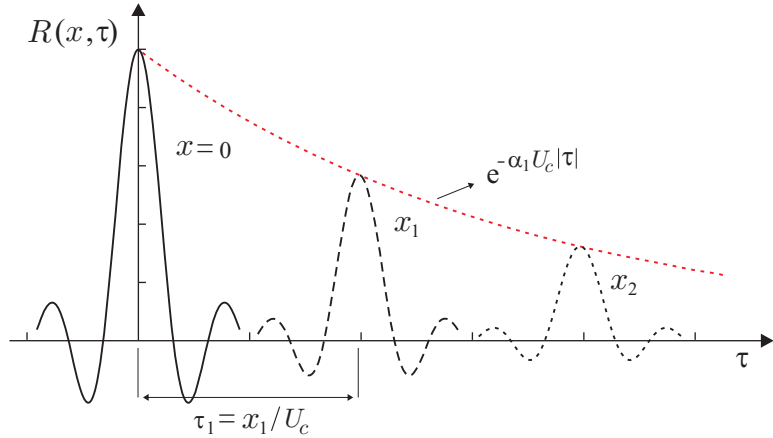


**Fig. 8.13.** Boundary layer noise: cross correlation functions for various streamwise distances  $x_i$ ; the maximum takes place after a delay  $\tau_i = x_i/U_c$  and its magnitude is attenuated as  $e^{-\alpha_1|x_i|}$ .

spatial correlation with the separation between the points in the boundary layer; the argument  $\tau - x/U_c$  accounts for the fact that the cross correlation between two points separated by  $x$  in the flow direction is maximum after a time  $x/U_c$  (Fig. 8.13), which corresponds to the time necessary to transport the disturbance downstream over the distance  $x$  with the convection velocity  $U_c$ . It follows that

$$\Phi(x, y, \omega) = \Phi_0 \cdot \mathcal{C}(x, y, \omega) = \Phi_0(\omega) \exp\left(-\frac{j\omega x}{U_c}\right) e^{-\alpha_1|x|} e^{-\alpha_2|y|} \quad (8.75)$$

where  $\Phi_0(\omega)$  is the PSD of the pressure field at any point (which can be measured easily with a microphone), and the complex exponential arises from the translation theorem of the Fourier transform. The foregoing form of the co-spectrum is a nice generic form which can fit many situations, such as acoustic fatigue of panels; it has only three free parameters,  $U_c$ ,  $\alpha_1$  and  $\alpha_2$  which can be determined experimentally relatively easily.

#### 8.8.4 Wind response of a tall building

The flow around a massive structure is very complicated; however, it is a common practice to evaluate the along-wind response by assuming that the drag forces can be expressed in terms of the unperturbed flow. The drag force at a node reads

$$f_j(t) = \frac{1}{2} \rho A_j C_D u_j^2(t) \quad (8.76)$$

where  $\varrho$  is the air density,  $A_j$  is the tributary area associated with the node  $j$ ,  $C_D$  is the drag coefficient and  $u_j(t)$  is the *unperturbed* wind velocity at the altitude of the node  $j$ . Since the turbulent component of the wind velocity is small compared to the mean wind  $\bar{u}_j$ , one can write

$$u_j(t) = \bar{u}_j[1 + \varepsilon_j(t)] \quad (8.77)$$

where  $\varepsilon_j(t)$  is the non-dimensional turbulent velocity, assumed to be a zero-mean Gaussian process and such that  $|\varepsilon_j(t)| \ll 1$ . It follows that the drag force acting at node  $j$  can be *linearized*:<sup>9</sup>

$$f_j(t) \simeq \frac{1}{2} \varrho A_j C_D \bar{u}_j^2 [1 + 2\varepsilon_j(t)] \quad (8.78)$$

The first term is the static loading of the mean wind; it is constant and can be treated separately. The fluctuating part of the response is excited by a zero-mean Gaussian random field of drag forces of PSD function

$$\Phi_{f_i f_j}(\omega) = 4\nu_i \nu_j \Phi_{\varepsilon_i \varepsilon_j}(\omega) \quad (8.79)$$

where

$$\nu_j = \frac{1}{2} \varrho A_j C_D \bar{u}_j^2 \quad (8.80)$$

is the static drag force associated to node  $j$ .

The direction of the mean wind does not change significantly with the altitude, but the velocity profile in the boundary layer depends on the ground roughness. Above the *gradient height*  $z_g$  the velocity is constant and equal to the *gradient velocity*  $u_g$ , and below  $z_g$ , the wind profile can be represented by the power law

$$\bar{u}_j = u_g \left( \frac{z_i}{z_g} \right)^\alpha \quad (8.81)$$

where  $z_g$  and  $\alpha$  are constant parameters depending on the terrain conditions (the following values are typical: city:  $z_g \simeq 500$  m,  $\alpha \simeq 0.4$ ; seaside:  $z_g \simeq 250$  m,  $\alpha \simeq 0.16$ ).

The turbulent velocity at one point may be represented by the following PSD, known as *Davenport's spectrum*:

$$\Phi_{uu}(\omega) = \frac{2\kappa u_{10}^2}{|\omega|} \frac{\left( \frac{600\omega}{\pi u_{10}} \right)^2}{[1 + (\frac{600\omega}{\pi u_{10}})^2]^{4/3}} \quad (8.82)$$

---

<sup>9</sup> Neglecting the term in  $\varepsilon_j^2$  is justified in wind engineering and the drag forces are also Gaussian. Such an approximation is no longer acceptable in the analysis of off-shore structures under wave excitation.

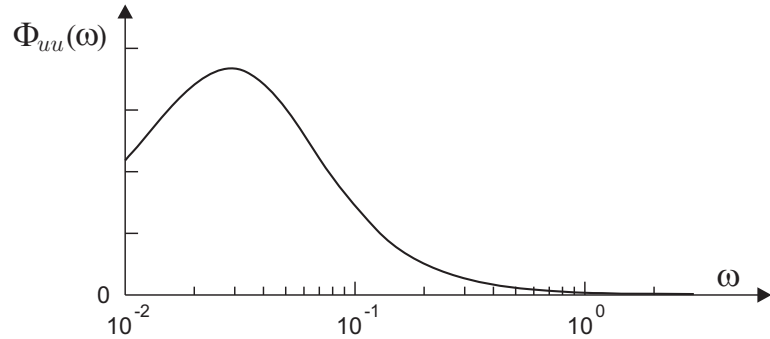


**Fig. 8.14.** Davenport's spectrum for the turbulent wind velocity (amplitudes in linear scale). The first natural frequency of all existing tall buildings is in the tail of the spectrum.

where  $\kappa$  is a constant depending on the terrain roughness and  $u_{10}$  is the mean wind reference velocity at 10 m above the ground. The shape of this PSD is shown in Fig. 8.14; the first natural frequency of all existing tall buildings is in the tail of the spectrum.<sup>10</sup> The cross PSD of the reduced turbulent velocity  $\varepsilon(t, z)$  at two points at heights  $z_i$  and  $z_j$  is

$$\Phi_{\varepsilon_i \varepsilon_j}(z_i, z_j, \omega) = \frac{2\kappa u_{10}^2}{\bar{u}_i \bar{u}_j |\omega|} \frac{\left(\frac{600\omega}{\pi u_{10}}\right)^2}{[1 + (\frac{600\omega}{\pi u_{10}})^2]^{4/3}} e^{-\frac{|\omega|}{2\pi u_{10}} C |z_i - z_j|} \quad (8.83)$$

where  $C$  is a correlation constant,  $C \approx 7$ .

### 8.8.5 Vehicle moving on a rough road

The road profile  $w(x)$  may be regarded as a process with exponential correlation,  $R_{ww}(x) = \sigma^2 e^{-a|x|}$ , where  $\sigma^2$  is the MS value and  $a$  is a parameter describing the road roughness (Fig. 8.15). If the car is moving at the speed  $v$ , the road profile  $w(t)$  seen by a wheel in a frame attached to the car is a function of time which is obtained by the change of variables  $v\tau = x$ ; the autocorrelation function of  $w(t)$  is:

$$R_{ww}(\tau) = \sigma^2 e^{-av|\tau|} \quad (8.84)$$

The corresponding PSD is

$$\Phi_{ww}(\omega) = \frac{\sigma^2}{\pi} \frac{av}{\omega^2 + a^2 v^2} \quad (8.85)$$

---

<sup>10</sup> e.g. see (7.71).

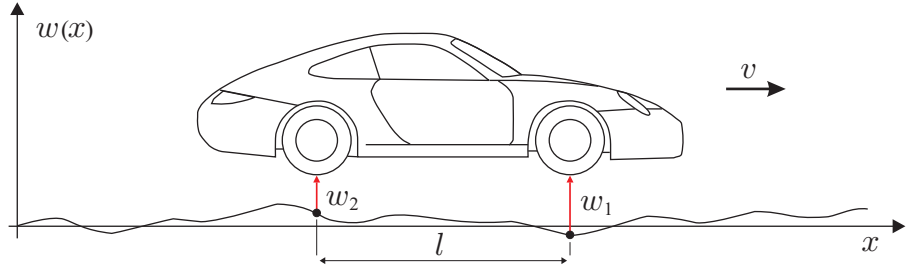


**Fig. 8.15.** Car moving on a rough road of profile  $w(x)$ . The rear wheels are at a distance  $l$  from the front wheel, corresponding to a delay  $\Delta = l/v$ .

If the rear wheel is at a distance  $l$  from the front wheel, it perceives the same road profile with a delay  $\Delta = l/v$ ,  $w_2(t) = w_1(t - l/v)$ . The correlation matrix may be constructed as follows:

$$R_w(\tau) = \begin{bmatrix} E[w_1(t + \tau)w_1(t)] & E[w_1(t + \tau)w_2(t)] \\ E[w_2(t + \tau)w_1(t)] & E[w_2(t + \tau)w_2(t)] \end{bmatrix}$$

Upon substituting  $w_2$ ,

$$R_w(\tau) = \begin{bmatrix} R_{ww}(\tau) & R_{ww}(\tau + l/v) \\ R_{ww}(\tau - l/v) & R_{ww}(\tau) \end{bmatrix} \quad (8.86)$$

Using the translation theorem of the Fourier transform, one gets the corresponding PSD matrix:

$$\Phi_w(\omega) = \frac{\sigma^2}{\pi} \frac{av}{\omega^2 + a^2v^2} \begin{bmatrix} 1 & e^{j\omega l/v} \\ e^{-j\omega l/v} & 1 \end{bmatrix} \quad (8.87)$$

## 8.9 Mean square response

We have seen earlier in the previous section that the PSD of the response quantity is

$$\Phi_r(\omega) = \mathbf{b}^T \Phi_z(\omega) \mathbf{b} = \sum_{i,j} b_i b_j \Phi_{ij}(\omega)$$

The MS value is

$$\sigma_r^2 = \int_{-\infty}^{\infty} \Phi_r(\omega) d\omega = \sum_i b_i^2 \beta_{ii} + \sum_i \sum_{j \neq i} b_i b_j \beta_{ij} \quad (8.88)$$

where the double sum has been partitioned into the diagonal and non-diagonal components and

$$\beta_{ii} = \int_{-\infty}^{\infty} \Phi_{ii}(\omega) d\omega \quad \beta_{ij} = \int_{-\infty}^{\infty} \Phi_{ij}(\omega) d\omega \quad (8.89)$$

$\beta_{ii}$  is called the *modal autocorrelation* and  $\beta_{ij}$  the *modal cross-correlation*. An interesting practical question is the following: under what condition may we neglect the contribution of the cross-correlations in front of that of the autocorrelations? If it may be done, the global MS response can be computed simply by adding up the MS responses of the various modes, without taking into account their correlation; this is the so-called “SRSS” rule (*square root of the sum of the squares*) which is frequently used in practice.<sup>11</sup> It turns out that this assumption is justified provided that the spacing between the natural frequencies is large, compared with the bandwidth of the modal response,

$$\frac{|\omega_i - \omega_j|}{\omega_i + \omega_j} \gg \xi_i \quad (8.90)$$

Before illustrating this with an example, consider the *mass-averaged mean square displacement* in the structure,

$$E[\mathbf{x}^T M \mathbf{x}] = \sum_{i,j} M_{ij} E[x_i x_j]$$

Changing into modal coordinates,  $\mathbf{x} = \Psi \mathbf{z}$ , where  $\Psi = (\phi_1, \dots, \phi_m)$  is the matrix of the mode shapes, one finds

$$E[\mathbf{x}^T M \mathbf{x}] = E[\mathbf{z}^T \Psi^T M \Psi \mathbf{z}] = \sum_i \mu_i E[z_i^2] \quad (8.91)$$

after using the orthogonality condition of the mode shapes,  $\phi_i^T M \phi_k = \mu_i \delta_{ik}$ . Thus, all the cross-correlations have disappeared. This result indicates that the cross-correlations contribute to the local variations of the mean square response, but not to the mass-averaged response over the entire structure. The following example illustrates this.

### 8.9.1 Role of the cross-correlations

Consider the system of Fig.8.16 (Elishakoff, 1982). It consists of two identical oscillators connected by a variable spring and damper. A white noise

---

<sup>11</sup> particularly in “back-of-an-envelope” calculations, because the global response is treated as the sum of independent responses of linear oscillators.

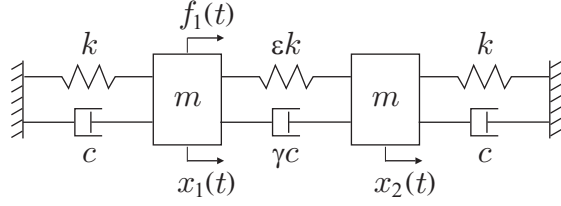


**Fig. 8.16.** Two identical oscillators connected by a variable spring and damper (this system degenerates into two independent oscillators as \$\varepsilon, \gamma \rightarrow 0\$).

force  $f_1$  of PSD  $\Phi_0$  is applied to the oscillator  $x_1$ . The mass, stiffness and damping matrices are

$$M = m \begin{bmatrix} 1 & 0 \\ 0 & 1 \end{bmatrix} \quad K = k \begin{bmatrix} 1 + \varepsilon & -\varepsilon \\ -\varepsilon & 1 + \varepsilon \end{bmatrix} \quad C = c \begin{bmatrix} 1 + \gamma & -\gamma \\ -\gamma & 1 + \gamma \end{bmatrix}$$

The natural frequencies are

$$\omega_1 = \left(\frac{k}{m}\right)^{1/2} \quad \omega_2 = \left(\frac{k}{m}\right)^{1/2} \cdot (1 + 2\varepsilon)^{1/2} \quad (8.92)$$

The corresponding mode shapes (normalized to  $\mu_i = 1$ ) are

$$\Psi = \frac{1}{\sqrt{2m}} \begin{bmatrix} 1 & 1 \\ 1 & -1 \end{bmatrix}$$

and the modal damping ratios

$$\xi_1 = \frac{c}{2\sqrt{km}} \quad \xi_2 = \frac{c}{2\sqrt{km}} \frac{1 + 2\gamma}{\sqrt{1 + 2\varepsilon}}$$

We will assume that  $1 + 2\gamma = \sqrt{1 + 2\varepsilon}$ , so that  $\xi_1 = \xi_2 = \xi$ . The parameter  $\varepsilon$  controls the spacing between the two modes.

According to the procedure described above,

$$\Phi_f = \Phi_0 \begin{bmatrix} 1 & 0 \\ 0 & 0 \end{bmatrix} \quad \Phi_p = \Psi^T \Phi_f(\omega) \Psi = \frac{\Phi_0}{2m} \begin{bmatrix} 1 & 1 \\ 1 & 1 \end{bmatrix}$$

and the PSD of the displacements  $x_1$  and  $x_2$  are respectively

$$\Phi_{11}(\omega) = \frac{\Phi_0}{4m^2} \{ |H_1(\omega)|^2 + |H_2(\omega)|^2 + 2Re[H_1(\omega)H_2^*(\omega)] \}$$

$$\Phi_{22}(\omega) = \frac{\Phi_0}{4m^2} \{ |H_1(\omega)|^2 + |H_2(\omega)|^2 - 2Re[H_1(\omega)H_2^*(\omega)] \}$$

where the identity  $H_1(\omega)H_2^*(\omega) + H_1^*(\omega)H_2(\omega) = 2Re[H_1(\omega)H_2^*(\omega)]$  has been used. After some calculations, the MS displacements read

$$E[x_1^2] = \frac{\pi\Phi_0}{4m^2} \left\{ \frac{1}{2\xi\omega_1^3} + \frac{1}{2\xi\omega_2^3} + \frac{8\xi}{(\omega_1 + \omega_2)[(\omega_1 - \omega_2)^2 + 4\xi^2\omega_1\omega_2]} \right\} \quad (8.93)$$

$$E[x_2^2] = \frac{\pi\Phi_0}{4m^2} \left\{ \frac{1}{2\xi\omega_1^3} + \frac{1}{2\xi\omega_2^3} - \frac{8\xi}{(\omega_1 + \omega_2)[(\omega_1 - \omega_2)^2 + 4\xi^2\omega_1\omega_2]} \right\} \quad (8.94)$$

In these expressions, the first two terms represent the autocorrelations  $\beta_{ii}$  and the third one is the contribution of the cross-correlations  $\beta_{ij}$ . They contribute identically to the MS responses of  $x_1$  and  $x_2$ , but with opposite signs; the cross correlations tend to increase the response of the d.o.f.  $x_1$  where the excitation is applied, and to decrease the response of  $x_2$ , but the sum  $E[x_1^2] + E[x_2^2]$  is unchanged. The ratio between the contributions of the cross-correlation and the autocorrelation may be expressed approximately by

$$\frac{\text{Cross-correlation}}{\text{Autocorrelation}} \approx \frac{1}{1 + \alpha^2} \quad (8.95)$$

where

$$\alpha = \frac{\omega_2 - \omega_1}{\xi(\omega_1 + \omega_2)} \quad (8.96)$$

expresses the ratio between the frequency difference between the two modes and their half power bandwidth. If this ratio is large, the contribution of the cross-correlations may be neglected without significant error on the MS response, and the SRSS rule is justified: the modal contributions may be treated separately and the global MS response is the sum of the modal MS responses. The SRSS rule may lead to substantial errors if the modes are closely spaced ( $\alpha$  close to 1).

### 8.10 Example: The seismic response of a n-storey building

Consider a shear frame with 10 identical floors (Fig.2.11), with  $m = 10^5$  kg and  $k = 16 \times 10^7$  N/m [these values fit the empirical formula (7.71)]. The damping is assumed uniform in all modes,  $\xi_i = 0.01$ . The structure is excited seismically by a stationary ground acceleration with a Kanai-Tajimi PSD profile (8.34) such that the RMS value is  $\sigma_g = 1$  m/s<sup>2</sup>, the central frequency is  $\omega_g = 12.56$  rad/sec (2 Hz), and  $\xi_g = 0.1$ .

The intensity  $\Phi_0$  of the excitation fitting  $\sigma_g^2 = 1$  may be calculated from Equ.(8.102) [Problem 8.8]

$$\Phi_0 = \frac{\sigma_g^2}{\pi\omega_g(\frac{1}{2\xi_g} + 2\xi_g)} = 4.87 \times 10^{-3} \quad \left[ \frac{(\text{m/s}^2)^2}{(\text{rad/s})} = \frac{\text{m}^2}{\text{s}^3\text{rad}} \right]$$

The one-sided PSD of the ground acceleration,  $\bar{\Phi}_g(\omega) = 2\Phi_g(\omega)$  is represented in Fig.8.17.a. The seismic response of the n-storey building has been analyzed in section 7.3; the transmissibility between the ground acceleration and the acceleration of the various floors is given by Equ.(7.70), where the acceleration of floor  $k$ , component  $k$  of the acceleration vector,  $\ddot{\mathbf{X}}_1(k)$ , corresponds to the component  $k$  of the mode shapes,  $\phi_i(k)$ . Figure 8.17.b shows the one-sided PSD of the acceleration of floor 1 and floor 10. Figure 8.17.c shows the cumulative RMS value of the floor acceleration, again of floor 1 and floor 10.

$$\sigma_{\ddot{x}_k}(\omega) = \left[ \int_{\omega}^{\infty} \bar{\Phi}_{\ddot{x}_k}(\nu) d\nu \right]^{1/2} \quad (8.97)$$

The value for  $\omega = 0$  is the RMS acceleration; the amplitude of the various steps at the natural frequencies indicate how the corresponding mode contributes to the global response. Figure 8.18 shows the evolution of the RMS response within the building; the figure illustrates how the ground acceleration is amplified within the structure; one sees that higher floors experience a larger acceleration than the lower one. This is a general observation, and this is why precision equipments are rarely placed on the upper floors, to minimize their sensitivity to vibrations coming from the environment (traffic, etc...).

The transmissibility between the ground acceleration and the support reaction is given by (8.69) and the spectral density of the reaction force is given by (8.70). The one sided PSD of the non-dimensional reaction force  $f_0/\sigma_g m_T$  is represented in Fig.8.17.d and the cumulative RMS value is represented in Fig.8.17.e, for two values of the damping ratio ( $\xi = 0.01$  and  $\xi = 0.02$ ). Once again, the amplitude of the various steps indicate how the corresponding modes contribute to the global response (the reaction force is dominated by the first mode) and the comparison between the two curves illustrates the effect of the damping.<sup>12</sup> The value at  $\omega = 0$ ,

$$\frac{\sigma_{f_0}}{\sigma_g m_T}$$

ratio between the RMS reaction force and the inertia forces associated with the RMS ground acceleration, is a measure of the dynamic amplification of the shear force in the column of the first floor. One sees that a

---

<sup>12</sup> According to Equ.(8.30), the contribution of mode  $i$  to the RMS value varies according to  $\xi_i^{-1/2}$ .

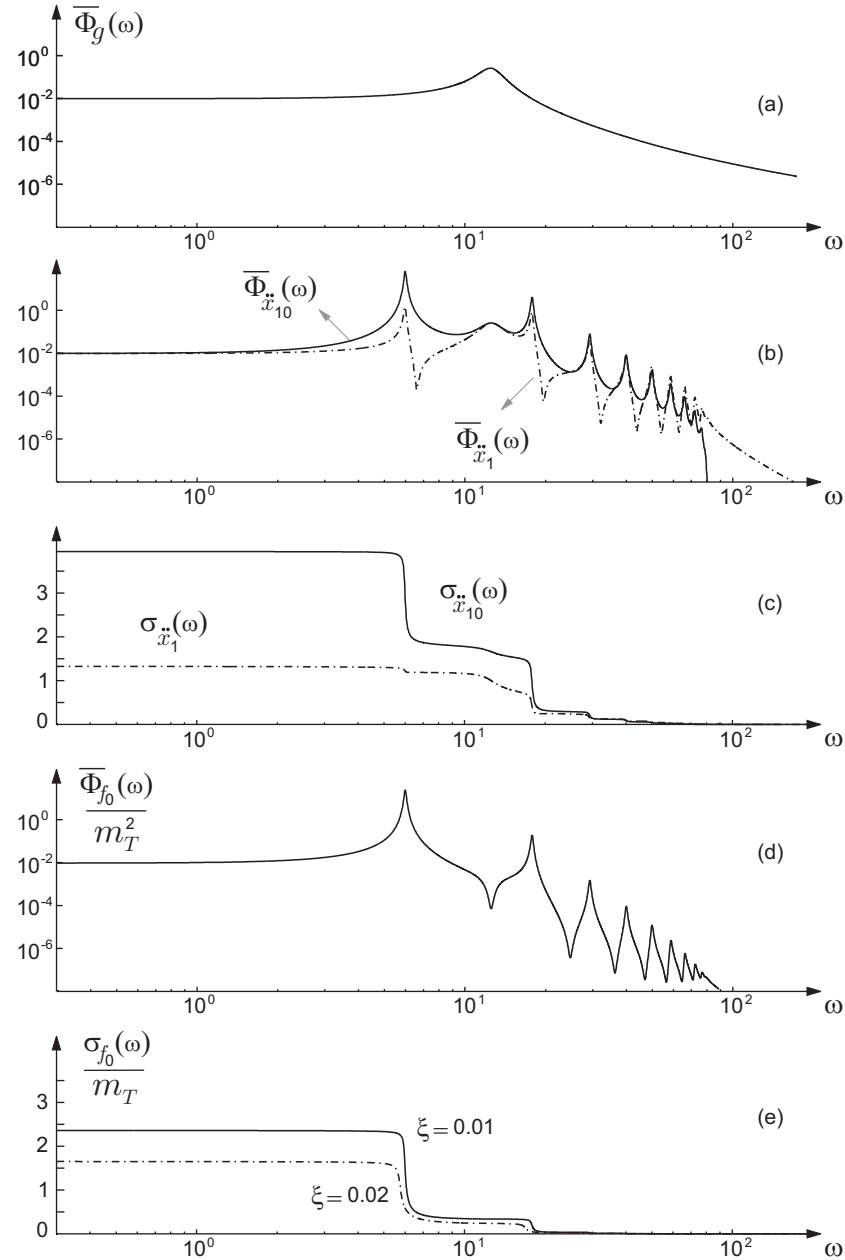


**Fig. 8.17.** Seismic response of a 10 storey shear frame. (a) One-sided PSD of the ground acceleration. (b) One-sided PSD of the acceleration of floor 1 and floor 10. (c) Cumulative RMS acceleration of floor 1 and floor 10. (d) One-sided PSD of the non-dimensional reaction force  $f_0/\sigma_g m_T$  ( $\xi = 0.01$ ). (e) Cumulative RMS value of the non-dimensional reaction force, for  $\xi = 0.01$  and  $\xi = 0.02$ .

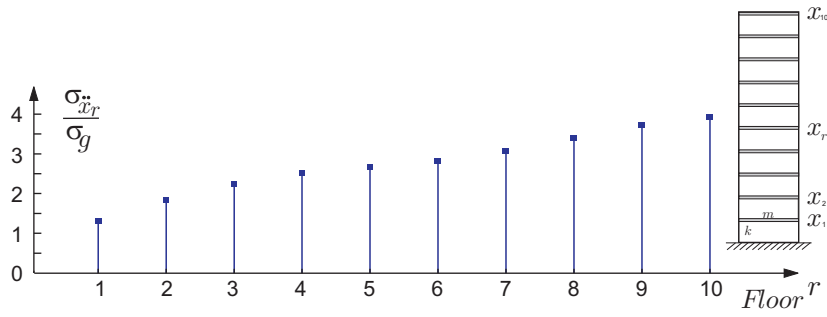


**Fig. 8.18.** Seismic response of a 10 storey shear frame. Evolution of the RMS floor acceleration  $\sigma_{\ddot{x}_k}/\sigma_g$  within the building.

significant reduction of the shear force may be achieved by increasing the damping of the first modes; various solutions to achieve this, passive and active, will be investigated in chapters 11 and 12.

## 8.11 Problems

**P.8.1** Starting from the definition of the autocorrelation function of a stationary process, show that

$$R_{\dot{x}x}(\tau) = R'_{xx}(\tau) \quad \text{and} \quad R_{\ddot{x}\dot{x}}(\tau) = -R''_{xx}(\tau)$$

**P.8.2** Show that the input-output relationships for the correlation function of a linear system of impulse response  $h(t)$  are

$$R_{yx}(\tau) = \int_0^\infty h(\xi) R_{xx}(\tau - \xi) d\xi \quad , \quad R_{yy}(\tau) = \int_0^\infty h(\xi) R_{yx}(\tau + \xi) d\xi$$

**P.8.3** Consider the seismic response of a linear oscillator to an stationary random acceleration of arbitrary, but slowly varying PSD  $\Phi_0(\omega)$ . Develop a numerical scheme for evaluating the variance of the relative displacement of the oscillator with more accuracy than the white noise approximation. [Hint: decompose the excitation into a sum of band limited white noise processes on adjacent intervals  $[\omega_i, \omega_{i+1}]$ , and for each of them use the analytical formula for a band limited white noise excitation].

**P.8.4** Consider the system governed by the first order differential equation

$$\dot{x} + ax = bf$$

and excited by a white noise  $\Phi_{ff}(\omega) = \Phi_0$ . Compute the PSD and the variance of the response. Does  $m_2$  exist for this process?

**P.8.5** The random variables  $x/\sigma_x$  and  $\dot{x}/\omega_0\sigma_x$  are independent, unity Gaussian variables [Equ.(8.45)]. Using a change of variables  $x = a \cos \theta$ ,  $y = \dot{x}/\omega_0 = a \sin \theta$  and expressing the conservation of the mass of probability associated with a small element  $dx dy = a da d\theta$ , show that the probability density function of the envelope  $a(t)$  follows the Rayleigh distribution (8.46).

**P.8.6** Let  $x(t)$  be a stationary random process with PSD  $\Phi_{xx}(\omega)$  and consider the smoothed process obtained by time averaging

$$y(t) = \frac{1}{2\varepsilon} \int_{t-\varepsilon}^{t+\varepsilon} x(\tau) d\tau \quad (8.98)$$

Show that  $y(t)$  may be seen as the response of a linear system of impulse response

$$h(t) = \frac{1}{2\varepsilon} \quad |t| < \varepsilon$$

[ $h(t)$  does not define a causal system]. Show that

$$\Phi_{yy}(\omega) = \Phi_{xx}(\omega) \frac{\sin^2 \varepsilon \omega}{\varepsilon^2 \omega^2} \quad (8.99)$$

What change to the integral would lead to a causal system? What would be the corresponding change in the PSD  $\Phi_{yy}(\omega)$ ?

**P.8.7** Consider the discrete averaging

$$y(t) = \frac{1}{4}x(t-T) + \frac{1}{2}x(t) + \frac{1}{4}x(t+T) \quad (8.100)$$

Show that the PSD of the stationary processes  $x(t)$  and  $y(t)$  are related by

$$\Phi_{yy}(\omega) = \Phi_{xx}(\omega) (\cos \frac{\omega T}{2})^4 \quad (8.101)$$

**P.8.8** Consider a random process with the Kanai-Tajimi spectrum (8.34); show that the variance is given by

$$\sigma_g^2 = \int_{-\infty}^{+\infty} \Phi_g(\omega) d\omega = \pi \Phi_0 \omega_g \left( \frac{1}{2\xi_g} + 2\xi_g \right) \quad (8.102)$$

---

## Peak factor & random fatigue

*Le premier pas vers la philosophie, c'est l'incrédulité.*  
Diderot, dernières paroles... 1784

### 9.1 Introduction

In the previous chapter, we have analyzed how the statistics of the structural response can be evaluated from the statistics of the random excitation. If the excitation process is Gaussian with zero mean (and the structure behaves linearly), the statistical information about the random response is entirely contained in the PSD functions, from which one can calculate the RMS value and the central frequency of the response, but this is not enough to assess the reliability of the structure. In this chapter, we consider the two most important failure mechanisms: threshold crossing and fatigue.

#### 9.1.1 Threshold crossings

In some situations, the design must guarantee that the stress level or the displacements remain below a given limit (e.g. vibration amplitude of a rotor remaining lower than the existing gap with the stator, or the stress level remaining below the yield stress or a given regulatory limit for a design earthquake in a nuclear plant). In these circumstances, the designer is interested in the probability distribution of the *largest* value  $x_{max}$  of the response over the duration of the excitation. This largest value is related to the RMS value  $\sigma_x$  by

$$x_{max} = \eta_e \sigma_x \quad (9.1)$$

where  $\eta_e$  is the *peak factor* (it is dimensionless).  $\eta_e$  is an increasing function of the duration of the phenomenon (it also depends on the probability of exceedance that is accepted). This chapter considers only the simplest case of a stationary Gaussian process of zero mean.

### 9.1.2 Fatigue

In many cases, the structural failure occurs after a fairly large number of cycles, while the nominal stress never exceeds the yield stress of the material. This situation is called *high-cycle fatigue*; the structure remains linear and, if the excitation is Gaussian, the response is also Gaussian. This chapter considers high-cycle fatigue of uniaxial as well as multi-axial stress fields; however, the discussion is limited to stress fields with zero mean. It has been observed that a constant compression stress does not affect the endurance limit, while a constant tension stress reduces the endurance limit. The models describing the effect of a constant stress are not examined in this chapter.

## 9.2 Peak factor

This section analyzes the probability distribution of the largest extremum over some duration  $T$ . We begin with the distribution of the maxima.

### 9.2.1 Maxima

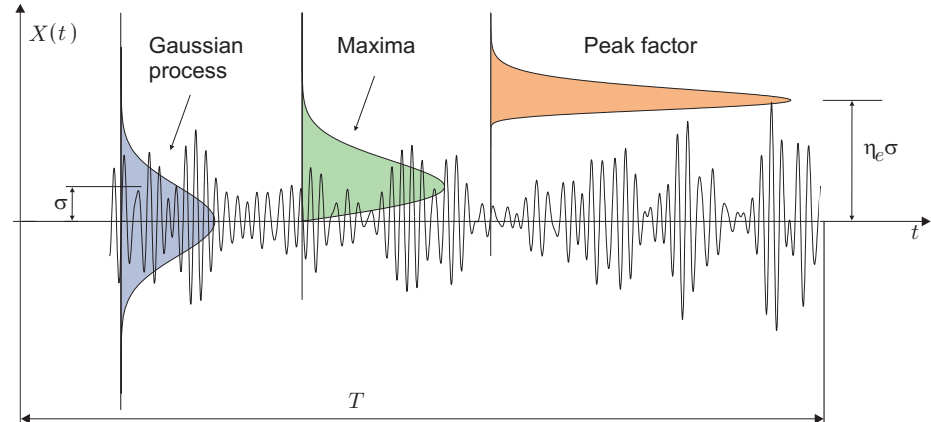


**Fig. 9.1.** Sample of duration  $T$ , of a stationary Gaussian process  $x(t)$  of zero mean and RMS value  $\sigma$ . Probability density functions of the process  $x(t)$ , of the maxima  $b$  (the curve shown is a Rayleigh distribution which corresponds to a narrow band process). Probability density function of the largest maximum  $x_{max}(T)$  over the duration  $T$ . The peak factor is defined by  $x_{max}(T) = \eta_e(T) \sigma$ .

Consider the Gaussian stationary random process of zero mean  $x(t)$  (Fig.9.1); the distribution of the maxima  $b$  is fairly complicated and depends on the bandwidth of the process. It can be shown that the probability density function  $q(\eta)$  of the reduced maxima  $\eta = b/\sigma$  is given by (Cartwright & Longuet-Higgins, 1956)

$$q(\eta) = \frac{1}{(2\pi)^{1/2}} [\varepsilon e^{-\eta^2/2\varepsilon^2} + (1 - \varepsilon^2)^{1/2} \eta e^{-\eta^2/2} \int_{-\infty}^{\eta(1-\varepsilon^2)^{1/2}/\varepsilon} e^{-x^2/2} dx] \quad (9.2)$$

where  $\varepsilon$  is a parameter which characterizes the bandwidth of the process and can be expressed in terms of the spectral moments according to

$$0 \leq \varepsilon^2 = 1 - \frac{m_2^2}{m_0 m_4} = 1 - \left(\frac{\nu_0}{\nu_1}\right)^2 \leq 1 \quad (9.3)$$

According to the discussion of section 8.5, the average number of maxima per unit of time,  $\nu_1$  tends to be close to the central frequency  $\nu_0$  for a narrow band process, and  $\varepsilon^2$  is close to 0. On the contrary,  $\nu_1 \gg \nu_0$  for a wide band process and  $\varepsilon^2$  is close to 1. For a wide band process, the maxima can assume negative as well as positive values (as illustrated in Fig.8.7.b) and, when  $\varepsilon \rightarrow 1$ ,  $q(\eta)$  is Gaussian; for  $\varepsilon \rightarrow 0$ , it becomes identical to the Rayleigh distribution

$$q(\eta) = \eta \exp(-\frac{\eta^2}{2}) \quad (\eta \geq 0) \quad (9.4)$$

represented in Fig.8.9.

### 9.2.2 First-crossing problem

Let  $x(t)$  be a stationary Gaussian process of zero mean and standard deviation  $\sigma$ . The *reliability*  $W(T, \eta)$  is the probability that  $x(t)$  remains in the safe domain  $|x(t)| < \eta\sigma$  during the observation period:

$$W(T, \eta) = \text{Prob}\{|x(t)| < \eta\sigma ; 0 \leq t < T\} \quad (9.5)$$

$W(T, \eta)$  represents the fraction of samples which have not left the safe domain after the duration  $T$ .

The probability density function of the first-crossing time is

$$p_1(T) = -\frac{\partial W(T, \eta)}{\partial T} \quad (9.6)$$

because  $p_1(T)dT$  represents the probability that the first-crossing occurs in the time interval  $[T, T + dT[$ .

Alternatively,  $W(T, \eta)$  is the probability that the largest extremum during the observation period  $T$  remains below  $b = \eta\sigma$ , that is (by definition) the probability distribution function of the largest extremum (during the observation period  $T$ ).<sup>1</sup> It follows that the probability density function of the peak factor is

$$p_e(T, \eta) = \frac{\partial W(T, \eta)}{\partial \eta} \quad (9.7)$$

$p_e(T, \eta)d\eta$  represents the probability that the largest extremum during the observation period  $T$  belongs to the interval  $[\eta, \eta + d\eta[$ .

The literature about the first-crossing problem is considerable and can only be touched in this text. A model for the reliability can be built by considering the extreme point process  $y(n)$  constructed as indicated in Fig.9.2; if the process is narrow band, the time interval between two consecutive points is  $\Delta \simeq 1/2\nu_0$  ( $\nu_0 = \omega_0/2\pi$  is the central frequency).

If  $h(n)$  stands for the probability that the  $n^{th}$  extremum is the first one beyond the threshold  $\eta\sigma$  (under the condition that all previous ones are below the threshold),

$$h(n) = P[y(n) > \eta\sigma \mid \bigcap_{i=1}^{n-1} y(i) < \eta\sigma] \quad (9.8)$$

The reliability can be written

$$W(T, \eta) = \prod_{n=1}^N [1 - h(n)] \quad (9.9)$$

where  $N$  is the total number of extreme points over the duration  $T$ .<sup>2</sup> From this expression, various models can be built by making assumptions on the way the extrema occur.

The simplest of all possible assumptions is that of *independent* extrema; in this case, the condition disappears from Equ.(9.8). If, in addition

---

<sup>1</sup> The *probability distribution function*  $F(x)$  of a random variable is related to its probability density function  $p(x)$  by

$$F(x) = \int_{-\infty}^x p(a) da \quad \text{or} \quad p(x) = \frac{dF(x)}{dx}$$

<sup>2</sup>  $1 - h(n)$  is the probability that the  $n^{th}$  extremum is also below the threshold  $\eta\sigma$  if all the previous extrema are below the threshold.

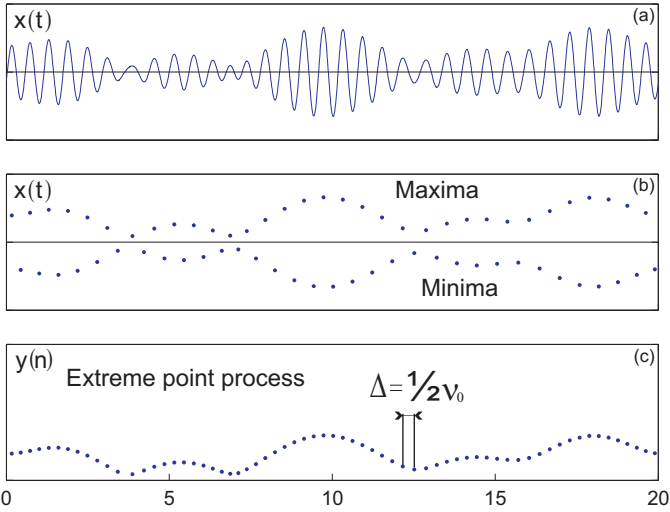


**Fig. 9.2.** (a) Sample of a narrow band process  $x(t)$ . (b) Maxima and minima; the time interval between two maxima is  $\simeq 1/\nu_0$ . (c) Absolute extrema of the process,  $y(n) = |x(t)|_{max}$  the time interval between two consecutive points is  $\Delta \simeq 1/2\nu_0$ .

to this, the process is assumed narrow band, the maxima are distributed according to the Rayleigh distribution (9.4) and  $N = 2\nu_0 T$  is the number of half-cycles over the duration  $T$ . It follows that

$$h(n) = P[y(n) > \eta\sigma] = \int_{\eta}^{\infty} xe^{-x^2/2} dx = e^{-\eta^2/2} \quad (9.10)$$

and

$$W(T, \eta) = \prod_{n=1}^{N} [1 - h(n)] = (1 - e^{-\eta^2/2})^N \quad (9.11)$$

For large values of  $N$ , using the asymptotic form of the exponential  $\lim_{n \rightarrow \infty} (1 + \frac{x}{n})^n = e^x$ , this result may be written alternatively

$$W(T, \eta) = \exp[-Ne^{-\eta^2/2}] = \exp[-2\nu_0 Te^{-\eta^2/2}] \quad (9.12)$$

This is the simplest model for the reliability. The assumption of independent extrema may be criticized, particularly for narrow band signals, because the extrema (which belong to the envelope process) tend to vary smoothly rather than being independent, as illustrated in Fig. 9.2. However, this model is conservative and tends to overestimate the peak factor. The probability density function of the peak factor is obtained by partial derivation with respect to  $\eta$ . There is a single parameter which is the number of half-cycles,  $N = 2\nu_0 T$ .

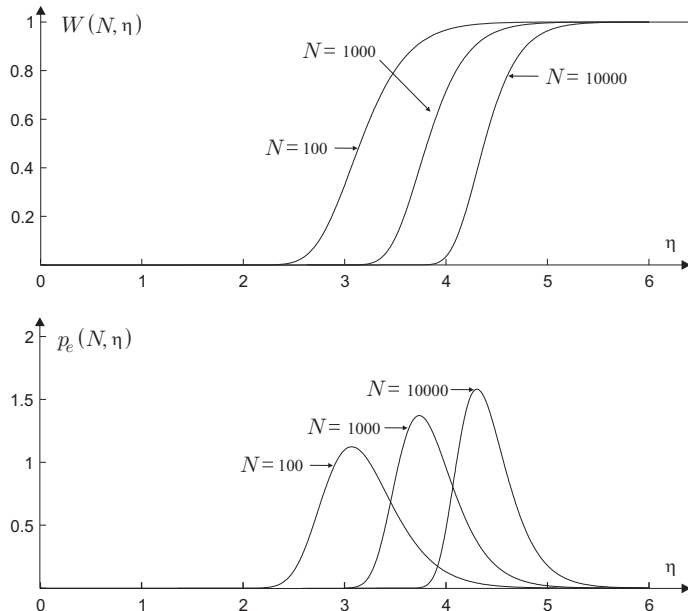
### 9.2.3 Peak factor

Figure 9.3 shows  $W(N, \eta)$  for several values of  $N$ ; the reliability is by definition the probability distribution function of the peak factor and  $p_e(N, \eta)$  is given by Equ.(9.7); the maximum value of  $p_e(N, \eta)$  tends to increase with  $N$  and it occurs for larger values of  $\eta$  (typically between 3 and 5); the dispersion of  $p_e$  about its maximum decreases with  $N$ . The average and standard deviation of the peak factor can be approximated by (Davenport, 1964)

$$E[\eta_e] \simeq (2 \ln N)^{1/2} + \frac{\gamma}{(2 \ln N)^{1/2}} \quad (9.13)$$

$$\sigma[\eta_e] \simeq \frac{\pi}{\sqrt{6}} \frac{1}{(2 \ln N)^{1/2}} \quad (9.14)$$

where  $\gamma = 0.5772$  (Euler's constant).



**Fig. 9.3.** (a) Reliability  $W(N, \eta) = \exp[-Ne^{-\eta^2/2}]$  for various values of the number of half-cycles  $N$  (the reliability is by definition the probability distribution function of the peak factor). (b) Corresponding probability density function of the peak factor ( $p_e = \partial W / \partial \eta$ ) based on independent extrema. The maximum of  $p_e$  occurs for typical values of  $\eta_e$  between 3 and 5.

### 9.3 Response spectrum

In earthquake engineering, there is a tradition of using the concept of *response spectrum*. For a given accelerogram  $\ddot{x}_0$  (Fig.9.4), the *displacement spectrum*,  $S_d(\omega_n, \xi)$ , is defined as the maximum of the absolute value of the relative displacement  $y$  of a single d.o.f. oscillator of natural frequency  $\omega_n$  and damping  $\xi$  in response to the acceleration  $\ddot{x}_0$ . The relative displacement  $y$  is solution of Equ.(8.24);  $S_d(\omega_n, \xi)$  is regarded as a function of  $\omega_n$ , with  $\xi$  as a parameter [for every different value of  $\omega_n$  and  $\xi$ , the relative response  $y(t)$  is different, and so is  $|y|_{max} = S_d(\omega_n, \xi)$ ]. The most frequent representation is a log-log diagram of the *pseudo-velocity spectrum*, defined by

$$S_v(\omega_n, \xi) = \omega_n S_d(\omega_n, \xi) \quad (9.15)$$

The *pseudo-acceleration spectrum* is defined by

$$S_a(\omega_n, \xi) = \omega_n S_v(\omega_n, \xi) = \omega_n^2 S_d(\omega_n, \xi) \quad (9.16)$$

$S_v$  is different from the maximum velocity of the response, but usually  $S_a$  is close to the maximum absolute acceleration of the oscillator. In the log-log diagram of the pseudo-velocity spectrum, constant values of the relative displacement ( $S_d$ ) and of the acceleration ( $S_a$ ) appear as straight lines.

For a given site, the expected characteristics of the ground acceleration (maximum acceleration, duration, frequency content) depend on the seismicity of the site and on the local geological conditions. Standard shapes of response spectra have been defined (Fig.9.5), corresponding to various local soil conditions (bedrock, alluvion); they are normalized with respect to the local seismicity, expressed by the maximum acceleration for the site (often called “ZPA”: *zero-period acceleration*, corresponding to the high frequency asymptote of the response spectrum). The maximum acceleration is generally expressed as a fraction of the acceleration of gravity,  $g$ ;  $a_{max}$  can be  $0.15g$  in areas of moderate seismicity and  $0.3g$  and above in area of high seismic activity; the duration is typically between 10 and 30 sec.<sup>3</sup>

The regulatory design response spectra are supposed to define an envelope for all possible ground motions at one site; they depend on the

---

<sup>3</sup> In the large earthquake that struck Japan in March 2011 (Magnitude 9 on the Richter scale), maximum ground accelerations above  $1g$  were observed at more than 100 km from the epicenter, and the duration of the strong ground motion was about 2 minutes.

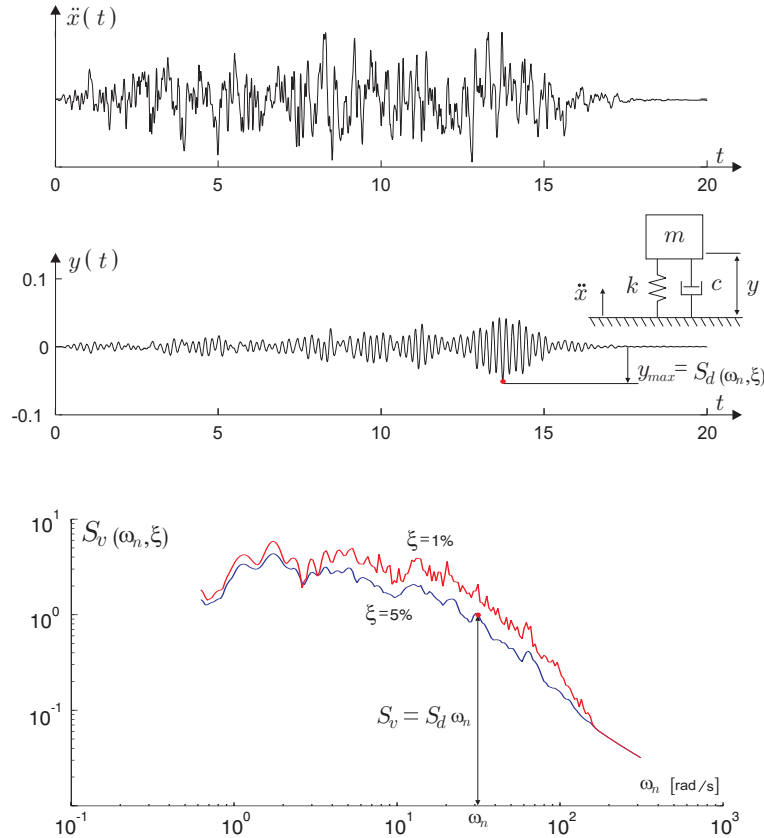


**Fig. 9.4.** (a) Artificial earthquake accelerogram. (b) Response  $y$  of the single d.o.f. oscillator for specific values  $(\omega_n, \xi)$  of the natural frequency and the damping ratio;  $S_d(\omega_n, \xi) = |y|_{max}$ , the maximum of the absolute value. (c) Pseudo-velocity spectrum  $S_v(\omega_n, \xi) = \omega_n S_d(\omega_n, \xi)$ , for two values of the damping ratio (the two curves have the same high frequency asymptote).

return period considered. In practice, for the design of nuclear power plants, two sets of response spectra are defined for a site: the *Operating Basis Earthquake* is the earthquake that the plant is likely to experience once during its lifetime, and after which it is supposed to restart after only minor repairs. The *Safe Shut-down Earthquake* is the maximum possible earthquake for the site, for which the plant must be safely shut down and maintained in a cool state, without any significant release of reactivity; no restart is expected.

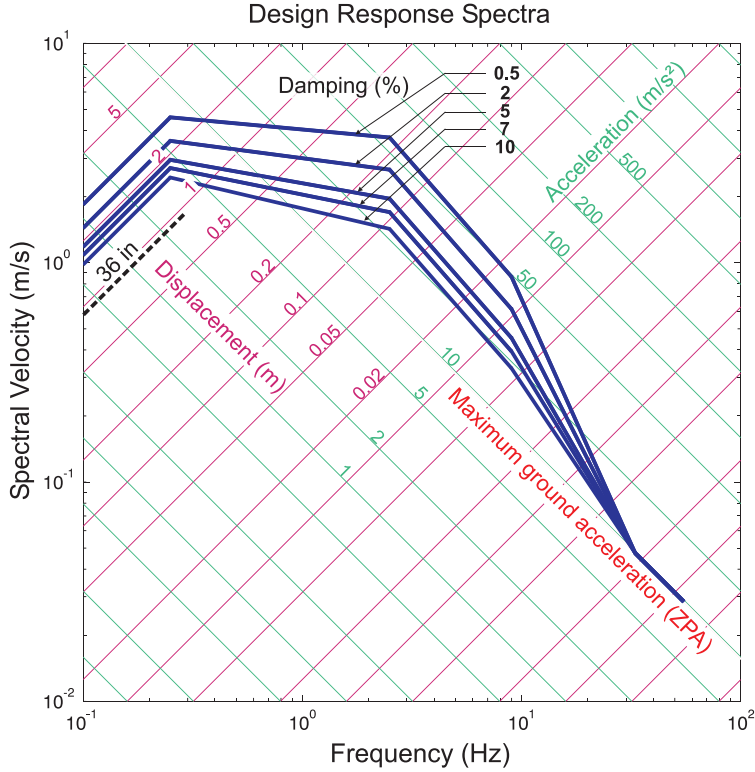


**Fig. 9.5.** Horizontal design response spectra of the US NRC Regulatory Guide 1.60, normalized to a maximum ground acceleration of ZPA=1g.

### 9.3.1 Maximum structural response

The historical reason for developing response spectra is that, if the structural response is dominated by a single mode, the maximum response can be directly evaluated from the response spectrum. Indeed, referring to Equ.(7.21), the modal response (of mode  $i$ ) is governed by

$$\mu_i \ddot{z}_i + 2\xi_i \mu_i \omega_i \dot{z}_i + \mu_i \omega_i^2 z_i = \Gamma_i \ddot{x}_0 \quad (9.17)$$

and the structural response

$$\mathbf{y} = \phi_i z_i \quad (9.18)$$

From the definition of the response spectrum, it follows that the maximum structural response of mode  $i$  is given by

$$\mathbf{y}_i^{max} = \phi_i \frac{\Gamma_i}{\mu_i} S_d(\omega_i, \xi_i) \quad (9.19)$$

where  $S_d(\omega_i, \xi_i)$  is the value of the response spectrum for the natural frequency  $\omega_i$  and the damping  $\xi_i$  of the dominant mode.

If several modes contribute to the structural response, the maximum response of each mode can still be evaluated in the same way. For well separated modes, we have seen in section 8.9 that the modal responses may be treated as independent and the global response may be evaluated by the SRSS rule:

$$y^{max} = \left\{ \sum_i [y_i^{max}]^2 \right\}^{1/2} \quad (9.20)$$

This combination rule may lead to substantial errors for closely spaced modes. Alternative combination rules have been proposed, but this topic is outside the scope of this textbook.

An elegant alternative to the use of response spectra would be to replace the specification of the ground motion by a finite duration stationary random process of specified power spectral density; the ground acceleration would be defined by a PSD  $\Phi_0(\omega)$  and a window function. However, the response spectra being defined by the regulatory authorities, the definition of a PSD consistent with a given response spectrum remains a subject of discussion. The relationship between the PSD and the response spectra is outlined below.

### 9.3.2 Relation between $S_v(\omega, \xi)$ and $\Phi_0(\omega)$

If the acceleration time-history  $\ddot{x}_0$  is known, the response spectrum  $S_d(\omega, \xi)$  is entirely determined; the reverse is not true. However, for a lightly damped oscillator, the response is strongly influenced by the energy contained in the excitation in the vicinity of the natural frequency of the oscillator. If one assumes that the oscillator response is a stationary random process of duration  $T$ , an approximate relationship between  $S_v(\omega, \xi)$  and  $\Phi_0(\omega)$  may be obtained by the following steps:

1. According to the white noise approximation, the RMS response of the oscillator of frequency  $\omega_n$  is related to the PSD of the excitation by Equ.(8.30)

$$\sigma^2 = \frac{\pi \Phi_0(\omega_n)}{2\xi \omega_n^3} \quad (9.21)$$

2. The maximum response is related to the RMS response by the peak factor  $\eta_e(N)$  which depends on the number of half-cycles. For a narrow band process, the central frequency may be approximated by the natural frequency of the oscillator,  $\nu_0 \simeq \omega_n/2\pi$ . Thus,  $N = 2\nu_0 T \simeq \omega_n T / \pi$  and the average value of the peak factor,  $E[\eta_e]$  may be evaluated from (9.13).

3. Finally, by definition, the response spectrum and the peak factor are related by

$$S_d(\omega_n, \xi) = \sigma E[\eta_e] \quad (9.22)$$

This leads to

$$\Phi_0(\omega_n) = \frac{2\xi\omega_n^3}{\pi} \left[ \frac{S_d(\omega_n, \xi)}{E[\eta_e]} \right]^2 \quad (9.23)$$

This simple model neglects all the transient effects present in the oscillator response, and is based on several simplifying assumptions; however, the estimator may be improved iteratively to fit the average response spectrum of a set of artificially generated accelerograms.<sup>4</sup>

## 9.4 Random fatigue

### 9.4.1 S-N curve

The characterization of the uniaxial fatigue behavior of materials is done by subjecting a sample to an alternating sine loading of constant amplitude  $S$  and counting the number of cycles  $N$  until the start of the first crack. The test is repeated for increasing values of the stress and the results are presented in the form of a curve  $S(N)$  which is known as the *Wöhler curve* of the material, or simply the “ $S - N$ ” curve. Some materials have an endurance limit,  $S_e$ , which is the limit stress under which the material can sustain an infinite number of cycles without initiation of a crack; some other materials do not have an endurance limit. For a large class of materials, the  $S - N$  curve may be approximated by<sup>5</sup>

$$NS^\beta = c \quad (9.24)$$

where  $\beta$  and  $c$  are material constants ( $5 < \beta < 20$ ). The present discussion is focused on alternating stress fields and does not discuss the situation where the alternating stress is superimposed on a constant stress. The random stress is assumed to be a zero mean stationary Gaussian process.

---

<sup>4</sup> Taking only the first contribution of (9.13), one gets the explicit formula:

$$\Phi_0(\omega_n) = \frac{2\xi\omega_n^3}{\pi} \cdot \frac{S_d(\omega_n, \xi)^2}{2 \ln(\omega_n T / \pi)}$$

<sup>5</sup> This relationship ignores the endurance limit and the statistical scatter in the material behavior; the  $S-N$  curve may also be defined in a probabilistic way.

### 9.4.2 Linear damage theory

Fatigue life for complex load histories can be treated by a cumulative damage analysis; the *linear damage theory* (also known as *Palmgren-Miner criterion*) assumes that  $n_i$  cycles at a stress level  $S_i$  produce a damage  $D_i = n_i/N_i$ , where  $N_i = cS_i^{-\beta}$  is the number of cycles of the  $S$ - $N$  curve under the constant amplitude  $S_i$ . According to the linear damage theory, the total damage associated with various levels of stress may be added linearly, producing a total damage

$$D = \sum_i \frac{n_i}{N_i} \quad (9.25)$$

and the crack initiates when the total damage reaches  $D = 1$ . This criterion does not take into account the order of application of the various stress levels; it is known to be inaccurate, but it has the enormous advantages of being simple and of relying on constant amplitude tests for which experimental data are widely available. Although inadequate as an absolute indicator of fatigue resistance, the linear damage  $D$  provides a valuable relative information and can be used for design purposes: a design leading to a smaller value of  $D$  is probably a better design. If the stress histories are available, the counting of the stress cycles can be done according to the *rainflow* method. In the present discussion which is concerned with random stress fields, the distribution of the stress cycles is derived from the PSD of the random stress.

### 9.4.3 Uniaxial loading

Let  $x(t)$  be a uniaxial Gaussian stress of zero mean and PSD  $\Phi(\omega)$ . The material has a  $S$ - $N$  curve of the form (9.24) and behaves according to the linear damage theory (9.25).

In the classical theory of random fatigue, the counting of the cycles is related to the occurrence of maxima. To account for the fact that fatigue damage is related to tension rather than compression stresses, it is assumed that every maximum with a positive amplitude  $b$  contributes for one cycle to the damage, and that a maximum with a negative amplitude does not contribute to the damage. Thus, the damage associated with one cycle of amplitude  $b$  is

$$D = \frac{1}{N} = \frac{1}{cb^{-\beta}} = b^\beta c^{-1} \quad (b > 0) \quad (9.26)$$

where  $N$  is the number of cycles of the  $S$ - $N$  curve corresponding to the stress level  $b$ . If the average number of maxima per unit of time is  $\nu_1$  [given by Equ.(8.42)], the average number of maxima per unit of time in  $[b, b+db]$  is  $\nu_1 q(b)db$ , where  $q(b)$  is the probability density function of the maxima, given by Equ.(9.2). This leads to a rate of damage  $b^\beta c^{-1} \nu_1 q(b)db$ . The expected damage per unit of time is obtained by integrating the damage rate over all possible values of the stress amplitude  $b$ ,

$$E[D] = \nu_1 c^{-1} \int_0^\infty b^\beta q(b) db \quad (9.27)$$

Introducing the reduced stress,  $\eta = b/\sigma_x$ ,

$$E[D] = \nu_1 c^{-1} \sigma_x^\beta \int_0^\infty \eta^\beta q(\eta) d\eta \quad (9.28)$$

where  $\sigma_x = m_0^{1/2}$  is the standard deviation (RMS value) of the stress. For a narrow band process,  $q(\eta)$  is the Rayleigh distribution (9.4) and the rate of maxima  $\nu_1$  may be approximated by the central frequency  $\nu_0$ , leading to

$$E[D] = c^{-1} \nu_0 \sigma_x^\beta \int_0^\infty \eta^{\beta+1} e^{-\eta^2/2} d\eta$$

or

$$E[D] = c^{-1} \nu_0 \sigma_x^\beta 2^{\beta/2} \Gamma(\beta/2 + 1) \quad (9.29)$$

where  $\Gamma(\cdot)$  is the Gamma function.<sup>6</sup> Upon substituting  $\sigma_x = m_0^{1/2}$  and  $\nu_0 = \frac{1}{2\pi} (m_2/m_0)^{1/2}$ ,

$$E[D] = c^{-1} \frac{2^{\beta/2}}{2\pi} \Gamma(\beta/2 + 1) m_0^{(\beta-1)/2} m_2^{1/2} \quad (9.30)$$

This result was first derived by (Miles, 1954). It can also be used as an approximation for a wide band process, but it tends to be conservative. Alternative prediction models have been proposed, based on other spectral moments, but they are outside this introductory text.

Note that Equ.(9.29) shows that the damage is proportional to  $\sigma_x^\beta$ , where  $\beta$  is the power of the  $S$ - $N$  curve. In fatigue testing, it is often

---

<sup>6</sup> The Gamma function is an extension of the factorial function  $\Gamma(n) = (n - 1)!$  for non integer numbers. It is defined by

$$\Gamma(x) = \int_0^\infty t^{x-1} e^{-t} dt$$

necessary to increase the level of excitation to reduce the duration of the tests; if the PSD  $\Phi_0(\omega)$  of the excitation is multiplied by a scalar  $a$  while keeping the frequency content unchanged, the moment  $m_0$  will also be multiplied by  $a$  and the RMS response  $\sigma_x$  by  $a^{1/2}$ . Thus, the damage per unit of time will be multiplied by  $a^{\beta/2}$  and the duration of the test leading to a given damage will be reduced accordingly (Problem 9.2).

#### 9.4.4 Biaxial loading

Biaxial stress states are very important, because cracks often initiate at the surface, where the stress is biaxial. The von Mises criterion has been found to correlate fairly well with a lot of experimental data for biaxial stress states. The equivalent von Mises stress is defined by a quadratic equation,

$$s_c^2 = s_x^2 + s_y^2 - s_x s_y + 3s_{xy}^2 \quad (9.31)$$

or

$$s_c^2 = \mathbf{s}^T Q \mathbf{s} \quad (9.32)$$

where  $\mathbf{s} = (s_x, s_y, s_{xy})^T$  is the stress vector and  $Q$  is defined by

$$Q = \begin{bmatrix} 1 & -1/2 & 0 \\ -1/2 & 1 & 0 \\ 0 & 0 & 3 \end{bmatrix} \quad (9.33)$$

If one considers this quadratic relationship in the strict sense, one would normally have to work in the time domain rather than in the frequency domain,<sup>7</sup> and the Gaussian property would also be lost. Alternatively, in what follows, we consider it in the mean square sense to define a new Gaussian scalar random process. Taking advantage of the relationship

$$\mathbf{s}^T Q \mathbf{s} = \text{Trace}\{Q[\mathbf{s}\mathbf{s}^T]\} \quad (9.34)$$

the mean square value of the von Mises stress reads

$$\mathbb{E}[s_c^2] = \mathbb{E}[\mathbf{s}^T Q \mathbf{s}] = \text{Trace}\{Q\mathbb{E}[\mathbf{s}\mathbf{s}^T]\} \quad (9.35)$$

where the expectation  $\mathbb{E}[\cdot]$  applies only to the random quantities.  $\mathbb{E}[\mathbf{s}\mathbf{s}^T]$  is the covariance matrix of the stress vector, related to the PSD matrix of the stress vector,  $\Phi_{ss}(\omega)$  by

---

<sup>7</sup> The frequency content of a time-history of  $s_c(t)$  is different from that of the stress components; if the stress components are harmonic at a frequency  $\omega$ ,  $s_c(t)$  has its frequency content centered on  $2\omega$ .

$$\mathbb{E}[\mathbf{s}\mathbf{s}^T] = \int_{-\infty}^{\infty} \Phi_{ss}(\omega) d\omega \quad (9.36)$$

Thus, if one defines a equivalent random stress  $s_c(t)$  as a zero mean Gaussian process with PSD

$$\Phi_c(\omega) = \text{Trace}\{Q\Phi_{ss}(\omega)\} \quad (9.37)$$

this process has indeed the same mean square value as the von Mises stress,

$$\mathbb{E}[s_c^2] = \int_{-\infty}^{\infty} \Phi_c(\omega) d\omega \quad (9.38)$$

Since a zero mean Gaussian process is entirely defined by its PSD, Equ.(9.37) may be regarded as the *definition* of an equivalent uniaxial alternating von Mises stress. Although this process varies noticeably from the time-histories defined by Equ.(9.31), it is meaningful from the physical point of view, because:

- (i) In the uniaxial case where only a single stress component  $s_x \neq 0$ ,  $\Phi_c(\omega) = \Phi_x(\omega)$ , so that  $s_c = s_x$ .
- (ii) The process  $s_c$  defined by (9.37) does have components at all the natural frequencies of the structure, unlike the time-histories obtained by (9.31).

#### 9.4.5 Finite element formulation

The stress vector at one point (or within one finite element) is related to the modal amplitudes by

$$\mathbf{s} = S \mathbf{z} \quad (9.39)$$

where  $S$  is the  $(3 \times m)$  modal stress matrix at this point. The corresponding  $(3 \times 3)$  PSD matrix of the stress vector is

$$\Phi_{ss}(\omega) = S \Phi_z(\omega) S^T \quad (9.40)$$

where  $\Phi_z(\omega)$  is the  $(m \times m)$  PSD matrix of the modal responses, computed according to section 8.8.  $\Phi_c(\omega)$  can be calculated by (9.37) and the procedure for uniaxial stress discussed above applies.

## 9.5 Problems

**P.9.1** Show that, according to the simplified model relating the response spectrum and the power spectral density developed in section 9.3.2, the

amplitudes of the response spectrum for two different values of the damping ratio are related by

$$\frac{S_d(\omega_n, \xi_1)}{S_d(\omega_n, \xi_2)} \approx \left(\frac{\xi_2}{\xi_1}\right)^{\frac{1}{2}}$$

**P.9.2** Accelerated fatigue test: a specimen must be subjected to a fatigue endurance test of duration  $T$  with a stationary random excitation of prescribed PSD  $\Phi(\omega)$ . In order to reduce the duration of the test, it is considered to scale up the excitation. Determine the scaling factor of the PSD, in order to produce the same damage in the reduced time  $T/\alpha$ .

# 10

---

## Rotor dynamics

*Alexandre voyait la terre comme une belle place bien propre à y établir un empire [...] un philosophe la voit comme une grosse planète qui va par les cieux, toute couverte de fous.*

Fontenelle, *Entretiens sur la pluralité des mondes*, 1686

### 10.1 Introduction

This chapter is an introduction to the basic phenomena encountered in rotor dynamics. It starts with the “Jeffcott rotor model” (1919) which involves only a point mass and two d.o.f., and explains the critical velocity, the stable operation at supercritical velocities as well as the self-centering observed at supercritical velocities; it is also sufficient to account for the destabilizing effect of the rotating damping at supercritical speeds.

Next, the gyroscopic effects are analyzed using again a two d.o.f. model obtained by the Rayleigh-Ritz approximation. The gyroscopic effects are due to the wobbling of the disk, resulting from the combined motion of spin and bending of the shaft; the angular momentum and the angular velocity vectors are no longer parallel and induce gyroscopic moments, which have a considerable impact on the rotor dynamics if the angular momentum is large. The dependence of the natural frequencies on the spin velocity is usually represented by the Campbell diagram. The dependency of the conical modes on the spin velocity is studied further with the analysis of a rigid rotor on elastic supports.

Finally, this chapter ends with the analysis of the effect of the anisotropy of the support and of the shaft on the dynamics of the rotor and its stability.

## 10.2 Jeffcott rotor

A perfectly balanced Jeffcott rotor (Fig.10.1.a) consists of a point mass  $m$  attached at the elastic center  $C$  of the cross section of a massless shaft. The system is undamped and axially symmetrical; the shaft rotates at the angular speed  $\Omega$  and has an overall stiffness  $k$ <sup>1</sup>; the disk remains aligned on the  $z$  axis and the gyroscopic effects are ignored. An unbalanced Jeffcott rotor is such that the point mass at  $P$  has a small eccentricity  $\varepsilon$  with respect to the elastic center  $C$ . In the description of the motion, the origin of time  $t$  is taken in such a way that  $CP$  is aligned on the axis  $Ox$  when  $t = 0$  (Fig.10.1.b).

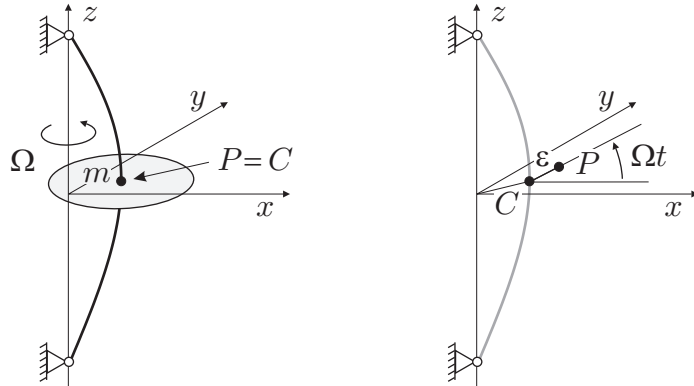


**Fig. 10.1.** Jeffcott rotor;  $C$  is the elastic center and the mass  $m$  of the disk is lumped at the center of mass  $P$ . (a) Perfectly balanced. (b) Unbalanced with eccentricity  $\varepsilon$ .

The reference frame  $Oxyz$  is fixed; the absolute coordinates of the elastic center  $C$  are taken as generalized coordinates,  $\mathbf{r}_c = (x_c, y_c)^T$ .

$$\mathbf{r}_p = \begin{Bmatrix} x_p \\ y_p \end{Bmatrix} = \begin{Bmatrix} x_c + \varepsilon \cos \Omega t \\ y_c + \varepsilon \sin \Omega t \end{Bmatrix}$$

It follows that the absolute velocity of the point mass is

$$\dot{\mathbf{r}}_p = \begin{Bmatrix} \dot{x}_c - \varepsilon \Omega \sin \Omega t \\ \dot{y}_c + \varepsilon \Omega \cos \Omega t \end{Bmatrix}$$

and the kinetic energy

---

<sup>1</sup> It does not matter whether the lateral stiffness comes from the bending of the shaft, from the supports, or both, but the stiffness is assumed isotropic, that is identical in all directions.

$$T = \frac{m}{2}(\dot{x}_p^2 + \dot{y}_p^2) = \frac{m}{2}[\dot{x}_c^2 + \dot{y}_c^2 + \varepsilon^2 \Omega^2 + 2\varepsilon\Omega(-\dot{x}_c \sin \Omega t + \dot{y}_c \cos \Omega t)] \quad (10.1)$$

The potential energy associated with the deformation of the shaft reads

$$V = \frac{1}{2}k(x_c^2 + y_c^2) \quad (10.2)$$

where  $k$  is the lateral stiffness accounting for the flexibility of the shaft and supports. If there are external forces acting on  $P$ , defined by  $F_x$  and  $F_y$  in the fixed reference frame, the generalized forces associated with the generalized coordinates  $x_c$  and  $y_c$  are also  $F_x$  and  $F_y$ , because  $\delta x_p = \delta x_c$  and  $\delta y_p = \delta y_c$ .<sup>2</sup>

From the above expressions of the kinetic and potential energies, the Lagrange equations read

$$\begin{aligned} m\ddot{x}_c + kx_c &= m\varepsilon\Omega^2 \cos \Omega t + F_x \\ m\ddot{y}_c + ky_c &= m\varepsilon\Omega^2 \sin \Omega t + F_y \end{aligned} \quad (10.3)$$

The first term in the right hand side represents the rotating unbalance force associated with the eccentricity  $\varepsilon$ .

### 10.2.1 Unbalance response

To analyze the unbalance response, it is assumed that  $F_x = F_y = 0$  in Equ.(10.3). A particular solution of the form of a synchronous forward whirl (i.e. a whirl at the same frequency and in the same direction as the rotating shaft)

$$\begin{cases} x_c = x_0 \cos \Omega t \\ y_c = y_0 \sin \Omega t \end{cases}$$

exists provided that

$$(k - m\Omega^2)x_0 = m\varepsilon\Omega^2$$

$$(k - m\Omega^2)y_0 = m\varepsilon\Omega^2$$

which yields

$$x_0 = y_0 = r_0 = \varepsilon \frac{m\Omega^2}{k - m\Omega^2} = \varepsilon \frac{\Omega^2}{\omega_n^2 - \Omega^2} \quad (10.4)$$

where  $\omega_n = \sqrt{k/m}$  is the critical speed, for which the unbalanced response is unbounded. More generally, *the critical speed is the shaft rotational*

---

<sup>2</sup> The displacement of  $P$  associated with the spin,  $\varepsilon \cos \Omega t$  does not contain any generalized coordinate and the virtual displacements are taken at constant time.

speed that corresponds to the peak of a (non critically damped) resonance frequency, when it is excited by the shaft imbalance.

Thus, the unbalanced response consists of a synchronous whirling with an amplitude  $r_0$  given above. In the subcritical region, for  $\Omega < \omega_n$ , the whirling amplitude grows from zero, tending to infinity for  $\Omega = \omega_n$ . In the supercritical region,<sup>3</sup> for  $\Omega > \omega_n$ ,  $r_0$  decreases and eventually,  $r_0 \rightarrow -\varepsilon$  as  $\Omega \rightarrow \infty$ ; the response is  $180^\circ$  out of phase with the excitation, meaning that  $P$  tends to return to the origin. Thus, the rotor tends to be *self centering* at high speed (Fig.10.2).

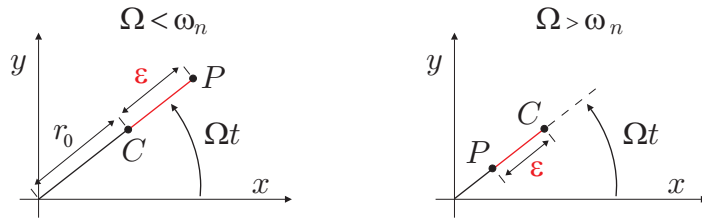


**Fig. 10.2.** Unbalanced response of the Jeffcott rotor;  $r_0 = \varepsilon\Omega^2/(\omega_n^2 - \Omega^2)$ . (a) In the subcritical region ( $\Omega < \omega_n$ ). (b) In the supercritical region ( $\Omega > \omega_n$ ) the rotor tends to be self centering.

### 10.2.2 Complex coordinates

As an alternative to the vector representation  $\mathbf{r}_c$  considered in the previous section, one can consider the complex number  $z_c(t) = x_c(t) + jy_c(t)$ . The use of complex coordinates is useful to represent the whirling motion of rotors. Multiplying the second equation (10.3) by  $j$  and adding to the first equation, one gets

$$m\ddot{z}_c + kz_c = m\varepsilon\Omega^2 e^{j\Omega t} + F_n \quad (10.5)$$

where  $F_n = F_x + jF_y$  denotes the non rotating forces. With these notations, the unbalance response ( $F_n = 0$ ) can be analyzed as follows: a

---

<sup>3</sup> Before the Jeffcott model, the Rankine shaft model was essentially that of Fig.3.8.a, where a linear oscillator is constrained to vibrate along an axis rotating with a constant velocity  $\Omega$ . As we saw in section 3.6.5, this system is subject to a divergent instability when  $\Omega > \sqrt{k/m}$  and cannot operate at supercritical velocities. Apparently, the Swedish engineer C. Laval was the first to run a steam turbine at a supercritical speed in 1889, demonstrating the weakness of Rankine's model.

particular solution of the form  $z_c(t) = z_0 e^{j\Omega t}$  exists with the complex amplitude  $z_0$  given by

$$(-m\Omega^2 + k)z_0 = m\varepsilon\Omega^2$$

or

$$z_0 = \varepsilon \frac{\Omega^2}{\omega_n^2 - \Omega^2} \quad (10.6)$$

Since  $\varepsilon$  is real, so is  $z_0$ , which means that the unbalanced response consists of a forward synchronous whirl aligned on the unbalance force. Once again, one observes the self centering property at supercritical speeds: for  $\Omega \rightarrow \infty$ ,  $z_0 \rightarrow -\varepsilon$ .

### 10.2.3 Free whirl

Consider the free motion in complex coordinates; it is governed by the homogeneous equation

$$m\ddot{z}_c + kz_c = 0$$

The solution has the form  $z_c = z_0 e^{st}$  provided that there exists a non trivial solution to the algebraic equation

$$(ms^2 + k)z_0 = 0$$

The solution exists if  $s = \pm j\omega_n$  and

$$z_c(t) = Z_1 e^{j\omega_n t} + Z_2 e^{-j\omega_n t} = z_f(t) + z_b(t) \quad (10.7)$$

where  $Z_1$  and  $Z_2$  are complex numbers depending on the initial conditions. The solution is the sum of two rotating vectors; the first one,  $z_f(t) = Z_1 e^{j\omega_n t}$  describes a circular forward whirl in the same direction as the spin of the shaft; the second one,  $z_b(t) = Z_2 e^{-j\omega_n t}$  describes a backward whirl in the direction opposed to the spin of the shaft (Fig.10.3). Both rotations take place at the frequency  $\omega_n = \sqrt{k/m}$  of the non rotating system. The distribution between the forward and the backward whirl depends on the initial conditions.

### 10.2.4 Jeffcott rotor with viscous damping

In most problems of structural dynamics, the damping has a beneficial effect: it attenuates the resonances and increases the stability. However, the effect of damping on rotor dynamics has unexpected features. One must

distinguish between the *stationary* damping forces which are associated with the stationary (non rotating) part of the machine and the *rotating* damping which is directly associated with the motion of the rotor. The stationary damping is always stabilizing while the rotating damping tends to be destabilizing at supercritical speeds.

The stationary damping may be introduced in Equ.(10.3) by adding external forces proportional to the absolute velocity

$$\mathbf{F}_s = \begin{Bmatrix} F_x \\ F_y \end{Bmatrix} = -c_s \begin{Bmatrix} \dot{x}_c \\ \dot{y}_c \end{Bmatrix}$$

where  $c_s$  is the stationary damping coefficient. Similarly, the rotating damping forces are associated with the velocity in the rotating frame

$$\mathbf{F}_r = \begin{Bmatrix} F_u \\ F_v \end{Bmatrix} = -c_r \begin{Bmatrix} \dot{u}_c \\ \dot{v}_c \end{Bmatrix}$$

where  $c_r$  is the rotating damping coefficient and  $u_c$  and  $v_c$  are the coordinates of  $C$  in rotating frame (Fig.10.4).  $\mathbf{F}_s$  is expressed in fixed frame and  $\mathbf{F}_r$  in rotating frame.  $u_c$  and  $v_c$  are related to the coordinates in stationary frame by

$$\begin{Bmatrix} u_c \\ v_c \end{Bmatrix} = \begin{bmatrix} \cos \Omega t & \sin \Omega t \\ -\sin \Omega t & \cos \Omega t \end{bmatrix} \begin{Bmatrix} x_c \\ y_c \end{Bmatrix} = R \begin{Bmatrix} x_c \\ y_c \end{Bmatrix} \quad (10.8)$$

It follows that

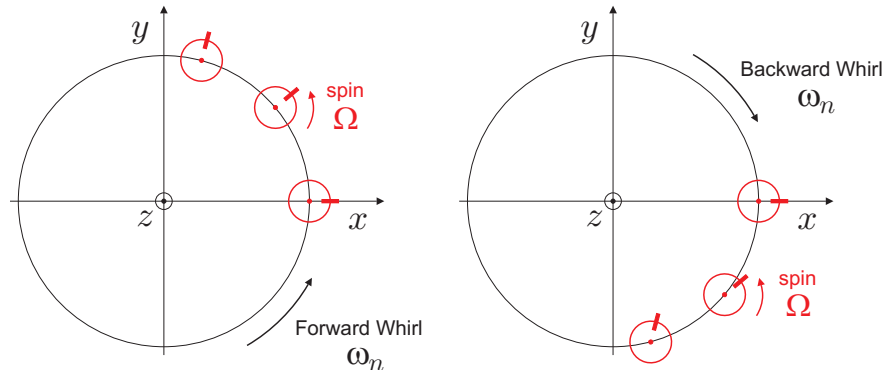


**Fig. 10.3.** (a) Forward whirl  $z_f(t) = Z_1 e^{j\omega_n t}$ : The spin velocity  $\Omega$  and the whirl velocity  $\omega_n$  are in the same direction; if  $\omega_n = \Omega$ , the whirl is synchronous. (b) Backward whirl  $z_b(t) = Z_2 e^{-j\omega_n t}$ : The spin velocity and the whirl velocity have opposite directions. The backward whirl mode is not excited by the imbalance forces.

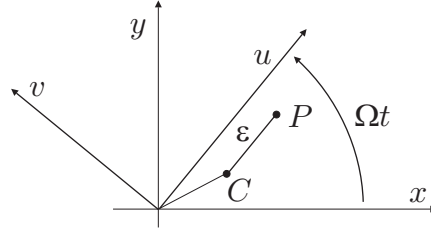


**Fig. 10.4.** Stationary frame and rotating frame; the coordinates of  $C$  are respectively  $(x_c, y_c)$  and  $(u_c, v_c)$ .

$$\begin{Bmatrix} \dot{u}_c \\ \dot{v}_c \end{Bmatrix} = \dot{R} \begin{Bmatrix} x_c \\ y_c \end{Bmatrix} + R \begin{Bmatrix} \dot{x}_c \\ \dot{y}_c \end{Bmatrix} \quad (10.9)$$

and the rotating damping forces are expressed in fixed frame as

$$\begin{Bmatrix} F_x \\ F_y \end{Bmatrix} = R^T \begin{Bmatrix} F_u \\ F_v \end{Bmatrix} = -c_r R^T \dot{R} \begin{Bmatrix} x_c \\ y_c \end{Bmatrix} - c_r \begin{Bmatrix} \dot{x}_c \\ \dot{y}_c \end{Bmatrix}$$

after using the property of a rotation matrix that  $R^T R = I$ . Besides, since

$$R^T \dot{R} = \Omega \begin{bmatrix} 0 & 1 \\ -1 & 0 \end{bmatrix} \quad (10.10)$$

one gets the following expression for the rotating damping forces expressed in stationary frame

$$\begin{Bmatrix} F_x \\ F_y \end{Bmatrix} = -c_r \Omega \begin{bmatrix} 0 & 1 \\ -1 & 0 \end{bmatrix} \begin{Bmatrix} x_c \\ y_c \end{Bmatrix} - c_r \begin{Bmatrix} \dot{x}_c \\ \dot{y}_c \end{Bmatrix} \quad (10.11)$$

Overall, after including the rotating and the stationary damping, Equ.(10.3) becomes

$$\begin{bmatrix} m & 0 \\ 0 & m \end{bmatrix} \begin{Bmatrix} \ddot{x}_c \\ \ddot{y}_c \end{Bmatrix} + \begin{bmatrix} c_s + c_r & 0 \\ 0 & c_s + c_r \end{bmatrix} \begin{Bmatrix} \dot{x}_c \\ \dot{y}_c \end{Bmatrix} + \begin{bmatrix} k & \Omega c_r \\ -\Omega c_r & k \end{bmatrix} \begin{Bmatrix} x_c \\ y_c \end{Bmatrix} = m\varepsilon\Omega^2 \begin{Bmatrix} \cos \Omega t \\ \sin \Omega t \end{Bmatrix} + \begin{Bmatrix} F_x \\ F_y \end{Bmatrix} \quad (10.12)$$

The rotational damping is responsible for a skew-symmetric term in the stiffness matrix, proportional to the spin velocity  $\Omega$ .

If one uses the complex coordinate  $z_c = x_c + jy_c$ , the equation governing the complex amplitude can be constructed by adding the first equation to the second one after multiplying by  $j$ ; one finds

$$m\ddot{z}_c + (c_s + c_r)\dot{z}_c + (k - jc_r\Omega)z_c = m\varepsilon\Omega^2 e^{j\Omega t} + F_n \quad (10.13)$$

The skew-symmetric term in the stiffness matrix in real coordinates appears as an imaginary term in the stiffness in complex coordinate.

### 10.2.5 Stability in presence of damping

The free whirling of the system with damping may be analyzed from the homogeneous part of either of the above equations (after cancelling the right hand side). Starting from Equ.(10.12),

$$\begin{bmatrix} m & 0 \\ 0 & m \end{bmatrix} \begin{Bmatrix} \ddot{x}_c \\ \ddot{y}_c \end{Bmatrix} + \begin{bmatrix} c_s + c_r & 0 \\ 0 & c_s + c_r \end{bmatrix} \begin{Bmatrix} \dot{x}_c \\ \dot{y}_c \end{Bmatrix} + \begin{bmatrix} k & \Omega c_r \\ -\Omega c_r & k \end{bmatrix} \begin{Bmatrix} x_c \\ y_c \end{Bmatrix} = 0 \quad (10.14)$$

Assuming a free response of the form  $\mathbf{r}_c = \mathbf{r}_0 e^{st}$ , the system is stable if the solutions  $s$  satisfy  $\text{Re}(s) \leq 0$ . Upon substituting  $\mathbf{r}_c$  in the previous equation,

$$\begin{bmatrix} ms^2 + (c_s + c_r)s + k & \Omega c_r \\ -\Omega c_r & ms^2 + (c_s + c_r)s + k \end{bmatrix} \begin{Bmatrix} x_0 \\ y_0 \end{Bmatrix} = 0 \quad (10.15)$$

A non trivial solution exists if the determinant vanishes. This gives the characteristic equation

$$[ms^2 + (c_s + c_r)s + k]^2 + \Omega^2 c_r^2 = 0 \quad (10.16)$$

Notice that, because of the rotating damping, the characteristic equation depends on the spin velocity  $\Omega$ . The stability may be analyzed with the Routh-Hurwitz stability criterion. After going through the burden of the algebra (which is omitted here), one can show that the system becomes unstable for

$$\Omega > \sqrt{\frac{k}{m}} \cdot (1 + \frac{c_s}{c_r}) \quad (10.17)$$

Thus, in the supercritical range, the stability is control by the ratio between the stationary damping  $c_s$  and the rotating damping  $c_r$ ; increasing the rotating damping will tend to reduce the spin velocity leading to instability; the rotating damping destabilizes the system.

### 10.3 Gyroscopic effects

The Jeffcott rotor assumes that the rotating disk can be represented by a point mass and ignores the angular momentum of the rotating disk. Such a simplistic representation cannot account for the gyroscopic effects, which result from the interaction between the spin of the disk and the bending of the shaft. This issue is considered below in the simplest way, using a two d.o.f. model obtained with the Rayleigh-Ritz method.

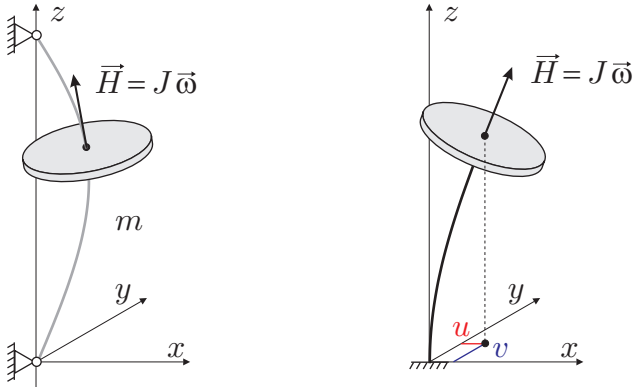


**Fig. 10.5.** Description of the kinematics of the bending of the shaft; the frame  $\{x, y, z\}$  is inertial; the  $z$  axis is aligned on the undeformed shaft and the disk is located at  $z = a$ . The bending of the shaft is assumed of the form  $u = f(z).q_1(t)$  and  $v = f(z).q_2(t)$ .

The shaft is assumed to be symmetric and massless; the disk is located at  $z = a$  along the shaft; it is characterized by its mass  $m$  and polar moment of inertia  $I_z$  and transversal moment of inertia  $I_x$ . Following the Rayleigh-Ritz approximation (Chapter 5), the transverse displacements in inertial frame are assumed of the form

$$\begin{aligned} u &= f(z).q_1(t) \\ v &= f(z).q_2(t) \end{aligned} \quad (10.18)$$

where  $f(z)$  is a shape function satisfying the geometric boundary conditions (Fig. 10.5) and  $q_1(t)$  and  $q_2(t)$  are the two generalized coordinates representing the transverse vibration of the shaft in the  $(x, z)$  plane and the  $(y, z)$  plane, respectively. The function  $f(z)$  is chosen in such a way that  $f(a) = 1$ , so that  $q_1(t)$  and  $q_2(t)$  are the displacements  $u$  and  $v$  of the elastic center of shaft at the location of the disk. The rotor is assumed to remain orthogonal to the shaft; its wobbling is represented by the two angles describing the slope of the rotor. Let  $\theta$  be the rotation of the disk about  $x$  and  $\psi$  the rotation about  $y$  ( $\theta$  and  $\psi$  are assumed to be small,  $\ll 1$ ). From Fig. 10.6 and the foregoing equation,

$$\begin{aligned} \theta &= -[\frac{\partial v}{\partial z}]_{z=a} = -f'(a).q_2(t) \\ \psi &= [\frac{\partial u}{\partial z}]_{z=a} = f'(a).q_1(t) \end{aligned} \quad (10.19)$$

[the negative sign for the first equation is due to the definition of the angle  $\theta$  about the  $x$  axis which is opposite to the definition of the slope of  $f(z)$  in the  $(y, z)$  plane].

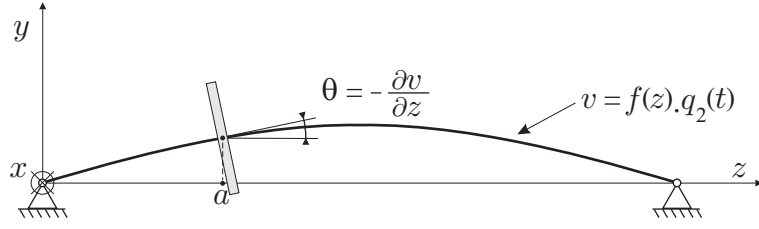


**Fig. 10.6.** Relation between the rotation of the disk and the bending of the shaft;  $\theta = -(\partial v / \partial z)_{z=a}$ . A similar figure may be drawn for the bending in the  $(x, z)$  plane, leading to  $\psi = (\partial u / \partial z)_{z=a}$ .

The strain energy may be expressed in the same form as for the Jeffcott rotor. Assuming that the shaft behaves as a Bernoulli beam without prestress, the strain energy reads<sup>4</sup>

$$V = \frac{1}{2} \int_0^L EI \left[ \left( \frac{\partial^2 u}{\partial z^2} \right)^2 + \left( \frac{\partial^2 v}{\partial z^2} \right)^2 \right] dz \quad (10.20)$$

Substituting  $u$  and  $v$  from Equ.(10.18), one finds

$$V = \frac{1}{2} k (q_1^2 + q_2^2) \quad (10.21)$$

where

$$k = \frac{1}{2} \int_0^L EI [f''(z)]^2 dz$$

This equation has exactly the form of Equ.(10.2). The kinetic energy is more complicated, because it includes not only the translational energy (associated with the translation of the center of mass), but also the rotational energy of the disk, which can be expressed simply only in a frame moving with the disk. Such a frame is obtained by performing two rotations as explained below.

### 10.3.1 Kinetic energy of a rigid disk

Since the disk is axisymmetric, two rotations are needed to transform the inertial frame  $\{x, y, z\}$  aligned on the undeformed axis of rotation into a moving frame where the tensor of inertia is diagonal (and constant):

1. Rotation  $\psi$  about the axis  $y$  of the inertial frame

---

<sup>4</sup> The Rayleigh-Ritz method may handle more complicated situations if the appropriate expression of the strain energy is used.

$$\{x, y, z\} \Rightarrow \{x_1, y, z_1\}$$

The rotation matrix is

$$R_\psi = \begin{bmatrix} \cos \psi & 0 & \sin \psi \\ 0 & 1 & 0 \\ -\sin \psi & 0 & \cos \psi \end{bmatrix} \quad (10.22)$$

**2.** Rotation  $\theta$  about the axis  $x_1$  of the moving frame

$$\{x_1, y, z_1\} \Rightarrow \{x_1, y_2, z_2\}$$

The rotation matrix is

$$R_\theta = \begin{bmatrix} 1 & 0 & 0 \\ 0 & \cos \theta & -\sin \theta \\ 0 & \sin \theta & \cos \theta \end{bmatrix} \quad (10.23)$$

The axis  $z_2$  is aligned on the deformed shaft; in the reference frame  $\{x_1, y_2, z_2\}$ , the disk rotates about  $z_2$  at  $\Omega$  (spin) and the inertia tensor about the center of mass is diagonal,

$$J = \begin{bmatrix} I_x & 0 & 0 \\ 0 & I_x & 0 \\ 0 & 0 & I_z \end{bmatrix} \quad (10.24)$$

The rotation velocity of the disk can be obtained as follows:

$$\vec{\omega} = \Omega \vec{z}_2 + \dot{\theta} \vec{x}_1 + \dot{\psi} \vec{y} \quad (10.25)$$

The first two components belong to the same reference frame; the third component may be transformed into the moving frame  $\{x_1, y_2, z_2\}$  using the rotation matrix  $R_\theta^T$ , and the result may be further simplified by taking advantage of small rotations, according to which  $\cos \theta \simeq 1$ ,  $\sin \theta \simeq \theta$ ,

$$\begin{bmatrix} 1 & 0 & 0 \\ 0 & \cos \theta & \sin \theta \\ 0 & -\sin \theta & \cos \theta \end{bmatrix} \begin{Bmatrix} 0 \\ \dot{\psi} \\ 0 \end{Bmatrix} = \begin{Bmatrix} 0 \\ \dot{\psi} \cos \theta \\ -\dot{\psi} \sin \theta \end{Bmatrix} \simeq \begin{Bmatrix} 0 \\ \dot{\psi} \\ -\dot{\psi} \theta \end{Bmatrix}$$

Finally, the absolute velocity is expressed in moving frame:

$$\boldsymbol{\omega} = \begin{Bmatrix} \dot{\theta} \\ \dot{\psi} \\ \Omega - \dot{\psi} \theta \end{Bmatrix} \quad (10.26)$$

and the rotational kinetic energy reads

$$\begin{aligned} T_\omega &= \frac{1}{2}\boldsymbol{\omega}^T J \boldsymbol{\omega} = \frac{1}{2}I_x(\dot{\theta}^2 + \dot{\psi}^2) + \frac{1}{2}I_z(\Omega - \dot{\psi}\theta)^2 \\ &\simeq \frac{1}{2}[I_x(\dot{\theta}^2 + \dot{\psi}^2) + I_z(\Omega^2 - 2\Omega\dot{\psi}\theta)] \end{aligned} \quad (10.27)$$

after deleting the higher order term  $(\dot{\psi}\theta)^2$ . As discussed in chapter 3, the rotational kinetic energy has the form  $T_\omega = T_2 + T_1 + T_0$  where  $T_2 = I_x/2(\dot{\theta}^2 + \dot{\psi}^2)$  is homogeneous quadratic in the generalized velocities  $\dot{\theta}$  and  $\dot{\psi}$ ,  $T_1 = -I_z\Omega\dot{\psi}\theta$  is homogeneous linear and  $T_0 = I_z\Omega^2/2$  is constant ( $T_0$  may be removed, because it will disappear in the derivatives of the Lagrange equations).  $T_1$  is responsible for the gyroscopic effects, proportional to the angular momentum  $I_z\Omega$  of the rotor.<sup>5</sup>

The total kinetic energy is the sum of the translational kinetic energy, associated with the motion of the center of mass, and the rotational kinetic energy,

$$T = \frac{1}{2}m[\ddot{u}^2(a) + \ddot{v}^2(a)] + \frac{1}{2}[I_x(\dot{\theta}^2 + \dot{\psi}^2) - 2I_z\Omega\dot{\psi}\theta] \quad (10.28)$$

Taking into account the kinematic assumptions (10.18) and the relationships between the angles and displacements, (10.19),

$$T = \frac{1}{2}M(\dot{q}_1^2 + \dot{q}_2^2) + \Omega\Theta \dot{q}_1 q_2 \quad (10.29)$$

where  $M = m + I_x f'(a)^2$  is the generalized mass and  $\Theta = I_z f'(a)^2$  is the gyroscopic constant (it is expressed in the same units as  $M$ ).

If a small eccentricity of the center of mass is included, in order to analyze the unbalance response of the rotor (Fig.10.1), the translational kinetic energy must be expressed according to Equ.(10.1), leading to the additional contribution

$$T_\varepsilon = m\varepsilon\Omega(-\dot{q}_1 \sin \Omega t + \dot{q}_2 \cos \Omega t) \quad (10.30)$$

As in the Jeffcott rotor, this term will be responsible for the rotating unbalanced forces.

---

<sup>5</sup> Note that the order in which the rotations were performed in this section was totally arbitrary; it could have been done in the opposite order,  $\theta$  first and  $\psi$  next; leading to  $\psi\dot{\theta}$  instead of  $\dot{\psi}\theta$  in the last term of  $T_\omega$ .

### 10.3.2 Dynamics including gyroscopic effects

Combining Equ.(10.21), (10.29) and (10.30), the Lagrangian of the system is

$$L = \frac{1}{2}M(\dot{q}_1^2 + \dot{q}_2^2) + \Omega\Theta \dot{q}_1 q_2 + m\varepsilon\Omega(-\dot{q}_1 \sin \Omega t + \dot{q}_2 \cos \Omega t) - \frac{1}{2}k(q_1^2 + q_2^2)$$

If there are external forces acting in the fixed reference frame, their virtual work is  $\delta W = F_1\delta q_1 + F_2\delta q_2$  and the Lagrange equations read

$$\begin{aligned} M\ddot{q}_1 + \Omega\Theta\dot{q}_2 + kq_1 &= m\varepsilon\Omega^2 \cos \Omega t + F_1 \\ M\ddot{q}_2 - \Omega\Theta\dot{q}_1 + kq_2 &= m\varepsilon\Omega^2 \sin \Omega t + F_2 \end{aligned} \quad (10.31)$$

or, in matrix form,

$$\begin{bmatrix} M & 0 \\ 0 & M \end{bmatrix} \ddot{\mathbf{q}} + \begin{bmatrix} 0 & \Omega\Theta \\ -\Omega\Theta & 0 \end{bmatrix} \dot{\mathbf{q}} + \begin{bmatrix} k & 0 \\ 0 & k \end{bmatrix} \mathbf{q} = m\varepsilon\Omega^2 \begin{Bmatrix} \cos \Omega t \\ \sin \Omega t \end{Bmatrix} + \mathbf{F} \quad (10.32)$$

with  $\mathbf{q} = (q_1, q_2)^T$  and  $\mathbf{F} = (F_1, F_2)^T$ . These equations may be further extended in a straightforward manner to include stationary and rotating damping as in section 10.2.4. They are identical to those of the Jeffcott rotor, except for the presence of the skew symmetric matrix of gyroscopic effects, whose magnitude is proportional to the angular momentum  $I_z\Omega$ .

If the complex coordinate  $z_c = q_1 + jq_2$  is used, the foregoing equations may be rewritten in the same way as in the previous section

$$M\ddot{z}_c - j\Omega\Theta\dot{z}_c + kz_c = m\varepsilon\Omega^2 e^{j\Omega t} + F_n \quad (10.33)$$

where  $F_n = F_1 + jF_2$ . Observe that, if  $\Theta = 0$  (i.e. if the angular momentum of the disk is neglected), this equation reduces itself to that of the Jeffcott rotor, Equ.(10.5).

### 10.3.3 Free whirl, Campbell diagram

The free motion of the rotor is governed (in complex coordinate) by

$$M\ddot{z}_c - j\Omega\Theta\dot{z}_c + kz_c = 0 \quad (10.34)$$

A solution of the form  $z_c = z_0 e^{st}$  exists where  $s$  is solution of the algebraic equation

$$Ms^2 - j\Omega\Theta s + k = 0 \quad (10.35)$$

The solutions are all imaginary,  $s = j\omega_1$  and  $s = -j\omega_2$  with

$$\omega_1 = \sqrt{\frac{k}{M} + \frac{\Omega^2 \Theta^2}{4M^2} + \frac{\Omega \Theta}{2M}}, \quad \omega_2 = \sqrt{\frac{k}{M} + \frac{\Omega^2 \Theta^2}{4M^2} - \frac{\Omega \Theta}{2M}} \quad (10.36)$$

The free response is

$$z_c = Z_1 e^{j\omega_1 t} + Z_2 e^{-j\omega_2 t} = z_f(t) + z_b(t) \quad (10.37)$$

where  $Z_1$  and  $Z_2$  are complex numbers depending on the initial conditions. Once again, the solution is the sum of two rotating vectors, a circular forward whirl (in the same direction as the spin of the shaft),  $z_f(t) = Z_1 e^{j\omega_1 t}$ , at the frequency  $\omega_1$  larger than the natural frequency of the non rotating shaft,  $\omega_n = \sqrt{k/M}$ , and a backward whirl (in the direction opposed to the spin of the shaft),  $z_b(t) = Z_2 e^{-j\omega_2 t}$ , at a frequency  $\omega_2 < \omega_n$ . Since the two eigenvalues are purely imaginary for all speeds, no instability occurs in absence of rotating damping. It is not difficult to extend the foregoing discussion to include viscous damping, following the same approach as in section 10.2. In presence of rotary damping, stability becomes an issue, as for the Jeffcott rotor.

The diagram of the natural frequencies as a function of the spin rotation is known as the *Campbell diagram* (Fig.10.7). The natural frequency of the forward whirl (FW),  $\omega_1$ , increases with  $\Omega$  while the of the backward whirl (BW),  $\omega_2$  decreases. Since many disturbances occur in relation with

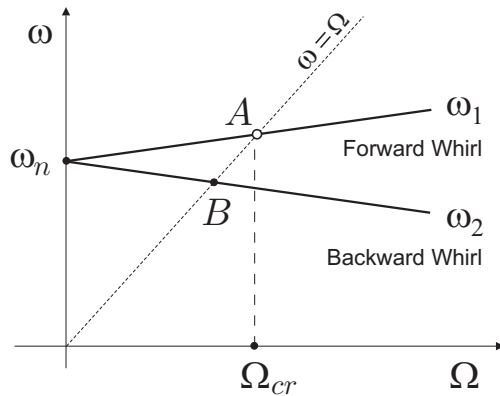


**Fig. 10.7.** Campbell diagram of the rotor with gyroscopic effects. The natural frequencies depend on the rotor speed. The straight line starting from the origin corresponds to  $\omega = \Omega$ . The critical speed  $\Omega_{cr}$  is the rotor speed when the imbalance excitation (at the rotor speed) is exactly tuned on the natural frequency  $\omega_1$  of the forward whirl, at point A in the diagram.

the spin velocity, it is important to avoid to operate at a spin velocity equal to a natural frequency of the rotor. For the forward whirl, this condition is achieved at the intersection between the natural frequency  $\omega_1$  and the line  $\omega = \Omega$ , for

$$\omega_1 = \sqrt{\frac{k}{M} + \frac{\Omega^2\Theta^2}{4M^2} + \frac{\Omega\Theta}{2M}} = \Omega$$

or

$$\Omega_{cr} = \sqrt{\frac{k}{M - \Theta}} \quad (10.38)$$

This spin velocity corresponds to point *A* on the Campbell diagram and  $\Omega_{cr}$  is the *critical velocity*. Observe that there is no solution for  $\Theta > M$  (we will come back to this later). For the backward whirl, the condition is

$$\omega_2 = \sqrt{\frac{k}{M} + \frac{\Omega^2\Theta^2}{4M^2} - \frac{\Omega\Theta}{2M}} = \Omega$$

or

$$\Omega = \sqrt{\frac{k}{M + \Theta}} \quad (10.39)$$

This corresponds to point *B* in the Campbell diagram.

More generally, some disturbances (e.g. from ball bearings) occur at frequencies related, but not equal to the spin velocity; the condition for the spin velocity to be a multiple of the natural frequency ( $\omega_i = \alpha\Omega$ ) is, for the forward whirl,

$$\omega_1 = \sqrt{\frac{k}{M} + \frac{\Omega^2\Theta^2}{4M^2} + \frac{\Omega\Theta}{2M}} = \alpha\Omega$$

or

$$\Omega = \sqrt{\frac{k}{\alpha(\alpha M - \Theta)}} \quad (10.40)$$

and for the backward whirl

$$\omega_2 = \sqrt{\frac{k}{M} + \frac{\Omega^2\Theta^2}{4M^2} - \frac{\Omega\Theta}{2M}} = \alpha\Omega$$

or

$$\Omega = \sqrt{\frac{k}{\alpha(\alpha M + \Theta)}} \quad (10.41)$$

### 10.3.4 Unbalance response

The unbalance response is governed by

$$M\ddot{z}_c - j\Omega\Theta\dot{z}_c + kz_c = m\varepsilon\Omega^2 e^{j\Omega t} \quad (10.42)$$

A particular solution of the form  $z_c(t) = z_0 e^{j\Omega t}$  of a forward whirl at the spin velocity exists with the complex amplitude

$$z_0 = \frac{m\varepsilon\Omega^2}{k + (\Theta - M)\Omega^2} \quad (10.43)$$

The amplitude of the response is illustrated in Fig.10.8. It tends to infinity at the critical frequency  $\Omega_{cr}$  defined by (10.38) (point *A* in the Campbell diagram of Fig.10.7). Thus, the critical speed is the rotor speed at which the unbalance excitation (at the rotor speed) is exactly tuned on the natural frequency of the forward whirl. Observe that the rotor does not respond to the mass unbalance at the frequency of the backward whirl (point *B* on the Campbell diagram). In general, rotors have more than one forward whirl modes and there are several critical speeds.

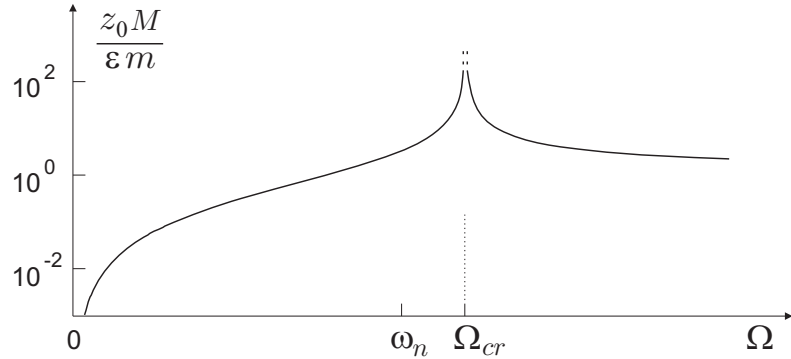


**Fig. 10.8.** Amplitude of the unbalanced response as a function of the spin velocity.

### 10.3.5 Response to an asynchronous force

The response to an asynchronous force corresponds to  $F_1 = F_0 \cos \omega t$  and  $F_2 = 0$  and  $\varepsilon = 0$ . Since  $\cos \omega t = \frac{1}{2}[e^{j\omega t} + e^{-j\omega t}]$ , Equ.(10.33) becomes

$$M\ddot{z}_c - j\Omega\Theta\dot{z}_c + kz_c = \frac{F_0}{2}[e^{j\omega t} + e^{-j\omega t}] \quad (10.44)$$

The excitation is the superposition of a forward rotating force at  $\omega$  and a backward rotating force of the same amplitude at the same frequency. The response may be found by superposition. The response to the forward rotating force has the form  $z_c = Z_1 e^{j\omega t}$  and, upon substituting in the foregoing equation, one finds

$$Z_1 = \frac{F_0/2}{k + \omega\Omega\Theta - \omega^2 M}$$

which has a resonance peak at  $\omega = \omega_1$  given by (10.36). Similarly, the response to the backward rotating force has the form  $z_c = Z_2 e^{-j\omega t}$  with

$$Z_2 = \frac{F_0/2}{k - \omega\Omega\Theta - \omega^2 M}$$

with a resonance peak at  $\omega = \omega_2$  given by (10.36). The overall response is the sum of these two contributions:

$$z_c = \frac{F_0}{2} \left[ \frac{e^{j\omega t}}{k + \omega\Omega\Theta - \omega^2 M} + \frac{e^{-j\omega t}}{k - \omega\Omega\Theta - \omega^2 M} \right] \quad (10.45)$$

The response is the sum of a forward whirl and a backward whirl whose amplitudes are illustrated in Fig. 10.9. The backward whirl dominates when  $\omega < \omega_n$  and the forward whirl dominates for  $\omega > \omega_n$ . Thus, the response to a sweeping asynchronous force has two peaks, respectively at  $\omega_1$  and  $\omega_2$  given by (10.36). This property may be used to reconstruct the Campbell diagram by performing tests at various rotor speeds.

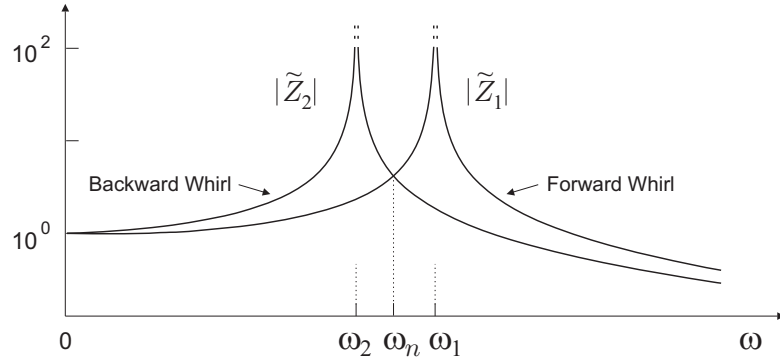


**Fig. 10.9.** Response to an asynchronous force  $F_1 = F_0 \cos \omega t$ . Amplification of the forward and the backward whirl;  $|\tilde{Z}_i| = 2k|Z_i|/F_0$ . The backward whirl dominates for  $\omega < \omega_n$  and the forward whirl dominates for  $\omega > \omega_n$ .

### 10.4 Rigid rotor on elastic supports

In this section, we consider a rigid rotor on elastic supports with isotropic stiffness  $k$  (Fig.10.10). The center of mass  $C$  of the rotor is located at distances  $a$  and  $b$  from the bearings; the polar moment of inertia is  $I_z$  and the transversal moment of inertia is  $I_x$  (identical in all directions orthogonal to  $z$ ). If  $I_z > I_x$ , the body is referred to as a *disk* (for a thin disk,  $I_z = 2I_x$ ); if  $I_x > I_z$ , it is called a *long rotor*. The system kinematics

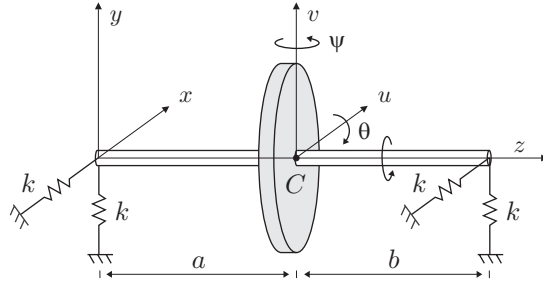


**Fig. 10.10.** Rigid axisymmetric rotor on isotropic elastic supports.

is described by 4 coordinates: the transverse displacements ( $u, v$ ) of the center of mass, and the (small) rotations of the system:  $\theta$  about  $x$  (positive according to the “corkscrew rule”) and  $\psi$  about  $y$ . With these coordinates, the displacements at the supports are respectively:

$$\begin{aligned} u_1 &= u - \psi a & u_2 &= u + \psi b \\ v_1 &= v + \theta a & v_2 &= v - \theta b \end{aligned} \quad (10.46)$$

The strain energy in the elastic supports reads

$$V = \frac{1}{2}k(u_1^2 + v_1^2 + u_2^2 + v_2^2)$$

and, combining with the equations describing the kinematics,

$$V = \frac{1}{2}k[2u^2 + 2v^2 + (\psi^2 + \theta^2)(a^2 + b^2) + (2u\psi - 2v\theta)(b - a)] \quad (10.47)$$

If the rotor is symmetric with respect to its supports,  $a = b$  and the last term disappears. The kinetic energy of the rigid rotor is the sum of the translational kinetic energy of the center of mass and the rotational

kinetic energy about the center of mass, given by Equ.(10.27). The total kinetic energy is

$$T = \frac{1}{2}m(\dot{u}^2 + \dot{v}^2) + \frac{1}{2}[I_x(\dot{\theta}^2 + \dot{\psi}^2) + I_z(\Omega^2 - 2\Omega\dot{\psi}\theta)] \quad (10.48)$$

From now on, we will assume that the rotor is symmetric with respect to its supports,  $a = b$ . The four Lagrange equations are

$$\begin{aligned} m\ddot{u} + 2ku &= 0 \\ m\ddot{v} + 2kv &= 0 \end{aligned} \quad (10.49)$$

$$\begin{aligned} I_x\ddot{\theta} + I_z\Omega\dot{\psi} + 2ka^2\theta &= 0 \\ I_x\ddot{\psi} - I_z\Omega\dot{\theta} + 2ka^2\psi &= 0 \end{aligned} \quad (10.50)$$

Thus, for a rotor with symmetric supports ( $a = b$ ), the equations are decoupled in two independent sets: the first two are those of a Jeffcott rotor (of stiffness  $2k$ ) while the other two are identical to (the left hand side of ) Equ.(10.31). Introducing the complex coordinates  $z_c = u + jv$  and  $q_c = \theta + j\psi$ , they are rewritten

$$m\ddot{z}_c + 2kz_c = 0 \quad (10.51)$$

$$I_x\ddot{q}_c - jI_z\Omega\dot{q}_c + K_\phi q_c = 0 \quad (10.52)$$

with the notation  $K_\phi = 2ka^2$ . The first equation has already been discussed for the Jeffcott rotor; it corresponds to a cylindrical mode whose frequency is not affected by the spin velocity  $\Omega$ . The second equation corresponds to a conical mode (Fig.10.11); the eigenvalues have already been analyzed in section 10.3.3; a solution of the form  $q_c = q_0 e^{st}$  exists if  $s$  is solution of the algebraic equation

$$I_x s^2 - jI_z\Omega s + K_\phi = 0 \quad (10.53)$$

The solutions are purely imaginary and consist of a *Forward Whirl* (FW) at  $s = j\omega_1$

$$\omega_1 = \sqrt{\frac{K_\phi}{I_x} + \frac{I_z^2\Omega^2}{4I_x^2}} + \frac{I_z\Omega}{2I_x} \quad (10.54)$$

and a *Backward Whirl* (BW) at  $s = -j\omega_2$

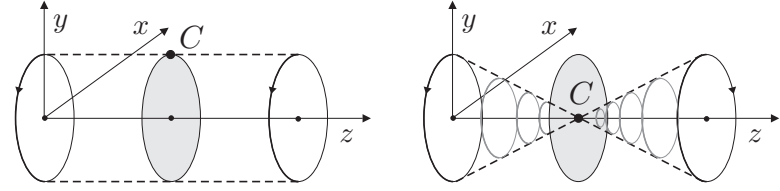


**Fig. 10.11.** Mode shapes of the rigid axisymmetric rotor on isotropic elastic supports.  
(a) Cylindrical mode. (b) Conical mode. The frequency of the cylindrical mode is not affected by gyroscopic effects.

$$\omega_2 = \sqrt{\frac{K_\phi}{I_x} + \frac{I_z^2 \Omega^2}{4I_x^2}} - \frac{I_z \Omega}{2I_x} \quad (10.55)$$

Using the ratio  $\delta = I_z/I_x$  and  $\omega_0 = \sqrt{K_\phi/I_x}$  ( $\omega_0$  is the natural frequency when the spin velocity is  $\Omega = 0$ )

$$\omega_1 = \sqrt{\omega_0^2 + \frac{\delta^2 \Omega^2}{4}} + \frac{\delta \Omega}{2} \quad (10.56)$$

$$\omega_2 = \sqrt{\omega_0^2 + \frac{\delta^2 \Omega^2}{4}} - \frac{\delta \Omega}{2} \quad (10.57)$$

The Campbell diagram of the conical modes is represented in Fig.10.12;

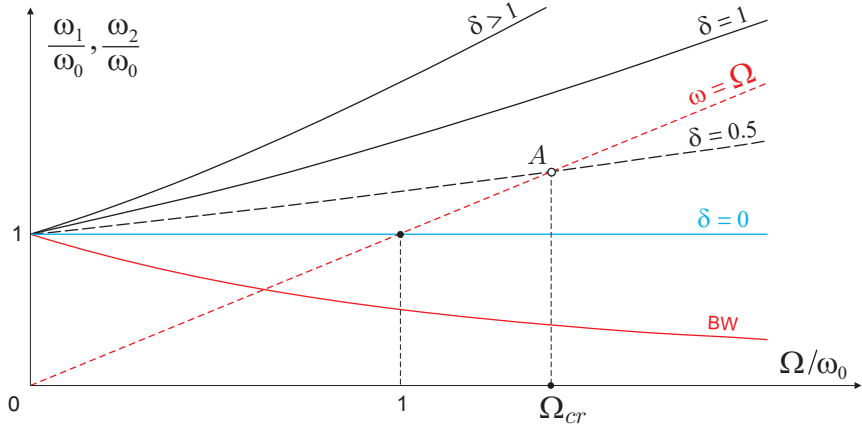


**Fig. 10.12.** Rigid axisymmetric rotor on isotropic elastic supports: Campbell diagram of the conical modes for various values of the ratio  $\delta = I_z/I_x$ . The downward curve BW refers to the backward mode. The increasing curves refer to the forward mode for various values of  $\delta = I_z/I_x$ . The critical speed corresponds to point A; there is no critical speed if  $\delta > 1$ .

the frequency  $\omega_2$  of the backward whirl decreases with  $\Omega$  and goes to 0 as  $\Omega \rightarrow \infty$ . The frequency  $\omega_1$  of the forward whirl is increasing with  $\Omega$  and is asymptotically  $\omega_1 = \delta\Omega$ . It follows that for a disk like rotor such that  $\delta > 1$ , there is no intersection with the line  $\omega = \Omega$ , which means that there is no critical speed. For a long rotor ( $\delta < 1$ ), there is a critical speed, given by Equ.(10.38); in this case

$$\Omega_{cr} = \sqrt{\frac{K_\phi}{I_x - I_z}} \quad (10.58)$$

The complete Campbell diagram of the rigid rotor is shown in Fig.10.13 for the two situations where the frequency  $\omega_0$  of the conical mode is either lower or higher than that of the cylindrical mode (which is not affected by the rotor speed).

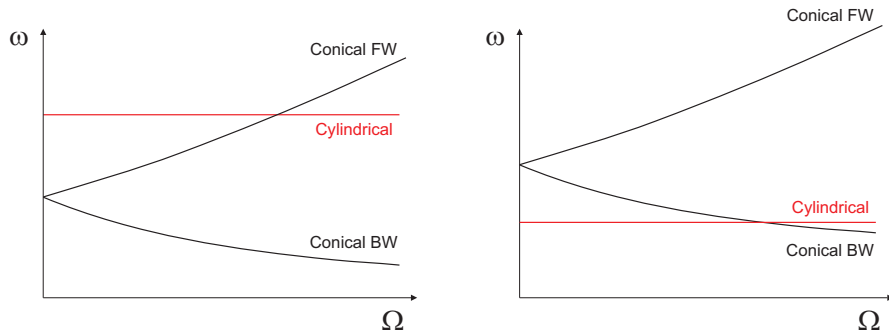


**Fig. 10.13.** Campbell diagram of the rigid rotor. (a) The frequency  $\omega_0$  of the conical mode is lower than that of the cylindrical mode. (b) Higher.

## 10.5 Anisotropy of the shaft and the supports

The Jeffcott rotor is sufficient to analyze various forms of anisotropy.

### 10.5.1 Anisotropic supports

If the supports have an anisotropic stiffness, a force applied in one direction produces, in general, a displacement in another direction (Fig.10.14). The polar diagram of the stiffness in fixed frame is an ellipse and we assume that the principal elastic axes are along  $Ox$  and  $Oy$ , with

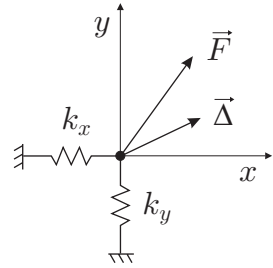


**Fig. 10.14.** Support with anisotropic stiffness; a force  $\vec{F}$  produces in general a displacement  $\vec{\Delta}$  in another direction.

$$F_x = -k_x x, \quad F_y = -k_y y$$

Assuming that the Jeffcott rotor consists of a rigid shaft supported by an elastic support, the entire stiffness of the system is provided by the support, leading to the governing equation

$$\begin{aligned} m\ddot{x}_c + k_x x_c &= m\varepsilon\Omega^2 \cos \Omega t + F_x \\ m\ddot{y}_c + k_y y_c &= m\varepsilon\Omega^2 \sin \Omega t + F_y \end{aligned} \quad (10.59)$$

where the right hand side contains, as in section 10.2, the unbalance force and the external force applied to the system. Considering the homogeneous equation, it is clear that there are two natural frequencies (assuming  $k_x < k_y$ )

$$\omega_1 = \sqrt{\frac{k_x}{m}} \quad \text{and} \quad \omega_2 = \sqrt{\frac{k_y}{m}}$$

Since the gyroscopic effects have been ignored, these are independent of the spin velocity, and the Campbell diagram consists of two horizontal straight lines. Proceeding as in section 10.2.1, the unbalanced response has the form

$$\begin{cases} x_c = x_0 \cos \Omega t \\ y_c = y_0 \sin \Omega t \end{cases}$$

with

$$x_0 = \varepsilon \frac{m\Omega^2}{k_x - m\Omega^2} \quad \text{and} \quad y_0 = \varepsilon \frac{m\Omega^2}{k_y - m\Omega^2} \quad (10.60)$$

The orbit in the  $(x, y)$  plane is an ellipse with the principal axes directed along  $x$  and  $y$ . There are two critical speeds,  $\Omega_{cr1} = \omega_1$  for which the motion occurs in a straight line along the  $x$  axis, and  $\Omega_{cr2} = \omega_2$  corresponding to a straight line along the  $y$  axis. For  $\Omega < \Omega_{cr1}$ , the response in the two planes have the same sign and are  $90^\circ$  out of phase; the orbit

is an ellipse in the forward direction, which elongates along the  $x$  axis as  $\Omega$  approaches  $\Omega_{cr1}$  (Fig. 10.15). For  $\Omega_{cr1} < \Omega < \Omega_{cr2}$ , the response along  $x$  is negative while that along  $y$  is positive; they produce an elliptical motion in the backward direction; the ellipse is elongated along the  $x$  axis when  $\Omega$  is close to  $\Omega_{cr1}$  and it is elongated along the  $y$  axis when  $\Omega$  approaches  $\Omega_{cr2}$ . For some value of  $\Omega$ , the trajectory is circular. It is quite remarkable that this backward synchronous whirl may be excited by the unbalance excitation which is, by nature, in the forward direction. For  $\Omega > \Omega_{cr2}$ , the amplitudes along the two axes have again the same sign, which corresponds to an elliptic orbit in the forward direction, initially elongated along the  $y$  axis when  $\Omega$  is close to  $\Omega_{cr2}$ , and it becomes eventually a circle as  $\Omega \rightarrow \infty$ , because both amplitudes  $x_0$  and  $y_0$  are asymptotically equal to  $-\varepsilon$ . Thus, the rotor tends to be self-centering, also with anisotropic supports.

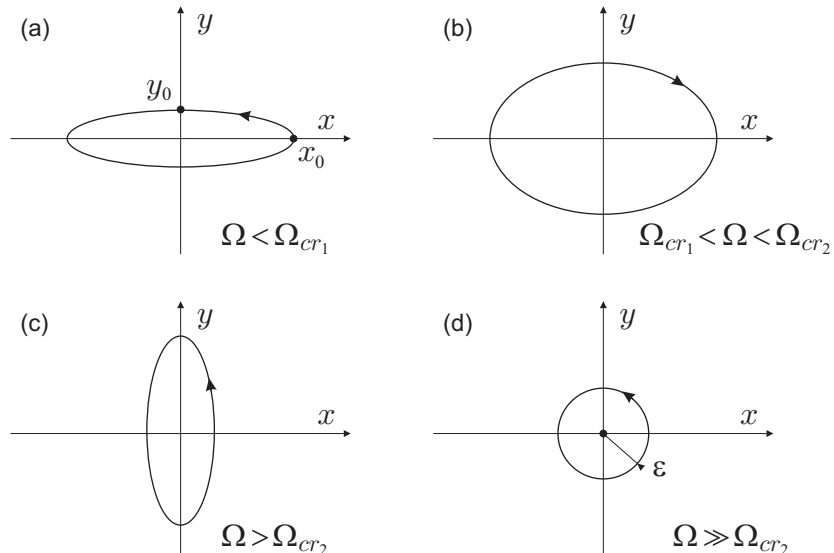


**Fig. 10.15.** Orbits of a Jeffcott rotor with anisotropic support, for various values of the spin velocity. For  $\Omega < \Omega_{cr1}$ , the orbit is an ellipse in the forward direction. When  $\Omega_{cr1} < \Omega < \Omega_{cr2}$ , the orbit is an ellipse in the backward direction. For  $\Omega > \Omega_{cr2}$ , the orbit is an ellipse in the forward direction again, and for  $\Omega \gg \Omega_{cr2}$ , the orbit becomes a circle of radius  $\varepsilon$  in the forward direction.

### 10.5.2 Anisotropic shaft

Consider the Jeffcott rotor with an anisotropic shaft (e.g. with a rectangular cross section, Fig.10.16.a) The polar diagram of the stiffness is an ellipse in rotating frame,<sup>6</sup> with its principal axis along  $Ou$  and  $Ov$ , and

$$\begin{Bmatrix} F_u \\ F_v \end{Bmatrix} = \begin{bmatrix} -k_u & 0 \\ 0 & -k_v \end{bmatrix} \begin{Bmatrix} u_c \\ v_c \end{Bmatrix} \quad (10.61)$$

Since the elastic properties are constant in the rotating frame  $Ouv$ , we shall write the equation of motion in rotating frame. The coordinates of the elastic center  $C$  expressed in two reference frames,  $\mathbf{r}_c = (x_c, y_c)^T$  in fixed frame and  $\mathbf{q}_c = (u_c, v_c)^T$  in rotating frame are related by the rotation matrix (10.8)

$$\mathbf{r}_c = \begin{Bmatrix} x_c \\ y_c \end{Bmatrix} = \begin{bmatrix} \cos \Omega t & -\sin \Omega t \\ \sin \Omega t & \cos \Omega t \end{bmatrix} \begin{Bmatrix} u_c \\ v_c \end{Bmatrix} = R^T \mathbf{q}_c \quad (10.62)$$

It follows that the absolute velocity is

$$\dot{\mathbf{r}}_c = \dot{R}^T \mathbf{q}_c + R^T \dot{\mathbf{q}}_c \quad (10.63)$$

or, after some elementary algebra,

$$\begin{aligned} \dot{x}_c &= \cos \Omega t (\dot{u}_c - \Omega v_c) - \sin \Omega t (\dot{v}_c + \Omega u_c) \\ \dot{y}_c &= \sin \Omega t (\dot{u}_c - \Omega v_c) + \cos \Omega t (\dot{v}_c + \Omega u_c) \end{aligned}$$

and, if one assumes that the mass  $m$  is located at the elastic center (no eccentricity) the kinetic energy reads

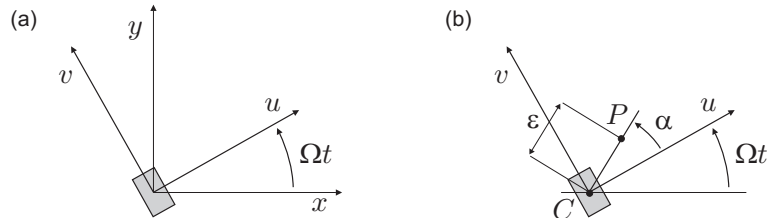


**Fig. 10.16.** (a) Rotor with anisotropic shaft. The elastic axes are assumed to coincide with  $Ou$  and  $Ov$ . (b) With eccentricity, the center of mass  $P$  is located at  $\varepsilon_u = \varepsilon \cos \alpha$  and  $\varepsilon_v = \varepsilon \sin \alpha$  in the rotating frame.

---

<sup>6</sup> in the previous section, the polar stiffness of the support was an ellipse in fixed frame.

$$T = \frac{1}{2}m(\dot{x}_c^2 + \dot{y}_c^2) = \frac{1}{2}m[(\dot{u}_c - \Omega v_c)^2 + (\dot{v}_c + \Omega u_c)^2] \quad (10.64)$$

This form is identical to Equ.(3.35) in section 3.6.6. The strain energy can be written similarly

$$V = \frac{1}{2}k_u u_c^2 + \frac{1}{2}k_v v_c^2 \quad (10.65)$$

Thus, the Lagrangian of the (perfectly balanced) Jeffcott rotor in rotating coordinates has the same form as that of the system considered in section 3.6.6; consequently, the inertia and elastic contributions to the governing equations will be the same. Let us examine the damping forces.

As in section 10.2.4, the damping forces consist of a stationary part, associated with the velocity in the fixed frame, and given in fixed frame by  $\mathbf{F}_s = -c_s \dot{\mathbf{r}}_c$ , and a rotating one, associated with the velocity in rotating frame, given (in rotating frame) by  $\mathbf{F}_r = -c_r \dot{\mathbf{q}}_c$ . The projection of the stationary damping forces in rotating frame is  $R\mathbf{F}_s$ . Overall, the damping forces expressed in rotating frame are

$$\mathbf{F}_q = R\mathbf{F}_s + \mathbf{F}_r \quad (10.66)$$

and, substituting  $\dot{\mathbf{r}}_c$  from Equ.(10.63), taking into account that  $RR^T = I$ , one finds

$$\mathbf{F}_q = -c_s(R\dot{R}^T)\mathbf{q}_c - (c_s + c_r)\dot{\mathbf{q}}_c \quad (10.67)$$

with

$$R\dot{R}^T = \Omega \begin{bmatrix} 0 & -1 \\ 1 & 0 \end{bmatrix} \quad (10.68)$$

Upon writing the Lagrange equations, one finds

$$\begin{bmatrix} m & 0 \\ 0 & m \end{bmatrix} \begin{Bmatrix} \ddot{u}_c \\ \ddot{v}_c \end{Bmatrix} + \begin{bmatrix} c_s + c_r & -2m\Omega \\ 2m\Omega & c_s + c_r \end{bmatrix} \begin{Bmatrix} \dot{u}_c \\ \dot{v}_c \end{Bmatrix} + \begin{bmatrix} k_u - \Omega^2 m & -c_s \Omega \\ c_s \Omega & k_v - \Omega^2 m \end{bmatrix} \begin{Bmatrix} u_c \\ v_c \end{Bmatrix} = 0 \quad (10.69)$$

The reader will observe that this equation is identical to (3.36), except for the damping term which, in the present case, consists of two identical components  $c_r$  along the rotating axis and two equal components  $c_s$  along the fixed frames.<sup>7</sup> Before examining the stability of this homogeneous equation, let us consider the effect of an eccentricity.

---

<sup>7</sup> In the analysis of the Jeffcott rotor with damping, the shaft stiffness was isotropic and Equ.(10.12) was written in fixed frame. On the contrary, Equ.(10.69) is written in rotating frame, because of the anisotropy of the shaft.

### 10.5.3 Unbalance response of an anisotropic shaft

If the eccentricity is added, the center of mass is located at  $\varepsilon$  at an angle  $\alpha$  from the axis  $Ou$  (Fig.10.16.b);  $P$  is at  $u_p = \varepsilon_u = \varepsilon \cos \alpha$  and  $v_p = \varepsilon_v = \varepsilon \sin \alpha$  in the rotating frame; It follows from Equ.(10.63) that the velocity of the center of mass in fixed frame is given by

$$\begin{Bmatrix} \dot{x}_p \\ \dot{y}_p \end{Bmatrix} = \dot{R}^T \begin{Bmatrix} u_c + \varepsilon_u \\ v_c + \varepsilon_v \end{Bmatrix} + R^T \begin{Bmatrix} \dot{u}_c \\ \dot{v}_c \end{Bmatrix} \quad (10.70)$$

The kinetic energy becomes slightly more complicated

$$\begin{aligned} T = \frac{1}{2}m(\dot{x}_p^2 + \dot{y}_p^2) &= \frac{1}{2}m[(\dot{u}_c - \Omega v_c)^2 + (\dot{v}_c + \Omega u_c)^2 \\ &\quad + 2(\dot{v}_c + \Omega u_c)\Omega \varepsilon_u - 2(\dot{u}_c - \Omega v_c)\Omega \varepsilon_v + \Omega^2 \varepsilon^2] \end{aligned} \quad (10.71)$$

Upon writing the Lagrange equations, the unbalance excitation appears in the right hand side of the equation; everything else remains the same.

$$\begin{aligned} \begin{bmatrix} m & 0 \\ 0 & m \end{bmatrix} \begin{Bmatrix} \ddot{u}_c \\ \ddot{v}_c \end{Bmatrix} + \begin{bmatrix} c_s + c_r & -2m\Omega \\ 2m\Omega & c_s + c_r \end{bmatrix} \begin{Bmatrix} \dot{u}_c \\ \dot{v}_c \end{Bmatrix} + \\ \begin{bmatrix} k_u - \Omega^2 m & -c_s \Omega \\ c_s \Omega & k_v - \Omega^2 m \end{bmatrix} \begin{Bmatrix} u_c \\ v_c \end{Bmatrix} = \begin{Bmatrix} m\Omega^2 \varepsilon_u \\ m\Omega^2 \varepsilon_v \end{Bmatrix} \end{aligned} \quad (10.72)$$

Thus, the unbalance excitation is constant in rotating frame, and the steady state response is solution of

$$\begin{bmatrix} k_u - \Omega^2 m & -c_s \Omega \\ c_s \Omega & k_v - \Omega^2 m \end{bmatrix} \begin{Bmatrix} u_c \\ v_c \end{Bmatrix} = \begin{Bmatrix} m\Omega^2 \varepsilon_u \\ m\Omega^2 \varepsilon_v \end{Bmatrix} \quad (10.73)$$

In absence of stationary damping,

$$u_c = \varepsilon_u \frac{m\Omega^2}{k_u - m\Omega^2} \quad \text{and} \quad v_c = \varepsilon_v \frac{m\Omega^2}{k_v - m\Omega^2} \quad (10.74)$$

This corresponds to a circular whirling with a constant amplitude in the fixed frame. There are two critical velocities for which the amplitude is unbounded:

$$\Omega_{cr1} = \omega_1 = \sqrt{\frac{k_u}{m}} \quad \text{and} \quad \Omega_{cr2} = \omega_2 = \sqrt{\frac{k_v}{m}} \quad (10.75)$$

#### 10.5.4 Stability of an anisotropic shaft

Let us now return to the homogeneous equation (10.69) and examine the conditions for stability in the absence of damping. Assuming a solution of the form  $\mathbf{q}_c = \mathbf{q}_0 e^{st}$ , the system is stable if the solutions  $s$  satisfy  $\text{Re}(s) \leq 0$ . Upon substituting (assuming  $c_r = c_s = 0$ ), one finds

$$\begin{bmatrix} ms^2 + k_u - \Omega^2 m & -2m\Omega s \\ 2m\Omega s & ms^2 + k_v - \Omega^2 m \end{bmatrix} \begin{Bmatrix} u_0 \\ v_0 \end{Bmatrix} = 0 \quad (10.76)$$

or

$$\begin{bmatrix} s^2 + \omega_1^2 - \Omega^2 & -2\Omega s \\ 2\Omega s & s^2 + \omega_2^2 - \Omega^2 \end{bmatrix} \begin{Bmatrix} u_0 \\ v_0 \end{Bmatrix} = 0 \quad (10.77)$$

A non trivial solution exists if the determinant vanishes. This gives the characteristic equation

$$s^4 + s^2[\omega_1^2 + \omega_2^2 + 2\Omega^2] + (\omega_1^2 - \Omega^2)(\omega_2^2 - \Omega^2) = 0 \quad (10.78)$$

The third coefficient is positive for  $\Omega < \omega_1$  and  $\Omega > \omega_2$  (assuming that  $\omega_1 < \omega_2$ ), which will lead to purely imaginary eigenvalues; the system is stable. However, for  $\omega_1 < \Omega < \omega_2$ , the third coefficient of the characteristic equation becomes negative and the system is unstable.<sup>8</sup> Thus, the elastic anisotropy of the shaft is responsible for a range of unstable spin velocities in the interval between the critical velocities,

$$\omega_1 < \Omega < \omega_2 \quad (10.79)$$

Figure 10.17 shows the evolution of the real and imaginary parts of the eigenvalues; these are purely imaginary, except for  $\omega_1 < \Omega < \omega_2$  where the system is unstable (one of the eigenvalues has a positive real part).

In presence of rotating damping alone, Equ.(10.77) may be rewritten

$$\begin{bmatrix} s^2 + 2\xi_1\omega_1 s + \omega_1^2 - \Omega^2 & -2\Omega s \\ 2\Omega s & s^2 + 2\xi_2\omega_2 s + \omega_2^2 - \Omega^2 \end{bmatrix} \begin{Bmatrix} u_0 \\ v_0 \end{Bmatrix} = 0$$

The characteristic equation reads

---

<sup>8</sup> When the characteristic equation is written in the form

$$d(s) = s^n + a_1 s^{n-1} + a_2 s^{n-2} + \dots + a_n = 0$$

if one coefficient becomes negative, the system is unstable.

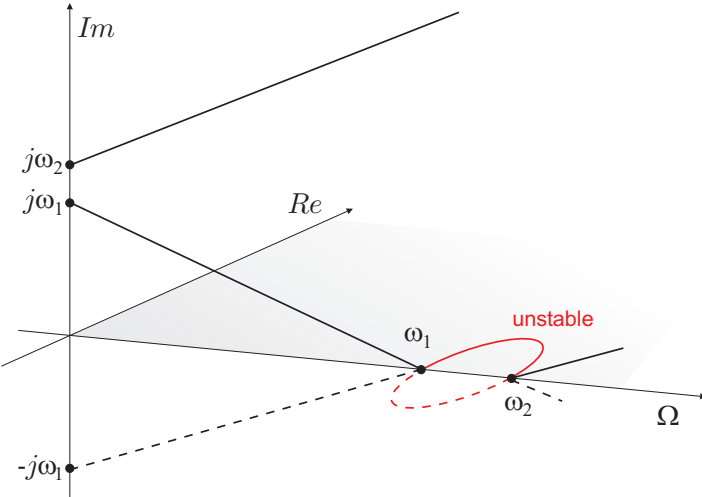


**Fig. 10.17.** Evolution with the spin velocity  $\Omega$  of the real and imaginary parts of the eigenvalues of an undamped rotor with anisotropic shaft. The imaginary part is the Campbell diagram starting from  $\omega_1$  and  $\omega_2$ . The eigenvalues are purely imaginary, except for  $\omega_1 < \Omega < \omega_2$  where they are real and one of them is positive.

$$\begin{aligned} s^4 + 2(\xi_1\omega_1 + \xi_2\omega_2)s^3 + [\omega_1^2 + \omega_2^2 + 2\Omega^2 + 4\xi_1\xi_2\omega_1\omega_2]s^2 + 2[\xi_1\omega_1 \\ (\omega_2^2 - \Omega^2) + \xi_2\omega_2(\omega_1^2 - \Omega^2)]s + (\omega_1^2 - \Omega^2)(\omega_2^2 - \Omega^2) = 0 \quad (10.80) \end{aligned}$$

The coefficients of the polynomial satisfy  $a_1 > 0$  and  $a_2 > 0$  for all  $\Omega$ ;  $a_4 < 0$  for  $\omega_1 < \Omega < \omega_2$  as in the undamped case, but

$$a_3 = 2[\xi_1\omega_1(\omega_2^2 - \Omega^2) + \xi_2\omega_2(\omega_1^2 - \Omega^2)] < 0$$

for all  $\Omega > \omega_2$ . Thus, in presence of rotating damping alone, the anisotropic rotor is unstable for all spin velocities above the critical frequencies. This result is consistent with Equ.(10.17) for an isotropic rotor. In more complicated situations, the frequency range of stability may be identified by tracking the eigenvalues of Equ.(10.69) for different values of the spin velocity  $\Omega$ .

## 10.6 Vibrating angular rate sensor

Angular rate sensors are used in many control systems, including satellite attitude control or car dynamic stability systems (known as ESP). Vibrating angular rate sensors are based on Coriolis forces and are governed by

the same equations as rotors, which justifies their treatment here.<sup>9</sup> The system involves two lightly damped high frequency resonators with natural frequencies close, or equal to each other; one of them is harmonically excited at a frequency close to the resonance, while the other is excited by the Coriolis force due to the rotation, and constitutes the output of the sensor.

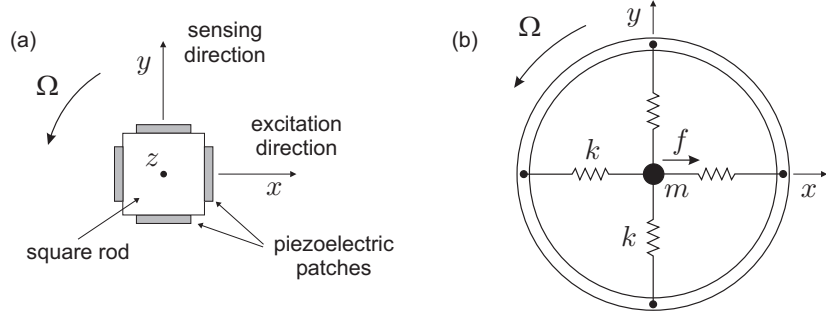


**Fig. 10.18.** Vibrating angular rate sensor. (a) Conceptual design: the rod with a square cross section is excited along  $Ox$  by piezoelectric patches acting as a bimorph actuator, while another set of piezoelectric patches constitutes the sensing element along the orthogonal direction  $Oy$ . (b) Model: point mass supported by two orthogonal springs with identical stiffness, mounted on a rotating support; the mass is excited by a force along  $Ox$ . The frequency of the oscillator is much larger than the angular speed to measure,  $\omega_n \gg \Omega$ .

Figure 10.18.a shows a conceptual design of such a sensor (there are many possible configurations); it consists of a rod with a square cross section is excited along  $Ox$  by piezoelectric patches acting as a bimorph actuator, while another set of piezoelectric patches constitutes the sensing element along the orthogonal direction  $Oy$ . Because of the square cross section, the two modes have the same natural frequency  $\omega_n$ , which is much larger than the angular velocity to measure,  $\omega_n \gg \Omega$ . The system may be modelled as in Fig.10.18.b, with the harmonic force  $f$  acting along the  $Ox$  axis (and rotating with it). This system has already been analyzed in section 3.6.6; the governing equations are

$$\begin{aligned} m\ddot{x} - 2m\Omega\dot{y} + kx - m\Omega^2x &= f \\ m\ddot{y} + 2m\Omega\dot{x} + ky - m\Omega^2y &= 0 \end{aligned} \quad (10.81)$$

<sup>9</sup> Note however that, contrary to rotors, the operating range of angular velocities  $\Omega$  is much smaller than the natural frequency of the vibrating system of the sensor.

where the damping has been neglected and the stiffness has been assumed isotropic. If the natural frequency  $\omega_n = \sqrt{k/m}$  is much larger than the angular speed to measure,  $\omega_n \gg \Omega$ , the centrifugal term may be neglected and the equation is rewritten

$$\begin{aligned}\ddot{x} - 2\Omega\dot{y} + \omega_n^2 x &= f/m \\ \ddot{y} + 2\Omega\dot{x} + \omega_n^2 y &= 0\end{aligned}\tag{10.82}$$

If the excitation is harmonic,  $f = f_0 e^{j\omega t}$ , the steady state response is also harmonic at the same frequency  $x = x_0 e^{j\omega t}$ ,  $y = y_0 e^{j\omega t}$ . Upon substituting in the foregoing equation, one finds the algebraic equation

$$\begin{bmatrix} \omega_n^2 - \omega^2 & -2j\omega\Omega \\ 2j\omega\Omega & \omega_n^2 - \omega^2 \end{bmatrix} \begin{Bmatrix} x_0 \\ y_0 \end{Bmatrix} = \begin{Bmatrix} f_0/m \\ 0 \end{Bmatrix}\tag{10.83}$$

leading to

$$\begin{aligned}x_0 &= \left[ \frac{\omega_n^2 - \omega^2}{(\omega_n^2 - \omega^2)^2 - 4\omega^2\Omega^2} \right] \frac{f_0}{m} \\ y_0 &= \left[ \frac{-2j\omega\Omega}{(\omega_n^2 - \omega^2)^2 - 4\omega^2\Omega^2} \right] \frac{f_0}{m} = \left[ \frac{-2j\omega\Omega}{\omega_n^2 - \omega^2} \right] x_0\end{aligned}\tag{10.84}$$

Thus, the Coriolis forces induce a vibration along the axis  $Oy$  orthogonal to the harmonic excitation; this vibration is  $90^\circ$  out of phase with the response along  $Ox$  and its amplitude is proportional to the rotation velocity  $\Omega$ . The sensitivity of the sensor is maximized if the excitation frequency  $\omega$  is close to the resonance frequency  $\omega_n$  (in practice the sensitivity is limited by the damping in the system and the dissipation in the transducting device).

## 10.7 Problems

**P.10.1** In the analysis of the gyroscopic effects (section 10.3.1), the rotation  $\psi$  was performed first followed by the rotation  $\theta$ ; in fact, the order is arbitrary. Show that, if the rotations are performed in the reverse order, the rotational kinetic energy in the disk may be written

$$T_\omega \simeq \frac{1}{2} [I_x(\dot{\theta}^2 + \dot{\psi}^2) + I_z(\Omega^2 + 2\Omega\psi\dot{\theta})]$$

instead of (10.27). Show that this eventually leads to the same set of equations (10.31).

**P.10.2** Consider a simply supported rotor; it consists of a steel shaft ( $E = 210$  GPa,  $\rho = 7800$  kg/m<sup>3</sup>) of  $l = 1$  m and 15 mm diameter, a steel disk of 300 mm diameter and 20 mm thickness, located at a distance  $a = 0.25$  m from a support.

1. Write the equations of the equivalent Jeffcott rotor.
2. Following the Rayleigh-Ritz method with  $f(z) = \sin(\pi z/l)$ , write the dynamic model including the gyroscopic effects.
3. Draw the Campbell diagram and calculate the critical velocity (if any).

**P.10.3** In the analysis of the rotor with gyroscopic effects (section 10.3), how would you handle a uniform axial preload acting on the shaft ?

**P.10.4** Rigid rotor on elastic support: Show that in the general case  $a \neq b$  (Fig.10.10), the equations of motion are no longer decoupled and become:

$$\begin{aligned} m\ddot{u} + 2ku + k(b-a)\psi &= 0 \\ m\ddot{v} + 2kv - k(b-a)\theta &= 0 \end{aligned} \quad (10.85)$$

$$\begin{aligned} I_x\ddot{\theta} + I_z\Omega\dot{\psi} + k(a^2 + b^2)\theta - k(b-a)v &= 0 \\ I_x\ddot{\psi} - I_z\Omega\dot{\theta} + k(a^2 + b^2)\psi + k(b-a)u &= 0 \end{aligned} \quad (10.86)$$

or in matrix form

$$M\ddot{\mathbf{q}} + G\dot{\mathbf{q}} + K\mathbf{q} = 0 \quad (10.87)$$

with  $\mathbf{q} = (u, v, \theta, \psi)^T$ ,  $M = \text{diag}(m, m, I_x, I_x)$ , and

$$G = \begin{bmatrix} 0 & 0 & 0 & 0 \\ 0 & 0 & 0 & 0 \\ 0 & 0 & 0 & I_z\Omega \\ 0 & 0 & -I_z\Omega & 0 \end{bmatrix} \quad K = \begin{bmatrix} 2k & 0 & 0 & k(b-a) \\ 0 & 2k & -k(b-a) & 0 \\ 0 & -k(b-a) & k(a^2 + b^2) & 0 \\ k(b-a) & 0 & 0 & k(a^2 + b^2) \end{bmatrix}$$

**P.10.5** Cantilever rotor (Stodola-Green rotor) with 4 d.o.f.: The rotor of Fig.10.19 consists of a disk of mass  $m$  and polar and transverse moments of inertia of respectively  $I_z$  and  $I_x$  and a shaft with uniform cross section. If the shaft is modeled as a massless cantilever single beam element, show that the equations of motion can be written in the form (10.87), with the same expression of the mass and the gyroscopic matrices, and the stiffness matrix:

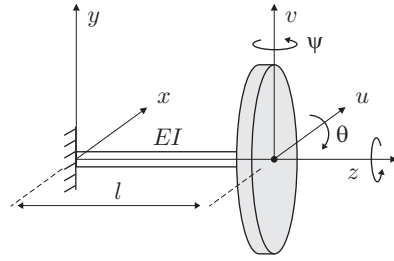


**Fig. 10.19.** Cantilever rotor (Stodola-Green rotor) with 4 d.o.f.

$$K = \begin{bmatrix} 12EI/l^3 & 0 & 0 & -6EI/l^2 \\ 0 & 12EI/l^3 & 6EI/l^2 & 0 \\ 0 & 6EI/l^2 & 4EI/l & 0 \\ -6EI/l^2 & 0 & 0 & 4EI/l \end{bmatrix}$$

Hint: the stiffness matrix of a beam element is given by Equ.(6.22); however the sign convention for the coordinates  $(v, \theta)$  describing the beam shape in the  $(z, y)$  plane is different from that used to describe the beam finite element. As a result, the stiffness matrix in  $(v, \theta)$  coordinates is

$$K = \frac{EI}{l^3} \begin{bmatrix} 12 & 6l \\ 6l & 4l^2 \end{bmatrix}$$

**P.10.6** Cantilever rotor with 2 d.o.f.: Assuming that the deformation of the shaft is that of a uniform beam statically loaded by a point force at the tip, the rotations are related to the translations by

$$\theta = -\frac{3}{2l}v, \quad \psi = \frac{3}{2l}u$$

Show that the equation of motion can be written

$$[m + I_x(\frac{3}{2l})^2] \begin{bmatrix} 1 & 0 \\ 0 & 1 \end{bmatrix} \begin{Bmatrix} \ddot{u} \\ \ddot{v} \end{Bmatrix} + I_z \Omega (\frac{3}{2l})^2 \begin{bmatrix} 0 & 1 \\ -1 & 0 \end{bmatrix} \begin{Bmatrix} \dot{u} \\ \dot{v} \end{Bmatrix} + \frac{3EI}{l^3} \begin{bmatrix} 1 & 0 \\ 0 & 1 \end{bmatrix} \begin{Bmatrix} u \\ v \end{Bmatrix} = 0$$

What is the condition for this system to have a critical speed? Establish the analytical expression of the critical speed.

# 11

---

## Vibration alleviation

*Un homme sage ni ne se laisse gouverner, ni ne cherche à gouverner les autres : il veut que la raison gouverne seule, et toujours.*

La Bruyère, *Les Caractères*, 1688

### 11.1 Introduction

Mechanical vibrations are sometimes beneficial (e.g. vibration transporters, ultrasonic vibration cleaning, or friction reduction), but most of the time they are harmful; they span amplitudes from meters (civil engineering) to nanometers (precision engineering) and frequencies from a fraction of a Hertz to several kHz. Their detrimental effect on systems may be of various natures:

**Failure:** vibration-induced structural failure may occur by excessive strain during transient events (e.g. building response to earthquake), by instability due to particular operating conditions (flutter of bridges under wind excitation), or simply by fatigue (mechanical parts in machines).

**Comfort:** examples where vibrations are detrimental to comfort are numerous: noise and vibration in helicopters, car suspensions, wind-induced sway of buildings.

**Operation of precision devices:** numerous systems in precision engineering, especially optical systems, put severe restrictions on mechanical vibrations. Precision machine tools, wafer steppers and telescopes are typical examples [*Moore's law* on the number of transistors on an integrated circuit could not hold without a constant improvement of the accuracy of wafer steppers and other precision machines]. The performances of large interferometers such as the VLTI<sup>1</sup> are limited by microvibrations affecting the various parts of the optical path.

---

<sup>1</sup> *Very Large Telescope Interferometer* built and operated by ESO in Paranal (Chili).

Vibration reduction can be achieved in many different ways, depending on the problem; the most common are stiffening, damping and isolation. *Stiffening* consists of shifting the resonance frequency of the structure beyond the frequency band of excitation. *Damping* consists of reducing the resonance peaks by dissipating the vibration energy. *Isolation* consists of preventing the propagation of disturbances to sensitive parts of the systems.

Damping may be achieved passively with fluid dampers, eddy currents, elastomers or hysteretic elements, which transform the kinetic energy into heat. One can also use transducers as energy converters, to transform vibration energy into electrical energy that is dissipated in electrical networks, or stored (energy harvesting). Recently, *semi-active* devices have become available; they consist of passive devices with controllable properties. The *Magneto-Rheological* (MR) fluid damper is a famous example, which is commonly used in modern car suspensions.

The first part of this chapter is devoted to the celebrated *Dynamic Vibration Absorbers* (DVA). The idea consists of transferring the kinetic energy of the vibrating structure to a properly tune and specially designed single d.o.f. oscillator, where it is dissipated.<sup>2</sup> Depending on the application, it can also be called *Tuned Mass Damper* (TMD). Dynamic Vibration Absorbers have been used very successfully to attenuate the wind response of tall buildings; they are also used extensively in helicopters.

The second part of this chapter is devoted to the vibration isolation between a disturbance source and a system which must remain quiet. This problem has also numerous applications in vehicles, precision machines and space structures.

## 11.2 Dynamic vibration absorber

Consider the single d.o.f. oscillator of mass  $m_1$ , excited by an external force  $f$  (Fig.11.1.a). The DVA consists of a secondary single d.o.f. system, attached to the first one, with properties such that the response of the primary system to the load  $f$  is reduced; the mass of the DVA is usually much smaller than that of the primary system, ( $m_2 \ll m_1$ ). The choice of the design parameters of the DVA,  $k_2$  and  $c_2$  depends on the nature of the excitation, and in particular if the excitation is wide band or harmonic.

---

<sup>2</sup> It was invented by H. Frahm in 1909; the underlying theory was developed by J. Ormondroyd and J.P. Den Hartog in 1928.

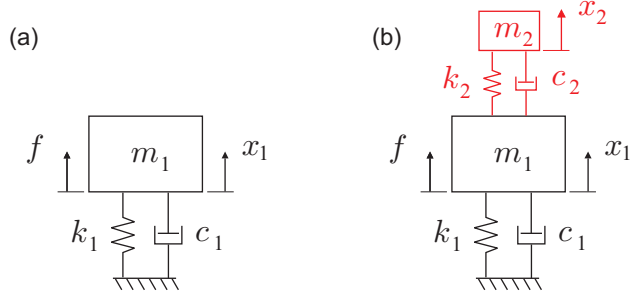


**Fig. 11.1.** (a) Single d.o.f. oscillator excited by an external force  $f$ . (b) Same system equipped with a DVA.

Let us first write the governing equations. The system of Fig.11.1.b is governed by the following equations:

$$\begin{bmatrix} m_1 & 0 \\ 0 & m_2 \end{bmatrix} \begin{Bmatrix} \ddot{x}_1 \\ \ddot{x}_2 \end{Bmatrix} + \begin{bmatrix} c_1 + c_2 & -c_2 \\ -c_2 & c_2 \end{bmatrix} \begin{Bmatrix} \dot{x}_1 \\ \dot{x}_2 \end{Bmatrix} + \begin{bmatrix} k_1 + k_2 & -k_2 \\ -k_2 & k_2 \end{bmatrix} \begin{Bmatrix} x_1 \\ x_2 \end{Bmatrix} = \begin{Bmatrix} f \\ 0 \end{Bmatrix}$$

or in Laplace form:

$$\begin{bmatrix} m_1 s^2 + (c_1 + c_2)s + (k_1 + k_2) & -c_2 s - k_2 \\ -c_2 s - k_2 & m_2 s^2 + c_2 s + k_2 \end{bmatrix} \begin{Bmatrix} x_1 \\ x_2 \end{Bmatrix} = \begin{Bmatrix} f \\ 0 \end{Bmatrix} \quad (11.1)$$

The determinant of the matrix is

$$\Delta(s) = [m_1 s^2 + (c_1 + c_2)s + (k_1 + k_2)][m_2 s^2 + c_2 s + k_2] - (c_2 s + k_2)^2 \quad (11.2)$$

and the solutions of the characteristic equation

$$\Delta(s) = 0 \quad (11.3)$$

are the poles of the system. Inverting Equ.(11.1), one easily gets

$$\begin{Bmatrix} x_1 \\ x_2 \end{Bmatrix} = \frac{1}{\Delta(s)} \begin{bmatrix} m_2 s^2 + c_2 s + k_2 & c_2 s + k_2 \\ c_2 s + k_2 & m_1 s^2 + (c_1 + c_2)s + (k_1 + k_2) \end{bmatrix} \begin{Bmatrix} f \\ 0 \end{Bmatrix} \quad (11.4)$$

This equation is the starting point for the analysis of the DVA.

### 11.3 Narrow band disturbance

Let us first consider the case of an harmonic excitation at the frequency  $\omega_0$ ,  $f = F e^{j\omega_0 t}$ . This is typically the case when the excitation comes

from the unbalance of a machine rotating at a constant speed, such as the rotor of an helicopter, which produces unbalance forces at a frequency multiple of the constant rotation frequency and the number of blades. The response of the system is also harmonic,  $x_1 = X_1 e^{j\omega_0 t}$  and  $x_2 = X_2 e^{j\omega_0 t}$ ; from Equ(11.4), one readily finds that

$$\frac{X_1}{F} = \frac{k_2 + j\omega_0 c_2 - \omega_0^2 m_2}{\Delta(j\omega_0)} \quad (11.5)$$

and

$$\frac{X_2}{X_1} = \frac{k_2 + j\omega_0 c_2}{k_2 + j\omega_0 c_2 - \omega_0^2 m_2} \quad (11.6)$$

The first of these equation suggests that if the excitation frequency  $\omega_0$  is constant, the best choice of the parameters is  $c_2 = 0$  and  $\omega_2 = \sqrt{k_2/m_2} = \omega_0$ . In this case, the transmission zero between  $f$  and  $x_1$  is purely imaginary and tuned on the frequency of the excitation, which is therefore canceled.  $c_2 = 0$  cannot be achieved exactly, but a small value will minimize the response  $X_1$ . The second equation may be rewritten

$$\frac{X_2}{X_1} \simeq \frac{1}{1 - (\omega_0/\omega_2)^2 + 2j\xi_2\omega_0/\omega_2} \quad (11.7)$$

This equation may be used to tune the DVA: The structure is excited harmonically at the frequency  $\omega_0$  while two sensors are used to measure  $x_1$  and  $x_2$ ; the frequency of the DVA is adjusted in such a way that the two signals  $x_1$  and  $x_2$  are  $90^\circ$  out of phase (see Fig.1.7). DVAs may be manufactured very simply with a cantilever plate with a tip mass whose position may be adjusted, Fig.11.2. The efficiency of the system depends very much on the quality of the tuning  $\omega_2 \simeq \omega_0$ .

## 11.4 Wide band disturbance

It is usual to introduce the following parameters:

$$\omega_1 = \sqrt{\frac{k_1}{m_1}}, \quad \omega_2 = \sqrt{\frac{k_2}{m_2}} \quad (11.8)$$

$$\xi_1 = \frac{c_1}{2m_1\omega_1}, \quad \xi_2 = \frac{c_2}{2m_2\omega_2} \quad (11.9)$$

$$\text{Mass ratio: } \mu = \frac{m_2}{m_1}, \quad \text{Frequency ratio: } \nu = \frac{\omega_2}{\omega_1} \quad (11.10)$$

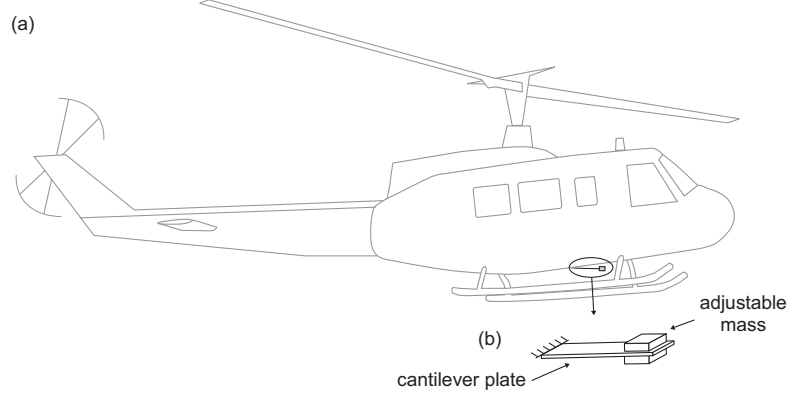


**Fig. 11.2.** (a) Helicopter with a DVA aimed at reducing the vibrations inside the cockpit. (b) DVA made of a cantilever plate with an adjustable tip mass.

Typically, the mass ratio is  $\mu \simeq 1$  to 3%, to limit the weight penalty associated with the DVA; the frequency ratio  $\nu$  and the damping ratio  $\xi_2$  of the DVA are the design parameters which are adjusted to optimize the performances of the absorber. The optimum values depend on the optimization criteria; in all cases,  $\nu$  is in general close to 1. From Equ.(11.4), the transmissibility between the disturbance  $f$  and the displacement of the primary mass is

$$\frac{x_1}{f} = \frac{m_2 s^2 + c_2 s + k_2}{(m_1 s^2 + c_1 s + k_1)(m_2 s^2 + c_2 s + k_2) + m_2 s^2(k_2 + c_2 s)} \quad (11.11)$$

In terms of the foregoing parameters, the dynamic amplification reads:

$$\frac{k_1 x_1}{f} = H(s) = \frac{s^2/\omega_2^2 + 2\xi_2 s/\omega_2 + 1}{(s^2/\omega_1^2 + 2\xi_1 s/\omega_1 + 1)(s^2/\omega_2^2 + 2\xi_2 s/\omega_2 + 1) + \mu s^2/\omega_1^2(1 + 2\xi_2 s/\omega_2)} \quad (11.12)$$

Figure 11.3 compares the dynamic amplification of the primary system alone (single d.o.f. oscillator  $m_1$ ) to that of the system equipped with the DVA, for fixed values of the mass ratio  $\mu$  and of the frequency ratio  $\nu$ , but for various values of the damping ratio  $\xi_2$  of the DVA. One sees that the single peak amplification of the primary system has been transformed into a double peak amplification. For small values of the damping ratio  $\xi_2$ , the curve consists of two marked peaks and one marked transmission zero (anti-resonance) in between; this zero has been exploited in the previous section to attenuate the harmonic excitation. For larger values of the damping ratio, the two peaks and the zeros are less marked. A remarkable feature of these curves is that they all cross each other at two fixed points

*A* and *B*. Let us now examine how the parameters  $\nu$  and  $\xi_2$  may be chosen to optimize the dynamic amplification.

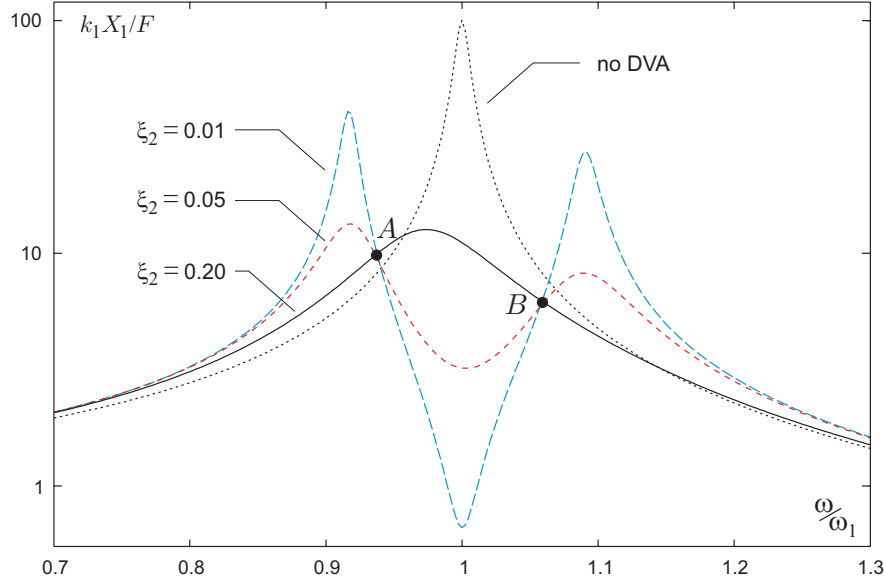


**Fig. 11.3.** Dynamic amplification of the primary system alone ( $\xi_1 = 0.01$ ) and equipped with a DVA. All the curves correspond to the same mass ratio ( $\mu = 0.03$ ) and frequency ratio ( $\nu = 1$ ). For small values of the damping ratio  $\xi_2$ , the curve consists of two marked peaks and one marked transmission zero in between. For larger values of the damping ratio, the two peaks and the zeros are less marked. All the curves cross each other at two fixed points *A* and *B*.

#### 11.4.1 Equal peak design

The most popular design method is the so-called “equal peak design”, which was historically developed by Den Hartog. The position of the two points *A* and *B* in Fig.11.3 depends only on the frequency ratio  $\nu$ ; a change of  $\nu$  will increase the amplitude of one of them and reduce the amplitude of the other; a reasonable choice for  $\nu$  is therefore that leading to equal amplitude at *A* and *B*; this is achieved when the frequency ratio is

$$\nu = \frac{\omega_2}{\omega_1} = \frac{1}{1 + \mu} \quad (11.13)$$

Besides, the damping ratio of the DVA is selected by enforcing that the points *A* and *B* constitute the maxima of the dynamic amplification curve;

this is achieve for

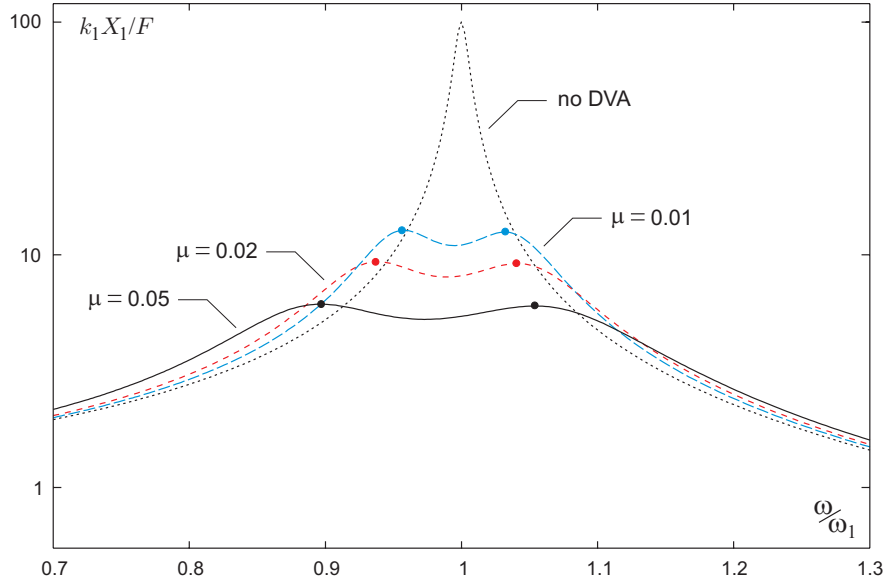
$$\xi_2 = \sqrt{\frac{3\mu}{8(1+\mu)}} \quad (11.14)$$

Figure 11.4 illustrates this design for various values of the mass ratio  $\mu$ . As  $\mu$  increases, the frequency difference between the two peaks at  $A$  and  $B$  increases and their amplitude is reduced. The maximum amplification (quality factor) at  $A$  and  $B$  of the equal peak design depends only on the mass ratio  $\mu$

$$H_{max} = Q = \sqrt{\frac{2+\mu}{\mu}} \simeq \sqrt{\frac{2}{\mu}} \quad (11.15)$$

Recall that, for a single d.o.f. system, the quality factor and the damping ratio are related by  $Q = 1/2\xi$ . Therefore, for a mass ratio  $\mu$ , the maximum amplification will be that of a single d.o.f. with an equivalent damping ratio  $\xi_e = \sqrt{\mu/8}$ ; for  $\mu = 0.01$ ,  $\xi_e \simeq 0.032$ ; for  $\mu = 0.02$ ,  $\xi_e \simeq 0.05$ , etc...

There are other ways of choosing the absorber parameters:  $\nu$  and  $\xi_2$  may be selected to minimize the MS response  $E[x_1^2]$  of the primary structure to a white noise excitation (Crandall & Mark), or to maximize the



**Fig. 11.4.** DVA with equal peak design, for various values of the mass ratio  $\mu$ . For each of them, the parameters of the vibration absorber are chosen according to  $\nu = 1/(1+\mu)$  and  $\xi_2 = \sqrt{3\mu}/8(1+\mu)$ . Larger values of  $\mu$  lead to more distant peaks  $A$  and  $B$ , with lower amplitudes. The maximum amplification is  $Q \simeq \sqrt{2/\mu}$ .

stability margin the poles of the system, solutions of the characteristic equation (11.3). Different optimization criteria will lead to slightly different values of  $\nu$  and  $\xi_2$  [Asami]. It turns out, however, that the optimum is reasonably flat, and that the DVA operates reasonably well even if the parameters differ from their optimum values. As always, this is a key to the practical implementation, and justifies that the DVAs are used extensively. A celebrated application in civil engineering is the wind response mitigation of very tall buildings. Figure 11.5 shows the DVA mounted at the top of the Taipei 101 building in Taiwan. This building has a height of 509 m and has 101 floors. The absorber consists of a pendulum with a mass of 730 tons suspended with four cables extending over 4 floors.<sup>3</sup>



**Fig. 11.5.** Dynamic Vibration Absorber of the Taipei 101 building. The DVA consists of a pendulum with a mass of 730 tons suspended with 4 cables extending over 4 floors.

---

<sup>3</sup> According to the rule of thumb (7.71), a building with 101 floors has a natural frequency  $T \approx 0.1N \approx 10$  s. Since the period of a pendulum of length  $l$  is  $T = 2\pi\sqrt{l/g}$ ; this corresponds to a length of  $l \approx 16$  m.

## 11.5 Multiple d.o.f. systems

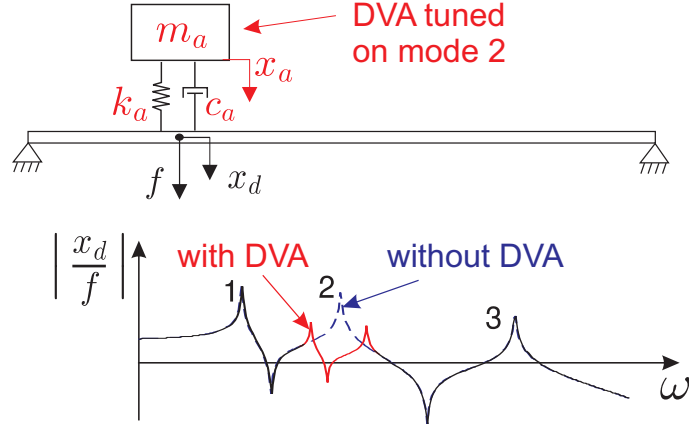


**Fig. 11.6.** Multiple d.o.f. system equipped with a DVA.

In order to apply DVAs to a multiple d.o.f. system, one needs to estimate what mass should be considered as  $m_1$  (the mass of the primary system) in the foregoing design procedure. In fact, it depends on the targeted mode and on the location of the DVA within the system. Consider a multiple d.o.f. system (defined by its mass and stiffness matrices  $M$  and  $K$ ) and a DVA which is located at a position defined by the input vector  $\mathbf{d}$ . The dynamics under the force  $f_d$  coming from the DVA is governed by (assuming no damping for simplicity),

$$M\ddot{\mathbf{x}} + K\mathbf{x} = \mathbf{d} f_d \quad (11.16)$$

In modal coordinates,  $\mathbf{x} = \Phi\mathbf{z}$ , every mode is governed by

$$\mu_i \ddot{z}_i + \mu_i \omega_i^2 z_i = \boldsymbol{\phi}_i^T \mathbf{d} f_d = \boldsymbol{\phi}_i(d) f_d \quad (11.17)$$

In this equation,  $\mu_i$  is the generalized mass of mode  $i$ ,  $\omega_i$  its natural frequency and  $\boldsymbol{\phi}_i(d) = \boldsymbol{\phi}_i^T \mathbf{d}$  the modal amplitude at the DVA location. If the modes are well separated and if the DVA is targeted at mode  $k$ , it is reasonable to assume that, for frequencies close to  $\omega_k$ , the response is dominated by mode  $k$ , and consequently that  $\mathbf{x} \sim \boldsymbol{\phi}_k z_k$ . This amounts to assuming that the modal amplitude  $z_k$  and the structural displacement at the DVA location are related by

$$z_k \sim \frac{x_d}{\phi_k(d)}$$

Substituting this into the modal equation for the targeted mode  $k$ , one gets

$$\mu_k \frac{\ddot{x}_d}{\phi_k(d)} + \mu_k \omega_k^2 \frac{x_d}{\phi_k(d)} = \phi_k(d) f_d$$

or alternatively

$$\frac{\mu_k}{\phi_k^2(d)} \ddot{x}_d + \frac{\mu_k}{\phi_k^2(d)} \omega_k^2 x_d = f_d \quad (11.18)$$

Upon comparing this result with the same equation for a single d.o.f. oscillator, one sees that the equivalent mass to take into account in the design is

$$m_1 = \frac{\mu_k}{\phi_k^2(d)} \quad (11.19)$$

Thus, the equivalent mass  $m_1$  is the generalized mass of mode  $k$  when the modal amplitude of mode  $k$  is normalized according to  $\phi_k(d) = 1$  at the d.o.f. where the DVA is attached. Once the mass  $m_1$  has been determined, the design of the DVA proceeds as for a single d.o.f. system. The mass ratio is selected by the designer and the frequency ratio and the damping ratio are computed from Equ.(11.13) and (11.14).

Observe from the previous equation that a larger modal amplitude will tend to decrease  $m_1$ , that is to increase the mass ratio for a given mass  $m_2$  of the DVA. Thus, in order to maximize its efficacy, the DVA should be located where the targeted mode has large modal amplitudes.

## 11.6 Example: n-storey building

Consider once again the shear frame with 10 identical floors (Fig.11.7); the eigenvalue problem was examined in section 2.7; its seismic response was analyzed in sections 7.3 and 8.10; it was observed that the shear force at the base,  $f_0$ , is dominated by the response of the first mode. The collapse of buildings during earthquakes is often associated with the maximum shear force exceeding the building resistance. In this section, we examine the use of a DVA (tuned on mode 1) to reduce the amplitude of the shear (reaction) force; all the data used here are identical to those used in section 8.10. We proceed in 3 steps: (i) construction of a model including the DVA, (ii) design of the DVA (determination of the constants  $k_a$  and  $c_a$ ), and (iii) calculation of the random response of the structure with DVA to the random seismic input.

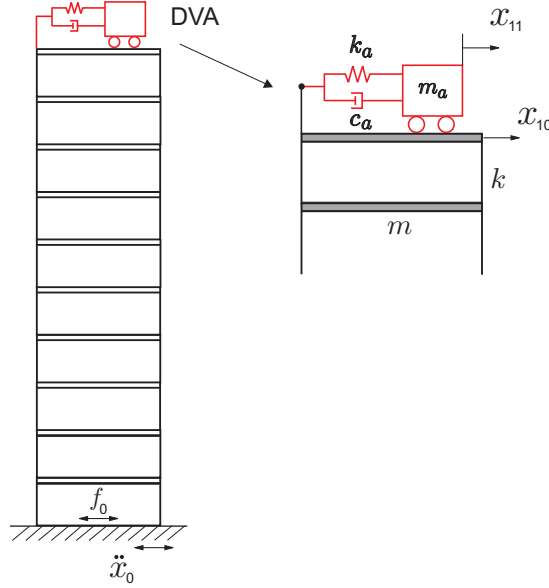


**Fig. 11.7.** 10-storey shear frame equipped with a DVA at the top. The mass ratio is defined as  $\varepsilon = m_a/m_T = m_a/10m$ .  $f_0$  is the shear force at the base; the stroke of the DVA is  $s = x_{11} - x_{10}$ .

### 11.6.1 Model construction

The structure is represented in Fig. 11.7; we assume that the mass of the DVA is only a small fraction of the total mass of the building,  $m_a = \varepsilon m_T$  with  $\varepsilon = 0.01$ . The  $(11 \times 11)$  mass and stiffness matrices of the global system can easily be constructed by inspection of Fig. 11.7; they read

$$M = \begin{bmatrix} mI_{10} & 0 \\ 0 & m_a \end{bmatrix} \quad (11.20)$$

$$K = \begin{bmatrix} 2k & -k & 0 & \dots & 0 & 0 \\ -k & 2k & -k & 0 & 0 & 0 \\ 0 & \dots & \dots & \dots & 0 & 0 \\ 0 & \dots & -k & 2k & -k & 0 \\ 0 & \dots & 0 & -k & k + k_a & -k_a \\ 0 & \dots & 0 & 0 & -k_a & k_a \end{bmatrix} \quad (11.21)$$

The construction of the damping matrix is more difficult, because the system consists of a shear frame where a uniform modal damping  $\xi$  is assumed and a discrete damper (the DVA) connecting  $x_{10}$  and  $x_{11}$ ; the

global system does not satisfy the assumption of modal damping. The  $(10 \times 10)$  damping matrix  $C^*$  of the shear frame alone can be reconstructed as follows: because of the uniform mass distribution within the frame,  $M^* = mI_{10}$  and the orthogonality condition reads

$$\Phi^T M^* \Phi = m \Phi^T \Phi = \text{diag}(\mu_i)$$

Thus, the mode shapes are orthogonal:

$$\Phi^T \Phi = \text{diag}\left(\frac{\mu_i}{m}\right)$$

It follows that

$$C^* = \Phi \text{ diag}\left(\frac{2m^2\xi_i\omega_i}{\mu_i}\right) \Phi^T \quad (11.22)$$

satisfies the assumption of modal damping, because  $\Phi^T C^* \Phi = \text{diag}(2\xi_i\omega_i\mu_i)$ . The global  $(11 \times 11)$  damping matrix of the system reads

$$C = \begin{bmatrix} C^* & & 0 \\ & C_{10,10}^* + c_a & -c_a \\ 0 & -c_a & c_a \end{bmatrix} \quad (11.23)$$

where  $C_{10,10}^*$  is the component  $(10,10)$  of the matrix  $C^*$  and  $c_a$  the damper constant of the DVA. In a more general case where the mode shapes are not orthogonal, a full damping matrix may be constructed by making use of the Rayleigh damping assumption (2.25); however, this model has only two free parameters and allows to assign only two values of the modal damping ratio, using (2.26).

### 11.6.2 Design of the DVA

The DVA is designed to operate on mode 1; it is placed at the top, where the amplitude of mode 1 is maximum. Once the mass  $m_a$  of the DVA has been chosen,  $m_a = \varepsilon m_T$  (with  $\varepsilon = 0.01$  in this case), the equivalent mass of mode 1 is calculated from Equ.(11.19); combining with (7.38), one finds

$$m_1 = \frac{\mu_1}{\phi_1^2(n)} = \frac{m \sum_{i=1}^n \phi_1^2(i)}{\phi_1^2(n)} \quad (11.24)$$

In this formula,  $n$  is the index of the upper floor ( $n = 10$  in this case).<sup>4</sup> Next, the mass ratio is calculated,  $\mu = \frac{m_a}{m_1}$ , and the optimum parameters of the absorber,  $k_a$  and  $c_a$ , are obtained from Equ.(11.13) and (11.14)

---

<sup>4</sup> Since the DVA is placed on the upper floor where the amplitude  $\phi_1(n)$  is maximum,  $m_1$  is significantly smaller than  $m_T$ , which makes the mass ratio  $\mu$  significantly larger than  $\varepsilon$ ;  $\mu = 1.89\varepsilon$  in this case. According to (11.15), the equivalent damping is  $\xi_e \simeq \sqrt{\mu/8} = 0.048$ , which is quite substantial.

$$\omega_a = \sqrt{\frac{k_a}{m_a}} = \frac{\omega_1}{1 + \mu}; \quad \xi_a = \frac{c_a}{2m_a\omega_a} = \sqrt{\frac{3\mu}{8(1 + \mu)}} \quad (11.25)$$

The parameters of the DVA,  $m_a$ ,  $k_a$  and  $c_a$  have all been determined; however, for practical applications, an important design parameter remains to be determined: the stroke, which depends on the seismic input; it will result from the calculation of the random response of the structure with DVA to the random seismic input.

### 11.6.3 Random response of the structure with DVA

The random response of the structure without DVA was analyzed in section 8.10. The analysis was performed in modal coordinates, because the structure satisfies the assumption of modal damping. In the present situation, the complete structure does not satisfy the assumption of modal damping and, owing to the small size of the model, it is convenient to perform the analysis in global coordinates. From Equ.(7.12), the relative displacement response satisfies

$$M\ddot{\mathbf{y}} + C\dot{\mathbf{y}} + K\mathbf{y} = -M\mathbf{1}\ddot{x}_0 \quad (11.26)$$

where  $M$ ,  $K$  and  $C$  are given above. Thus, the FRF between the relative displacement vector and the ground acceleration is

$$\mathbf{Y} = -(K + j\omega C - \omega^2 M)^{-1} M \mathbf{1} \ddot{X}_0 \quad (11.27)$$

The absolute accelerations of the various floors are obtained from (7.2):

$$\ddot{\mathbf{x}} = \mathbf{1}\ddot{x}_0 + \ddot{\mathbf{y}} \quad (11.28)$$

leading to the FRF

$$\ddot{\mathbf{X}} = [\mathbf{1} + \omega^2(K + j\omega C - \omega^2 M)^{-1} M \mathbf{1}] \ddot{X}_0 = \mathbf{H}_{\ddot{x}}(\omega) \ddot{X}_0 \quad (11.29)$$

Similarly, from Equ.(7.9), the reaction force is given by  $f_0 = \mathbf{1}^T M \ddot{\mathbf{x}}$ , leading to the FRF

$$F_0 = [m_T + \omega^2 \mathbf{1}^T M (K + j\omega C - \omega^2 M)^{-1} M \mathbf{1}] \ddot{X}_0 = H_{f_0}(\omega) \ddot{X}_0 \quad (11.30)$$

after using  $m_T = \mathbf{1}^T M \mathbf{1}$ .

The displacement of the DVA relative to the upper floor,  $s = y_{11} - y_{10}$  may be obtained by defining a vector  $\mathbf{b}^T = (0, \dots, 0, -1, 1)$  such that

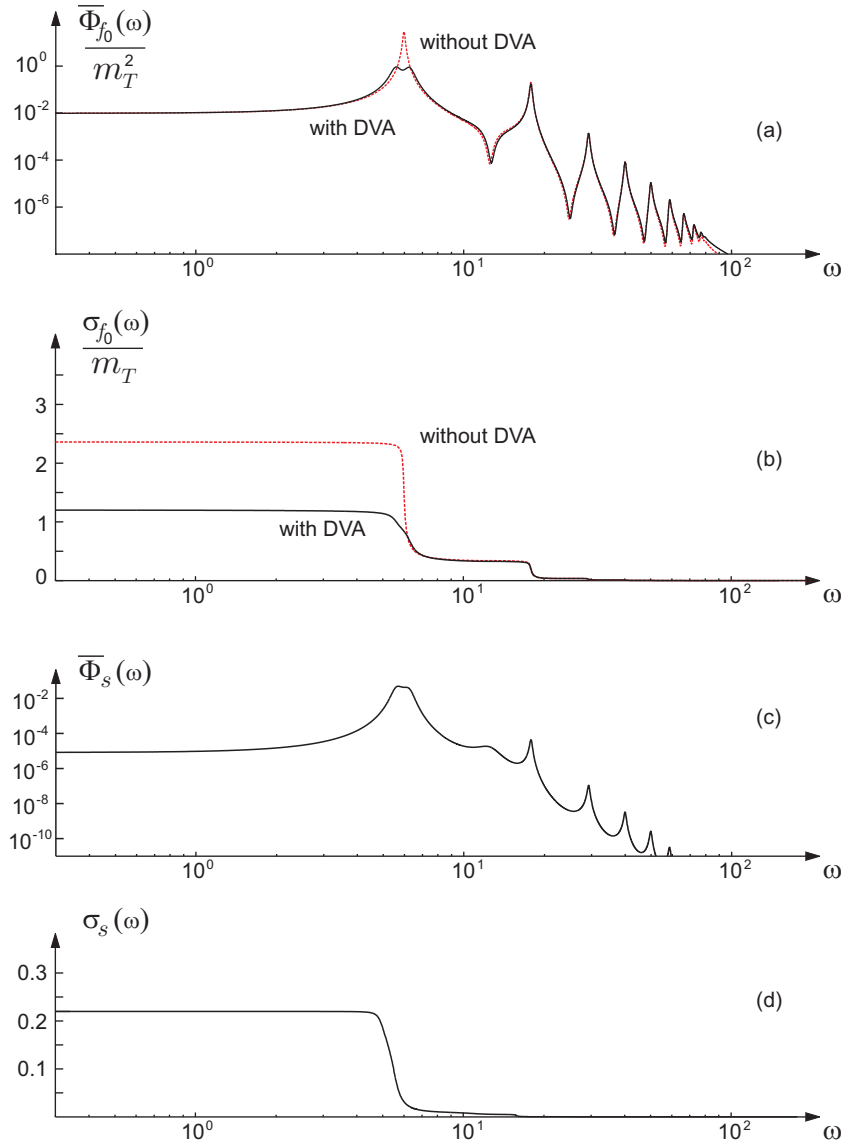


**Fig. 11.8.** Seismic response of a 10-storey shear frame equipped with a DVA at the top ( $\varepsilon = 0.01$ ). (a) One-sided response PSD of the non-dimensional reaction force  $f_0/\sigma_g m_T$  with and without DVA. (b) Cumulative RMS value of the non-dimensional reaction force, with and without DVA. (c) One-sided PSD of the relative displacement of the DVA,  $s = x_{11} - x_{10}$ . (d) Cumulative RMS value of the relative displacement,  $\sigma_s(\omega)$  [m].

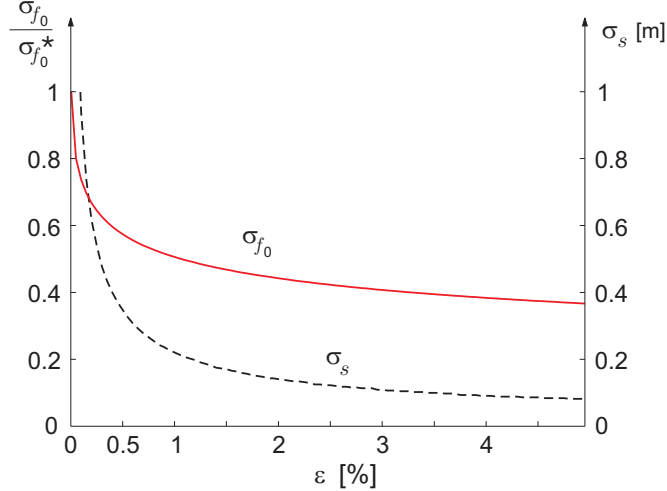


**Fig. 11.9.** 10-storey shear frame equipped with a DVA at the top. Influence of the fraction of mass  $\varepsilon = m_a/m_T$  on the reduction of the reaction force ( $\sigma_{f_0}^*$  refers to the response without DVA) and on the RMS relative displacement  $\sigma_s$ .

$s = \mathbf{b}^T \mathbf{y}$ ; the FRF between the complex amplitudes of  $s$  and  $\ddot{x}_0$  is given by

$$S = -\mathbf{b}^T(K + j\omega C - \omega^2 M)^{-1}M\mathbf{1}\ddot{X}_0 = H_s(\omega)\ddot{X}_0 \quad (11.31)$$

The power spectral density of the relative displacement  $s$  is obtained from the fundamental input-output relationship (8.23)

$$\Phi_s(\omega) = |H_s(\omega)|^2 \Phi_{\ddot{x}_0} \quad (11.32)$$

and similarly for all the response quantities. Figure 11.8 shows the influence of the DVA on the structural response. Figure 11.8.a shows the impact of the DVA on the resonance peak of the first mode in the reaction force  $f_0$ . The reduction of the RMS of the shear force is illustrated in Fig.11.8.b. The relative response of the DVA with respect to the top floor is illustrated in Fig.11.8.c and d. Finally, Fig.11.9 illustrate the influence of the mass of the DVA on the attenuation of the RMS reaction force  $\sigma_{f_0}$  and on the stroke  $\sigma_s$ . For every value of the mass fraction  $\varepsilon$ , the parameters are those of the equal peak design.

## 11.7 Vibration isolation

There are two broad classes of problems in which vibration isolation is necessary: (i) Operating equipments generate oscillatory forces which can

propagate into the supporting structure (Fig.11.10.a). This situation corresponds to that of an engine in a car. (ii) Sensitive equipments may be supported by a structure which vibrates appreciably (Fig.11.10.b); in this case, it is the support motion which constitutes the source of excitation; this situation corresponds to, for example, a telescope in a spacecraft, a wafer stepper or a precision machine tool in a workshop, or a passenger seated in a car. The disturbance may be either deterministic, such as the unbalance of a motor, or random as in a passenger car riding on a rough road (section 8.8.5).

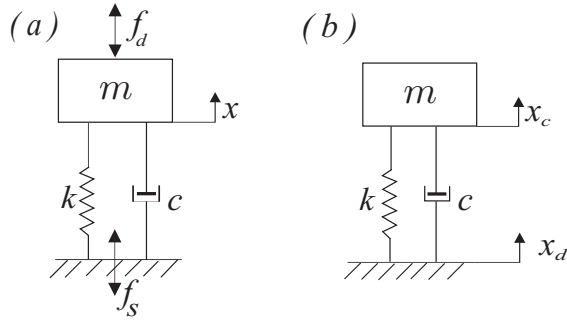


**Fig. 11.10.** (a) Operating equipment generating a disturbance force  $f_d$ . (b) Equipment subjected to a support excitation  $x_d$ .

## 11.8 Linear isolator

Consider the system depicted in Fig.11.10.a, excited by a disturbance force  $f_d$ . If the support is fixed, the governing equation is:

$$m\ddot{x} + c\dot{x} + kx = f_d \quad (11.33)$$

The force transmitted to the support is given by

$$f_s = kx + c\dot{x} \quad (11.34)$$

In the Laplace domain,

$$X(s) = \frac{F_d(s)}{m(s^2 + 2\xi\omega_n s + \omega_n^2)} \quad (11.35)$$

$$F_s(s) = m(\omega_n^2 + 2\xi\omega_n s)X(s) \quad (11.36)$$

where  $X(s)$ ,  $F_d(s)$  and  $F_s(s)$  stand for the Laplace transform of respectively  $x(t)$ ,  $f_d(t)$  and  $f_s(t)$ , and with the usual notations  $\omega_n^2 = k/m$  and  $2\xi\omega_n = c/m$ . The *transmissibility* of the support is defined in this case as the transfer function between the disturbance force  $f_d$  applied to the mass and the force  $f_s$  transmitted to the support structure; combining the foregoing equations, we get

$$\frac{F_s(s)}{F_d(s)} = \frac{1 + 2\xi s/\omega_n}{1 + 2\xi s/\omega_n + s^2/\omega_n^2} \quad (11.37)$$

Next, consider the second situation illustrated in Fig. 11.10.b; the disturbance is the displacement  $x_d$  of the supporting structure and the system output is the displacement  $x_c$  of the sensitive equipment. Proceeding in a similar way, it is easily established that the transmissibility of this isolation system, defined in this case as the transfer function between the support displacement and the absolute displacement of the mass  $m$ , is given by (Problem 11.2)

$$\frac{X_c(s)}{X_d(s)} = \frac{1 + 2\xi s/\omega_n}{1 + 2\xi s/\omega_n + s^2/\omega_n^2} \quad (11.38)$$

which is identical to the previous one; the two isolation problems can therefore be treated in parallel. The amplitude of the corresponding FRF,

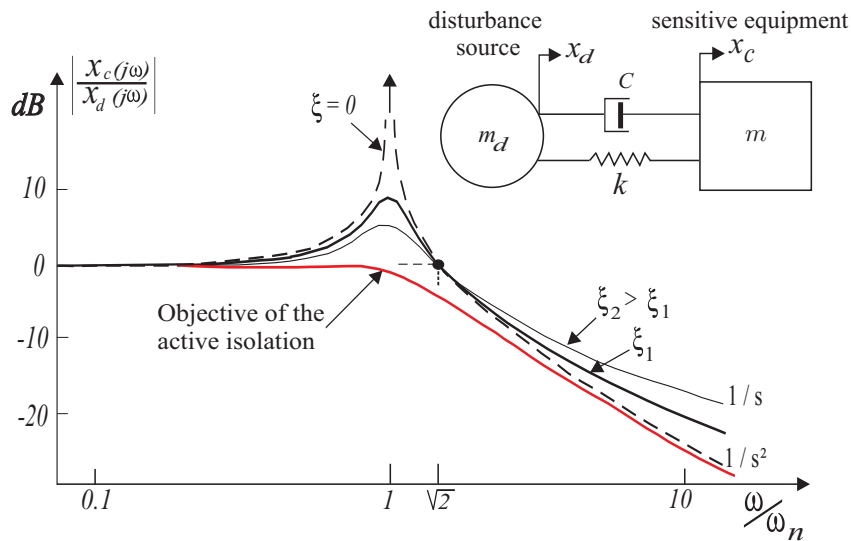


**Fig. 11.11.** Transmissibility of the linear isolator for various values of the damping ratio  $\xi$ . The performance objectives of active isolation are a high frequency decay like  $s^{-2}$  together with no overshoot at resonance.

for  $s = j\omega$ , is represented in Fig.11.11 for various values of the damping ratio  $\xi$ . We observe that: (i) All the curves are larger than 1 for  $\omega < \sqrt{2}\omega_n$  and become smaller than 1 for  $\omega > \sqrt{2}\omega_n$ . Thus the critical frequency  $\sqrt{2}\omega_n$  separates the domains of amplification and attenuation of the isolator. (ii) When  $\xi = 0$ , the high frequency decay rate is  $s^{-2}$ , that is -40 dB/decade, while very large amplitudes occur near the corner frequency  $\omega_n$  (the natural frequency of the spring-mass system).

Figure 11.11 illustrates the trade-off in passive isolator design: large damping is desirable at low frequency to reduce the resonant peak while low damping is needed at high frequency to maximize the isolation. One may already observe that if the disturbance is generated by a rotating unbalance of a motor operating at a variable speed, there is an obvious benefit to use a damper with variable damping characteristics which can be adjusted according to the rotation velocity: high when  $\omega < \sqrt{2}\omega_n$  and low when  $\omega > \sqrt{2}\omega_n$ . Such variable (*adaptive*) systems may be implemented, e.g. with controllable fluids or electromagnetic devices. Figure 11.11 also shows the target of an ideal (*active*) isolation system which combines a decay rate of -40 dB/decade with no overshoot at resonance; such an active isolator will be analyzed in the following chapter. Next section discusses one way of improving the high frequency isolation using only passive components.

## 11.9 Relaxation isolator

In the *relaxation* isolator, the viscous damper  $c$  is replaced by a Maxwell unit consisting of a damper  $c$  and a spring  $k_1$  in series (Fig.11.12). The governing equations are

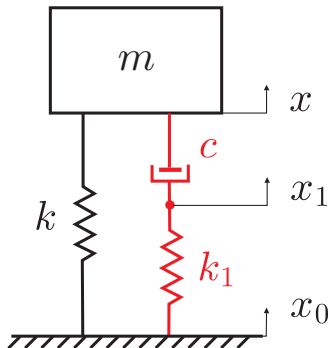


**Fig. 11.12.** Relaxation isolator consisting of a spring in parallel with a Maxwell unit.

$$m\ddot{x} + k(x - x_0) + c(\dot{x} - \dot{x}_1) = 0 \quad (11.39)$$

$$c(\dot{x} - \dot{x}_1) = k_1(x_1 - x_0) \quad (11.40)$$

or, in matrix form using the Laplace variable  $s$ ,

$$\begin{bmatrix} ms^2 + cs + k & -cs \\ -cs & k_1 + cs \end{bmatrix} \begin{Bmatrix} x \\ x_1 \end{Bmatrix} = \begin{Bmatrix} k \\ k_1 \end{Bmatrix} x_0 \quad (11.41)$$

It follows that the transmissibility reads

$$\begin{aligned} \frac{x}{x_0} &= \frac{(k_1 + cs)k + k_1 cs}{(ms^2 + cs + k)(k_1 + cs) - c^2 s^2} \\ &= \frac{(k_1 + cs)k + k_1 cs}{(ms^2 + k)(k_1 + cs) + k_1 cs} \end{aligned} \quad (11.42)$$

One sees that the asymptotic decay rate for large frequencies (obtained by keeping only the highest power in  $s$  at the numerator and the denominator) is in  $s^{-2}$ , that is  $-40 \text{ dB/decade}$ . Physically, this corresponds to the fact that, at high frequency, the viscous damper tends to be blocked, and

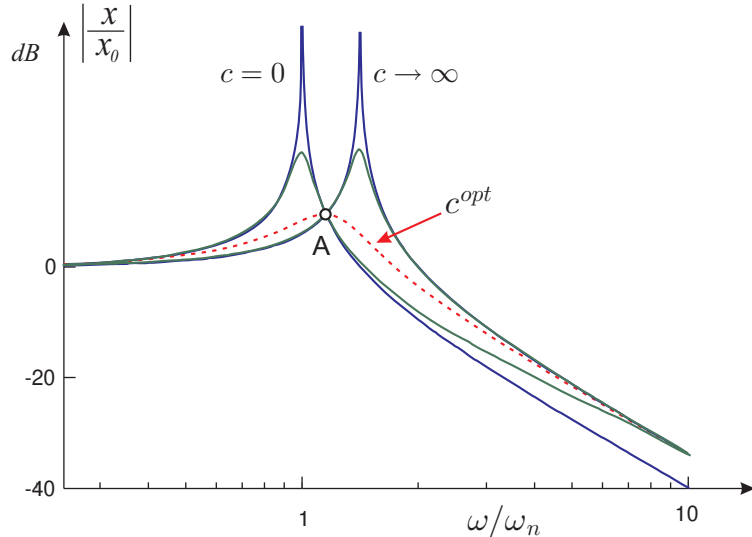


**Fig. 11.13.** Transmissibility of the relaxation isolator for fixed values of  $k$  and  $k_1$  and various values of  $c$ . The first peak corresponds to  $\omega = \omega_n = (k/m)^{1/2}$ ; the second one corresponds to  $\omega = \Omega_n = [(k + k_1)/m]^{1/2}$ . All the curves cross each other at  $A$  and have an asymptotic decay rate of  $-40 \text{ dB/decade}$ . The curve corresponding to  $c_{opt}$  is nearly maximum at  $A$ .

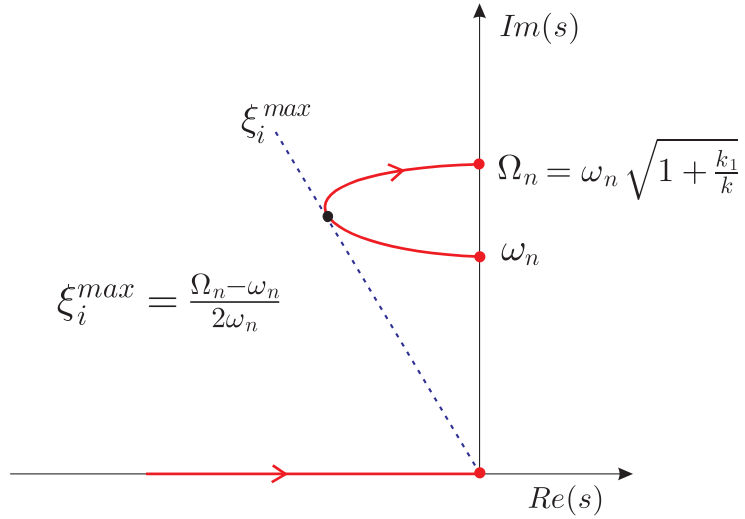


**Fig. 11.14.** Root locus of the solutions of Equ.(11.43) as  $c$  goes from zero to infinity. The maximum damping is achieved for  $k_1/c = \Omega_n^{3/2}\omega_n^{-1/2}$ .

the system behaves like an undamped isolator with two springs acting in parallel. Figure 11.13 compares the transmissibility curves for given values of  $k$  and  $k_1$  and various values of  $c$ . For  $c = 0$ , the relaxation isolator behaves like an undamped isolator of natural frequency  $\omega_n = (k/m)^{1/2}$ . Likewise, for  $c \rightarrow \infty$ , it behaves like an undamped isolator of frequency  $\Omega_n = [(k + k_1)/m]^{1/2}$ . In between, the poles of the system are solution of the characteristic equation

$$(ms^2 + k)(k_1 + cs) + k_1cs = (ms^2 + k)k_1 + cs(ms^2 + k + k_1) = 0$$

which can be rewritten in root locus form

$$1 + \frac{k_1}{c} \frac{s^2 + \omega_n^2}{s(s^2 + \Omega_n^2)} = 0 \quad (11.43)$$

It is represented in Fig.11.14 when  $c$  varies from 0 to  $\infty$ ; it can be shown that the maximum damping ratio is achieved for

$$\frac{k_1}{c} = \frac{\Omega_n^{3/2}}{\omega_n^{1/2}} \quad (11.44)$$

and the corresponding damper constant is

$$c_{opt} = \frac{k_1}{\Omega_n} \left( \frac{\omega_n}{\Omega_n} \right)^{1/2} = \frac{k_1}{\Omega_n} (1 + \frac{k_1}{k})^{-1/4} = \frac{k_1}{\omega_n} (1 + \frac{k_1}{k})^{-3/4} \quad (11.45)$$

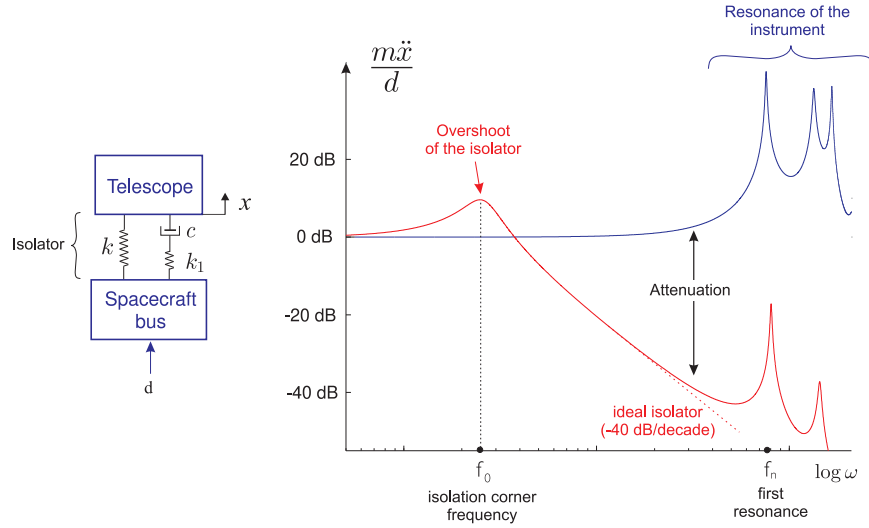


**Fig. 11.15.** Effect of the isolator on the transmissibility between the spacecraft bus and the telescope.

The transmissibility corresponding to  $c_{opt}$  is also represented in Fig.11.13; it is nearly maximum at  $A$ . The relaxation isolator can be realized with viscoelastic materials or with an electromechanical system consisting of voice coil transducer and a  $RL$  circuit.

The importance of achieving a high frequency decay rate of  $-40$   $dB/decade$  is illustrated in Fig.11.15 which considers a spacecraft carrying a precision payload (e.g. a telescope). The spacecraft bus is excited by all sorts of disturbances generated by the unbalanced mass of the attitude control wheels and gyros. A vibration isolator is inserted between the bus and the telescope to attenuate the jitter. If the isolator is designed in such a way that its transmissibility exhibits a decay rate of  $-40dB/decade$ , the jitter can be reduced by a factor 100 by selecting the isolator corner frequency,  $f_0$ , one decade lower than the first flexible mode of the payload,  $f_n$  (Fig.11.15). Extremely sensitive payloads may even involve several isolation layers.

## 11.10 Six-axis isolator

To fully isolate two rigid bodies with respect to each other, six single-axis isolators judiciously placed are needed. Let us consider a payload isolated by six identical isolators (Fig.11.16); if the isolators consist of

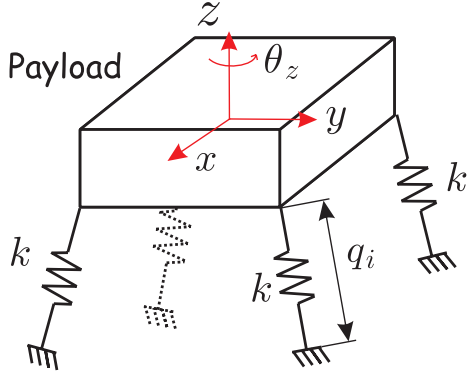


**Fig. 11.16.** Six-axis isolator (only four legs are represented). The connection between the leg and the support as well as the payload is done with spherical joints. The coordinates of the payload  $\mathbf{x} = (x, y, z, \theta_x, \theta_y, \theta_z)^T$  and the leg extensions  $\mathbf{q} = (q_1, \dots, q_6)^T$  are related by  $\mathbf{q} = J\mathbf{x}$  where  $J$  is the Jacobian of the isolator.

simple springs of stiffness  $k$ , the six suspension modes are solution of an eigenvalue problem

$$(M\mathbf{s}^2 + K)\mathbf{x} = 0 \quad (11.46)$$

where  $x$  is a vector of 6 coordinates describing the position of the payload, e.g.  $\mathbf{x} = (x, y, z, \theta_x, \theta_y, \theta_z)^T$  (the payload frame is attached to the center of mass). The mass matrix  $M$  can be obtained by writing the kinetic energy in terms of  $\dot{\mathbf{x}}$ , leading to

$$M = \begin{bmatrix} mI_3 & 0 \\ 0 & I_c \end{bmatrix} \quad (11.47)$$

where  $m$  is the mass of the payload,  $I_3$  is the unity matrix, and  $I_c$  is the inertia tensor about the center of mass. Similarly, the stiffness matrix is obtained by writing the strain energy in terms of  $\mathbf{x}$ . The strain energy in the system is  $V = \frac{1}{2}k\mathbf{q}^T\mathbf{q}$ , where  $\mathbf{q} = (q_1, \dots, q_6)^T$  is the vector of the spring extensions in the isolator and  $k$  is the stiffness common to all springs. If  $J$  is the Jacobian matrix connecting the spring extensions  $\mathbf{q}$  to the coordinates  $\mathbf{x}$  ( $J$  depends on the topology of the isolator),

$$\mathbf{q} = J\mathbf{x} \quad (11.48)$$

one gets that

$$V = \frac{1}{2}k\mathbf{q}^T\mathbf{q} = \frac{1}{2}k\mathbf{x}^T J^T J \mathbf{x} \quad (11.49)$$

which means that the stiffness matrix is

$$K = kJ^T J \quad (11.50)$$

The solutions of the eigenvalue problem

$$(K - \omega_i^2 M) \phi_i = 0 \quad (11.51)$$

are the six eigenfrequencies and mode shapes of the suspension.

If the linear spring is replaced by a relaxation isolator, the leg stiffness becomes frequency dependent; the common stiffness  $k$  must be replaced by the dynamic stiffness relating the force  $F$  in the relaxation spring to its extension  $x - x_0$ . From Fig.11.12,

$$F = k(x - x_0) + cs(x - x_1)$$

$x_1$  may be eliminated by using Equ.(11.40) which provides

$$x_1 = \frac{csx + k_1x_0}{cs + k_1}$$

leading to the dynamic stiffness:

$$\frac{F}{x - x_0} = k(s) = k[1 + \frac{k_1cs}{k(k_1 + cs)}] \quad (11.52)$$

(the stiffness is  $k$  at low frequency and  $k+k_1$  at high frequency). Thus, the (frequency-dependent) stiffness matrix of the six-axis relaxation isolator reads

$$K(s) = J^T J \ k[1 + \frac{k_1cs}{k(k_1 + cs)}] = K[1 + \frac{k_1cs}{k(k_1 + cs)}] \quad (11.53)$$

The eigenvalue problem (11.46) becomes

$$\{Ms^2 + K[1 + \frac{k_1cs}{k(k_1 + cs)}]\}\mathbf{x} = 0 \quad (11.54)$$

If  $\omega_i$  and  $\Phi = (\phi_1, \dots, \phi_6)$  are the solution of the eigenvalue problem (11.51), normalized according to  $\Phi^T M \Phi = I$ , one can transform (11.54) into modal coordinates,  $\mathbf{x} = \Phi \mathbf{z}$ ; using the orthogonality conditions, one finds a set of decoupled equations

$$s^2 + \omega_i^2 [1 + \frac{k_1cs}{k(k_1 + cs)}] = 0 \quad (11.55)$$

Upon introducing

$$\Omega_i^2 = \omega_i^2 \left(1 + \frac{k_1}{k}\right) \quad (11.56)$$

the previous equation may be rewritten

$$\frac{k_1}{c} (s^2 + \omega_i^2) + s(s^2 + \Omega_i^2) = 0$$

or

$$1 + \frac{k_1}{c} \frac{s^2 + \omega_i^2}{s(s^2 + \Omega_i^2)} = 0 \quad (11.57)$$

which is identical to (11.43). Thus, according to the foregoing equation, the six suspension modes follow independent root-loci connecting  $\omega_i$  and  $\Omega_i$  (Fig.11.14). However,  $k_1/c$  being a single scalar parameter, the optimal damping cannot be reached simultaneously in the six modes, because of the *modal spread* ( $\omega_1 < \omega_6$ ). A good design will aim at minimizing the modal spread, so that all the modes can be as close as possible to the optimal damping.

### 11.11 Isolation by kinematic coupling

When the disturbance is harmonic with a constant frequency, a very effective isolation may be achieved with the system described in Fig.11.17 [Krysinski & Malburet]. The strategy consists of introducing a transmission zero<sup>5</sup> in the transmissibility between the disturbance  $w$  and the structural response  $x$  by adding a mechanism involving a mass  $m_1$  connected kinematically to the structure and its support as indicated in the figure. The system is easily modelled with the Lagrange equations, using the two coordinates  $x$  (absolute vertical displacement of the structure) and  $y$  (absolute vertical displacement of the mass  $m_1$ ). The absolute displacement

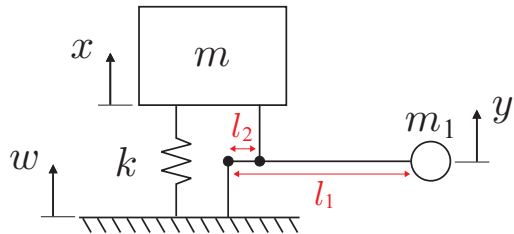


**Fig. 11.17.** Isolation by kinematic coupling.

---

<sup>5</sup> also called a *notch* filter.

of the support  $w$  is the input of the system. For small angles of rotation, the kinematics of the mechanism follows

$$y = \frac{l_1}{l_2}x - \frac{l_1 - l_2}{l_2}w = \alpha x - (\alpha - 1)w \quad (11.58)$$

where  $\alpha = l_1/l_2$  ( $> 1$ ). The kinetic energy reads

$$T = \frac{1}{2}m\dot{x}^2 + \frac{1}{2}m_1\dot{y}^2$$

and using the previous equation,

$$T = \frac{1}{2}m\dot{x}^2 + \frac{1}{2}m_1[\alpha\dot{x} - (\alpha - 1)\dot{w}]^2$$

The potential energy associated with the spring  $k$  is

$$V = \frac{1}{2}k(x - w)^2$$

The partial derivative of the kinetic energy is

$$\frac{\partial T}{\partial \dot{x}} = m\dot{x} + m_1\alpha[\alpha\dot{x} - (\alpha - 1)\dot{w}]$$

and the Lagrange equation reads

$$m\ddot{x} + m_1\alpha[\alpha\ddot{x} - (\alpha - 1)\ddot{w}] + k(x - w) = 0$$

or

$$(m + m_1\alpha^2)\ddot{x} + kx = m_1\alpha(\alpha - 1)\ddot{w} + kw \quad (11.59)$$

Finally, the transfer function between  $w$  and  $x$  reads

$$\frac{X(s)}{W(s)} = \frac{k + s^2m_1\alpha(\alpha - 1)}{k + s^2(m + m_1\alpha^2)} = \frac{1 + s^2/z^2}{1 + s^2/\omega_0^2} \quad (11.60)$$

where the transmission zeros  $\pm jz$  and the poles  $\pm j\omega_0$  are defined by

$$z^2 = \frac{k}{m_1\alpha(\alpha - 1)} > \omega_0^2 = \frac{k}{m + m_1\alpha^2} \quad (11.61)$$

The transmissibility  $X(\omega)/W(\omega)$  is represented in Fig.11.18. By adjusting the length ratio  $\alpha = l_1/l_2$ , the system is tuned in such a way that the frequency  $z$  of the transmission zero matches the frequency of the harmonic disturbance. Some damping will always be present in the system, which will tend to modify the transmissibility in the vicinity of the  $\omega_0$  and  $z$ . This concept has been applied to helicopters.

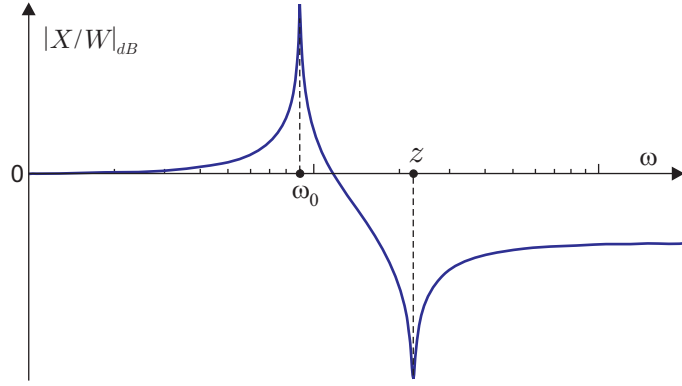


**Fig. 11.18.** Transmissibility of the isolator by kinematic coupling. The system is tuned in such a way that the frequency  $z$  of the transmission zero matches the frequency of the harmonic disturbance.

### 11.12 Centrifugal Pendulum Vibration Absorber

Internal combustion engines are subject to torsional oscillations due to the sharp variations of the pressure during the cycle. For a four stroke, four cylinder in-line engine, the disturbing torque is usually at an order  $n = 2$  of the engine speed,  $\omega = 2\Omega$ . The performance of the engine may be improved by the addition of a torsional oscillation absorber.

The linear torsional oscillation absorber (Fig.11.19) is easily modeled as

$$I_1 \ddot{\theta}_1 + k_\theta(\theta_1 - \theta_2) = M(t)$$

$$I_2 \ddot{\theta}_2 + k_\theta(\theta_2 - \theta_1) = 0$$

For a given harmonic excitation,  $M(t) = M_0 e^{j\omega t}$ , the response is also harmonic,  $\theta_1(t) = X_1 e^{j\omega t}$ ,  $\theta_2(t) = X_2 e^{j\omega t}$ . Upon substituting in the foregoing equations,

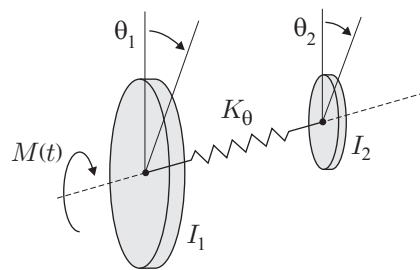


**Fig. 11.19.** Linear torsional oscillation absorber.

$$\begin{bmatrix} k_\theta - \omega^2 I_1 & -k_\theta \\ -k_\theta & k_\theta - \omega^2 I_2 \end{bmatrix} \begin{Bmatrix} X_1 \\ X_2 \end{Bmatrix} = \begin{Bmatrix} M_0 \\ 0 \end{Bmatrix}$$

and one finds easily

$$X_1 = \frac{k_\theta - \omega^2 I_2}{\omega^2 [I_1 I_2 - k_\theta (I_1 + I_2)]} M_0 \quad (11.62)$$

Thus, by tuning the torsional vibration absorber on the anti-resonance, with  $k_\theta = I_2 \omega^2$ , the effect of the disturbance may be entirely canceled. The centrifugal pendulum discussed in Problem 3.11 is an efficient way of doing this [see Equ.(3.73)]; once the centrifugal pendulum vibration absorber has been tuned ( $\omega_1 = \omega = n\Omega$ ), it remains tuned for any engine speed, as long as the pendulum behaves linearly. Note however, that for large amplitudes, the frequency of the centrifugal pendulum varies with varying pendulum amplitudes [Denman]. The pendulum trajectory leading to an eigenfrequency independent of the pendulum amplitude (*tautochronic* problem) is an epicycloid path.

### 11.13 Model of a car suspension

A two-d.o.f. model of a car suspension is represented in Fig.11.20; such a model is called a “quarter-car” model;  $m_s$  (sprung mass) represents one fourth of the mass of the body of the car (assumed rigid) and  $m_{us}$  (unsprung mass) is that of the wheel and part of the suspension.  $k$  and  $c$  are the characteristics of the suspension and  $k_t$  is the stiffness of the tyre;  $w(t)$  is the road profile (a random model of the road profile has been considered in section 8.8.5). Since  $m_s \gg m_{us}$  and  $k_t \gg k$ , the first mode is essentially the body resonance, close to  $\omega_n = \sqrt{k/m_s}$  while the second mode corresponds to the tyre resonance, close to  $\omega_t = \sqrt{k_t/m_{us}}$ .

Ride comfort requires good vibration isolation while vehicle handling requires good road holding. The ride comfort is usually measured by the car body acceleration, or sometimes its derivative called *jerk*. According to the literature, there is an excellent correlation between the RMS acceleration and the subjective ride rating. The road holding is often measured by the tyre deflection (proportional to the contact force), or sometimes by the unsprung mass (wheel) velocity. In addition to the car body acceleration and the tyre deflection which define the performance of the suspension, there are design constraints on the suspension travel, that is the relative displacement between the car body and the wheel. It is convenient to develop a model where all these important quantities appear

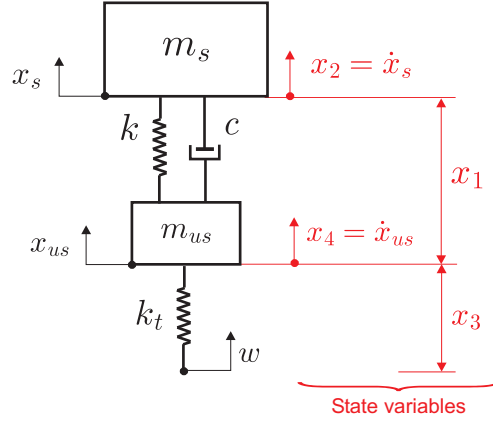


**Fig. 11.20.** Quarter-car suspension model with two-d.o.f. and description of the state variables.

as coordinates. This is achieved by the choice of the four *state variables*:  $x_1 = x_s - x_{us}$  is the relative displacement of the sprung mass with respect to the wheel,  $x_2 = \dot{x}_s$  is the absolute velocity of the car body,  $x_3 = x_{us} - w$  is the tyre deflection, and  $x_4 = \dot{x}_{us}$  is the absolute wheel velocity. With these coordinates, the equations of motion read

$$\begin{aligned} m_s \ddot{x}_2 &= -kx_1 + c(x_4 - x_2) \\ m_{us} \ddot{x}_4 &= -k_t x_3 + kx_1 + c(x_2 - x_4) \\ \dot{x}_1 &= x_2 - x_4 \\ \dot{x}_3 &= x_4 - \dot{w} \end{aligned}$$

and, upon defining  $\omega_n^2 = k/m_s$  ( $\omega_n$  is the body resonance),  $c/m_s = 2\xi\omega_n$ ,  $\omega_t^2 = k_t/m_{us}$  ( $\omega_t$  is the tyre resonance) and  $\mu = m_{us}/m_s$ , they are rewritten in matrix form:

$$\begin{Bmatrix} \dot{x}_1 \\ \dot{x}_2 \\ \dot{x}_3 \\ \dot{x}_4 \end{Bmatrix} = \begin{bmatrix} 0 & 1 & 0 & -1 \\ -\omega_n^2 & -2\xi\omega_n & 0 & 2\xi\omega_n \\ 0 & 0 & 0 & 1 \\ \frac{\omega_n^2}{\mu} & \frac{2\xi\omega_n}{\mu} & -\omega_t^2 & \frac{-2\xi\omega_n}{\mu} \end{bmatrix} \begin{Bmatrix} x_1 \\ x_2 \\ x_3 \\ x_4 \end{Bmatrix} + \begin{Bmatrix} 0 \\ 0 \\ -1 \\ 0 \end{Bmatrix} \dot{w} \quad (11.63)$$

or

$$\dot{\mathbf{x}} = A\mathbf{x} + \mathbf{b}\dot{w} \quad (11.64)$$

with the state vector  $\mathbf{x} = (x_1, x_2, x_3, x_4)^T$ , the input vector  $\mathbf{b} = (0, 0, -1, 0)^T$  and the system matrix

$$A = \begin{bmatrix} 0 & 1 & 0 & -1 \\ -\omega_n^2 & -2\xi\omega_n & 0 & 2\xi\omega_n \\ 0 & 0 & 0 & 1 \\ \frac{\omega_n^2}{\mu} & \frac{2\xi\omega_n}{\mu} & -\omega_t^2 & \frac{-2\xi\omega_n}{\mu} \end{bmatrix} \quad (11.65)$$

The input  $v = \dot{w}$  is the road velocity. Upon transforming Equ.(11.64) in the Laplace domain, the transfer function between the road velocity and the state vector is easily obtained

$$\mathbf{X}(s) = (sI - A)^{-1}\mathbf{b}V(s) \quad (11.66)$$

from which the transmissibility of all the response quantities follow by setting  $s = j\omega$ . This is illustrated in Fig.11.21 with numerical values [Chaliasani]:  $k_t = 160000$  N/m (tyre stiffness),  $k = 16000$  N/m (suspension spring stiffness),  $m_s = 240$  kg (car body),  $m_{us} = 36$  kg (wheel); three values of the suspension damping coefficient  $c$  are considered:  $c = 200$  Ns/m, 980 Ns/m, 4000 Ns/m. Figure 11.21.a shows the transmissibility between the road velocity and the body acceleration,  $T_{\ddot{x}_s v}(\omega) = |j\omega X_2(\omega)/V(\omega)|$ , Fig. 11.21.b shows the cumulative RMS value of the body acceleration, defined as

$$\sigma_{\ddot{x}_s}(\omega) = [\int_{\omega}^{\infty} |T_{\ddot{x}_s v}(\nu)|^2 d\nu]^{1/2} \quad (11.67)$$

Fig.11.21.c shows the transmissibility between the road velocity and the tyre deflection  $T_{x_3 v}(\omega) = |X_3(\omega)/V(\omega)|$  and Fig.11.21.d shows the cumulative RMS value,  $\sigma_{x_3}(\omega)$ . For the smallest value of  $c$ , one sees clearly the two peaks associated with the body resonance (sprung mass) and the tyre resonance (unsprung mass); the corresponding resonance frequencies are very close to  $\omega_n = \sqrt{k/m_s}$  and  $\omega_t = \sqrt{k_t/m_{us}}$ , respectively.<sup>6</sup> As the damping increases, the amplitude of the two peaks is reduced; one sees clearly that the passive damping cannot control the body resonance without deteriorating the isolation at higher frequency. The tyre deflection (i.e. road holding) depends also very much on the damping constant. In the following chapter, we will examine the behavior of an *active* suspension.

## 11.14 Problems

**P.11.1** Consider a plane shear frame with  $n = 10$  floors (section 2.7); the mass of one floor is  $m = 10^5$  kg and the stiffness is  $k = 16 \times 10^7$

---

<sup>6</sup> The body resonance is at 7.8 rad/s and the tyre resonance is at 69.5 rad/s, while  $\omega_n = \sqrt{k/m_s} = 8.16$  rad/s and  $\omega_t = \sqrt{k_t/m_{us}} = 66.7$  rad/s.

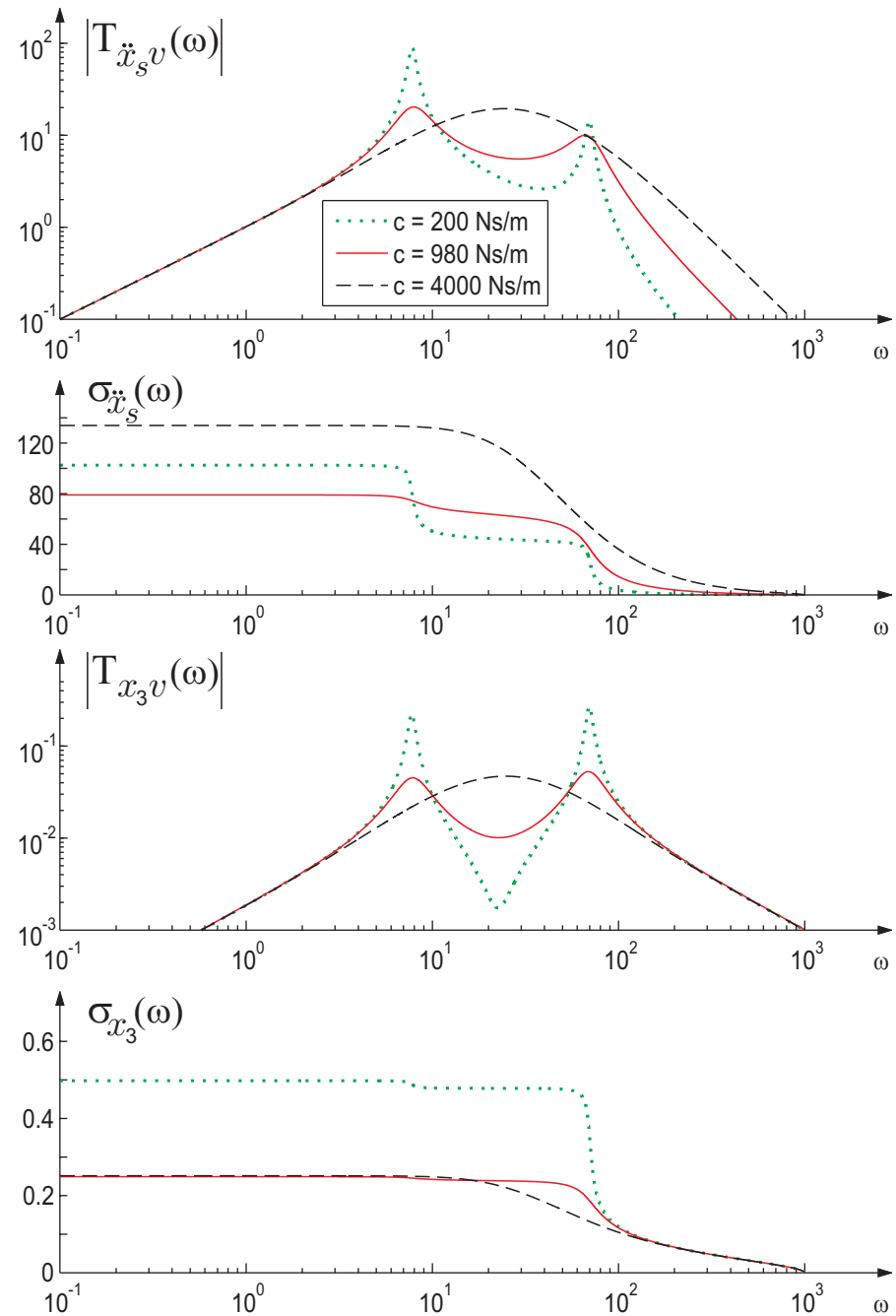


**Fig. 11.21.** Passive suspension of a rigid body with two d.o.f. (a) Transmissibility between the road velocity and the body acceleration, for three values of the suspension damping coefficient  $c$ . (b) Cumulative RMS value of the body acceleration; (c) Transmissibility between the road velocity and the tyre deflection. (d) Cumulative RMS value of the tyre deflection.

N/m. The excitation is represented by a point force  $f$  acting at the top of the frame; the passive damping is assumed uniform in all modes and equal to  $\xi_i = 0.01$ . Design a DVA targeted at mode 1 with a mass being respectively 1 % and 3 % of the total mass of the frame. Compare the transmissibility  $x_{10}/f$  of the system with DVA with that of the initial system.

**P.11.2** Consider the passive isolator of Fig.11.10.b. Find the transmissibility  $X_c(s)/X_d(s)$  of the isolation system.

**P.11.3** Consider the rigid body with two d.o.f. ( $y, \theta$ ) of Fig.11.22; the mass is  $m$  and the moment of inertia about the center of mass is  $I$ ; it is supported by two identical isolators of stiffness  $k$  placed symmetrically at  $x = \pm l/2$ . Find the distance between the isolators which minimizes the modal spread (by making  $\omega_1 = \omega_2$ ).

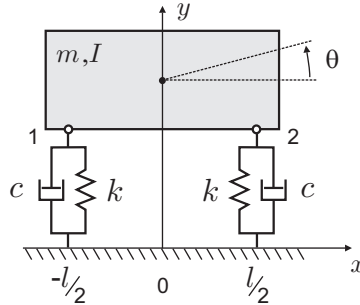


**Fig. 11.22.** Passive suspension of a rigid body with two d.o.f..

**P.11.4** Car suspension: For the example discussed at the end of section 11.13, calculate (a) the transmissibility  $T_{x_1v}(\omega)$  between the road velocity and the suspension stroke,  $x_1 = x_s - x_{us}$  and (b) the cumulative RMS value of the suspension stroke.



## 12

---

### Introduction to active vibration control

*La gloire et le repos sont choses  
qui ne peuvent loger en même  
gîte.*

Montaigne, *Essais*, 1572-1588

This chapter serves as an application of the theory discussed in the previous chapters and a brief introduction to the active control of vibrations. The reader is assumed to have an elementary knowledge of the linear system theory. The first section illustrates the fundamental difference between collocated and non-collocated control systems and the inherent stability associated with the interlacing properties of the poles and zeros of a collocated system. The second section considers the quarter car model of an active suspension; this popular example is used to illustrate the state space formulation and the state feedback control. The third section considers the active damping of a shear frame with an inertial actuator; such systems are representative of existing devices placed on the upper floors of high rise buildings. Finally, the fourth section examines the active damping of a truss with an active strut (e.g. piezoelectric) capable of axial extension, collocated with a force sensor; this problem is representative of a large space truss structure.

#### 12.1 The virtue of collocated control

The diagonal terms of the dynamic flexibility matrix were examined in section 2.6. These terms correspond to *collocated* and *dual* configurations, in which the excitation force is applied to the d.o.f. where the sensor is attached. If the system is undamped, these diagonal terms read

$$G_{kk}(\omega) = \sum_{i=1}^m \frac{\phi_i^2(k)}{\mu_i(\omega_i^2 - \omega^2)} + R_{kk} \quad (12.1)$$

Because all the residues are positive, they have *alternating poles and zeros on the imaginary axis*. Thus the pole/zero pattern of any collocated (dual) control systems is that of Fig.2.8; if the system is undamped, the poles

and zeros lie on the imaginary axis; if the system is lightly damped, they are slightly in the left half plane, close to the imaginary axis (refer to Fig 1.2.a for the relationship between the damping and the position of the poles in the complex plane). The corresponding Bode plots and Nyquist plots are shown in Fig.2.9; we note that the phase diagram never exceeds  $-180^\circ$  (a phase lag of  $180^\circ$  takes place at the natural frequencies  $\omega_i$  and a phase lead of  $180^\circ$  occurs at the transmission zeros or anti-resonances  $z_i$ ). In section 2.6, it was established that the anti-resonance frequencies are the resonance frequencies of the system obtained by adding a kinematic constraint along the d.o.f. on which the external force and the sensor operate.

To illustrate the fundamental difference between collocated and non-collocated control systems, consider the two-mass problem of Fig.12.1. The system has a rigid body mode along the  $x$  axis; it is controlled by a force  $f$  applied to the main body  $M$ . A flexible appendage  $m$  is connected to the main body by a spring  $k$  and a damper  $c$ . A position control system will be designed, using a sensor placed on the main body (collocated), measuring  $y_1$ , and a sensor attached to the flexible appendage measuring  $y_2$ .

The system equations are :

$$M\ddot{y}_1 + c(\dot{y}_1 - \dot{y}_2) + k(y_1 - y_2) = f \quad (12.2)$$

$$m\ddot{y}_2 + c(\dot{y}_2 - \dot{y}_1) + k(y_2 - y_1) = 0 \quad (12.3)$$

With the notations

$$\omega_o^2 = k/m, \quad \mu = m/M, \quad 2\xi\omega_o = c/m \quad (12.4)$$

the transfer functions between the input force  $f$  and  $y_1$  and  $y_2$  are respectively :

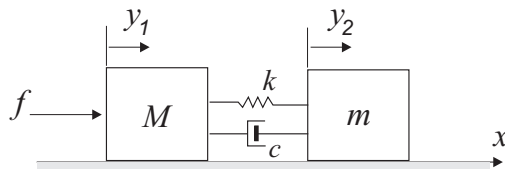


**Fig. 12.1.** Two mass problem.

$$G_1(s) = \frac{Y_1(s)}{F(s)} = \frac{s^2 + 2\xi\omega_0 s + \omega_0^2}{Ms^2 [s^2 + (1 + \mu)(2\xi\omega_0 s + \omega_0^2)]} \quad (12.5)$$

$$G_2(s) = \frac{Y_2(s)}{F(s)} = \frac{2\xi\omega_0 s + \omega_0^2}{Ms^2 [s^2 + (1 + \mu)(2\xi\omega_0 s + \omega_0^2)]} \quad (12.6)$$

$$G_2(s) \simeq \frac{\omega_0^2}{Ms^2 [s^2 + (1 + \mu)(2\xi\omega_0 s + \omega_0^2)]}$$

for low damping ( $\xi \ll 1$ ).<sup>1</sup> There are two poles at the origin and two poles near the imaginary axis; they appear at the denominator of both transfer functions. In  $G_1(s)$ , which refers to the collocated sensor, there are two zeros also near the imaginary axis, at  $(-\xi\omega_0 \pm j\omega_0)$ ; these zeros are identical to the poles of the constrained system where the main body has been blocked. On the contrary,  $G_2(s)$  possesses a single far away zero on the real axis, at  $s = -\omega_0/2\xi$ .

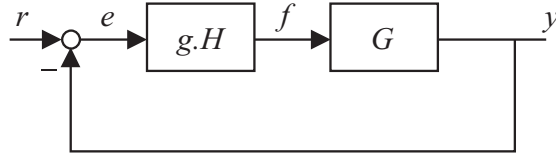


**Fig. 12.2.** Block diagram of the feedback control.

The block diagram of the control system is shown in Fig.12.2.  $G(s)$  is the transfer function of the plant,  $H(s)$  is the transfer function of the compensator;  $g$  is a scalar gain.

A *lead compensator* is used in this example:

$$H(s) = \frac{Ts + 1}{\alpha Ts + 1} \quad (\alpha < 1) \quad (12.7)$$

It includes one pole and one zero located on the negative real axis; the pole is to the left of the zero.

The relationship between the system output  $y$  and the reference input  $r$  is

$$\frac{y}{r} = \frac{gGH}{1 + gGH} \quad (12.8)$$

The *root-locus method* will be used to compare the two system configurations  $G_1(s)$  and  $G_2(s)$  with the same compensator  $H(s)$ . The root-locus

<sup>1</sup> the far away zero will not influence the closed-loop response.

method is a very powerful tool which allows to analyze the effect of a single parameter, the gain  $g$ , on the closed-loop poles, solutions of the characteristic equation:  $1 + gGH(s) = 0$ . The analysis begins with the mapping of the poles and zeros of the open-loop transfer function  $GH(s)$  ( $G$  and  $H$  appear only as a product: the combined effect of the plant and the compensator). The locus consists of  $n$  branches starting from the  $n$  open-loop poles for  $g = 0$  (marked by  $\times$ );  $m$  of them go to the  $m$  open-loop zeros (marked by  $\circ$ ) for  $g \rightarrow \infty$ . The  $n - m$  remaining branches ( $n \geq m$ ) go asymptotically to infinity. There exist a set of rules which allow to sketch the general shape of the root-locus by hand, but the easiest way to get the plot is with a computer aided design software such as Matlab.

The parameters of the system used in the following example are as follows:  $\omega_0 = 1$ ,  $M = 1$ ,  $\xi = 0.02$  and  $\mu = 0.1$ . The parameters of the compensator are  $T = 10$  and  $\alpha = 0.004$ . We examine below the main difference in the behavior of the closed-loop system, when the sensor  $y_1$  (collocated) or  $y_2$  (non-collocated) are used.

### 12.1.1 Collocated control

The open-loop transfer function  $G_1(s)$  is used in this case. Figure 12.3 shows the root locus plot, showing the evolution of the closed loop poles when the control gain  $g$  increases from 0 to  $\infty$ . Since the prod-

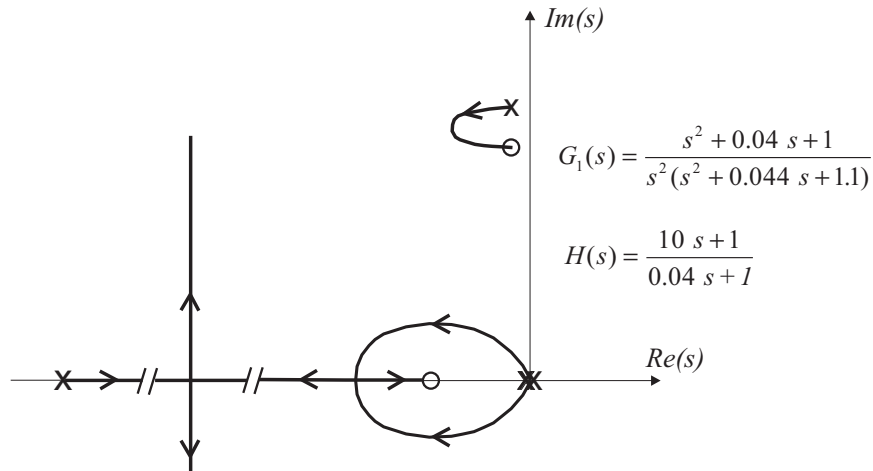


**Fig. 12.3.** Two-mass problem, root locus plot for the collocated control with a lead compensator (the plot is symmetrical with respect to the real axis, only the upper part is shown).

uct  $G_1(s)H(s)$  has two more poles than zeros ( $n - m = 2$ ), the root locus has two asymptotes at  $\pm 90^\circ$ . One observes that the system is stable for all values of the gain, and that the bandwidth of the control system can be a substantial part of  $\omega_0$ . The lead compensator *always* increases the damping of the flexible mode.

Note that in a more complex situation (e.g. see Problem 12.1), if there are not one but several flexible modes, because of the interlacing property of the poles and zeros recalled in the previous section, there are as many pole-zero pairs and the number of poles in excess of zeros remains the same ( $n - m = 2$  in this case), so that the angles of the asymptotes remain  $\pm 90^\circ$  and the root locus never leaves the stable region. The lead compensator increases the damping ratio of *all* the flexible modes, but especially those having their natural frequency between the pole and the zero of the compensator.<sup>2</sup>

### 12.1.2 Non-collocated control

Figure 12.4 shows the root locus plot for the lead compensator applied to the non-collocated open-loop system characterized by the transfer function  $G_2(s)$ , Equ.(12.6), with the same numerical data as in the previous example. The change of sensor affects only the transmission zeros, but

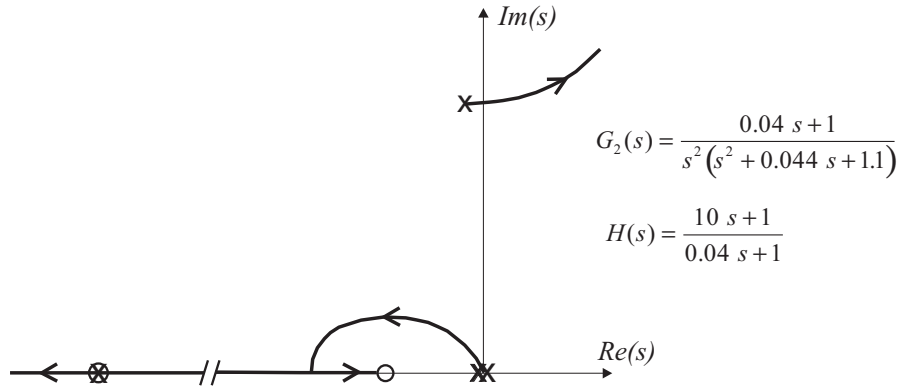


**Fig. 12.4.** Two-mass problem, root locus plot for the non-collocated control with a lead compensator (the plot is symmetrical with respect to the real axis, only the upper part is shown).

<sup>2</sup> Of course, we have assumed that the sensor and the actuator have perfect dynamics; if this is not the case, the foregoing conclusions may be considerably modified, especially for large gains.

leave the poles unchanged;  $G_2(s)$  has a single zero, far left on the real axis. The excess number of poles is in this case  $n - m = 3$  so that, for large gains, the flexible modes are heading towards the asymptotes at  $\pm 60^\circ$ , in the right half plane. The system can operate only for small gains, and only because of the structural damping; a system without damping would be unstable for all gains.

## 12.2 Active suspension: the “sky-hook” damper

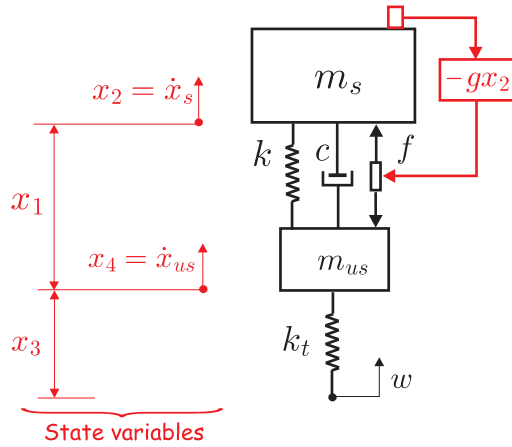


**Fig. 12.5.** Quarter car model with active suspension. The “sky-hook” damper consists of a partial state feedback  $f = -g\dot{x}_s$ . The absolute velocity of the car body may be obtained either by integrating the output of an accelerometer, or directly from a geophone.

The passive suspension has been analyzed in section 11.13. The active suspension consists of a force actuator  $f$  acting in parallel with the spring and damper, between the wheel and the body (Fig. 12.5). Using the same state variables as for the passive suspension, the equations of motion read

$$\begin{aligned} m_s \ddot{x}_2 &= f - kx_1 + c(x_4 - x_2) \\ m_{us} \ddot{x}_4 &= -f - k_t x_3 + kx_1 + c(x_2 - x_4) \\ \dot{x}_1 &= x_2 - x_4 \\ \dot{x}_3 &= x_4 - \dot{w} \end{aligned}$$

and, using again the notations  $\omega_n^2 = k/m_s$  ( $\omega_n$  is the body resonance),  $c/m_s = 2\xi\omega_n$ ,  $\omega_t^2 = k_t/m_{us}$  ( $\omega_t$  is the tyre resonance) and  $\mu = m_{us}/m_s$ , they are rewritten in matrix form:

$$\begin{Bmatrix} \dot{x}_1 \\ \dot{x}_2 \\ \dot{x}_3 \\ \dot{x}_4 \end{Bmatrix} = \begin{bmatrix} 0 & 1 & 0 & -1 \\ -\omega_n^2 & -2\xi\omega_n & 0 & 2\xi\omega_n \\ 0 & 0 & 0 & 1 \\ \frac{\omega_n^2}{\mu} & \frac{2\xi\omega_n}{\mu} & -\omega_t^2 & \frac{-2\xi\omega_n}{\mu} \end{bmatrix} \begin{Bmatrix} x_1 \\ x_2 \\ x_3 \\ x_4 \end{Bmatrix} + \begin{Bmatrix} 0 \\ 1/m_s \\ 0 \\ -1/m_{us} \end{Bmatrix} f + \begin{Bmatrix} 0 \\ 0 \\ -1 \\ 0 \end{Bmatrix} \dot{w} \quad (12.9)$$

or

$$\dot{\mathbf{x}} = A\mathbf{x} + \mathbf{b}f + \mathbf{e}v \quad (12.10)$$

$$y = \mathbf{c}^T \mathbf{x} \quad (12.11)$$

with the state vector  $\mathbf{x} = (x_1, x_2, x_3, x_4)^T$ , the control input vector  $\mathbf{b} = (0, 1/m_s, 0, -1/m_{us})^T$ , the disturbance input vector  $\mathbf{e} = (0, 0, -1, 0)^T$  (the disturbance  $v = \dot{w}$  is the road velocity), and the system matrix

$$A = \begin{bmatrix} 0 & 1 & 0 & -1 \\ -\omega_n^2 & -2\xi\omega_n & 0 & 2\xi\omega_n \\ 0 & 0 & 0 & 1 \\ \frac{\omega_n^2}{\mu} & \frac{2\xi\omega_n}{\mu} & -\omega_t^2 & \frac{-2\xi\omega_n}{\mu} \end{bmatrix} \quad (12.12)$$

The sensor measures the absolute velocity of the car body, corresponding to  $\mathbf{c} = (0, 1, 0, 0)^T$  in the sensor output equation (12.11).

This is the standard control form of a single input single output system. The state feedback reads

$$f = -\mathbf{g}^T \mathbf{x} = -gx_2 = -g\dot{x}_s = -gy \quad (12.13)$$

where  $\mathbf{g} = (0, g, 0, 0)^T$  is the state feedback gain vector. It is called “sky hook” damper because the feedback acts on the car body in the same way as a damper of constant  $g$  connected to a fixed point in space. Note that, in this particular case, the feedback involves only one state, which is directly available from the sensor output ( $y = x_2$ ); thus, no state observer is needed. Combining Equ.(12.10) and (12.13), one finds

$$\dot{\mathbf{x}} = (A - \mathbf{b}\mathbf{g}^T)\mathbf{x} + \mathbf{e}v \quad (12.14)$$

$A - \mathbf{b}\mathbf{g}^T$  is the closed-loop system matrix; its eigenvalues are the closed loop poles of the system. Upon transforming in the Laplace domain, one finds the transfer function between the road velocity and the state vector:

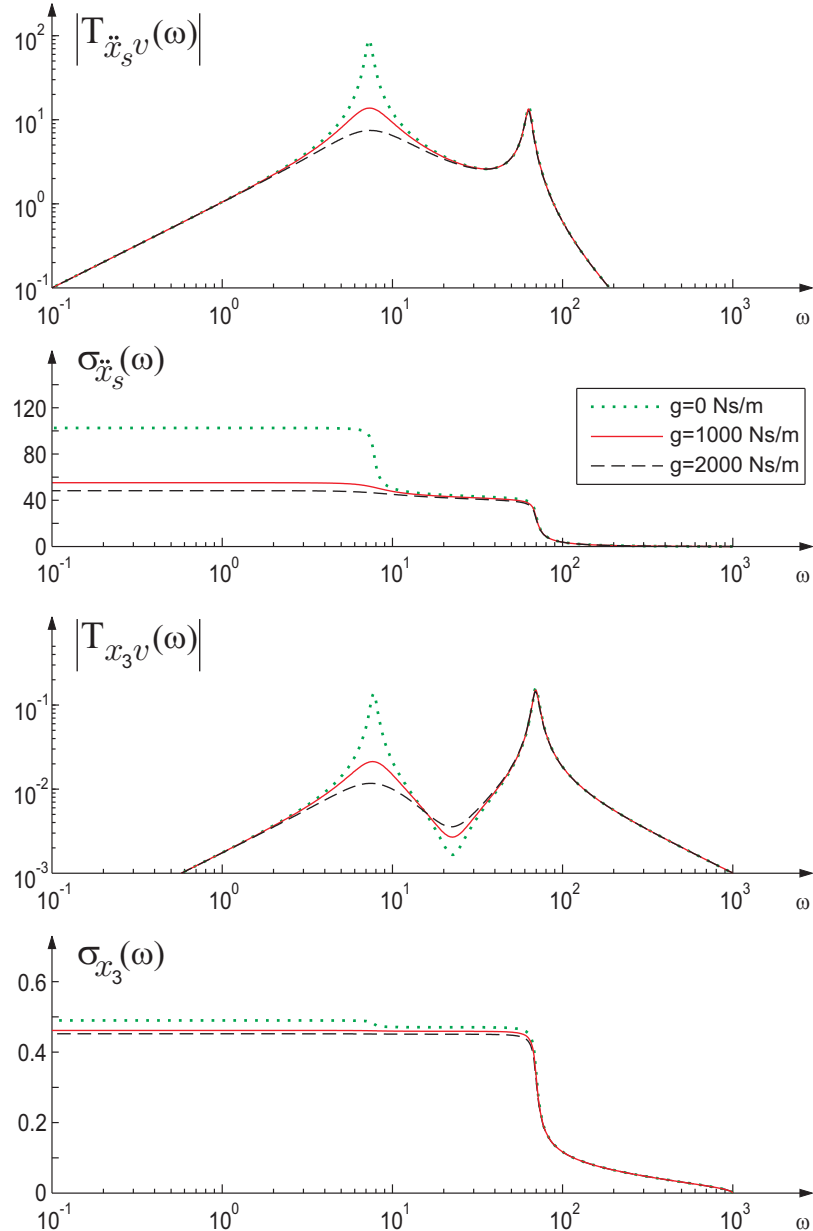


**Fig. 12.6.** Active suspension ( $c = 200$  Ns/m) with sky hook damper  $f = -g\dot{x}_s$ , for 3 values of the control gain  $g = 0, 1000$  and  $2000$  Ns/m. (a) Transmissibility between the road velocity and the body acceleration. (b) Cumulative RMS value of the body acceleration. (c) Transmissibility between the road velocity and the tyre deflection. (d) Cumulative RMS value of the tyre deflection.

$$\mathbf{X}(s) = [sI - (A - \mathbf{b}\mathbf{g}^T)]^{-1} \mathbf{e}V(s) \quad (12.15)$$

The quarter car model of a passive suspension was considered in section 11.13; the effect of the active suspension is illustrated in Fig.12.6. Only the lowest value  $c = 200$  Ns/m of the suspension damping coefficient is considered here, for clarity. One can see that the active control acts very effectively on the body resonance (the first peak at a frequency close to  $\omega_n = \sqrt{k/m_s}$ ) and that (on the contrary to increasing  $c$ ) the attenuation is achieved without deteriorating the high frequency isolation. However, the active control is unable to reduce the wheel resonance (second peak) and has little impact on the road holding in this case (the road holding is measured by the tyre deflection).

### 12.3 Active mass damper

In this section, we reexamine the reduction of the seismic response of the 10-storey building already analyzed in section 11.6, but the Dynamic Vibration Absorber (DVA) is replaced by an Active Mass Damper (AMD). The AMD consists of a spring mass system similar to a DVA, with the addition of a force actuator  $f$  acting in parallel with the spring  $k_a$  and damper  $c_a$  (Fig.12.7). Two notable differences, however, are that (i) the stiffness  $k_a$  is significantly lower than that of a DVA, so that the natural frequency of the AMD satisfies:

$$\omega_a = \sqrt{\frac{k_a}{m_a}} \ll \omega_1 \quad (12.16)$$

(ii) the damper  $c_a$  is selected to introduce a significant damping in the actuator system:

$$0.5 \leq \xi_a = \frac{c_a}{2m_a\omega_a} \leq 0.7 \quad (12.17)$$

With these characteristics, the inertial actuator behaves as a near-perfect force actuator in the frequency band containing the flexible modes of the structure. We assume that the system is equipped with a sensor measuring the horizontal velocity of the top floor,  $\dot{x}_{10}$ .<sup>3</sup> Note that, although both the velocity sensor and the AMD are attached to the same floor, the control system is not *collocated*, because the system output  $\dot{x}_{10}$  is the top floor velocity while the system input  $f$  consists of a pair of opposing forces acting

---

<sup>3</sup> This can be obtained either with a *geophone*, or by integrating the output signal of an accelerometer (although accelerometers do not work well at low frequency).

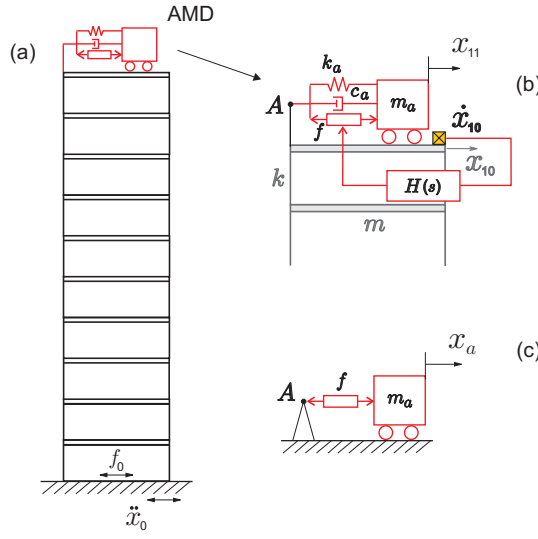


**Fig. 12.7.** (a) 10-storey building with an Active Mass Damper (AMD) at the top. (b) Active Mass Damper: a force actuator  $f$  operates in parallel with the spring  $k_a$  and the damper  $c_a$ . The parameters are selected according to  $m_a = \varepsilon m_T$ ,  $\omega_a = \sqrt{k_a/m_a} \ll \omega_1$ ,  $0.5 \leq \xi_a = c_a/2m_a\omega_a \leq 0.7$ . (c) Perfect inertial actuator.

respectively on the top floor and on the inertial mass  $m_a$ . However, if the inertial actuator parameters are chosen as explained before, it behaves closely to a perfect force actuator  $f$  applied to the top floor (collocated), and the open-loop FRF,  $G = \dot{x}_{10}/f$ , exhibits alternating poles and zeros.<sup>4</sup>

<sup>4</sup> To better understand the functioning of an AMD, consider first a perfect inertial actuator attached to a fixed point A (Fig.12.7.c). It consists of a force actuator acting on a mass  $m_a$ . Expressing the equilibrium of the massless actuator, the force applied to A is  $f = -m_a\ddot{x}_a$  (positive in traction). Next consider the AMD acting on a fixed point A (Fig.12.7.b with  $x_n = 0$ ). The governing equation is

$$m_a\ddot{x}_a + c_a\dot{x}_a + k_a x_a = -f$$

(with again  $f$  being positive in traction). Thus, the transfer function between  $f$  and  $x_a$  is

$$x_a = \frac{-f}{m_a s^2 + c_a s + k_a};$$

the force  $F$  applied to point A is  $F = -m_a\ddot{x}_a$  and the transfer function between  $f$  and  $F$  is that of a high-pass filter:

$$\frac{F}{f} = \frac{s^2}{s^2 + 2\xi_a\omega_a s + \omega_a^2} \quad (12.18)$$

where  $\xi_a$  and  $\omega_a$  are defined according to Equ.(12.16) and (12.17). Thus, when A is fixed, the AMD behaves as a perfect force generator for frequencies  $\omega \gg \omega_a$ .

### 12.3.1 System modeling

As compared to the system considered in section 11.6, the only difference is the presence of a force  $f$  acting between the top floor  $x_{10}$  and the inertial mass  $x_{11}$ . The governing equation is

$$M\ddot{\mathbf{y}} + C\dot{\mathbf{y}} + K\mathbf{y} = -M\mathbf{1}\ddot{x}_0 + \mathbf{b}_a f \quad (12.19)$$

where  $\mathbf{b}_a = (0, \dots, 0, 1, -1)^T$  is the influence vector of the control force ( $f$  assumed positive in traction). The matrices  $M$ ,  $C$  and  $K$  have been constructed in section 11.6.1. Introducing the state vector

$$\mathbf{z} = (\mathbf{y}^T, \dot{\mathbf{y}}^T)^T \quad (12.20)$$

it can be rewritten in state variable form (as a system of first order differential equations)

$$\dot{\mathbf{z}} = A\mathbf{z} + \mathbf{b}f + \mathbf{e}\ddot{x}_0 \quad (12.21)$$

where  $A$  is the system matrix

$$A = \begin{bmatrix} 0 & I \\ -M^{-1}K & -M^{-1}C \end{bmatrix}, \quad \mathbf{b} = \left\{ \begin{array}{c} \mathbf{0} \\ M^{-1}\mathbf{b}_a \end{array} \right\}, \quad \mathbf{e} = \left\{ \begin{array}{c} \mathbf{0} \\ -\mathbf{1} \end{array} \right\} \quad (12.22)$$

(the size of the control input vector  $\mathbf{b}$  and disturbance input vector  $\mathbf{e}$  is twice the number of d.o.f., 22 in this case).

The sensor output is the velocity of the top floor,

$$v = \dot{x}_{10} = \dot{x}_0 + \mathbf{b}_s^T \dot{\mathbf{y}} \quad (12.23)$$

where the vector  $\mathbf{b}_s = (0, \dots, 1, 0)^T$  defines the sensor location (note that  $\mathbf{b}_s \neq \mathbf{b}_a$ , because the control force is acting also on  $m_a$ ). This equation is rewritten in state space form

$$v = \mathbf{c}^T \mathbf{z} + \dot{x}_0 \quad (12.24)$$

with the output vector  $\mathbf{c}^T = (\mathbf{0}^T, \mathbf{b}_s^T)$ . In addition to the system equation (12.21) and the output equation (12.24), the feedback control law relates the control input to the sensor output; in this case a direct velocity feedback is used:

$$f = -gv \quad (12.25)$$

$g$  is the control gain.

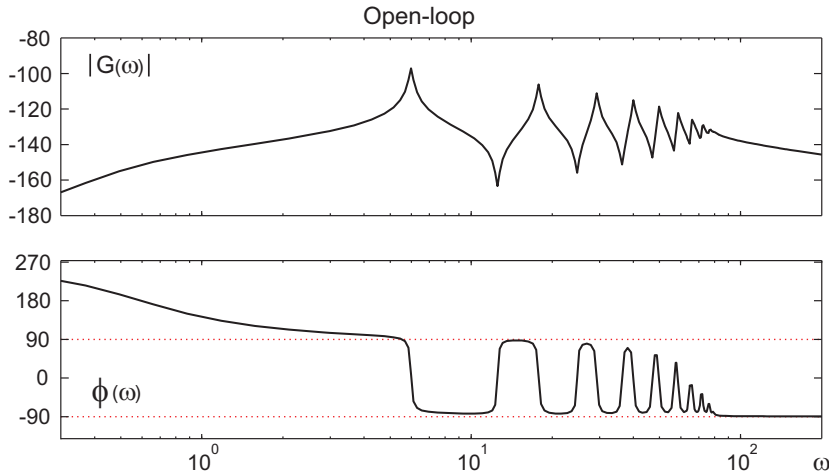


**Fig. 12.8.** 10-storey building with an Active Mass Damper (AMD) at the top. Open-loop FRF  $G = v/f$  between the force  $f$  in the actuator and the velocity of the top floor (amplitude in dB and phase). The FRF exhibits alternating poles and zeros above  $\omega_1$ .

### 12.3.2 System response

The open-loop transfer function of the system is the relationship between the control input  $f$  and the sensor output  $v$  without feedback control control and without disturbance; it is readily obtained from Equ.(12.21) and (12.24):

$$G(s) = \mathbf{c}^T(sI - A)^{-1}\mathbf{b} \quad (12.26)$$

The open-loop FRF  $G(j\omega)$  is obtained by substituting  $s = j\omega$ . It is represented in Fig.12.8. The FRF exhibits alternating poles and zeros for all flexible modes ( $\omega_1$  and above), typical of collocated control systems. The closed-loop system equation is obtained by combining Equ.(12.21), (12.24) and (12.25); one finds easily

$$\dot{\mathbf{z}} = (A - g\mathbf{b}\mathbf{c}^T)\mathbf{z} - g\mathbf{b}\dot{x}_0 + \mathbf{e}\ddot{x}_0 \quad (12.27)$$

The eigenvalues of the closed-loop system matrix  $A - g\mathbf{b}\mathbf{c}^T$  are the closed-loop poles. Their evolution for increasing values of the gain  $g$  is represented in the root locus of Fig.12.9. The transmissibility (in the frequency domain) between the ground acceleration  $\ddot{x}_0$  and the state  $\mathbf{z}$  is

$$\mathbf{Z}(j\omega) = [j\omega I - (A - g\mathbf{b}\mathbf{c}^T)]^{-1}\left(-\frac{g\mathbf{b}}{j\omega} + \mathbf{e}\right)\ddot{X}_0(j\omega) \quad (12.28)$$

Consider the response to the stationary seismic excitation of the ground acceleration already considered in section 8.10. The shear force at the base is given by Equ.(7.13). Using the state vector,

$$f_0 = -\mathbf{1}^T(K\mathbf{y} + C\dot{\mathbf{y}}) = -\mathbf{1}^T(K, C)\mathbf{z} \quad (12.29)$$

The closed-loop transmissibility between the ground acceleration  $\ddot{x}_0$  and  $f_0$  is readily obtained by combining with the previous equation. Figure 12.10.a shows the PSD of the shear force  $f_0$  resulting from the steady state response to a seismic acceleration with a Kanai-Tajimi profile considered in section 8.10, for various control gains, respectively  $g_1$  leading to a damping ratio of  $\xi = 0.05$  in the first mode,  $g_2$  leading to  $\xi = 0.1$  and  $g_3$  to  $\xi = 0.15$ . The corresponding values of the closed-loop poles are indicated in Fig.12.9. An important observation is that the AMD damps all the modes, unlike the DVA. The cumulative RMS value of the non-dimensional shear force is shown in Fig.12.10.b, for the same values of the gain, and the cumulative RMS control force  $f$  is represented in Fig.12.10.c; this figure shows the the control effort increases rapidly with

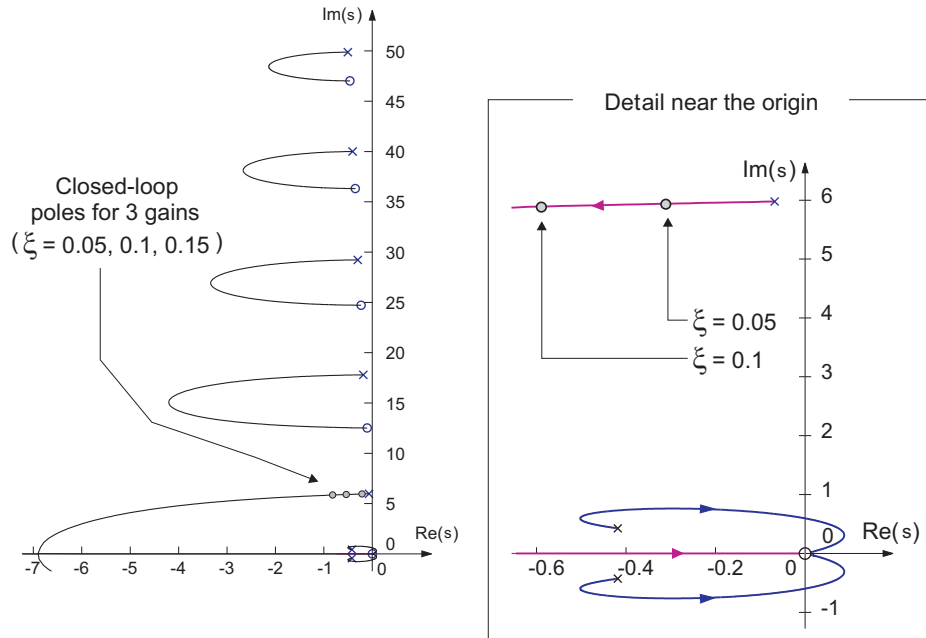


**Fig. 12.9.** 10-storey building with an Active Mass Damper (AMD) at the top and velocity feedback. Evolution of the closed-loop poles for increasing values of the control gain  $g$  (root locus).

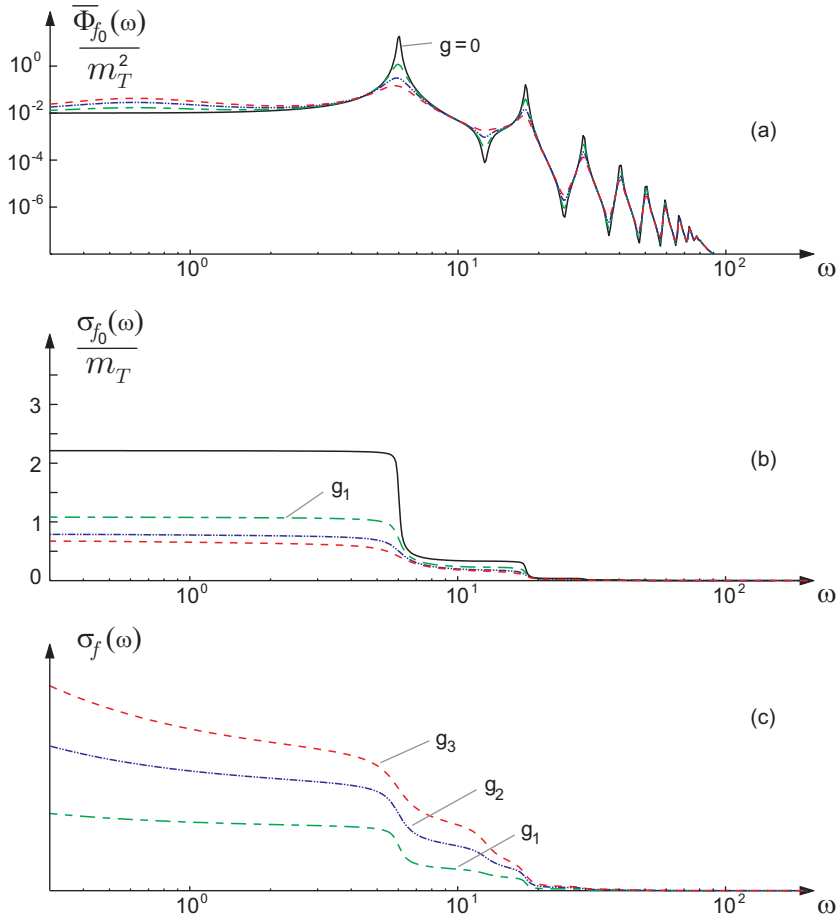


**Fig. 12.10.** 10-storey building with an Active Mass Damper (AMD) at the top ( $\varepsilon = 0.01$ ) and velocity feedback. (a) PSD of the shear force  $f_0$  due to the seismic acceleration with Kanai-Tajimi profile considered in section 8.10, for various values of the control gain, leading respectively to  $\xi$  of 5%, 10% and 15 % in the first mode. (b) Cumulative RMS value of the non-dimensional reaction force. (c) Cumulative RMS value of the control force.

the gain. Note that the control effort will eventually fix the size of the actuator.

## 12.4 Active truss

Consider the truss structure of Fig.12.11, where one of the bars has been replaced by an active strut consisting of a displacement actuator and a collocated force sensor. The constitutive equation of the active strut is

$$\Delta = \delta + f/K_a = g_a u + f/K_a \quad (12.30)$$

where  $\delta = g_a u$  is the unconstrained expansion induced by the control input  $u$  ( $g_a$  is the actuator gain),  $f$  is the force (positive in traction) acting on the strut and  $K_a$  is the strut stiffness.<sup>5</sup> This equation expresses that the total extension of the active strut is the sum of the (unconstrained) control extension and the elastic extension. The sensor output is the force  $f$  in the strut,

$$f = K_a(\Delta - \delta) = K_a(\mathbf{b}^T \mathbf{x} - \delta) \quad (12.31)$$

where  $\mathbf{b}^T$  is the vector defining the position of the active strut in the truss, such that its total extension is  $\Delta = \mathbf{b}^T \mathbf{x}$ . For the situation depicted in Fig.12.11,  $\Delta = x_5 - x_3$ . If the generalized coordinates are the nodal displacements along  $x$  and  $y$ ,  $\mathbf{x} = (x_1, y_1, x_2, y_2, \dots, x_{14}, y_{14})^T$ ,  $\mathbf{b}^T$  is a row

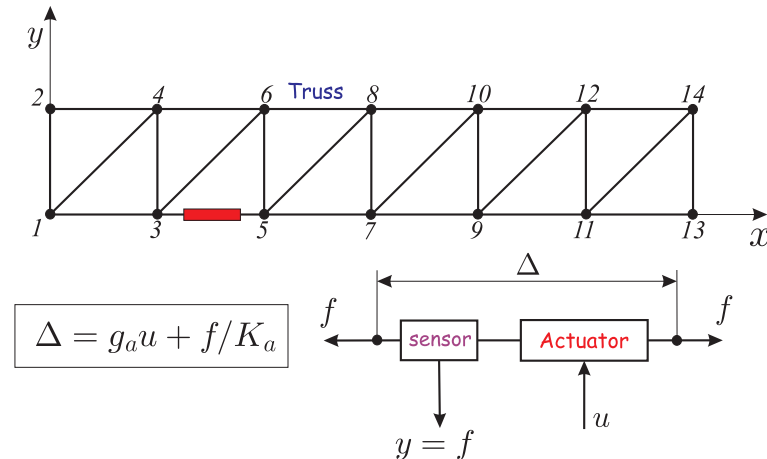


**Fig. 12.11.** Active truss with an active strut consisting of a displacement actuator and a force sensor.  $\delta = g_a u$  is the unconstrained extension of the strut induced by the control  $u$ . The passive stiffness of the strut is  $K_a$  and  $f/K_a$  is the elastic extension.  $\Delta = b^T x$  is the total extension of the active strut.

<sup>5</sup> This constitutive equation applies to a broad variety of actuators: for a piezoelectric actuator,  $u$  is a voltage and the gain  $g_a$  is expressed in  $m/V$ ; for a magnetostrictive actuator,  $u$  will be the input current and the gain is expressed in  $m/A$ , etc...

vector of dimension 28, with all entries being 0 except those corresponding to the components along  $x$  at nodes 3 and 5

$$\mathbf{b}^T = (0, 0, 0, 0, -1, 0, 0, 0, 1, 0, 0, \dots, 0)$$

If the active strut were placed instead of the bar at  $45^0$  connecting node 1 to node 4, the influence vector of the strut would become

$$\mathbf{b}^T = (-1/\sqrt{2}, -1/\sqrt{2}, 0, 0, 0, 0, 1/\sqrt{2}, 1/\sqrt{2}, 0, \dots, 0)$$

If  $K^*$  stands for the stiffness matrix of the truss without active strut, the equation of motion of the truss (active strut removed and assuming no damping)

$$M\ddot{\mathbf{x}} + K^*\mathbf{x} = -\mathbf{b}f \quad (12.32)$$

where the right hand side is the force exerted by the active strut on the truss. Note that the influence vector  $\mathbf{b}$  appearing in this equation is the same as that involved in the sensor output equation because the actuator and the sensor are collocated and dual (acting on the same nodes and in the same direction); the negative sign is due to the fact that the force  $f$  is positive in traction in the strut and the forces acting on the truss is opposing the force acting on the strut. Substituting  $f$  from the sensor equation, one finds the equation governing the dynamics of the active truss:

$$M\ddot{\mathbf{x}} + (K^* + \mathbf{b}\mathbf{b}^T K_a)\mathbf{x} = \mathbf{b}K_a\delta \quad (12.33)$$

or

$$M\ddot{\mathbf{x}} + K\mathbf{x} = \mathbf{b}K_a\delta \quad (12.34)$$

where  $K = K^* + \mathbf{b}\mathbf{b}^T K_a$  is the global stiffness matrix.  $\mathbf{b}\mathbf{b}^T K_a$  is the contribution of the active strut in the global stiffness matrix.  $\mathbf{b}K_a\delta$  is the control force, equal to the product of the free expansion  $\delta$  and the strut stiffness  $K_a$ .<sup>6</sup>

#### 12.4.1 Open-loop transfer function

Let  $\phi_i$  be the normal modes and  $\omega_i$  the natural frequencies of the system, solutions of the eigenvalue problem

$$(K - \omega_i^2 M)\phi_i = 0 \quad (12.35)$$

---

<sup>6</sup> The mass of the strut may be accounted for by adding the appropriate contribution to  $M$ .

They satisfy the usual orthogonality conditions

$$\phi_i^T M \phi_j = \mu_i \delta_{ij} \quad (12.36)$$

$$\phi_i^T K \phi_j = \mu_i \omega_i^2 \delta_{ij} \quad (12.37)$$

If the global displacements are expanded into modal coordinates,

$$\mathbf{x} = \sum_i z_i \phi_i \quad (12.38)$$

the modal amplitudes  $z_i$  are solutions of

$$\mu_i (\ddot{z}_i + \omega_i^2 z_i) = \phi_i^T \mathbf{b} K_a \delta \quad (12.39)$$

Upon taking the Laplace transform, one easily gets

$$\mathbf{x} = \sum_{i=1}^n \frac{\phi_i \phi_i^T}{\mu_i (\omega_i^2 + s^2)} \mathbf{b} K_a \delta \quad (12.40)$$

and the total extension of the active strut

$$\Delta = \mathbf{b}^T \mathbf{x} = \sum_{i=1}^n \frac{K_a (\mathbf{b}^T \phi_i)^2}{\mu_i \omega_i^2 (1 + s^2 / \omega_i^2)} \delta \quad (12.41)$$

From Equ.(12.37),  $\mu_i \omega_i^2 / 2$  is clearly the strain energy in the structure when it vibrates according to mode  $i$ , and  $K_a (\mathbf{b}^T \phi_i)^2 / 2$  represents the strain energy in the active strut when the structure vibrates according to mode  $i$ . Thus, the ratio

$$\nu_i = \frac{K_a (\mathbf{b}^T \phi_i)^2}{\mu_i \omega_i^2} \quad (12.42)$$

is readily interpreted as the *fraction of modal strain energy* in the active strut for mode  $i$ . With this notation, the previous equation is rewritten

$$\Delta = \mathbf{b}^T \mathbf{x} = \sum_{i=1}^n \frac{\nu_i}{(1 + s^2 / \omega_i^2)} \delta \quad (12.43)$$

and the sensor output equation reads

$$f = K_a \left[ \sum_{i=1}^n \frac{\nu_i}{(1 + s^2 / \omega_i^2)} - 1 \right] \delta \quad (12.44)$$

Thus, the open-loop FRF between the actuator free expansion  $\delta$  and the sensor force  $f$  is obtained by substituting  $s = j\omega$

$$\frac{f}{\delta} = K_a \left[ \sum_{i=1}^n \frac{\nu_i}{(1 - \omega^2/\omega_i^2)} - 1 \right] \quad (12.45)$$

A typical plot is represented in Fig.12.12. All the residues  $\nu_i$  being positive, there will be alternating poles and zeros along the imaginary axis. This important property was already stressed in the beginning of this chapter; it is typical of collocated system and it is responsible for their built-in robustness.

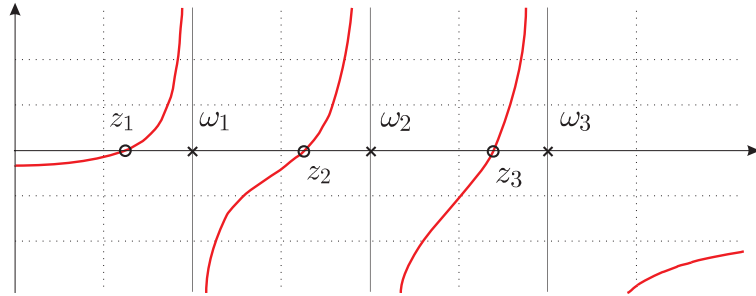


**Fig. 12.12.** Open-loop FRF  $f/\delta$  of the active strut mounted in the truss (undamped).

#### 12.4.2 Active damping by integral force feedback

The truss can be actively damped by a (positive) integral force feedback control law:

$$\delta = \frac{g}{K_a s} f \quad (12.46)$$

(the constant  $K_a$  at the denominator is for normalization purpose;  $f/K_a$  is the elastic extension of the strut). The block diagram of the system is represented in Fig.12.13. The pole-zero pattern of the system is shown in Fig 12.14. It consists of interlacing pole-zero pairs on the imaginary axis ( $z_1 < \omega_1 < z_2 < \omega_2 \dots$ ) and the pole at  $s = 0$  from the controller. The root-locus plot consists of the negative real axis and a set of loops going from the open-loop poles  $\pm j\omega_i$  to the open-loop zeros  $\pm jz_i$ . All the loops are entirely contained in the left half plane, so that the closed-loop system is unconditionally stable, for all values of the gain  $g$ . Note that this property is maintained, even if the poles and zeros are moved slightly

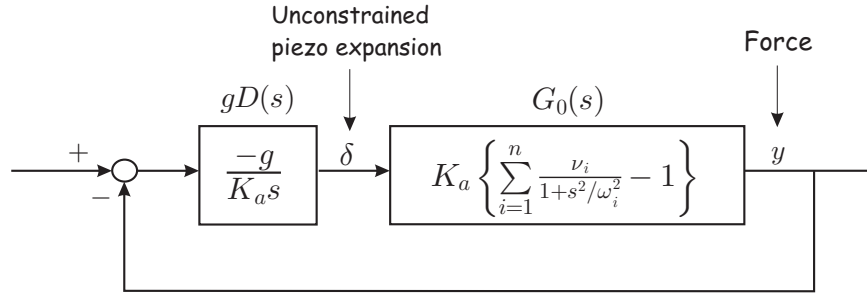


**Fig. 12.13.** Block diagram of the IFF controller.

along the imaginary axis, provided that the interlacing property of the poles and zeros holds, which is guaranteed because of the actuator/sensor collocation. Combining (12.31) and (12.46) one gets

$$\delta = \frac{g}{s+g} \mathbf{b}^T \mathbf{x} \quad (12.47)$$

and further combining with the dynamic equation (12.34), one gets the closed-loop characteristic equation

$$[Ms^2 + (K^* + \mathbf{b}\mathbf{b}^T K_a) - \mathbf{b}\mathbf{b}^T K_a \frac{g}{s+g}] \mathbf{x} = 0 \quad (12.48)$$

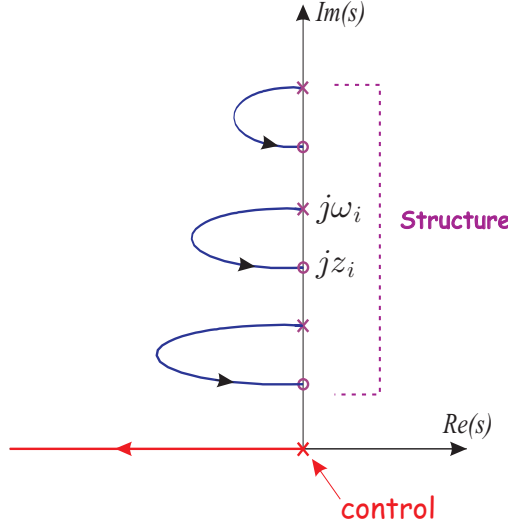


**Fig. 12.14.** Pole-zero pattern of the active truss (undamped) and root-locus of the IFF controller (the root-locus is symmetrical with respect to the real axis, only the upper part is shown).

For  $g = 0$ , the eigenvalues are indeed the open-loop poles,  $\pm j\omega_i$ . Asymptotically, for  $g \rightarrow \infty$ , the eigenvalue problem becomes

$$[Ms^2 + K^*]x = 0 \quad (12.49)$$

where  $K^*$  is the stiffness matrix of the structure without the active strut. Thus, the open-loop zeros  $\pm jz_i$  are the natural frequencies of the truss after removing the active strut. For well separated modes, the individual loops in the root-locus of Fig 12.14 are, to a large extent, independent of each other, and the root locus of a single mode can be drawn from the asymptotic values  $\pm j\omega_i$  and  $\pm jz_i$  only (Fig 12.15). The corresponding characteristic equation is

$$1 + g \frac{(s^2 + z_i^2)}{s(s^2 + \omega_i^2)} = 0 \quad (12.50)$$

The actual root-locus, Fig.12.14, which includes the influence of the other modes, is only slightly different from that of Fig 12.15, with the same asymptotic values at  $\pm j\omega_i$  and  $\pm jz_i$ . It can be shown that the maximum modal damping for mode  $i$  is given by

$$\xi_i^{max} = \frac{\omega_i - z_i}{2z_i} \quad (z_i \geq \omega_i/3) \quad (12.51)$$

It is achieved for  $g = \omega_i \sqrt{\omega_i/z_i}$ . The IFF controller is very efficient for providing active damping, but reduces the static stiffness of the structure; this problem is examined below.

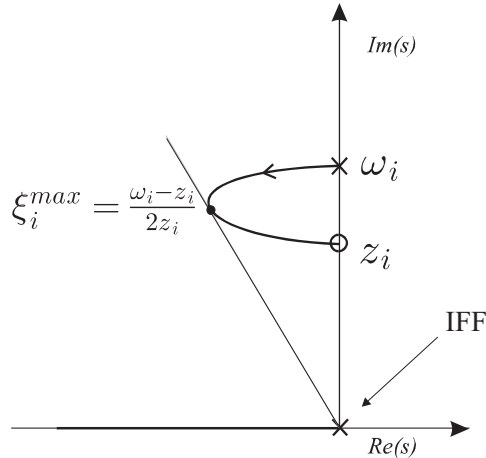


**Fig. 12.15.** (a) IFF root locus of a single mode (the root-locus is symmetrical with respect to the real axis, only the upper part is shown).

### 12.4.3 Beta controller

If the truss is subjected to external disturbances  $\mathbf{f}_d$ , the governing equation is

$$M\ddot{\mathbf{x}} + K\mathbf{x} = \mathbf{b}K_a\delta + \mathbf{f}_d \quad (12.52)$$

with the sensor output equation

$$f = K_a(\mathbf{b}^T \mathbf{x} - \delta) \quad (12.53)$$

A more general controller is assumed:

$$\delta = \frac{H(s)}{K_a} \cdot f \quad (12.54)$$

Combining the foregoing equations, one gets  $\delta = H(s)/[1 + H(s)] \cdot \mathbf{b}^T \mathbf{x}$  and the closed-loop system is governed by

$$[Ms^2 + K - K_a \mathbf{b} \mathbf{b}^T \frac{H(s)}{1 + H(s)}] \mathbf{x} = \mathbf{f}_d \quad (12.55)$$

For the particular case of the IFF,  $H(s) = g/s$ ; the foregoing equation becomes

$$[Ms^2 + K - K_a \mathbf{b} \mathbf{b}^T \frac{g}{s + g}] \mathbf{x} = \mathbf{f}_d \quad (12.56)$$

The closed-loop static stiffness is obtained for  $s = 0$ :

$$K^{stat} = K - K_a \mathbf{b} \mathbf{b}^T = K^* \quad (12.57)$$

which corresponds to the structure where the active strut has been removed. Such a stiffness reduction is not acceptable in many applications; however, examining Equ.(12.55), one sees that this problem can be solved if the control law is be changed in such a way that  $H(0) = 0$ . This condition is met by adding a high-pass filter to the IFF, leading to the “Beta controller”:

$$H(s) = \frac{gs}{(s + \beta)^2} \quad (12.58)$$

where  $\beta$  is a small positive number such that  $\beta \ll z_1$ . As compared to the IFF, the pole at the origin is replaced by one zero at the origin and a pair of poles at  $s = -\beta$ , near the origin. For well separated modes, the individual loops of the root locus may again be treated independently and Equ(12.50) is replaced by

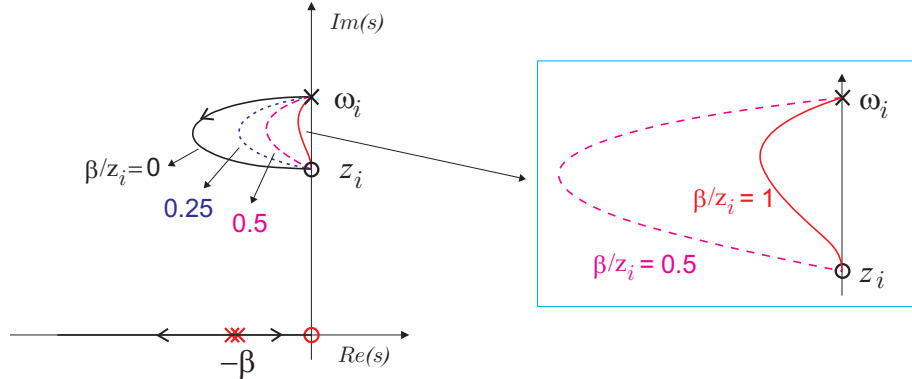


**Fig. 12.16.** Root locus of the closed-loop poles with the Beta controller  $gs/(s + \beta)^2$ , for various values of the ratio  $\beta/z_i$ . The IFF controller corresponds to  $\beta = 0$ . The locus is always stable for  $\beta < z_i$ ; for  $\beta = z_i$ , it is tangent to the imaginary axis at the zero  $\pm jz_i$ .

$$1 + \frac{gs}{(s + \beta)^2} \frac{(s^2 + z_i^2)}{(s^2 + \omega_i^2)} = 0 \quad (12.59)$$

It is represented in Fig.12.16. When  $\beta = 0$ , there is a pole-zero cancellation and the control is reduced to the IFF. As  $\beta$  increases, the root locus has two branches on the real axis, starting from  $s = -\beta$  in opposite directions; one of the closed-loop poles remains trapped between 0 and  $-\beta$ ; the loops still go from  $\pm j\omega_i$  to  $\pm jz_i$ , but they tend to be smaller, leading to less active damping; this is the price to pay for recovering the static stiffness. Analyzing the root locus in detail, one can show that the system is unconditionally stable (for all modes) provided that  $\beta < z_1$ .

The effect of the Beta controller on the dynamic response of the structure is illustrated in Fig.12.17, which shows the dynamic compliance at the top of a telescope (collocated force excitation and displacement) for various values of  $\beta$ . The open-loop FRF is in dotted line. One sees that the FRF of the Beta controller matches the open-loop FRF in a low frequency band which increases with  $\beta$ , but at the expense of the damping of the dominant mode of the system.

## 12.5 Problems

**P.12.1** Consider the three-mass system of Fig.12.18, with a control force  $f$  acting on mass  $M$ . Assuming that a collocated displacement sensor measures the displacement  $x_1$ , (a) calculate the transmission zeros in the

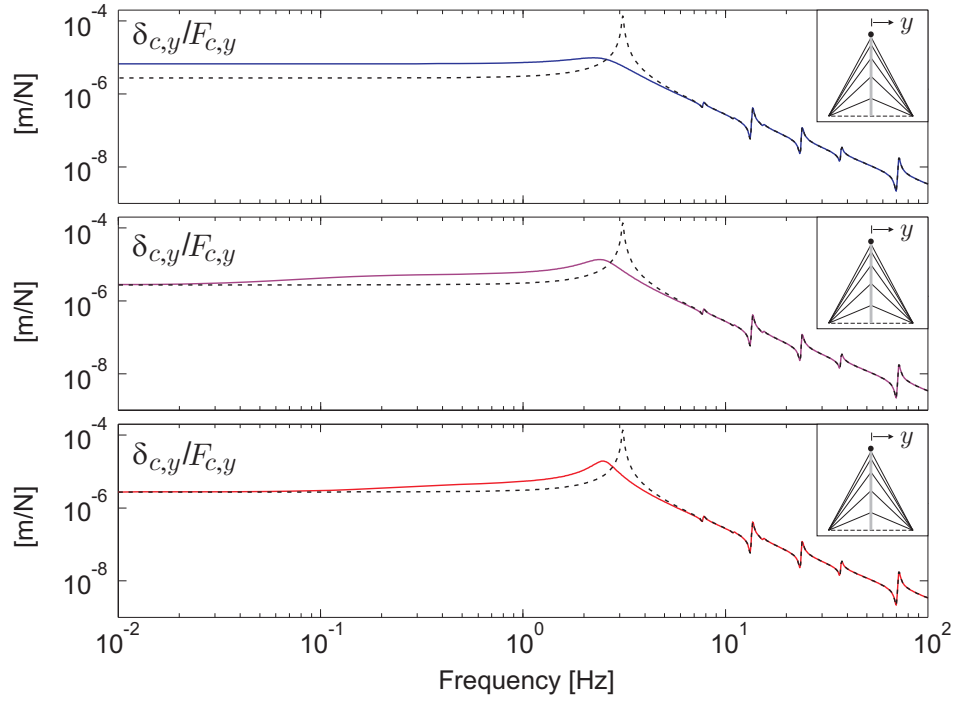


**Fig. 12.17.** Frequency response functions of a telescope structure actively damped with a  $\beta$  controller: (a)  $\beta = 0$  (IFF), (b)  $\beta/\omega_1 = 0.25$ , (c)  $\beta/\omega_1 = 0.5$ .

open-loop transfer function ; (b) draw the pole-zero plot of the open-loop system; (c) draw the root-locus for the collocated control with a lead compensator and compare it with the two-mass system of Fig.12.3. (d) Sketch the root-locus if more spring mass d.o.f. ( $m, k$ ) are added to the right of  $x_3$ . [Hint: the anti-resonance frequencies are the resonance frequencies of the constrained system.]

**P.12.2 Hybrid Mass Damper (HMD):** Consider the 10 storey building with a AMD tuned according to the equal peak design of a TMD,

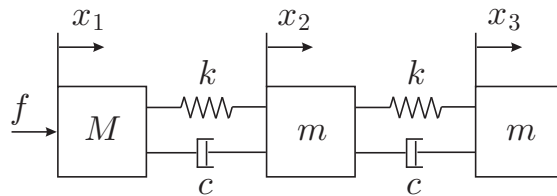


**Fig. 12.18.** Three-mass system.

Equ.(11.25). (a) Draw the evolution of the closed-loop poles for increasing values of the control gain. (b) Calculate the transmissibility between the ground acceleration  $\ddot{x}_0$  and the shear force at the base,  $f_0$ , for various values of the gain. (c) Suggest ways of changing the tuning of the AMD to improve the structural response [Preumont & Seto, section 3.5].

## Bibliography

---

- ASAMI, T., NISHIHARA, O. & BAZ, A.M. Analytical solutions to  $H_\infty$  and  $H_2$  optimization of dynamic vibration absorbers attached to damped linear systems, *ASME Journal of Vibration and Acoustics*, Vol.124, 284-295, April 2002.
- BATHE, K.J. & WILSON, E.L. *Numerical Methods in Finite Element Analysis*, Prentice-Hall, 1976.
- BENDAT, J. & PIERSOL, A. *Random Data: Analysis and Measurement Procedures*, Wiley-Interscience, 1971.
- BENDAT, J. & PIERSOL, A. *Engineering Applications of Correlation and Spectral Analysis*, Wiley-Interscience, 1980.
- BLEVINS, R.D. *Formulas for natural frequency and mode shape*, Van Nostrand Reinhold, 1979.
- BOURCIER de CARBON, Ch. Perfectionnement à la suspension des véhicules routiers. Amortisseur relaxation. Comptes Rendus de l'Académie des Sciences de Paris, Vol.225, pp. 722-724, Juillet-Déc. 1947.
- BRACEWELL, R.N. *The Fourier Transform and its Applications*, McGraw-Hill, 1978.
- CANNON, R.H. *Dynamics of Physical Systems*, McGraw-Hill, 1967.
- CARTWRIGHT, D.E. & LONGUET-HIGGINS, M.S. The statistical distribution of the maxima of a random function, *Proc. Roy. Soc. Ser. A*, 237, 212-232, 1956.
- CHALASANI, R.M., Ride Performance Potential of Active Suspension Systems, Part 1: Simplified Analysis based on a Quarter-Car Model, ASME Symposium on Simulation and Control of Ground Vehicles and Transportation Systems, Anaheim, CA, Dec. 1984.
- CLOUGH, R.W. & PENZIEN, J. *Dynamics of Structures*, McGraw-Hill, 1975.
- CRAIG, R.R. *Structural Dynamics*, Wiley, 1981.
- CRAIG, R.R., BAMPTON, M.C.C. Coupling of Substructures for Dynamic Analyses, *AIAA Journal*, Vol.6(7), 1313-1319, 1968.
- CRANDALL, S.H. & MARK, W.D. *Random Vibration in Mechanical Systems*, Academic Press, 1963.
- CRANDALL, S.H., KARNOPP, D.C., KURTZ, E.F, Jr., PRIDMORE-BROWN, D.C. *Dynamics of Mechanical and Electromechanical Systems*, McGraw-Hill, N-Y, 1968.
- CRANDALL, S.H. The role of damping in vibration theory *J. of Sound and Vibration* 11 (1), pp.3-18, 1970.
- DAVENPORT, A.G. The application of statistical concepts to the wind loading of structures, *Proc. Inst. Civ. Eng.*, Vol.19, pp.449-471, August 1961.
- DAVENPORT, A.G. Note on the distribution of the largest value of a random function with application to gust loading, *Proc. Inst. Civ. Eng.*, Vol.28, 187-196, 1964.
- DAVENPORT, A.G. The treatment of wind loading on tall buildings, Proc. of the symposium on Tall Buildings, University of Southampton, Pergamon Press, London, 1966.
- DEN HARTOG, J.P. *Mechanical Vibrations*, 4th Edition, Dover, 1985.
- DENMAN, H.H. Tautochronic bifilar pendulum torsion absorbers for reciprocating engines, *Journal of Sound and Vibration*, 159(2), 251-277, 1992.

- ELISHAKOFF, I. *Probabilistic Methods in the Theory of Structures*, Wiley, 1982.
- EWINS, D.J. *Modal Testing: Theory and Practice*, Wiley, 1984.
- FUNG, Y.C. *An Introduction to the Theory of Aeroelasticity*, Dover, 1969.
- GAWRONSKI, W.K. *Advanced Structural Dynamics and Active Control of Structures*, Springer, 2004.
- GAWRONSKI, W.K. *Dynamics and Control of Structures - A Modal Approach*, Springer, 1998.
- GENTA, G. *Dynamics of Rotating Systems*, Springer, 2005.
- GERADIN, M. & RIXEN, D. *Mechanical Vibrations, Theory and Application to Structural Dynamics*, Second Edition, Wiley, 1997.
- GOLDSTEIN, H. *Classical Mechanics*, Second Edition, Addison-Wesley, 1980.
- HAGEDORN, P. *Non-linear oscillations*, Clarendon Press, 1981.
- HROVAT, D., Survey of Advanced Suspension Developments and Related Optimal Control Applications, *Automatica*, Vol.33, No 10, 1781-1817, 1997.
- HUGHES, P.C. Dynamics of flexible space vehicles with active attitude control, *Celestial Mechanics Journal*, Vol.9, 21-39, March 1974.
- HUGHES, P.C. Space structure vibration modes: how many exist? which ones are important? *IEEE Control Systems Magazine*, February 1987.
- HUGHES, T.J.R. *The Finite Element Method, Linear Static and Dynamic Finite Element Analysis*, Prentice-Hall, 1987.
- IKEGAMI, R. & JOHNSON, D.W. The design of viscoelastic passive damping treatments for satellite equipment support structures, Proceedings of DAMPING'86, AFWAL-TR-86-3059, 1986.
- INMAN, D.J. *Vibration, with Control, Measurement, and Stability*. Prentice-Hall, 1989.
- INMAN, D.J. *Vibration with Control*, Wiley 2006.
- JEFFCOTT, H.H. The lateral vibration of loaded shafts in the neighborhood of a whirling speed, *Phil. Mag.*, Vol.6, No 37, pp.304-314, 1919.
- JONES, D.I.G. *Handbook of Viscoelastic Vibration Damping*, Wiley, 2001.
- JUNKINS, J.L. & KIM, Y. *Introduction to Dynamics and Control of Flexible Structures*, AIAA Education Series, 1993.
- KAILATH, T. *Linear Systems*, Prentice-Hall, 1980.
- KARNOPP, D.C., TRIKHA, A.K., Comparative study of optimization techniques for shock and vibration isolation, *Trans. ASME, J. of Engineering for Industry, Series B*, 91, 1128-1132, 1969.
- KRENK, S. Frequency analysis of the tuned mass damper, *J. of Applied Mechanics*, 72: 936-942, 2005.
- KRYSINSKI, T. & MALBURET, F. *Origine et contrôle des vibrations mécaniques, méthodes passives et actives*, Hermès-science, 2003.
- LALANNE, M. & FERRARIS, G. *Rotordynamics Prediction in Engineering*, 2nd Edition, Wiley, 1998.
- LEISSA, A.W. Vibration of Plates, NASA SP-160, 1969.
- LIN, Y.K. *Probabilistic Theory of Structural Dynamics*, McGraw-Hill, 1967.
- MEIROVITCH, L. *Computational Methods in Structural Dynamics*, Sijthoff & Noordhoff, 1980.
- MEIROVITCH, L. *Dynamics and Control of Structures*, Wiley, 1990.
- MEIROVITCH, L. *Methods of Analytical Dynamics*, McGraw-Hill, 1970.
- MIU, D.K. Physical interpretation of transfer function zeros for simple control systems with mechanical flexibilities. *ASME J. Dynamic Systems Measurement and Control*, Vol.113, September, 419-424, 1991.

- MIU, D.K. *Mechatronics - Electromechanics and Contromechanics*, Springer-Verlag, 1993.
- MILES, J.W. On structural fatigue under random loading, *J. of Aeronautical Sciences*, 21, 753-762, 1954.
- NAYFEH, A.H. & MOOK, D.T. *Nonlinear Oscillations*, Wiley, 1979.
- NELSON, F.C. A brief history of early rotor dynamics, *Sound and Vibration*, June, pp.8-11, 2003.
- NEWMARK, N.M. & ROSENBLUETH, E. *Fundamental of Earthquake Engineering*, Prentice Hall, 1971.
- PAPOULIS, A. *The Fourier Integral and its Applications*, McGraw-Hill, 1962.
- ORMONDROYD, J., DEN HARTOG, J.P., The theory of the damped vibration absorber, *Trans. ASME, J. of Applied Mechanics*, 50:7, 1928.
- PREUMONT, A. *Random Vibration and Spectral Analysis*, Kluwer, 1994.
- PREUMONT, A. *Mechatronics, Dynamics of Electromechanical and Piezoelectric Systems*, Springer, 2006.
- PREUMONT, A. *Vibration Control of Active Structures, An Introduction*, 3rd Edition, Springer 2011.
- PREUMONT, A. & SETO, K. *Active Control of Structures*, Wiley, 2008.
- REDDY, J.N., *Energy and Variational Methods in Applied Mechanics*, Wiley, 1984.
- SHAKER, F.J. Effect of axial load on mode shapes and frequencies of beams, NASA Technical Note TN D-8109, December 1975.
- SPECTOR, V.A. & FLASHNER, H. Sensitivity of structural models for noncollocated control systems. *ASME J. Dynamic Systems Measurement and Control*, Vol.111, No 4, December, 646-655, 1989.
- STRANG, G. *Linear Algebra and its Applications*, Harcourt Brace Jovanovich, 3rd Edition, 1988.
- SWANSON, E., POWELL C.D. & WEISSMAN, S. A Practical Review of Rotating Machinery Critical Speeds and Modes, *Sound and Vibration*, 10-17, May 2005.
- von KARMAN, Th. & BIOT, M. *Mathematical Methods in Engineering*, McGraw-Hill, 1940.
- WANG, Y.Z. & CHENG, S.H. The optimal design of dynamic absorber in the time domain and the frequency domain. *Applied Acoustics*, 28: 67-87, 1989.
- WIBERG, D.M. *State Space and Linear Systems*, McGraw-Hill Schaum's Outline Series in Engineering, 1971.
- WILDHEIM, S.J. Excitation of Rotationally Periodic Structures, *Transaction of the ASME, Journal of Applied Mechanics*, Vol.46, 878-882, Dec. 1979.
- WILLIAMS, J.H., Jr *Fundamentals of Applied Dynamics*, Wiley, 1996.
- ZIENKIEWICZ, O.C., & TAYLOR, R.L. *The Finite Element Method*, Fourth edition (2 vol.), McGraw-Hill, 1989.



---

## Index

- Accelerated fatigue test, 222
- Accelerogram, 213
- Active damping, 304
- Active mass damper (AMD), 295
- Active strut, 301
- Active suspension, 292
- Active truss, 301
- Active vibration control, 287
- Angular rate sensor, 250
- Anisotropic shaft, 246
  - stability, 249
  - unbalance response, 248
- Anisotropic support (rotor), 243
- Anti-resonance, 34, 259, 288
- Assembly, 143
- Assumed modes method, 117, 139
- Asymptotic method, 92
- Asynchronous force, 238
- Autocorrelation, 176
- Autocovariance, 176
- Backward whirl, 227, 236, 241
- Bar, 98, 120
  - finite element, 140
- Beam
  - Euler-Bernoulli, 81, 122
  - finite element, 144
  - free vibration, 87
  - free-free, 91
  - prestress, 85, 125
  - simply supported, 89
- Beat phenomenon, 10
- Bending stiffness, 83
- Beta controller, 307
- Bode plots, 7, 37
- Boundary layer noise, 195
- Buckling, 76
  - beam, 100
  - clamped-free beam, 102
  - critical load, 101
  - simply supported beam, 101
- Campbell diagram, 66, 235, 242
- Cantilever rotor, 253
- Car on a random road, 198
- Car suspension
  - active, 292
  - passive, 281
- Cascade analysis, 172
- Causality, 191
- Central frequency, 186
- Central limit theorem, 180
- Centrifugal pendulum, 80, 281
- Centrifugal Pendulum Vibration
  - Absorber, 80, 280
- Co-spectrum, 195
- Coherence function, 189
- Collocated control, 287, 290
- Collocated system, 34
- Complex coordinates, 226
- Conical mode, 241
- Conservation laws, 67
- Conservation of energy, 52, 69
- Conservative force, 52
- Consistent mass matrix, 146
- Constitutive equation

- active strut, 301
- linear elastic material, 74
- plane stress, 104
- Constrained system, 37, 154, 158, 289
- Convection velocity, 196
- Convergence, 149
- Convolution integral, 4, 181
- Coriolis force, 250
- Correlation
  - function, 176, 195
  - integral, 181
  - matrix, 191, 193
- Covariance matrix, 220
- Craig-Bampton reduction, 158
- Critical speed, 226, 237, 238
- Cross-correlation, 176
  - role of-, 200
- Cumulative mean square response, 179
- D'Alembert principle, 51
- Damping, 25, 26, 125
  - modal, 25
  - Rayleigh, 26
  - rotating, 228, 230
- Davenport spectrum, 197
- Degree of freedom (d.o.f.), 46, 117
- Den Hartog, 260
- Difference equation, 40
- Discretization, 117
- Disk, 240
- Dissipation function, 58
- Dynamic amplification, 7, 28
- Dynamic flexibility matrix, 27
- Dynamic mass, 165, 172
- Dynamic Vibration Absorber (DVA), 256
- Effective force, 51
- Effective modal mass, 166
- Elastic support, 240
- Envelope (narrow band process), 187
- Epicycloid, 281
- Equal peak design (DVA), 260
- ESP, 250
- Euler
  - Bernoulli beam, 81
  - critical buckling load, 101, 127
  - theorem on homogeneous functions, 69
- Fast Fourier Transform (FFT), 178
- Fatigue, 208
  - random-, 217
- Feedthrough, 12, 29
- Finite elements, 139
- First-crossing problem, 209
- Flexural rigidity (plate), 104
- Forward whirl, 225, 227, 236, 241
- Fourier transform, 9
- Fraction of critical damping, 2
- Fraction of modal strain energy, 303
- Frahm, 256
- Frequency Response Function (FRF), 8
- FRF estimation, 189
- Gaussian process, 180
- Generalized coordinates, 46, 55, 140
- Generalized momentum, 70
- Geometric stiffness matrix, 75, 126
  - planar beam element, 151
- Geometric strain energy, 71, 75
- Gradient height, 197
- Gradient velocity, 197
- Gravity loads, 132
- Green strain tensor, 71
- Guyan
  - mass matrix, 159, 171
  - reduction, 152
  - stiffness matrix, 159
- Gyroscopic effect, 56, 63, 230
- Gyroscopic forces, 64
- Half power bandwidth, 183
- Hamilton's principle, 52
- High-cycle fatigue, 208
- Holonomic constraint, 46, 67
- Homogeneous (random field), 195
- Homogeneous functions, 69
- Ignorable coordinate, 69
- Impulse response, 3
- Integral force feedback, 304
- Interlacing, 35, 287, 304
- Isolator
  - by kinematic coupling, 278
  - corner frequency, 275
  - Linear-, 270
  - Passive-, 271
  - Relaxation-, 272
  - Six-axis-, 275

- Jacobi integral, 67
- Jeffcott rotor, 63, 224
- Jitter, 275
- Kanai-Tajimi spectrum, 185, 202
- Kinematic constraint, 46
- Kirchhoff plate, 103
- Kronecker delta, 23
- Lagrange multipliers, 66
- Lagrange's equation, 55
  - with constraints, 66
- Lagrangian, 53, 56
- Lagrangian dynamics, 45
- Laplacian  $\Delta$ 
  - Cartesian coordinates, 105
  - polar coordinates, 107
- Laval, 226
- Lead compensator, 289
- Linear damage theory, 218
- Linear oscillator
  - Bode plots, 7
  - Dynamic amplification, 7
  - Free response, 1
  - Impulse response, 3
  - Nyquist plot, 8
  - Quality factor, 8
  - Random response, 182
  - State space form, 11
- Localization matrix, 143
- Long rotor, 240
- Lumped mass matrix, 146
- Mass matrix
  - bar, 121
  - bar element, 142
  - beam, 124
  - lumped, 146
  - planar beam element, 146
- Master-slave (d.o.f.), 152
- Maxwell unit, 272
- Mean square (MS), 176, 177, 199
  - mass averaged-, 200
- Memory, 4
- Modal
  - damping, 25
  - decomposition, 25, 95
  - mass, 22, 95
  - participation factor, 164
- participation matrix, 170
- truncation, 26
- Modal density, 107
- Modal spread, 278
- Mode shape, 20
- Moment-curvature relationship, 104
- Multi-axis excitation, 168
- Multiple natural frequencies, 23
- N-storey building, 39, 174
  - AMD, 295
  - DVA design, 264
  - random response, 202
  - random response with DVA, 267
  - seismic response, 166
- Nabla  $\nabla$ 
  - Cartesian coordinates, 105
- Narrow band process, 187
- Natural boundary conditions, 85
- Natural frequency, 20
- Nodal
  - circles, 111, 112
  - diameters, 111, 112
  - lines, 107
- Non-conservative force, 53
- Non-holonomic constraint, 47, 67
- Normal modes, 23
- Nyquist plot, 8, 37
- Operating Basis Earthquake, 214
- Orthogonal functions, 119
- Orthogonality, 22, 93
- Painlevé integral, 69
- Palmgren-Miner criterion, 218
- Parseval's theorem, 9
- Participation factor, 164
- Peak factor, 207, 208, 212
- Periodic structures, 112
- Phase plane, 187
- Plane truss, 140
- Plate
  - circular, 107
  - Kirchhoff, 103
  - rectangular, 106
- Pole-zero pattern, 35, 287, 304
- Power spectral density, *see* PSD
- Prestress, 71, 85, 100, 125
- Principle of stationarity, 129

- Principle of virtual work, 49
- Projection matrix, 43
- PSD
  - definition, 177
  - estimation, 178
  - input-output (MIMO), 192
  - input-output (SISO), 181
  - matrix, 192, 193
  - one sided-, 179
- Pseudo-acceleration spectrum, 213
- Pseudo-velocity spectrum, 213
- Quality factor, 8, 28, 261
- Quarter-car model, 281
- Quasi-static correction, 29, 166
- Rainflow, 218
- Random fatigue, 217
- Random vibration, 175
- Rankine's model, 226
- Rayleigh
  - damping, 26
  - distribution, 188
  - Quotient, 22, 95, 127
- Rayleigh-Ritz method, 117, 230
- Reduction
  - Craig-Bampton, 158
  - Guyan, 152
- Relaxation isolator, *see* Isolator
- Reliability, 209
- Residual mode, 29
- Resonance
  - frequency, 20
  - linear oscillator, 2
  - rotating force, 113, 114
- Response spectrum, 213
- Rice formulae, 186
- Rigid body mode, 23, 30
- Root locus, 274, 289, 298, 305
- Rotating force, 112
- Rotating mode, 111
- Rotor dynamics, 223
- Routh-Hurwitz stability, 230
- S-N curve, 217
- Safe Shut-down Earthquake, 214
- Scleronomic constraint, 46
- Seismic excitation, 161
- Self-centering, 226
- Semi-positive definite (matrix), 18
- Shape function, 118, 139, 145
- Signal to noise ratio, 191
- Single axis excitation, 161
- Sky-hook damper, 292
- Slave (d.o.f.), 152
- Spatial coherence, 195
- Spectral moments, 186
- SRSS rule, 200, 216
- Stability, 230
- Standard deviation, 176
- State feedback, 293
- State variables, 12, 282, 292, 297
- Stationary process, 175
- Stiffness matrix
  - bar, 120
  - bar element, 141
  - beam, 123
  - geometric, 126
  - planar beam element, 146
- Stodola-Green rotor, 253
- Strain energy density, 74, 104
- String, 96
- Strouhal number, 195
- Supercritical velocity, 226
- Support reaction, 165, 171
- Taipei 101, 261
- Tautochronic problem, 281
- Threshold crossing, 207
- Torsional stiffness, 14
- Transmissibility, 271, 275
- Traveling wave, 111, 113, 114
- Tuned Mass Damper (TMD), 256
- Unbalance response, 225, 238
- Variance, 176
- Vibration isolation, 269
- Virtual displacement, 48
- Virtual work, 49
- von Mises stress, 220
- Wöhler curve, 217
- Whirl, 227, 235
- White noise
  - approximation, 184, 216
  - band limited-, 184
  - process, 180
- Wind response, 196
- Zero (transmission-), 37, 258, 278, 288
- Zero-period acceleration (ZPA), 213